Zeitschrift: IABSE publications = Mémoires AIPC = IVBH Abhandlungen
Band: 35 (1975)

Teilband: IABSE Publications = Mémoires AIPC = IVBH Abhandlungen

ASSOCIATION INTERNATIONALE DES PONTS ET CHARPENTES
INTERNATIONALE VEREINIGUNG FÜR BRÜCKENBAU UND HOCHBAU
INTERNATIONAL ASSOCIATION FOR BRIDGE AND STRUCTURAL ENGINEERING

MÉMOIRES
ABHANDLUNGEN

35-II

1975

PUBLIÉS PAR LE SECRÉTARIAT GÉNÉRAL À ZURICH
HERAUSGEGEBEN VOM GENERALSEKRETARIAT IN ZÜRICH
PUBLISHED BY THE GENERAL SECRETARIAT IN ZURICH

Editeur - Verleger - Publisher

Association Internationale des Ponts et Charpentes
Ecole Polytechnique Fédérale de Zurich

Internationale Vereinigung für Brückenbau und Hochbau
Eidgenössische Technische Hochschule Zürich

International Association for Bridge and Structural Engineering
Swiss Federal Institute of Technology, Zurich

Printed in Switzerland
ISBN 3 85748 008 4

Préface

Les constructions de qualité présentent toutes au moins deux points communs: une conception générale idoine et des détails particulièrement bien étudiés.

L'action de notre association s'exerce sur les deux plans. Le présent volume des Mémoires en est un exemple nouveau. En effet, à côté d'études portant sur des aspects de détail importants, plusieurs auteurs ont fourni des contributions de caractère général donnant un effort en faveur de la compréhension des phénomènes généraux. Cette approche multiple des problèmes montre une fois de plus l'intérêt de nos publications pour l'ensemble des intéressés à la construction d'un ouvrage.

Nous remercions très vivement les auteurs pour leur participation, en espérant que nos Mémoires permettent toujours mieux l'approche de structures parfaites.

Zurich, septembre 1975.

Le Président de l'AIPC:

Prof. MAURICE COSANDEY
Président de l'Ecole Polytechnique Fédérale de Lausanne

Les Secrétaires Généraux:

Dr. sc. techn. HANS VON GUNTEN
Professeur à l'Ecole Polytechnique Fédérale de Zurich

Dr. sc. techn. PIERRE DUBAS
Professeur à l'Ecole Polytechnique Fédérale de Zurich

JÖRG SCHNEIDER
Professeur à l'Ecole Polytechnique Fédérale de Zurich

Vorwort

Wertvolle Bauwerke weisen mindestens zwei gemeinschaftliche Punkte auf: Geeignete Allgemeinkonzeption einerseits, und besonders durchgearbeitete Einzelheiten anderseits.

Die Tätigkeit unserer Vereinigung macht sich nach beiden Richtungen geltend, und der vorliegende Band unserer «Abhandlungen» bietet dafür ein neuerliches Beispiel. Neben Untersuchungen über verschiedene Aspekte von wichtigen Einzelheiten haben nämlich mehrere Verfasser Beiträge generellen Charakters beigestauert und damit die Bestrebungen zum Verständnis allgemeiner Phänomene aufgezeigt. Dieses vielfältige Näherrücken der Probleme beweist einmal mehr die unserer Veröffentlichungen entgegengebrachte Aufmerksamkeit aller interessierten Kreise bei der Konstruktion von Bauten.

Wir danken den Verfassern lebhaft für ihre Mitarbeit und hoffen, dass unsere «Abhandlungen» je länger je mehr die Annäherung zum Entstehen vollkommener Bauwerke gestatten werden.

Zürich, September 1975.

Der Präsident der IVBH:

Prof. MAURICE COSANDEY
Präsident der Eidgenössischen Technischen Hochschule Lausanne

Die Generalsekretäre:

Dr. sc. techn. HANS VON GUNTEN
Professor an der Eidgenössischen Technischen Hochschule Zürich

Dr. sc. techn. PIERRE DUBAS
Professor an der Eidgenössischen Technischen Hochschule Zürich

JÖRG SCHNEIDER
Professor an der Eidgenössischen Technischen Hochschule Zürich

Preface

All of the excellent structures have at least two points in common; a well planned general concept and thoroughly well elaborated details. The material produced through our Association is clearly becoming effective in both aspects.

The present volume of the "Memoires" has an additional attribute for which we have sought; while there are studies dealing with various aspects of detail having a narrow but no less important scope, there are also contributions from several authors aimed at making a general appreciation of the total concept. This embracing approach to problems gives our publications an interest and appeal to all of those whose interests are the actual construction of structures.

We acknowledge the co-operation of the authors in our aims and offer them our sincere thanks. We are confident that the Memoires will contribute more than ever to the advancement of the concept and the final realization of structures.

Zurich, September 1975

The President of IABSE:

Prof. MAURICE COSANDEY
President of the Swiss Federal Institute of Technology, Lausanne

The General Secretaries:

Dr. sc. techn. HANS VON GUNTEN
Professor of the Swiss Federal Institute of Technology, Zurich

Dr. sc. techn. PIERRE DUBAS
Professor of the Swiss Federal Institute of Technology, Zurich

JÖRG SCHNEIDER
Professor of the Swiss Federal Institute of Technology, Zurich

Leere Seite
Blank page
Page vide

Table des matières - Inhaltsverzeichnis - Table of Contents

Effect of Variation of Interface Connection Modulus in Elastically connected Elements of Composite Beams

Influence de la variation de la déformabilité des connecteurs dans les poutres mixtes élastiques

Einfluss der Änderung des Verformungsmoduls der Verbundmittel bei elastischen Verbundträgern

A.O. ADEKOLA
Professor and Head of Civil Engineering
Department of Civil Engineering,
University of Lagos, Nigeria

Abstract

Various forms of shear connectors are the medium through which interaction in composite beams is ensured. The connectors most commonly in use nowadays are the flexible type either in the form of studs, spiral shear connectors or cleats connected to the beam element and embedded in the concrete. In the present analysis an attempt is made to study the effect of distribution of shear connectors in a span where they are needed for ensuring interaction. Implicit in the analysis is the assumption that the profile for the shear connection modulus is analogous to that defining the juxtaposition of the shear connectors. This is of course only partially true since other effects like the flexural rigidity of the connectors, totally embedded within an "elastic" medium which itself undergoes deformation due to bending, and the presence of the connectors come into play. The mechanics by which flexible connectors ensure interaction is too complex, that only a simplified and idealised model like that used in this work can provide some insight into connector interaction behaviour.

The analysis shows quite clearly that for a given number of connectors to be employed for the transfer of interacting axial forces from one element to the other of a composite section the best arrangement is not the evenly spaced type, nor is the arrangement whereby connectors are concentrated near the point of maximum moment to be recommended. The best arrangement is the one that ensures that the greater number of connectors to be used are concentrated in the regions of zero external moments.

Introduction

The design of flexible shear connectors in composite beams is usually based on conditions at ultimate loads or collapse. The design objective is to ensure that at collapse there will be enough connectors, based on some predetermined connector design capacity obtained from standard push-out tests, to transfer the total axial force developed as a result of interaction from one to the other of the interacting steel beam and concrete slab. This design capacity is chosen on the basis of a limiting slip at failure as the design criterion. CHAPMAN and YAM [1] suggested that the juxtaposition of the connectors should be determined by spacing evenly over the distance between two adjacent points of maximum and zero or minimum moments the shear connectors needed to resist the maximum interacting axial force developed at ultimate load conditions between such points. They presented results for inelastic behaviour of continuous composite beams employing a predictor-corrector method of numerical integration.

Although it is an accepted design practice, and indeed the vogue, to select structural elements on the basis of conditions at collapse, safe structures however generally remain "elastic", or at any rate are far from collapse, at working loads. The present paper is therefore an attempt to examine the influence of shear connectors and their distributions on interaction under so called elastic conditions. It is believed that the insight gained from this work will lead to a better understanding of interaction at working loads and may result in more rational design basis or economy or both.

Previous interaction analyses of composite beams have assumed constant interface connection modulus along the length of the beams irrespective of the type of imposed loading or whether the beams are simply supported or continuous. In the present analysis a variation of the interface connection modulus is assumed in the form of an exponential function. Harmonic representation can also be used to study this variation. This representation enables a number of variations which idealise possible distributions of shear connectors to be studied as well as the limiting cases of partial interaction with constant interface connection modulus, the complete interaction and no interaction. Because in the design of a bridge deck system one is normally considering moment envelopes, the present analysis has been limited to simply supported beams of symmetrical loading.

Formulation of the problem

We will consider a system of an infinite number of steel beams supported over finite and equal spans equally spaced transversely, interacting with a concrete slab extending over the entire beam system, with each steel beam identically loaded. We choose as our origin the middle plane of the concrete slab at a point midway between two adjacent beams for the y coordinate in the transverse direction and midspan for the x coordinate in the spanwise direction.

The assumed representation for the interface connection modulus is of the form $Ae^{r\frac{|x|}{a}}$ for all cases of symmetrical loading over a continuous or a simply supported span. This will enable the effect of any one of the four spanwise variations of the connection modulus shown in Fig. 1 to be studied.

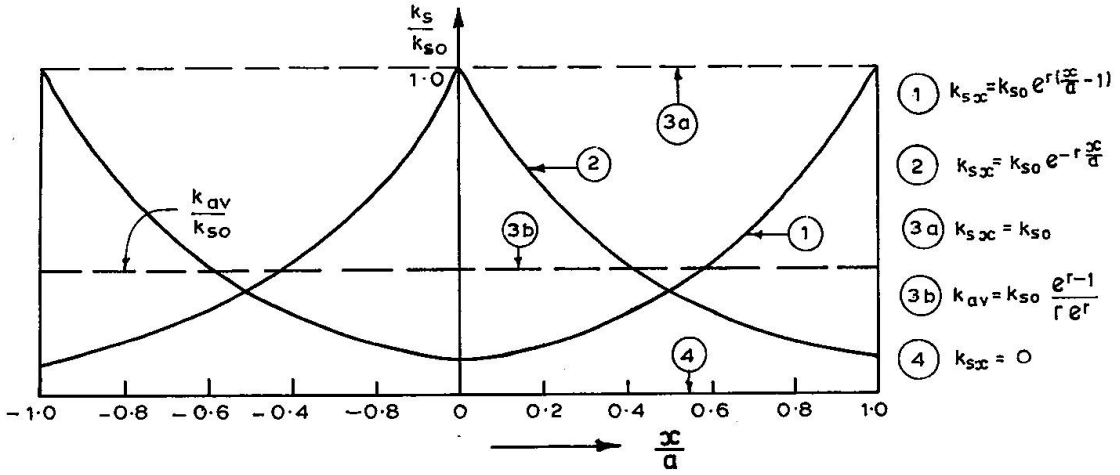

Fig. 1. Assumed variations of foundation modulus over the span of simply supported beam.

In general

$$k_{sx} = \begin{Bmatrix} \frac{k_{so}}{p} e^{\frac{|x|}{a} lnp} \\ \\ k_{so}\, e^{-\frac{|x|}{a} lnp} \end{Bmatrix} \tag{1}$$

according as whether the profile of 1 or 2 is assumed. Both representations yield the average value (3) when the connectors are assumed evenly spread but with the same overall resistance to slip over the span as in the expressions (1) and (2), and comply with the limiting case (4) of no interaction when p is $-\infty$ for representation (2), whilst complete interaction condition may be simulated by setting p to $+\infty$ for (1) and $-\infty$ for (2).

The equilibrium and compatibility conditions to be satisfied at the cross-section of each longitudinal steel beam, assumed prismatic, are given by [3]

$$\begin{aligned} &-E_s I_s w_{,1111} + \tfrac{d}{2}\cdot F_{,11} - Q_{c,1} + p_n = 0, \\ &[E_s R_s]^{-1}\cdot F + \frac{(d+t)}{2}\cdot w_{,11} - u_{x,1} = (k_{sx}^{-1}\cdot F_{,1})_{,1} \end{aligned} \tag{2}$$

where w is the transverse deflexion, u_x the longitudinal in-plane slab displacement, $E_s I_s, R_s$ and d refer to the elastic modulus, the second moment of area, cross-sectional area and overall depth of each of the steel beams; t the slab thickness; k_{sx} the interaction modulus at x, F the interacting axial forces and p_n the component of a Fourier representation for the loading.

$$Q_{c,1} = -2[D_y \cdot w_{,222} + H \cdot w_{,112}] \tag{4}$$

A comma, followed by 1 or 2 implies differentiation with respect to x or y respectively.

The displacement and membrane stress relations satisfying equilibrium conditions in the absence of body forces for a special case of isotropy are as follows:

$$\left.\begin{aligned} u_x &= \Psi_{,1} - 4(1+\nu)^{-1}\phi_1 \\ \alpha u_y &= \alpha\Psi_{,2} - 4(1+\nu)^{-1}\phi_2 \\ c_{11}^{-1}\sigma_{xx} &= \Psi_{,11} + \alpha^2\nu\Psi_{,22} - 4(1+\nu)^{-1}(\phi_{1,1} + \alpha\nu\phi_{2,2}) \\ \alpha^{-2}c_{11}^{-1}\sigma_{yy} &= \nu\Psi_{,11} + \alpha^2\Psi_{,22} - 4(1+\nu)^{-1}(\nu\phi_{1,1} + \alpha\phi_{2,2}) \\ \alpha^{-2}c_{11}^{-1}\sigma_{xy} &= (1-\nu)\left[\Psi_{,12} - 2(1+\nu)^{-1}(\phi_{1,2} + \alpha\phi_{2,1})\right] \end{aligned}\right\} \tag{5}$$

where

$$\Psi = \phi_0 + x\phi_1 + Y\phi_2,\ Y = \alpha^{-1}y, \tag{6}$$

$$\phi_0 = \sum_{n=1}^{\infty}[A_{n1}\cos h(K_nY)\cos(K_nx) + B_{n1}\cos h(L_nX)\cos(L_ny)], \tag{7}$$

$$\phi_1 = \sum_{n=1}^{\infty} B_{n2}\sin h(L_nX)\cos(L_ny), \tag{8}$$

$$\phi_2 = \sum_{n=1}^{\infty} A_{n2}\sin h(K_nY)\cos(K_nx), \tag{9}$$

Similarly we write the relation giving the deflexion surface satisfying equilibrium conditions for a plate having properties that result in a special case of isotropy as follows:

$$w(x,y) = \sum_{n=1}^{\infty}[K_n^{-4}q_n + \bar{A}_{n1}\cos h(K_n\bar{Y}) + \bar{A}_{n2}\bar{Y}\sin h(K_n\bar{Y})]\cos(K_nx), \tag{10}$$

where

$$q = D_x\sum_{n=1}^{\infty} q_n\cos(K_nx),\ K_n = (2n-1)\tfrac{\pi}{2a},\ L_n = \tfrac{2a}{b}\cdot K_n,\ X = \alpha x,\ \bar{Y} = \lambda^{-1}y, \tag{11}$$

By our choice of the eigen-values we have ensured the satisfaction of the condition for simply supported edges, namely $w = M_x = 0$ at $x = \pm a$. The conditions that $\sigma_{xx} = \sigma_{xy} = 0$ at $x = \pm a$ are satisfied provided

$$B_{n1} = L_n^{-1}(\alpha^2c_{11} - c_{12})^{-1}\left[2(1-\nu)(1+\nu)^{-1}c_{11} - (\alpha^2c_{11} - c_{12})L_na\tan h(L_n\alpha a)\right]\cdot B_{n2} \tag{12}$$

$$B_r = L_r\left[\frac{(1-\nu)(\alpha^2c_{11} + c_{12})}{(1+\nu)(\alpha^2c_{11} - c_{12})}\sin h(L_r\alpha a) + L_r\alpha a/\cos h(L_r\alpha a)\right]\cdot B_{r2}, \tag{13}$$

$$B_r = 4b^{-1}\sum_{m=1}^{\infty}\frac{(-1)^mL_rK_m\alpha^{-1}\sin h(K_mb\alpha^{-1})}{\alpha^{-2}K_m^2 + L_r^2}\left[(1+\nu)^{-1} - \frac{K_m^2}{K_m^2 + \alpha^2L_r^2}\right]\cdot A_{m2} \tag{14}$$

The other conditions to be satisfied from a consideration of the symmetry of the problem are

$$u_y = 0 \text{ at } y = 0 \text{ and } y = \pm b \text{ for } ||x| < a$$

$$w_{,2} = 0 \text{ at } y = 0 \text{ and } y = \pm b \text{ for } |x| < a$$

These are automatically satisfied if

$$A_{n1} = K_n^{-1}[(3 - \nu)(1 + \nu)^{-1} - K_n b\alpha^{-1} \coth(K_n b\alpha^{-1})] \cdot A_{n2} \tag{15}$$

$$\bar{A}_{n1} = -K_n^{-1}[1 + K_n b\lambda^{-1} \coth(K_n b\lambda^{-1})] \cdot \bar{A}_{n2} \tag{16}$$

Using the result in (15) above we obtain the interacting axial force as

$$F = \tau_o t \sum_{n=1}^{\infty} A_{n2} \sin h(K_n b\alpha^{-1}) \cos(K_n x) \tag{17}$$

In satisfying the compatibility condition (3) using the new representation for k_s as $k_{s0} e^{r\frac{|x|}{a}}$, that is case 1 of Fig. 1, and employing orthogonality relations for taking out from under the summation signs the extractable superposition coefficients we encounter the integrals

$$\int_{-a}^{a} e^{-r\frac{|x|}{a}} \cdot \sin(K_n x) \cos(K_m x)\, dx \tag{18}$$

$$\int_{-a}^{a} e^{-r\frac{|x|}{a}} \cdot \cos(K_n x) \cos(K_m x)\, dx \tag{19}$$

which upon solution reduces to zero for (18) and for (19) to

$$g_{mn} = \frac{r}{a}\left[\frac{(-1)^{n-m+1}e^{-r} + 1}{\frac{r^2}{a^2} + (K_n - K_m)^2} + \frac{(-1)^{n+m} \cdot e^{-r} + 1}{\frac{r^2}{a^2} + (K_n + K_m)^2}\right] \tag{20}$$

the case when the variation of k_s is of the type 2 of Fig. 1, namely $k_{s0} e^{-r\frac{|x|}{a}}$ is obtained by replacing r in (20) by $-r$.

The equilibrium and compatibility equations (2) and (3) now reduce respectively to

$$\bar{A}_{m2} J_m = E_s I_s q_m - p_m + \tau_0 t d K_m^2 \sin h(K_m b\alpha^{-1}) \cdot A_{m2} \tag{21}$$

$$A_{m2} + \tau_0 t V_m k_{s0}^{-1} \sum_{p=1}^{\infty} K_p^2 g_{mp} \sin h(K_p b\alpha^{-1}) \cdot A_{p2} + V_m \sum_{p=1}^{\infty} \sum_{n=1}^{\infty} R_{mp} S_{np} A_{n2} =$$

$$\frac{a(d+t)}{2} J_m^{-1} V_m[c_{1m} p_m + 4 q_m D_y \lambda^{-3} \sin h(K_m b\lambda^{-1})] \tag{22}$$

$$J_m = K_m^2[E_s I_s C_{1m} + 4 D_y \lambda^{-3} \sin h(K_m b\lambda^{-1})] \tag{23}$$

$$V_m^{-1} = a\left\{\tau_0 t \sin h(K_m b\alpha^{-1})\left[(E_s R_s)^{-1} + \frac{d(d+t)}{4} C_{1m} J_m^{-1} K_m^2\right] + C_{2m}\right\} \tag{24}$$

For a constant k_s

$$V_m^{-1} = a\left\{\tau_0 t \sin h(K_m b\alpha^{-1})\left[(E_s R_s)^{-1} + \frac{d(d+t)}{4} C_{1m} J_m^{-1} K_m^2 + K_s^{-1} K_m^2\right] + C_{2m}\right\} \quad (25)$$

since $g_{mp} = a$ when $p = m$ and zero
when $p \neq m$

where

$$C_{1m} = K_m(\cos h(K_m b\lambda^{-1}) + K_m b\lambda^{-1}/\sin h(K_m b\lambda^{-1})) \quad (26)$$

$$C_{2m} = K_m((3-\nu)(1+\nu)^{-1} \cos h(K_m b\alpha^{-1}) - K_m b\alpha^{-1}/\sin h(K_m b\alpha^{-1})) \quad (27)$$

$$R_{mp} = \frac{4\alpha L_p K_m(-1)^{m+1} \cos h(L_p \alpha a)}{K_m^2 + \alpha^2 L_p^2}\left[\frac{(1-\nu)c_{12}}{(1+\nu)(\alpha^2 c_{11} - c_{12})} - \frac{\alpha^2 L_p^2}{K_m^2 + \alpha^2 L_p^2}\right] \quad (28)$$

$$S_{np} = \frac{4S_p^{-1}(-1)^n \alpha L_p K_n \sin h(K_n b\alpha^{-1})}{K_n^2 + \alpha^2 L_p^2}\left[(1-\nu)^{-1} - \frac{K_n^2}{K_n^2 + \alpha^2 L_p^2}\right] \quad (29)$$

$$S_p = L_p b\left[\frac{(1-\nu)(\alpha^2 c_{11} + c_{12})}{(1+\nu)(\alpha^2 c_{11} - c_{12})} \sin h(L_p \alpha a) + L_p \alpha a/\cos h(L_p \alpha a)\right] \quad (30)$$

The method of analysing two-span continuous composite beams as well as the method of obtaining effective widths based on a comparison of the moment-curvature relationship of the composite assembly with that of the steel beams alone supporting the imposed loading have been discussed elsewhere [5].

Complete interaction is attained for type 1 variation of the k_s as r tends to infinity in equation (20) since g_{mn} will rend to zero correspondingly resulting in an earlier established result [4]. The case of no interaction is obtained by letting r tend to $-\infty$, thus leading to a zero k_s. Under this condition, equation (22) resulting from the interface compatibility condition becomes indeterminate since the coefficients of A_{r2} become infinite and the $A_{n2}^{'s}$ consequently take zero values. The surviving condition of equilibrium (21), also leads thereby to another earlier established result for no interaction case [4].

In the results that follow, degree of interaction, effective widths, steel bottom flange stress reduction, slip and deflexion profiles are all studied with the variation of r or p.

For the special case of isotropy considered in this analysis

$$\alpha = \lambda = (c_{22} c_{11}^{-1})^{1/4} = (D_y D_x^{-1})^{1/4}$$

and both become unity for the case of ordinary isotropy.

For the purpose of computations symmetrical and prismatic steel I sections are assumed to be interacting with a 152 mm thick concrete slab assumed isotropic. The dimensions of each steel beam are as follows:

Overall depth	625 mm
Flange width	254 mm

Flange thickness 24 mm
Web thickness 13 mm
$I_s = 1.309579 \times 10^{-3}\text{m}^4$
$R_s = 1.969300 \times 10^{-2}\text{m}^2$

The total load applied either as midspan point load or uniformly distributed over a span of 4.0 metre is 250 kN.

Concluding Remarks

The analysis demonstrates clearly the influence of the variation of shear connection modulus on interaction. It also once again confirms that considerable reduction in steel bottom flange stress and deflexions can be achieved at relatively low degree of interaction (see Tables 1 and 2 $\frac{k_s}{E_s}(1.5 - 2.5\%)$. It is assumed that the total number of connectors used partly determines the interface shear connection modulus of the composite element. Quite clearly the advantages to be gained by employing a large number of shear connectors to provide a shear connection modulus much above the range of values given above are minimal. What would seem to be paramount from the analysis is the physical arrangements of the connectors between adjacent points of minimum or zero moments.

If it is assumed that the physical arrangements of shear connectors bears a direct relation to the profile of shear connection modulus developed during interaction, then from the present analysis the more efficient distribution of connectors will be that which for a given number of shear connectors to be employed, varies from a minimum at the point of maximum positive or negative moment to a maximum at the point of zero moment. The system of evenly distributed shear connectors based on the above assumption would appear to be less efficient. However it must be pointed out that the method by which shear connectors develop interaction shear connection modulus is complex and least understood, and it could very well be that even the evenly distributed system of shear connectors does not offer a constant shear connection modulus in service.

Table 1

$100\frac{k_s}{E_s}$	Maximum Deflexion Span Ratio $\times 10^{-4}$ for $\frac{b}{a} = 0.4$, $p = 10$		
	Average Constant k_s	$\frac{k_{sx}}{k_{so}} = \frac{e}{p}\frac{x}{a}1n\,p$	$\frac{k_{sx}}{k_{so}} = e^{-\frac{x}{a}1np}$
0	22.6	22.6	22.6
0.125	18.5	14.0	17.2
0.250	16.4	12.5	15.0
0.500	14.3	11.5	13.1
1.000	12.6	11.0	11.7
1.500	11.9	10.6	11.2
2.000	11.5	10.5	10.9
2.500	11.2	10.4	10.7
∞	10.0	10.0	10.0

Table 2

$100\frac{k_s}{E_s}$ $p = 10$	Bottom Flange Stress Factor for $\frac{b}{a} = 0.4$, $p = 10$		
	Average Constant k_s	$\frac{k_{sx}}{k_{so}} = \frac{e}{p}^{\frac{1 \times 1}{a}} 1np$	$\frac{k_{sx}}{k_{so}} = e^{-\frac{1 \times 1}{a}} 1np$
0	0.934	0.934	0.934
0.125	0.894	0.852	0.880
0.250	0.874	0.836	0.857
0.500	0.853	0.824	0.837
1.000	0.835	0.815	0.822
1.500	0.827	0.811	0.816
2.000	0.822	0.808	0.812
2.500	0.818	0.806	0.811
∞	0.800	0.800	0.800

Fig. 2 demonstrates the performance of the various distributions of shear connection moduli assumed, in terms of bottom flange stress reduction and central deflexion reduction as compared with bottom flange stress and deflexion of the steel beams acting alone. The practical range of the diagram is from $p = 2$ to 10. Below this range one encounters infinite values of k_s and it will not be meaningful to draw conclusions from these.

Type 1 distribution as shown in fig. 1 is clearly the most efficient. Fig. 3 further demonstrates this fact in the degree of interaction achieved as defined by the

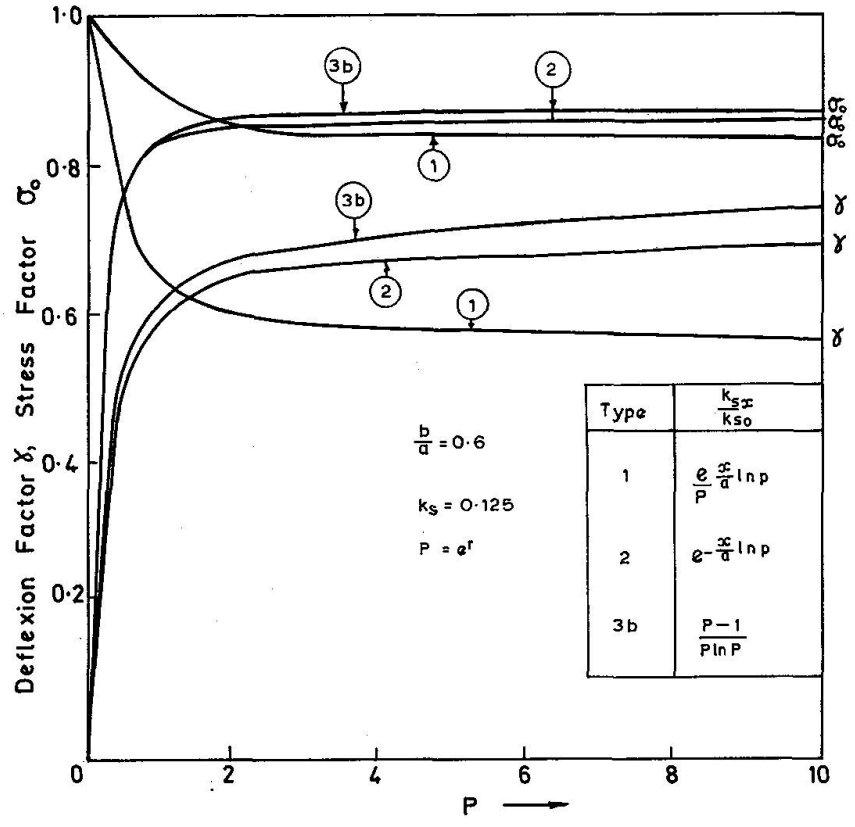

Fig. 2. The effect of foundation modulus reduction parameter p on deflexions and stresses.

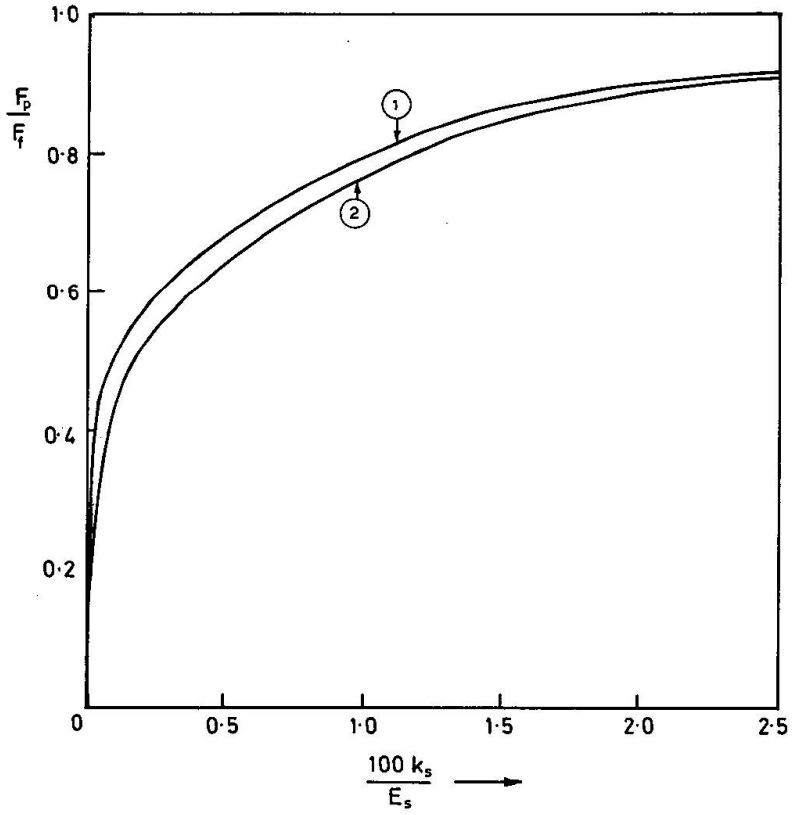

Fig. 3. Degree of interaction against foundation modulus.

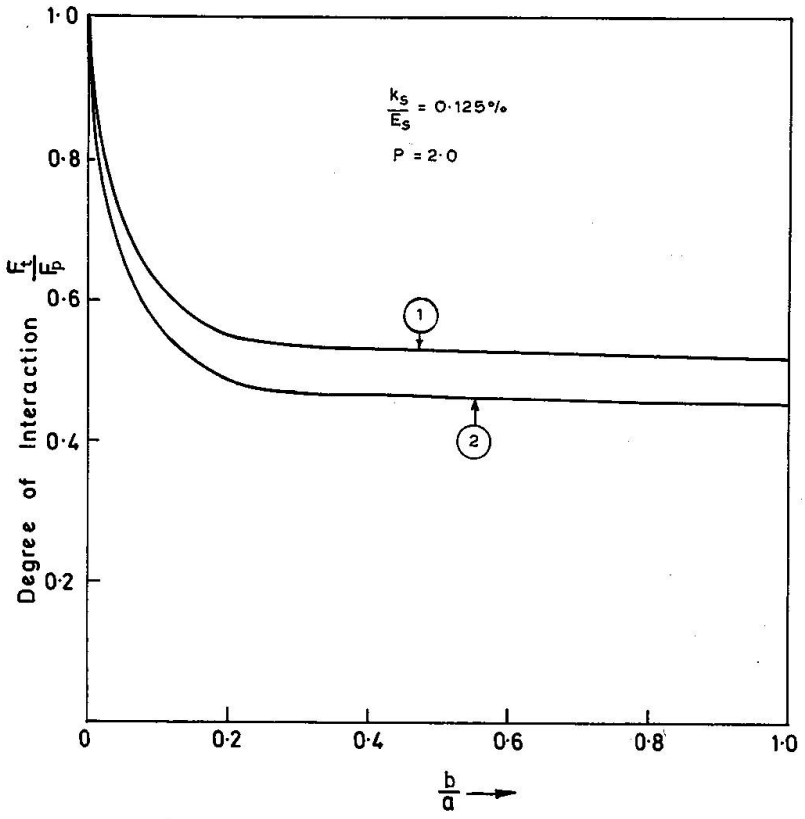

Fig. 4. Degree of interaction against aspect ratio.

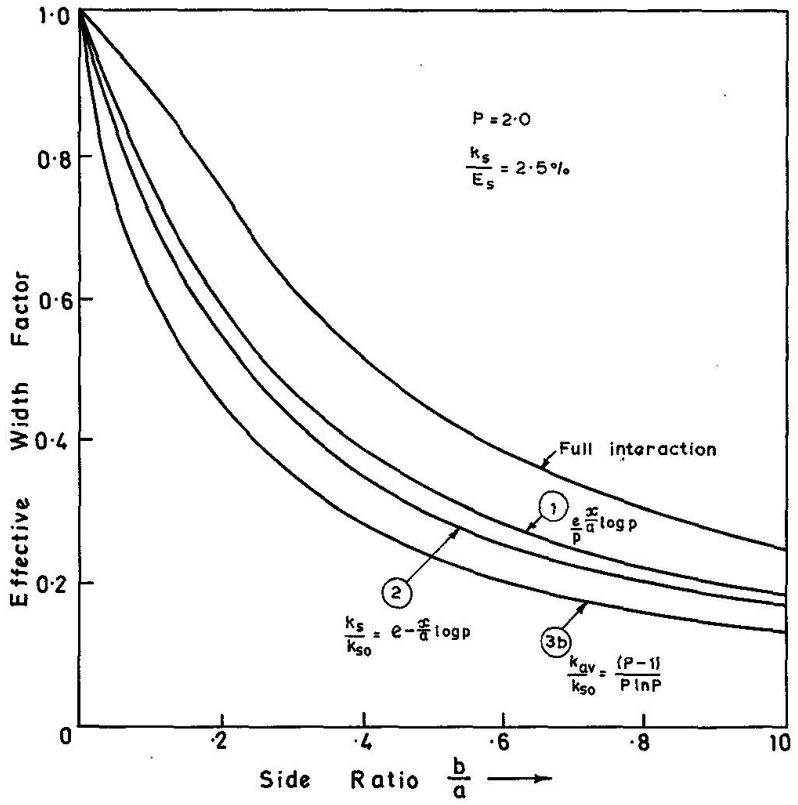

Fig. 5. Variation of Effective width with aspect ratio.

interacting axial force developed. Fig. 4 and 5 show respectively the variation of degree of interaction with aspect ratio $(\frac{b}{a})$ and the variation of effective width with aspect ratio for various distributions of shear connection modulus including full interaction. In all these the superiority of Type 1 distribution of Fig. 1 is manifested.

Finally mention must be made of the rather interesting slip profiles resulting from the various representations of shear connection moduli, Fig. 6a and 6b. Slip profile for the Type 2 representation of shear connection modulus of Fig. 1 has not been reported from any experimental work known for a beam simply supported. Slip profile for the Type 3b (Fig. 1) representation of modulus is however fairly well known. The slip profile similar to that for Type 1 representation of shear connection modulus of Fig. 1 was first observed in experiments performed by Balakrishnan [2] on simply supported composite beams subjected to symmetrical loading.

In conclusion the analysis has shown, first, that distribution of shear connectors is an important factor in achieving a high degree of interaction in composite beams under static working loads, and secondly, that the existence of small amount of interface slips does not negate the attainment of a high degree of interaction. Greater economy can therefore be achieved by seeking not to provide enough connectors to prevent slip totally but by providing sufficient number of connectors, distributed in accordance with the earlier observations in these concluding remarks, to develop an interface shear connection modulus not greater than 2.5% of the modulus of elasticity of the steel beam. The modulus offered by different types of connectors will still need to be determined from standard push-out tests.

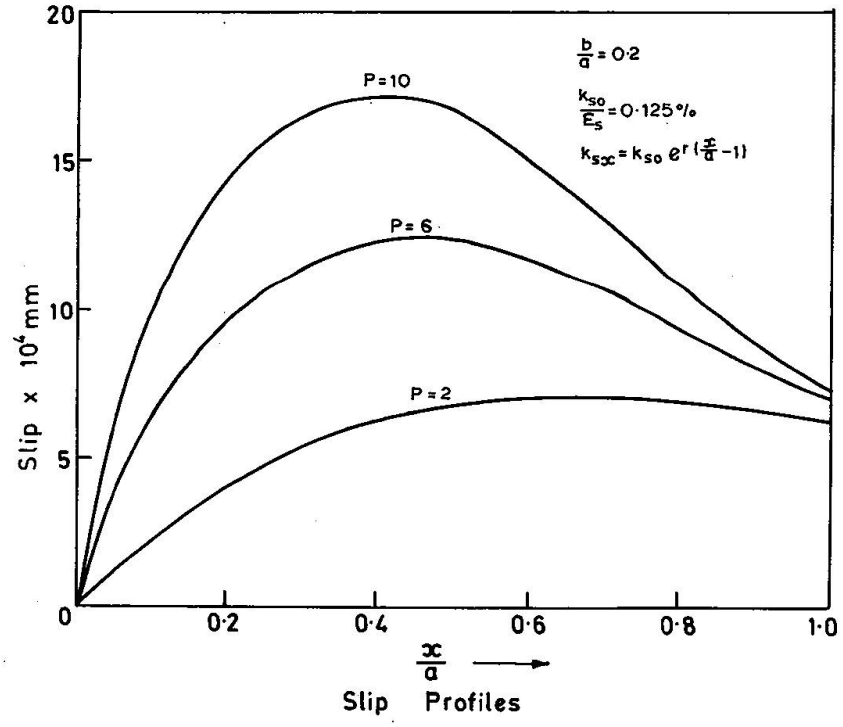

Fig. 6a. Slip Characteristics for Type 1 Spanwise variation of foundation modulus.

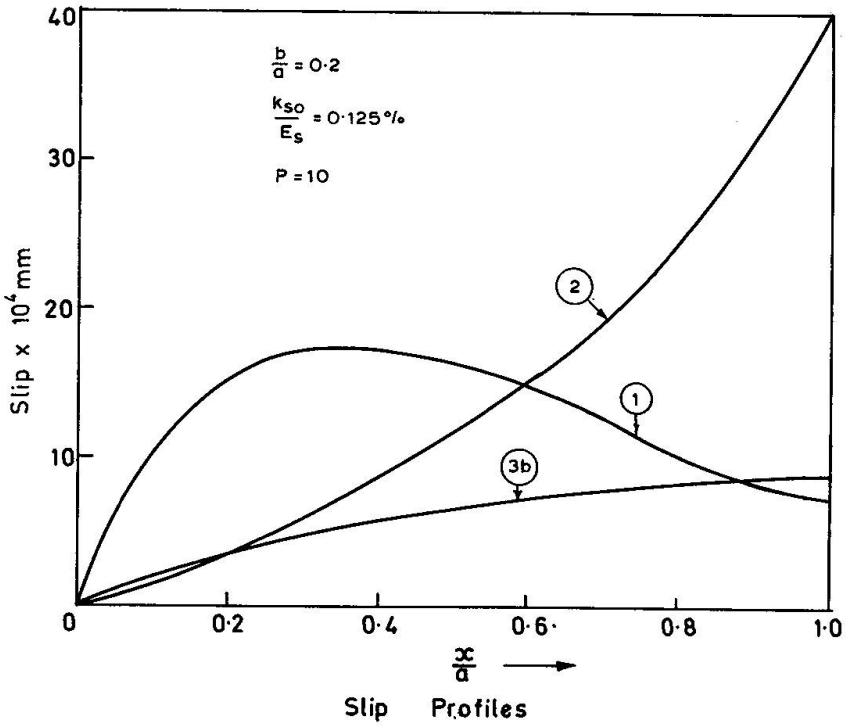

Fig. 6b. Slip Characteristics for different span-wise variation of foundation modulus.

Safety and Economy

Composite construction has been accepted in practice as an economic method of design. By exploiting the presence of the concrete slab when it is in compression and its steel reinforcement when the concrete is in tension, some reduction in sizes of the principal moment resisting elements (e.g. steel beams or concrete ribs) is effected. However the attainment of this reduction depends almost exclusively on the efficiency and reliability of the connecting mechanism — in this case shear connectors of various forms. Design techniques must therefore have as their goals not only reduction in beam sizes, but also the provision and arrangement within a beam of a number of shear connectors needed to ensure good performance and safety under working loads (i.e. not permitting excessive interface slips).

Distribution of shear connectors in a given beam could most probably influence the pattern or mode of failure of the connectors in the beam. It is reasonable to suppose that the worst strained connectors will be those located in the region of greatest slips within a beam. Such regions become the location for commencement of connector failures. The mathematical representations assumed in the present analysis for the variation of connection modulus along the span (and hence the spacing of connectors) are very idealised and such idealised distributions of modulus variation are not readily attainable in practice. It can however be inferred from the study that for reasons of safety, the best arrangement of shear connectors is one in which connector spacing is small in the regions of maximum shears or of maximum slips e.g. ends of a simply supported beam.

Current design practice is either based on connection modulus that will permit little or no interface slips or the attainment of ultimate carrying capacities by connectors at collapse of the composite beams. The objective is to eliminate or limit severely interface slip that can occur in a composite beam under working loads using the results of standard push-out tests. Consequently the value of working load connection modulus aimed at in practice by current design methods is rather high. The conclusion of the analysis that a high degree of interaction is attainable if sufficient number of connectors to develop an interface shear connection modulus not greater than 2.5% of the modulus of elasticity of the steel beam is employed should lead to some savings on the number of connectors.

Notations

a	half span.
b	distance between steel beams.
$c_{11}, c_{22}, c_{12}, c_{66}$	plate material elastic constants.
D_x, D_y	plate flaxural stiffness in the x and y directions.
d	overall depth of steel beams.
E_s	steel modulus of elasticity.
F	interacting axial force.
I_s	steel second moment of area.
k_{so}	maximum shear connection modulus.
p, r	non-dimensional parameters for the variation of k_s.

P_n harmonic component of loading.
q superimposed loading.
q_n harmonic component of superimposed loading.
R_s cross-sectional area of steel beam.
u, v plate displacements in the x, y directions.
w deflexion.
α non-dimensional parameter for plate plane stress.
λ non-dimensional parameter for plate bending.
τ_0 $8\, c_{66}\alpha^{-1}(1+\nu)^{-1}$.
ν Poisson's ratio.
σ_0 $\dfrac{\text{bottom flange stress of composite assembly}}{\text{bottom flange stress of steel beam alone}}$
$\dfrac{\text{deflexion of composite beam}}{\text{deflexion of steel beam alone}}$

References

1. L.C.P. YAM and J.C. CHAPMAN: The inelastic behaviour of continuous composite beams of steel and concrete. Paper 7551, Proc. I.C.E., Part 2, Vol. 53, 487–501 (1972).
2. S. BALAKSISHNAN: The behaviour of composite steel and concrete beams with welded stud shear connectors. Ph. D. thesis, London University (1962).
3. A.O. ADEKOLA: The effective width of composite beams of steel and concrete. Struct. Engr. 46 (a), 285–289 (1968).
4. A.O. ADEKOLA: The dependence of shear lag on partial interaction in composite beams. Int. J. Solids Struct. (10), 389–400 (1974).
5. A.O. ADEKOLA: On shear lag effects in orthotropic composite beams. Int. J. Solids Struct. (10), 735-754 (1974).
6. I.S. GRADSHTEYN and I.M. RYZHIK: Tables of Integrals, Series and Products. Academic Press, New York (1965).

Summary

Various forms of shear connectors, in the form of studs, spirals or cleats provide the means for ensuring composite action between beams and slabs. The present analysis attempts to study the influence, if any, of the span-wise variation in the shear connection modulus. This variation can be directly related to the physical arrangement of the connectors along the span of the beam. The results lead to the obvious conclusion that the concentration of shear connectors should be more in the region of large shears and that an even distribution of these connectors is not the most effective for ensuring composite action.

Résumé

Différents genres de connecteurs de cisaillement sous forme de goujons, spirales et profilés fournissent les moyens propres à assurer la transmission des efforts rasants entre poutres et dalles. L'auteur étudie l'influence éventuelle de la variation

le long de la portée de la déformabilité des connecteurs sur le comportement des poutres mixtes. Cette variation peut être directement mise en rapport avec la distribution des connecteurs. Les résultats obtenus mènent à la conclusion évidente que les connecteurs doivent être concentrés dans les régions à cisaillements élevés et qu'une distribution uniforme ne constitue pas le moyen le plus efficace à assurer la liaison.

Zusammenfassung

Zur Gewährleistung der Verbundwirkung zwischen Träger und Platte werden verschiedene Arten von Verbundmitteln in Form von Bolzen, Wendeln oder Knaggen verwendet. Der Einfluss der Änderung des Verformungsmoduls der Verbundmittel Diese Änderung kann direkt mit der Verteilung der Verbundmittel längs der Spannweite eines Trägers in Beziehung gebracht werden. Die Ergebnisse führen zum offensichtlichen Schluss, dass die Verbundmittel mehr im Bereich grosser Schubbeanspruchungen liegen sollten und eine gleichmässige Verteilung nicht das wirksamste Mittel zur Gewährleistung der Verbundwirkung darstellt.

Wieviel Spaltzugbewehrung ist nötig?

On the Necessary Amount of Transverse Reinforcement in the Anchorage Zone of Prestressed Beams

Quelle est l'armature de frettage nécessaire dans la zone d'ancrage des câbles de précontrainte?

DR. JOSEF ALMASI
Technische Universität Budapest, Ungarn

Einführung

Die Einleitung konzentrierter Kräfte in Stahlbetonscheiben führt in der Krafteinleitungszone zu Spaltzugspannungen. Diese treten im wesentlichen in einem Bereich auf, der nach einem Prinzip von St. Venant auf eine Länge gleich der grössten Querschnittsabmessung begrenzt ist. Diese praktische Begrenzung liess sich auch versuchstechnisch bestätigen und wird bei den folgenden Untersuchungen zugrundegelegt.

Es ist offensichtlich, dass die in der Krafteinleitungszone auftretenden Spaltzugkräfte in Stahlbetonscheiben zu Rissen führen können. Die Spaltzugkräfte müssen deshalb durch eine zweckmässig angeordnete und ausreichend bemessene Spaltzugbewehrung abgedeckt werden, um das Risseverhalten und die Rissbreiten günstig zu beeinflussen. Das sichere Erkennen von Zugzonen ist daher von besonderer Wichtigkeit. Die Berechnung der Grösse der Spaltzugkräfte selbst ist jedoch im allgemeinen nur näherungsweise möglich. Auch die Spannungen in der Spaltzugbewehrung lassen sich bis heute nicht direkt bestimmen.

Offensichtlich ist des weiteren, dass die Rissebildung im Beton der Krafteinleitungszone einen grossen Einfluss auf den Spannungszustand in der Stahlbetonscheibe hat. Die elastische Scheibentheorie ist nicht in der Lage, diesen Effekt zu berücksichtigen.

Zweck des vorliegenden Aufsatzes ist, ein Berechnungsverfahren bekannt zu machen, welches erlaubt, die Rissebildung zu berücksichtigen. Das Ergebnis einer Berechnung nach dem zu erläuternden Verfahren sind die Spannungen in Beton und Bewehrung sowie die Rissbreiten.

Anforderungen an die Spaltzugbewehrung

Die Spaltzugbewehrung soll die folgenden Anforderungen erfüllen:

— sie soll das Gleichgewicht der Kräfte sicherstellen;

— sie soll die Risse auf lokale Zonen beschränken;
— sie soll die Breite der Risse auf festzulegende Werte beschränken (zB 0,2 mm), bzw. der Zuwachs der Stahlspannung nach Bildung der Risse soll auf festzulegende Werte beschränkt bleiben (zB 1500 kp/cm^2);
— sie soll eine gleichmässige Lastverteilung fördern (Konstruktive Erwägung).

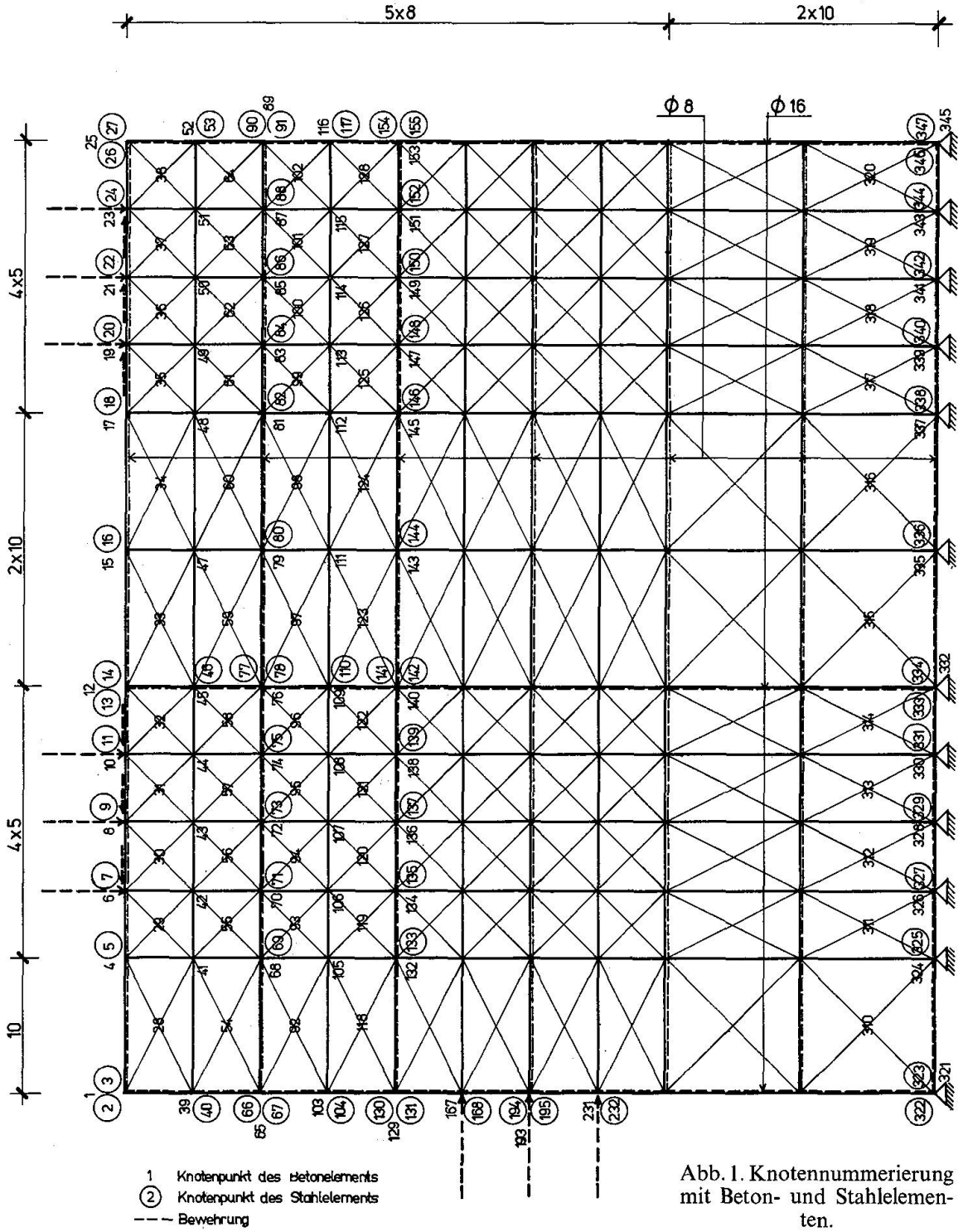

Abb. 1. Knotennummerierung mit Beton- und Stahlelementen.

Berechnungsverfahren

Das Berechnungsverfahren basiert auf der Methode der Finiten Elemente [1].

Für den Fall von Stahlbetonkonstruktionen ist hier nicht nur das Kontinuum in Elemente aufzuteilen, sondern auch die Bewehrung muss in Elemente aufgeteilt werden. Dass Zusammenwirken von Beton und Stahl ist durch «Federn» zu sichern, welche den Verbund charakterisieren. Zur Erläuterung dient Abb. 1.

Das der Berechnung zugrunde gelegte Modell muss die folgenden Anforderungen erfüllen:

— es soll die Eigenschaften des Stahlbetons möglichst gut wiedergeben;
— es muss auf die Tatsache Rücksicht nehmen, dass die Risse im Beton wie auch das Fliessen im Stahl lokal auftreten;
— es muss davon ausgehen, dass im Beton lokal grosse Betonstauchungen entstehen;
— es soll die Spannungen in der Bewehrung liefern;
— es soll die Abschätzung der Rissbreiten gestatten.

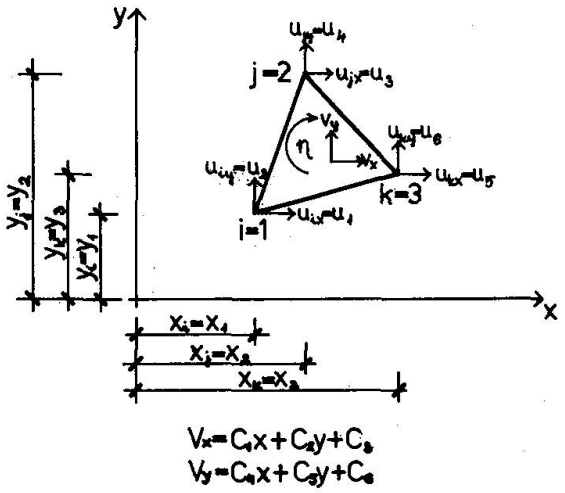

Abb. 2. Betonelement.

Die idealisierten Finiten Elemente

a) *Die Scheiben- oder Betonelemente*

Der Beton der Krafteinleitungszone wird in Dreieckelemente aufgeteilt. Die Dreieckelemente haben konstante Dehnungen. Die kinematischen Eigenschaften und die Ansätze sind in Abb. 2 angegeben. Durch «Kondensierung» am Elementniveau erhält man Viereckelemente. Die Elastizitätsmatrix entspricht für Spannungen im Hookeschen Bereich derjenigen für homogenes, isotropes Material:

$$[D_B] = \frac{E_1}{1-\nu^2}\begin{bmatrix} 1 & \nu & 0 \\ \nu & 1 & 0 \\ 0 & 0 & \frac{1-\nu}{2} \end{bmatrix}$$

Für Bereiche, in denen die Spannungen nicht proportional zu den Dehnungen sind, gilt die folgende Elastizitätsmatrix:

$$[\underline{D}_B] = \frac{E_1}{1 - \nu_{12} \cdot \nu_{21}} \begin{bmatrix} 1 & \nu_{12} & 0 \\ \nu_{21} & E_2/E_1 & 0 \\ 0 & 0 & \sqrt{\frac{1}{4} \cdot \frac{E_1}{1+\nu_{12}} \cdot \frac{E_2}{1+\nu_{21}}} \end{bmatrix}$$

Wenn die Zugspannungen in einem Element in einer Hauptrichtung bestimmte Werte überschreiten, so bildet sich aufgrund der gemachten Voraussetzungen ein Element mit orthotropen Eigenschaften und senkrecht zu den Hauptzugspannungen treten Risse auf. Für diesen Fall lautet die Elastizitätsmatrix:

$$[\underline{D}_B] = \begin{bmatrix} 0 & 0 & 0 \\ 0 & E_2 & 0 \\ 0 & 0 & 0 \end{bmatrix}$$

Im Sinne der eingangs erwähnten Anforderungen sind grosse Betonstauchungen zu gestatten. Erreicht die Betonstauchung die Bruchstauchung, so wird das betreffende Element nicht von der Tragwirkung ausgeschaltet, sondern nimmt weiter an der Kraftübertragung teil; einzig der zugehörige Elastizitätsmodul ist klein. Diese Vorstellung wird durch Versuchsergebnisse bestätigt, solange in der Umgebung liegende «stabile» Elemente Hilfe leisten. Versagen der Elemente auf Zug findet statt, wenn die Hauptzugdehnungen in den beiden Hauptrichtungen zugelassene Zugdehnungen überschreiten.

b) *Stab- oder Stahlelemente*

Stahlemente sind Stabelemente, welche nur in axialer Richtung und senkrecht dazu beansprucht sind. Die Anzahl der Knotenverschiebung ist demnach zwei (siehe Abb. 3). Die Elastizitätsmatrix hat die folgende Form:

$$[\underline{D}_s] = \begin{bmatrix} E_s F & 0 \\ 0 & 0 \end{bmatrix}$$

Lokales Fliessen der Stahlemente ist möglich. Ihr Elastizitätsmodul wird für weitere Laststufen auf denjenigen Wert festgelegt, der unmittelbar vor dem Fliessen gilt.

c) *Verbund- oder Federelemente*

Der Verbund zwischen Bewehrung und Beton wird mittels Federelementen simuliert. Die Federn ermöglichen Relativverschiebungen zwischen Bewehrung und Beton in Richtung der Bewehrung und senkrecht dazu.

Die Federn sind als dimensionslose Elemente zu betrachten (siehe Abb. 4). Wichtig sind ihre mechanischen Eigenschaften. Die Steifigkeit in Richtung der Bewehrung lässt sich wie folgt ausdrücken:

$$k_h = E_t \cdot m \cdot \pi \cdot d$$

In diesem Ausdruck ist

$$E_t = d\tau/du$$

und lässt sich aus Ausziehversuchen mit Stählen und Messung der Haftspannungs-Verschiebungs-Charakteristik bestimmen. m ist die Anzahl der Bewehrungsstäbe pro Federelement und d der Stabdurchmesser. Die Federsteifigkeit senkrecht zur Bewehrung wird im folgenden zu Null angenommen, da ausreichende Versuchsergebnisse nicht zur Verfügung stehen.

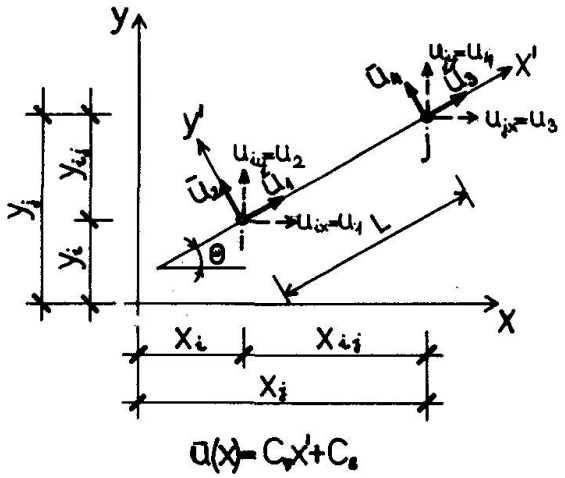

Abb. 3. Stahlelement.

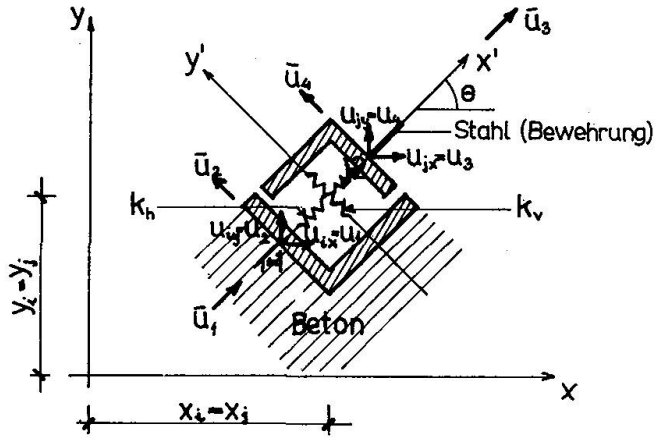

Abb. 4. Federelement.

Das Rechenprogramm

Auf der Basis der vorgestellten Finiten Elemente hat der Verfasser an der Eidg. Technischen Hochschule in Zürich ein Rechenprogramm geschrieben. Testläufe wurden im Rechenzentrum auf CDC 6400/6500 Computern durchgeführt.

Die Gleichgewichtsbedingung lautet:

$$[\underline{K}] \cdot \{\underline{u}\} - \{\underline{P}\} = \{\underline{0}\}.$$

Bei nichtlinearem Stoffgesetz ist der Zusammenhang zwischen Spannungen σ und Dehnungen ε wie folgt:

$$d\{\underline{\sigma}\} = [\underline{D}(\underline{\sigma})] \cdot d\{\underline{\varepsilon}\}.$$

Aufgrund dieser Gleichung ist die Steifigkeitsmatrix auch eine Funktion der Verschiebungen u.

$$[\underline{K}(\{\underline{u}\})] \cdot \{\underline{u}\} - \{\underline{P}\} = \{\underline{0}\}$$

und

$$[\underline{K}]\, d\{\underline{u}\} - d\{\underline{P}\} = \{\underline{0}\}.$$

Die Lösung dieser Gleichungen geschieht durch Iteration (siehe Abb. 5). Im Verlauf der Berechnung werden die angreifenden Kräfte schrittweise gesteigert und das jeweils zugehörige Spannungsfeld ermittelt. Die Festlegung einer vernünftigen Iterationsbedingung bereitet dabei einige Schwierigkeiten. Man kann zum Beispiel den maximalen Unterschied zwischen den Verschiebungen zweier Rechenschritte begrenzen, oder aber das Gleichgewicht kontrollieren.

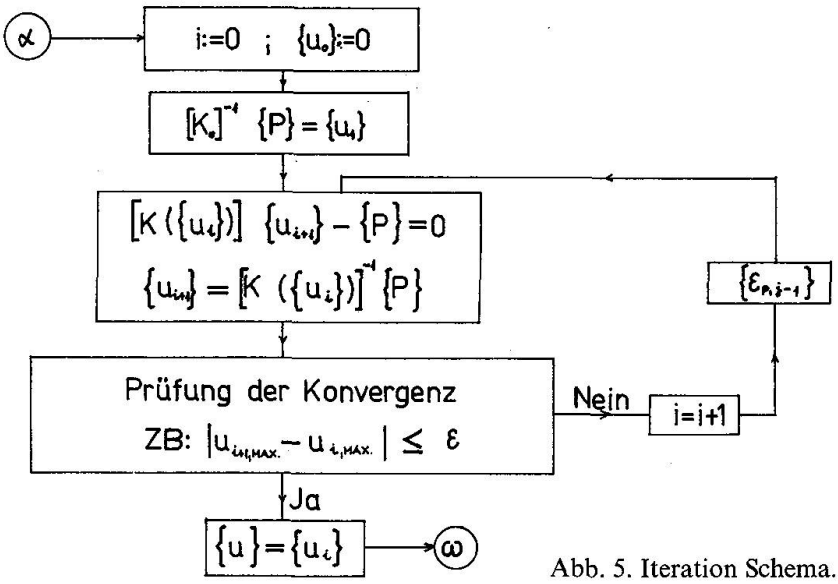

Abb. 5. Iteration Schema.

Numerische Ergebnisse

Zurückkehrend zu der im Titel dieses Aufsatzes gestellten Frage sollen in der Folge die Ergebnisse zweier numerischer Beispiele diskutiert werden.

Beispiel: Symmetrische Kräfteeinleitung

Die Situation entspricht Abb. 6. Mit einem elastischen Lösungsverfahren [4] erhält man bei $V = 44$ Mp bzw. 80 Mp Vorspannkraft eine maximale bezogene Spaltzugkraft von $N_y = 152$ kp/cm bzw. 280 kp/cm. Abb. 6 zeigt eine auf diese Beanspruchung hin etwa abgestimmte Bewehrung.

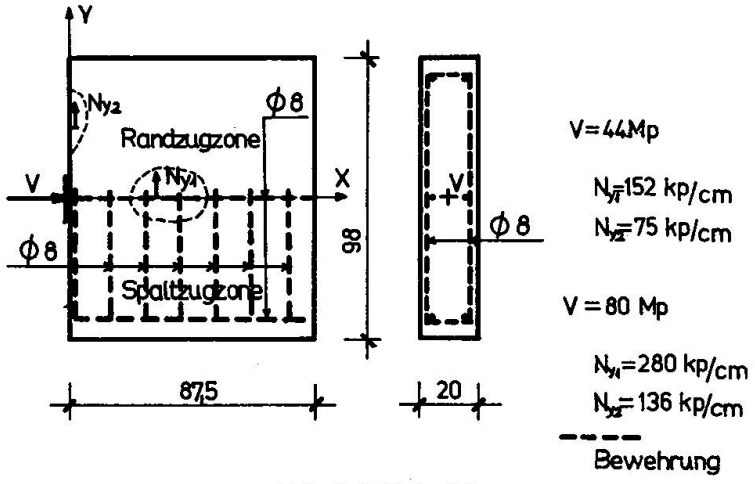

Abb. 6. 1. Beispiel.

Die Spannungen σ_x in X – Richtung unter $V = P + 2P + P = 44$ Mp sind in Abb. 7 dargestellt. Die auf die Elementlänge bezogenen Spaltzugkräfte sowie die Spannungen in den Bügeln und in der Längsbewehrung zeigt Abb. 8. Im Bereich maximaler Werte sind auch die Spaltzugkräfte pro Längeneinheit eingetragen. Diese entsprechen in der Spaltzugzone der elastischen Lösung und zeigen in der Randzugzone erhebliche Unterschiede. Die Ursache ist wohl darin zu suchen, dass die Risse zuerst in der Randzugzone auftreten und damit das Kräftespiel in der Scheibe beeinflussen.

Die unter $V = 80$ Mp entscheidenden Hauptspannungen σ_1 und σ_2 sind in Abb. 9 dargestellt. Die maximale Beton-Druckspannung beträgt -252 kp/cm^2, die Druckstauchung $-2{,}47‰$, die Zugdehnung $0{,}24‰$. Unter Annahme eines Rissabstandes von $\Delta l \cong 100$ mm lässt sich die Rissbreite zu $a_n = \Delta l \cdot \varepsilon_{max} = 100 \cdot 0{,}00024 = 0{,}024$ mm abschätzen. Die Grösse der Zugspannungen in Bügeln und Längsbewehrung können Abb. 10 entnommen werden. Die maximale Zugspannung in den Bügeln beträgt 97 kp/cm^2.

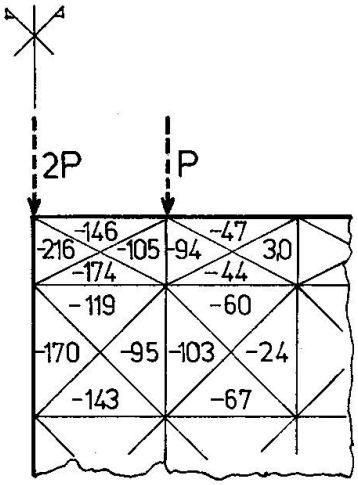

Abb. 7. Spannungen σ_x[kp/cm^2] bei $V = 44$ Mp.

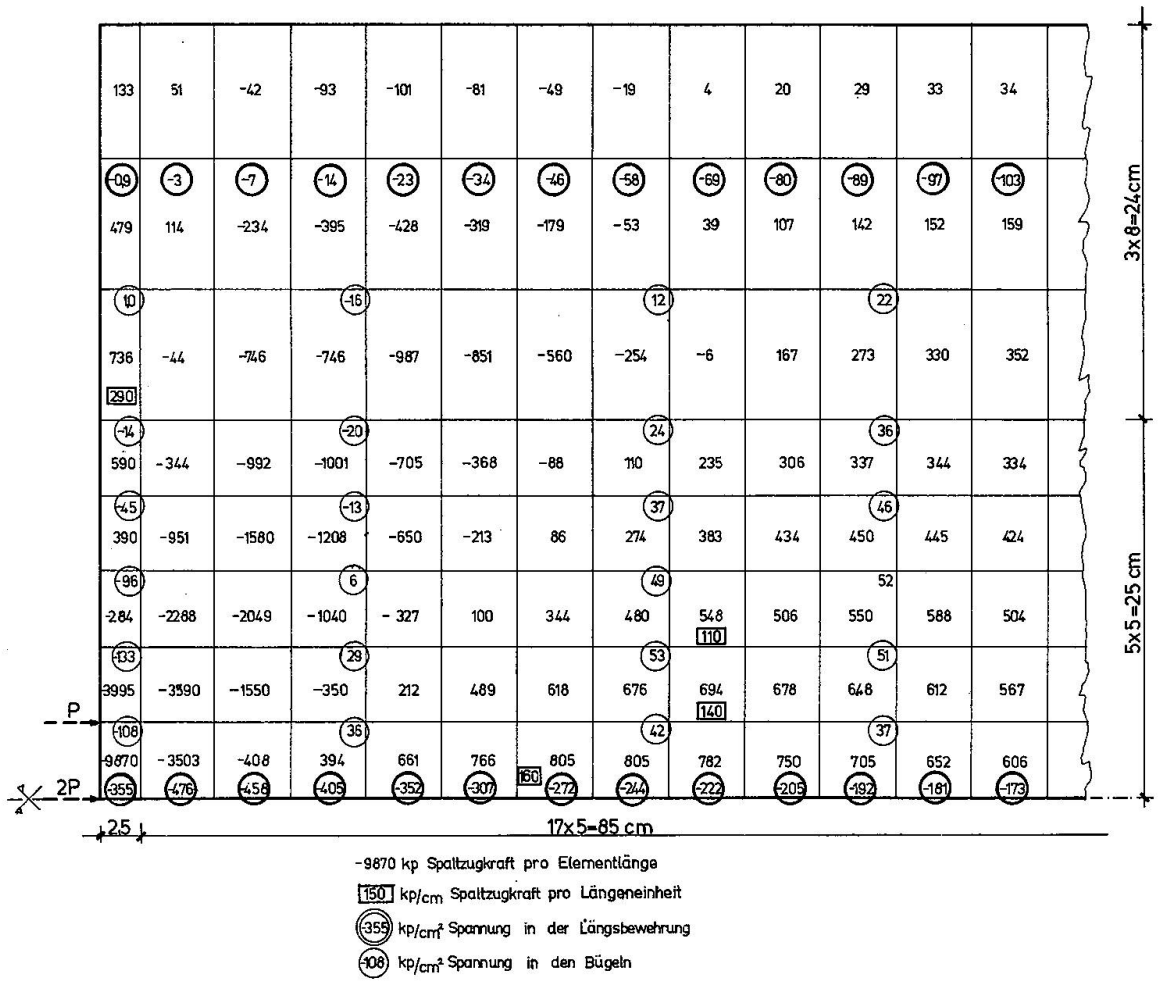

Abb. 8. Beanspruchung unter $V = 2 + 2P + P = 44\ Mp$.

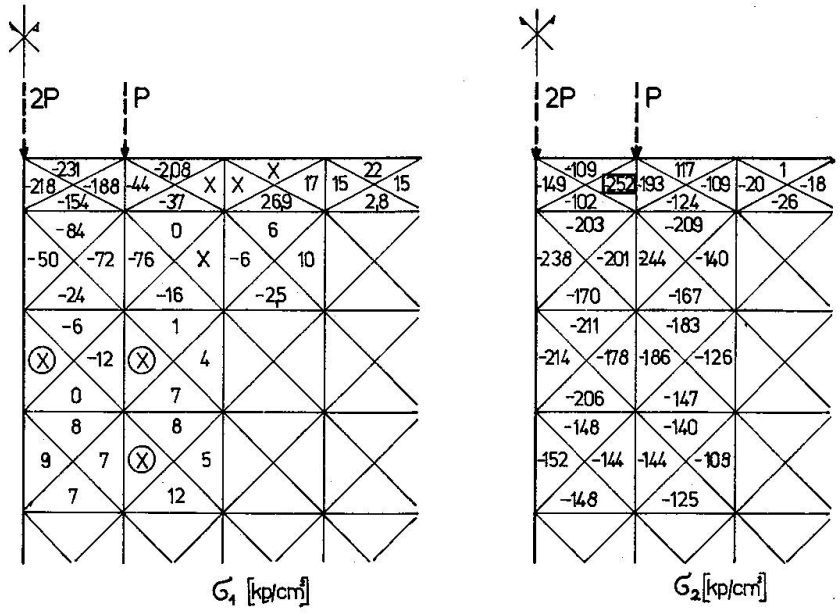

Abb. 9. Hauptspannungen bei $V = 80$ Mp.

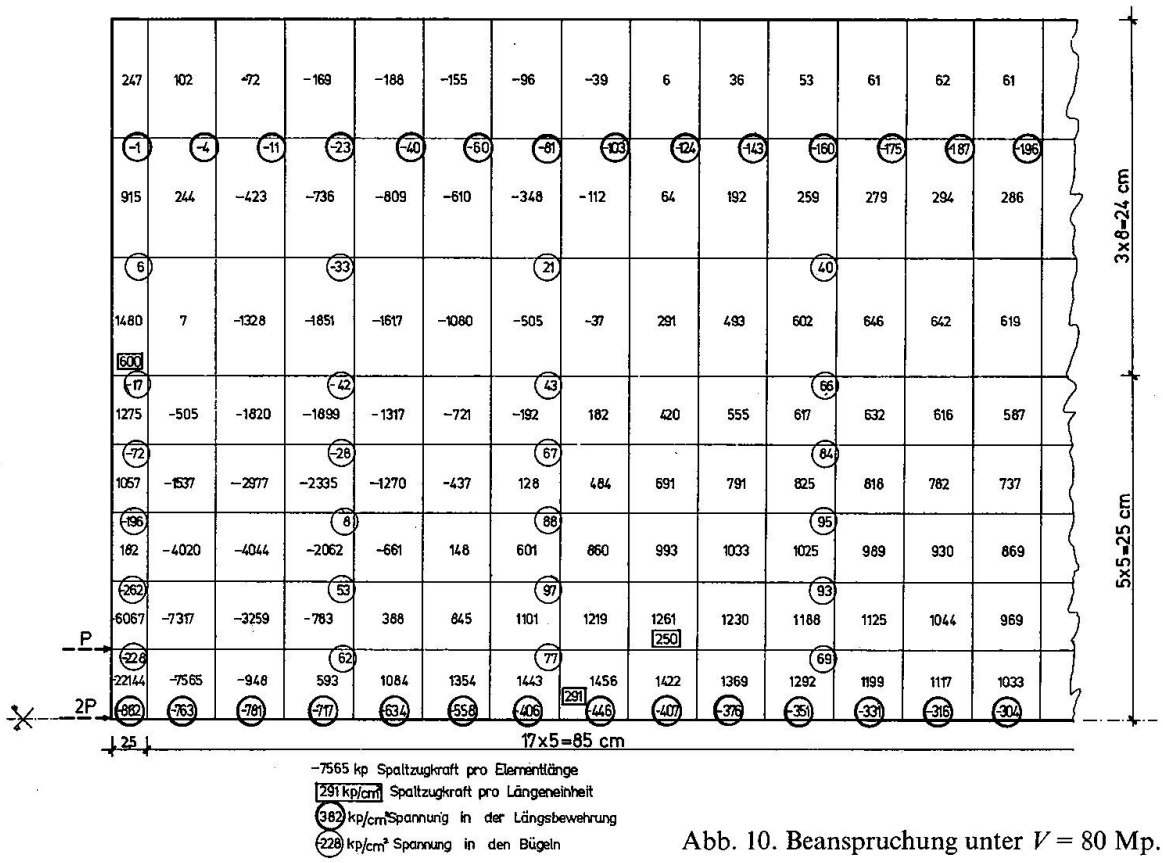

Abb. 10. Beanspruchung unter $V = 80$ Mp.

Beispiel: Unsymmetrische Krafteinleitung

Abb. 1 zeigt die idealisierte Krafteinleitungszone und ihre Bewehrung. Schräg gerichtete Vorspannkräfte werden in Komponenten zerlegt, desgleichen die Auflagekräfte. Die Laststeigerung erfolgt in zwölf Stufen. Das Anwachsen der auf die Längeneinheit bezogenen Kräfte Nx, Ny, der Spannungen σ_x und der Rissebildung ist aus den Abb. 11 bis 15 ersichtlich. Der erste Riss erscheint bei $V_1 = V_2 = 19$ Mp (siehe Abb. 11) in der Randzugzone. Die ersten Risse in der Spaltzugzone treten unter $V_1 = V_2 = 38$ Mp auf. Das Anwachsen der Zahl der gerissenen Elemente und die Rissbreiten lassen sich aus den Abb. 12 bzw. 13 entnehmen. Die Rissbreiten sind kleiner als etwa 0,1 mm. Die Spannungen σ_x und die bezogenen Spaltzugkräfte Ny unter der Höchstlast sind in Abb. 12 dargestellt. Die Spannungen in den Bügeln und in der Längsbewehrung zeigen schliesslich die Abb. 14 und 15. Die grössten Werte übersteigen 500 kp/cm^2 nicht.

Bei der Beurteilung der Ergebnisse ist allerdings zu beachten, dass sie stark von den getroffenen Annahmen abhängen. Eine Änderung dieser Annahmen wirkt erheblich auf die Ergebnisse zurück. Besonders empfindlich sind die Ergebnisse in Bezug auf die gewählte Verbundcharakteristik zwischen Beton und Bewehrung.

Vergleich der Ergebnisse mit Versuchen

Eine grosse Anzahl von Versuchen wurden mit Werkstoffen durchgeführt, die dem Verhalten des Stahlbetons nicht entsprechen. Hierzu gehören in erster Linie

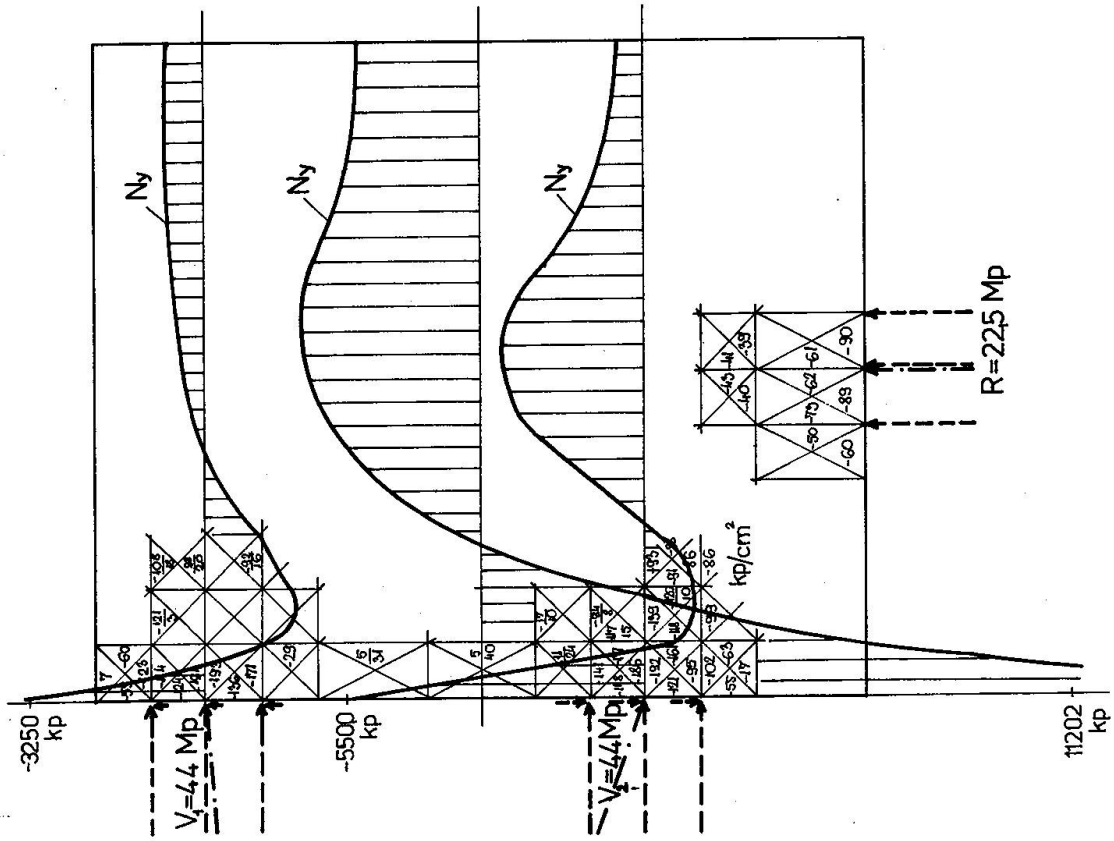

Abb. 12. Spannungen σ_x Kräfte N_y und Rissbild bei Laststufe 12.

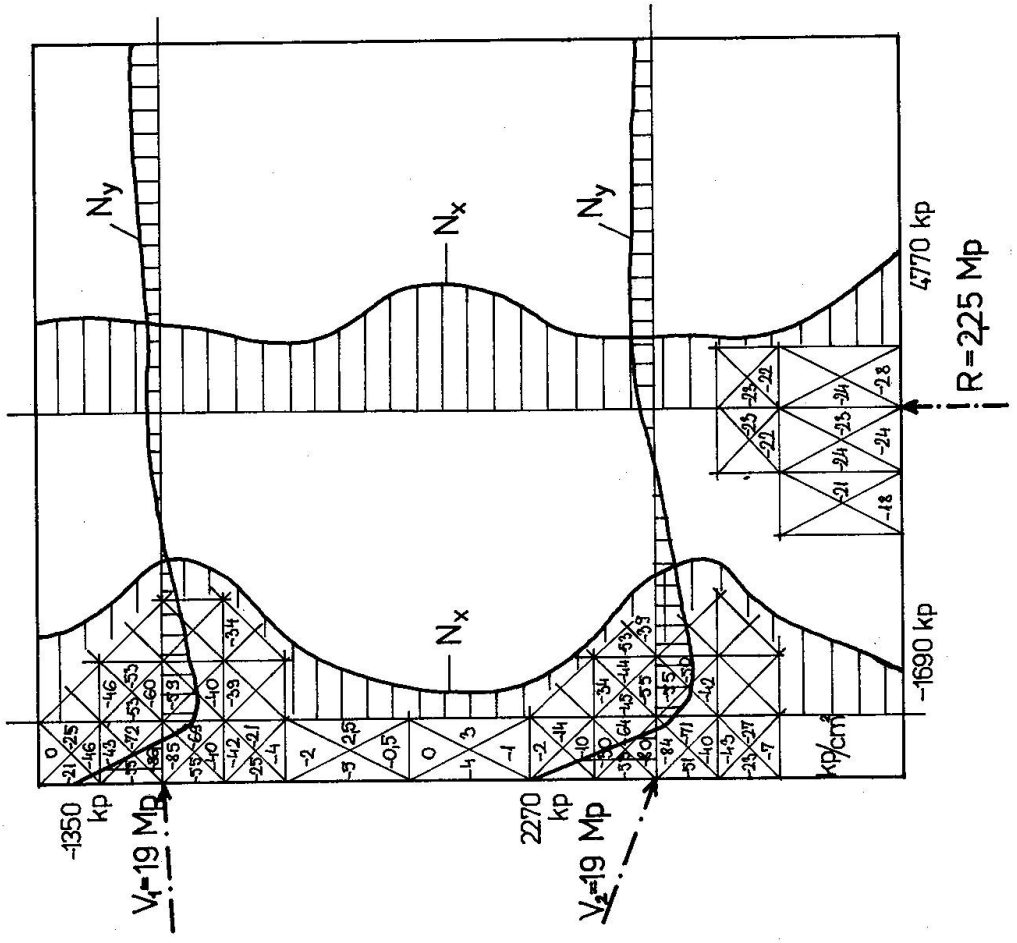

Abb. 11. Spannungen σ_x und Kräfte N_x bzw N_y bei Laststufe 3. (erste Risse).

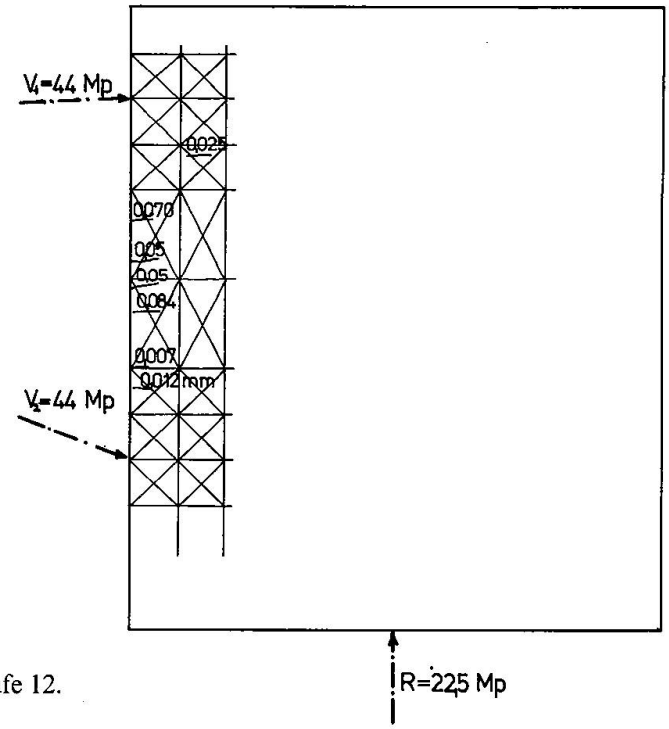

Abb. 13. Rissbreiten bei Laststufe 12.

spannungsoptische Versuche, die im Grunde genommen für den vorliegenden Fall nur Informationscharakter haben.

Versuche an Stahlbetonscheiben haben unter anderen TAYLOR [6] und TASSI-WINDISCH [5] durchgeführt. TAYLOR wiederholte die Versuche von Row und fand abweichende Ergebnisse. Ein Vergleich ist deshalb nur qualitativ möglich, insbesondere in Bezug auf das Rissbild. Sowohl für das erste als auch für das zweite Beispiel wurden die ersten Risse in der Randzugzone neben Krafteinleitungsstellen beobachtet und bestätigen damit die Ergebnisse der vorliegenden Berechnungsmethode.

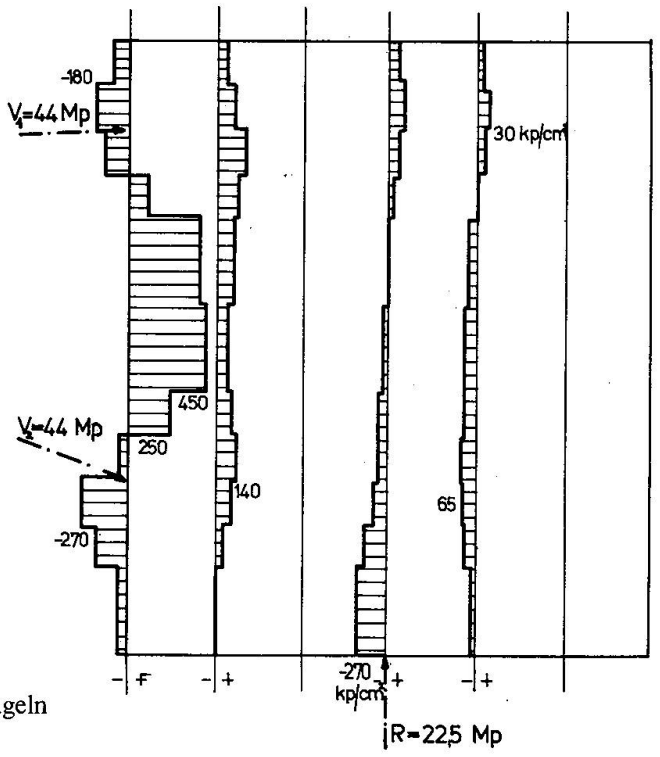

Abb. 14. Spannungen in den Bügeln bei Laststufe 12.

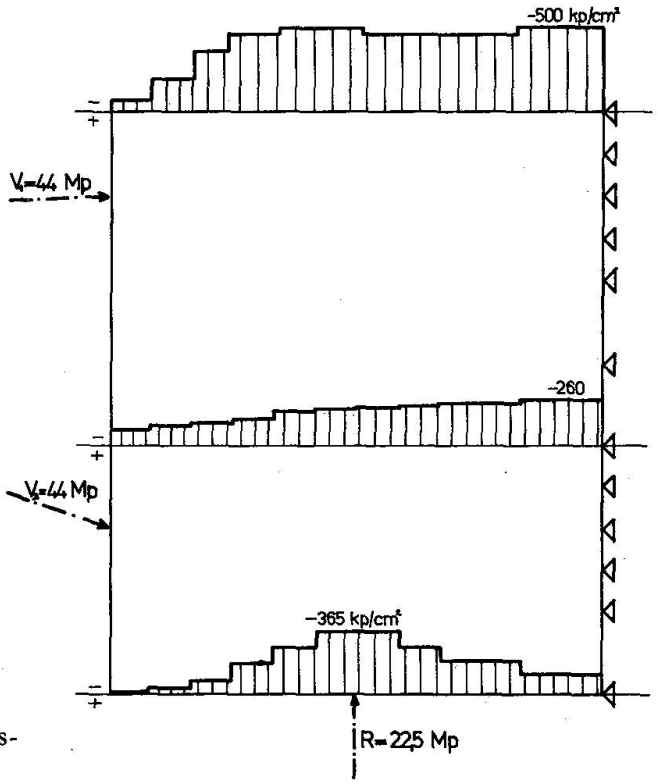

Abb. 15. Spannungen in der Längsbewehrung bei Laststufe 12.

Folgerungen

Sowohl die Ergebnisse der vorgeschlagenen Berechnungsmethode als auch die Versuche an Stahlbetonscheiben zeigen, dass die ersten Risse in der Randzugzone erscheinen. Diese Risse verändern das elastische Kräftespiel. Die Risse in der Spaltzugzone treten später auf, die Rissbreiten sind in dieser Zone kleiner und die auftretenden Zugkräfte näher bei den Ergebnissen einer plastischen Berechnung aufgrund der konventionellen Scheibentheorie. Es zeigt sich auch, dass es normalerweise nicht möglich ist, eine rissefreie Spaltzugzone zu erhalten. Es geht vielmehr darum, eine zweckmässig angeordnete und vernünftig bemessene Bewehrung einzulegen, mit welcher die Rissbreiten unter einer erwünschten Grösse gehalten werden.

Für die beiden Beispiele wurde die Bügelbewehrung nach der konventionellen elastischen Lösung bestimmt, und es zeigte sich, dass die — geschätzten — Rissbreiten kleiner als etwa 0,1 mm bleiben. Dies lässt den Schluss zu, dass eine konventionell bestimmte Bewehrung die Rissbreiten unter den normalerweise gewünschten Werten von 0,1 bis 0,2 mm halten kann. Inwieweit hier jedoch noch unausgeschöpfte Einsparungsmöglichkeiten bei der Bemessung der Bewehrung liegen, bedarf weiterer analytischer und experimenteller Untersuchungen.

Nachwort

Die vorliegende Arbeit entstand zu wesentlichen Teilen während meines Aufenthaltes am Lehrstuhl für Baustatik, Stahlbeton- und Brückenbau an der E.T.H. Zürich.

Ich möchte an dieser Stelle Herrn Prof. Jörg Schneider danken für die mir gewährte Unterstützung und auch für die Hilfe bei der Redaktion des Aufsatzes.

Literatur

1. ZIENKIEWICZ, O.C.: The Finite Element Method in Engineering Science. McGraw-Hill, London, 1971.
2. NGO, D. and SCORDELIS, A.: Finite Element Analysis of Reinforced Concrete Beams. J. ACI Procd., V. 64. No. 3, March 1967, pp. 152–163.
3. NILSON, A.: Nonlinear Analysis of Reinforced Concrete by the Finite Element Method. J. ACI Procd., V. 65, No. 9, Sept. 1968, pp. 757–766.
4. KAMMENHUBER, J. and SCHNEIDER, J.: Arbeitsunterlagen für die Berechnung vorgespannter Konstruktionen. Zürich, 1974.
5. TASSI, G. and WINDISCH, A.: Analysis and Model Testing of the Anchorage Zone of Post-Tensioned Beams. FIP VII, Congress, New York, 1974.
6. TAYLOR, S.J.: Anchorage bearing stresses. ICE, 1968, Conference on Prestressed Concrete Pressure Vessel, 1967.
7. ALMASI, J.: Berechnung von Stahlbeton-Elementen mit Hilfe der Methode der Finiten Elemente. Nicht publiziert, in ungarisch, Bp., 1974.

Zusammenfassung

Zweck des vorliegenes Aufsatzes ist, ein Berechnungsverfahren bekannt zu machen, welches erlaubt, Spannungszustände unter Berücksichtigung der Rissebildung zu bestimmen. Das Berechnungsverfahren basiert auf der Methode der finiten Elemente. Die praktische Anwendung wird anhand von zwei numerischen Beispielen erläutert, für welches die Spaltzugspannungen und die Rissebildung im Bereich der Krafteinleitungszone berechnet worden sind. Die beiden berechneten Beispiele zeigen, dass eine konventionell bestimmte Bügelbewehrung das Gleichgewicht sicherstellt und die Rissbreiten unter den normalerweise gewünschten Werten von 0,1 bis 0,2 mm halten kann.

Résumé

La contribution présente un procédé de calcul permettant de déterminer des états de tension en tenant compte de la formation de fissures. Le procédé de calcul est basé sur la méthode des éléments finis. L'application pratique est faite au moyen de deux exemples numériques pour lesquels les tensions dans la zone d'ancrage des câbles de précontrainte et la formation de fissures ont été calculés. Les deux exemples calculés montrent qu'une armature d'étriers déterminée selon les règles conventionnelles assure l'équilibre et que la largeur des fissures peut être maintenue au-dessous des valeurs normalement admissibles de 0,1 à 0,2 mm.

Summary

The aim of the present contribution is to notify a computation procedure which allows to determine tension states in taking into account the formation of cracks. The calculation procedure is based on the finite element method. The practical application is explained by two numerical examples wherein the tension in the anchorage zone of prestressed beams and the formation of cracks have been calculated. The two calculated examples show that the transverse reinforcement determined in the conventional manner assures the equilibrium and maintains the width of cracks below the usual values of 0.1 to 0.2 mm.

Leere Seite
Blank page
Page vide

Théorie des empilages élastiques

Theorie der aus elastischen Blöcken aufgebauten Säule

Theory of the Column made of the Elastic Blocks

M.C. BOURDON
Ingénieur principal à la SOCOTEC, Paris.

Généralités

Considérons un poteau en béton armé en équilibre fléchi sous une charge N appliquée avec une excentricité a. Il se comporte comme s'il était formé de l'association de deux poteaux fictifs constitués l'un par le béton seul, et l'autre par la cage d'armatures supposée entretoisée par les armatures transversales et des «bielles» de béton obliques.

La charge critique ultime de flambement d'ensemble du poteau a pour borne inférieure la somme des charges de la pièce en béton et de la cage d'armature, considérées isolément dans le même état déformé (le béton pouvant être fissuré si la flexion est assez importante).

On pourra donc aborder la question du flambement des poteaux en béton armé si l'on est en mesure:

a) de résoudre le problème théorique du poteau en béton dépouillé de son armature;

b) de déterminer l'influence des liaisons «béton-acier» sur les charges ultimes de chacune des deux colonnes, dans leur état limite déformé, ou ce qui revient au même, l'erreur commise en imposant à chaque poteau une déformée théorique déterminée, différente pour les besoins du calcul de la déformée commune dont le calcul ne peut être effectué, dans l'état actuel des connaissances, que pour des conditions d'extrémité particulières.

On admettra que la cage d'armature supposée seule subit une déformation sinusoïdale correspondant à la solution approximative donnée généralement à ce problème, dans le domaine élastique. Cette déformée sinusoïdale serait sous charge axiale, un arc complet de sinusoïde et, sous charge excentrée, un arc partiel de sinusoïde (voir Fig. 1).

Pour pouvoir raccorder notre étude aux hypothèses de calcul habituelles de la résistance des matériaux, nous admettrons:

— que le béton ne résiste pas à la traction, ce qui revient à assimiler la colonne à un empilage d'éléments élastiques de même hauteur, dont les faces sont normales à la ligne moyenne;

— que l'hypothèse de BERNOULLI (indéformabilité des sections) et la loi de HOOKE (proportionnalité des déformations aux contraintes) sont toutes les deux vérifiées pour la partie des éléments soumise aux efforts, et que la partie non sollicitée, correspondant à la zone fissurée, n'intervient pas dans la déformation des éléments.

Examinons pour simplifier le cas d'un empilage d'éléments rectangulaires de largeur b perpendiculairement au plan de flexion, et h parallèlement au plan de flexion.

Fig. 1

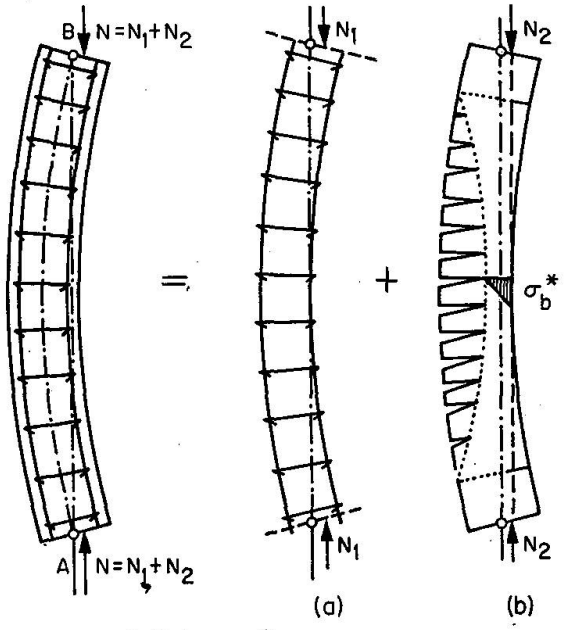

a) Colonne d'armatures.
b) Poteau en béton non armé.

Théorie élémentaire (voir Fig. 2)

Fig. 2.

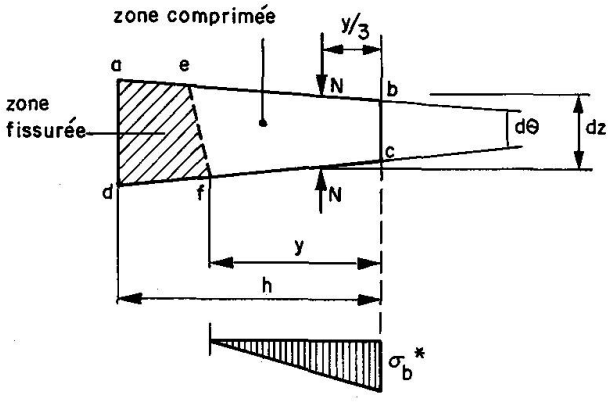

Soit N la charge appliquée,
y la largeur de repos d'un élément sur l'élément contigu,
z la cote de l'élément,
E le module d'élasticité du béton.

La contrainte maximale, sur la fibre la plus sollicitée, est:

$$\sigma = \frac{2N}{by} \tag{1}$$

Le raccourcissement unitaire de cette fibre est:

$$\varepsilon = -\frac{\sigma}{E} = -\frac{2N}{byE} \tag{2}$$

La rotation élémentaire:

$$\frac{d\theta}{dz} = -\frac{\varepsilon}{y} = \frac{2N}{by^2E} \tag{3}$$

Il résulte de la répartition triangulaire des contraintes que:

$$|\theta| = \frac{1}{3}\frac{dy}{dz}, \quad \text{d'où} \quad \left|\frac{d\theta}{dz}\right| = \frac{1}{3}\frac{d^2y}{dz^2}$$

$$\text{d'où} \quad \frac{d^2y}{dz^2} = \varepsilon \cdot \frac{6N}{by^2E} \tag{4} \qquad \text{avec } \varepsilon = \pm 1$$

soit x la déformation transversale de la section par rapport à la ligne d'action de N

$$x = \tfrac{h}{2} - \tfrac{y}{3} \tag{5} \qquad (\text{avec } y < h)$$

$$\text{d'où} \quad \frac{d^2x}{dz^2} = \varepsilon' \cdot \frac{2N}{by^2E} \tag{6} \qquad (\text{avec } \varepsilon' = \pm 1)$$

Le problème posé se ramène donc à l'intégration de l'équation différentielle du 2e ordre:

$$\boxed{y^2 \cdot y'' = \varepsilon \cdot A} \tag{7}$$

où A est une constante et $\varepsilon = \pm 1$

En appelant σ_b^* la contrainte maximale dans la section initiale ($z = 0$), pour laquelle la largeur d'appui est

$$y_0 = \frac{2N}{b\sigma_b^*} \tag{8}$$

et en prenant la variable auxiliaire:

$$u = \frac{y}{y_0} = \frac{\sigma_b^*}{\sigma_b} \tag{9}$$

on trouve les solutions de (7) sous les formes suivantes:

Premier cas:

$$\varepsilon = +1, \quad f_1(u) = Arg\ ch\sqrt{u} + \sqrt{u(u-1)} \tag{10}$$

$$\frac{z}{y_0} = \pm\sqrt{\frac{E}{6\sigma_b^*}} f_1(u) \tag{11}$$

Deuxième cas:

$$\varepsilon = -1, \quad f_2(u) = Arc\cos\sqrt{u} + \sqrt{u(u-1)} \tag{12}$$

$$\frac{z}{y_0} = \pm\sqrt{\frac{E}{6\sigma_b^*}}\, f_2(u) \tag{13}$$

Ces solutions correspondent aux Figs 3a et 3b. La rotation à la limite supérieure de l'empilage est:

$$\theta = \sqrt{\frac{2(\sigma_b^* - \sigma_1)}{3E}} \tag{14}$$

avec

$$\sigma_1 = \frac{2N}{bh} \tag{15}$$

Considérons maintenant une pile en béton non armé, axialement chargée, de hauteur l (section rectangulaire).

Fig. 3.

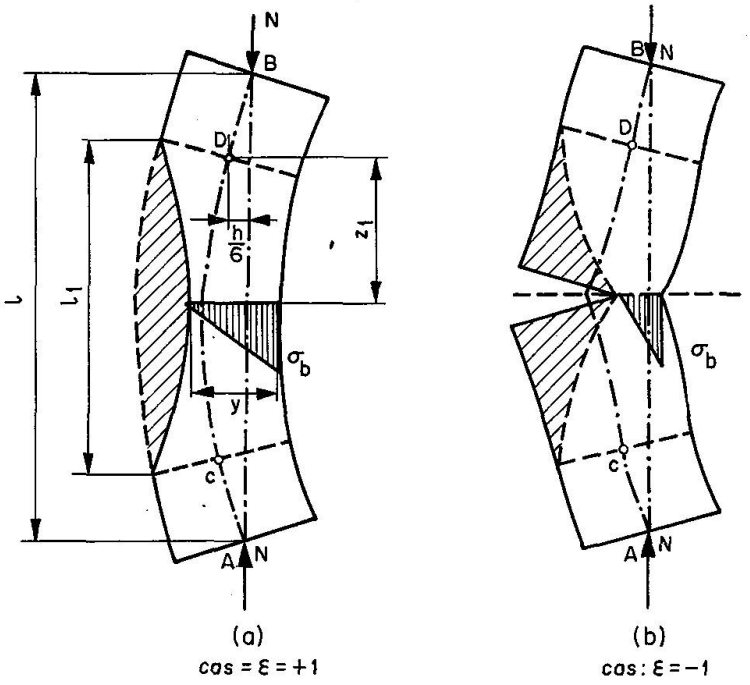

Soit $l_1 = 2z$, la longueur de la «zone fissurée» assimilable à un «empilage».
L'égalité des rotations à la limite de la zone fissurée conduit à la relation suivante:

$$tg\left[\sqrt{\frac{3\sigma_c}{E}}\frac{l}{h} - \frac{f_1(u_1)}{u_1\sqrt{u_1}}\right] = \frac{1}{2\sqrt{u_1 - 1}} \tag{16}$$

avec

$$u_1 = \frac{\sigma_b^*}{2\sigma_c} \tag{17}$$

σ_c = contrainte critique ultime de la pièce fissurée $= \dfrac{N_c}{bh}$ (18)

Si on compare σ_c à la contrainte critique eulérienne de la pièce

$$\sigma_e = \frac{\pi^2}{12} \cdot \frac{Eh^2}{l^2} \tag{19}$$

on obtient la courbe OA de la Fig. 4, et pour des pièces soumises à des charges excentrées le réseau des courbes telles que OB 1, OB 2..., qui montrent la variation du rapport de la charge ultime N à la charge critique d'Euler N_c en fonction de l'excentricité relative a/h pour diverses valeurs du paramètre u_1 défini plus haut.

L'intersection d'une courbe a/h avec la droite de pente

$$\frac{\sigma^* \lambda^2}{24E} = \frac{1}{2} \frac{\sigma_b^*}{E} \left(\frac{l}{h}\right)^2 \tag{20}$$

donne la solution du problème de l'équilibre fléchi de l'empilage d'élancement

$$\lambda = 2\sqrt{3}\, l/h$$

Fig. 4.

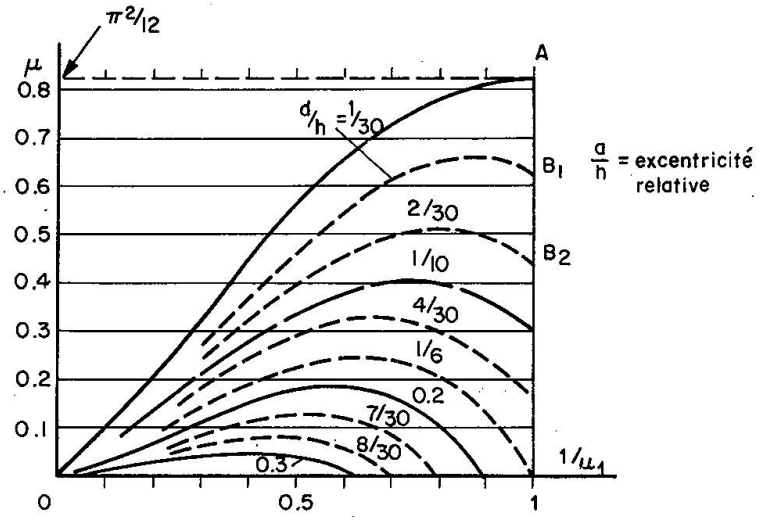

Portons en abscisse dans un diagramme rectangulaire les valeurs du paramètre

$$\tfrac{1}{2} \frac{\sigma_b^*}{E} \cdot \left(\frac{l}{h}\right)^2 \text{ et en ordonnée}$$

celles du coefficient

$$\mu = \frac{\pi^2}{12} \frac{N}{N_c}$$

on obtient le réseau des courbes de la Fig. 5 graduées en fonction de l'excentricité relative a/h.

Ces courbes comprennent, comme on pouvait s'y attendre, un segment de la droite OA passant par l'origine, de longueur variable, suivi d'un arc tel que EF ascendant et d'un arc plongeant FG.

Le segment OE correspond à l'équilibre non fissuré, l'arc EF à un équilibre fissuré stable, et l'arc EG à un équilibre instable.

On constate que pour des valeurs élevées de l'élancement, la théorie des empilages donne une charge ultime nulle.

Fig. 5.

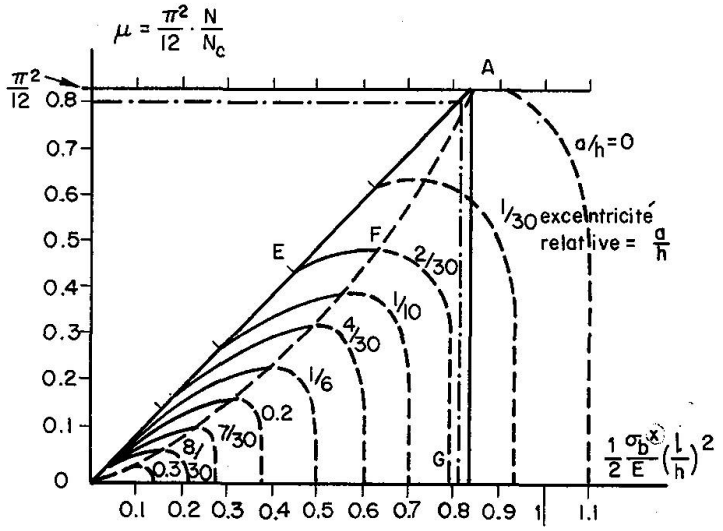

On peut aussi représenter l'effet de l'excentricité sur la stabilité d'un empilage élastique par le diagramme ci-dessous (Fig. 6).

Fig. 6.

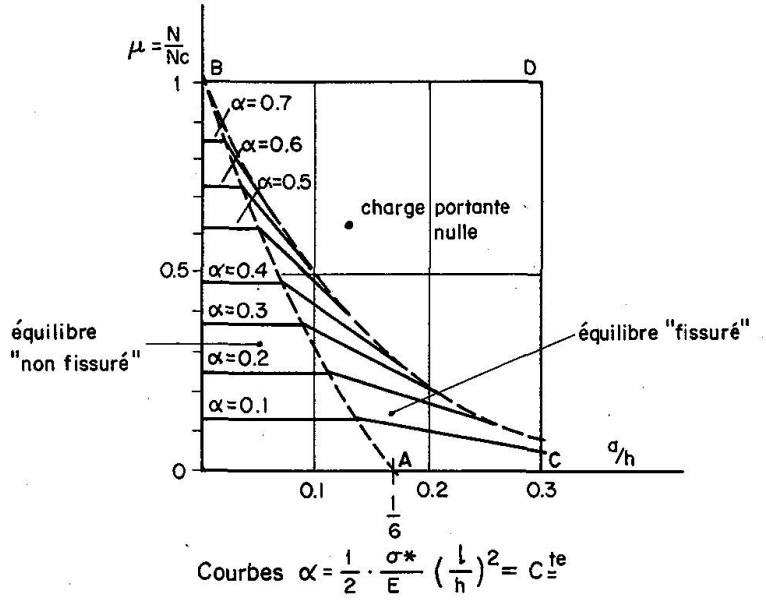

A chaque valeur de $\alpha = \frac{1}{2}\frac{\sigma_b^*}{E}\left(\frac{l}{h}\right)^2$ correspond une courbe $\frac{N}{N_c} = f\left(\frac{a}{h}\right)$ projection sur le plan $\left(\frac{a}{h}, \frac{N}{N_c}\right)$ de l'intersection par un plan parallèle à ces axes de la surface caractéristique de la charge limite admissible de la colonne.

Application aux poteaux en béton armé (Fig. 7)

Soit I_1 l'inertie de la section de béton non armé, I_2 l'inergie de la section des aciers et $(I_1 + mI_2)$ celle de la section homogénéisée.

On obtiendra une solution approchée du problème du poteau en béton armé de section rectangulaire, et à armatures symétriques en procédant à la construction indiquée sur la Fig. 7 qui réalise une interpolation géométrique entre les solutions correspondantes aux cas où $I_a = 0$ (empilage) et $I_b = 0$ (colonne fictive d'acier).

Nous avons procédé à la vérification du modèle proposé au moyen des résultats d'essais effectués sur deux séries de poteaux de 9 × 12,7 cm axialement chargés ayant des pourcentages d'armature de 1,5% et 2,5%.

Les résultats du calcul de la charge ultime par la théorie simplifiée et ceux des essais concordent de façon satisfaisante, eu égard à la dispersion assez élevée de ces derniers.

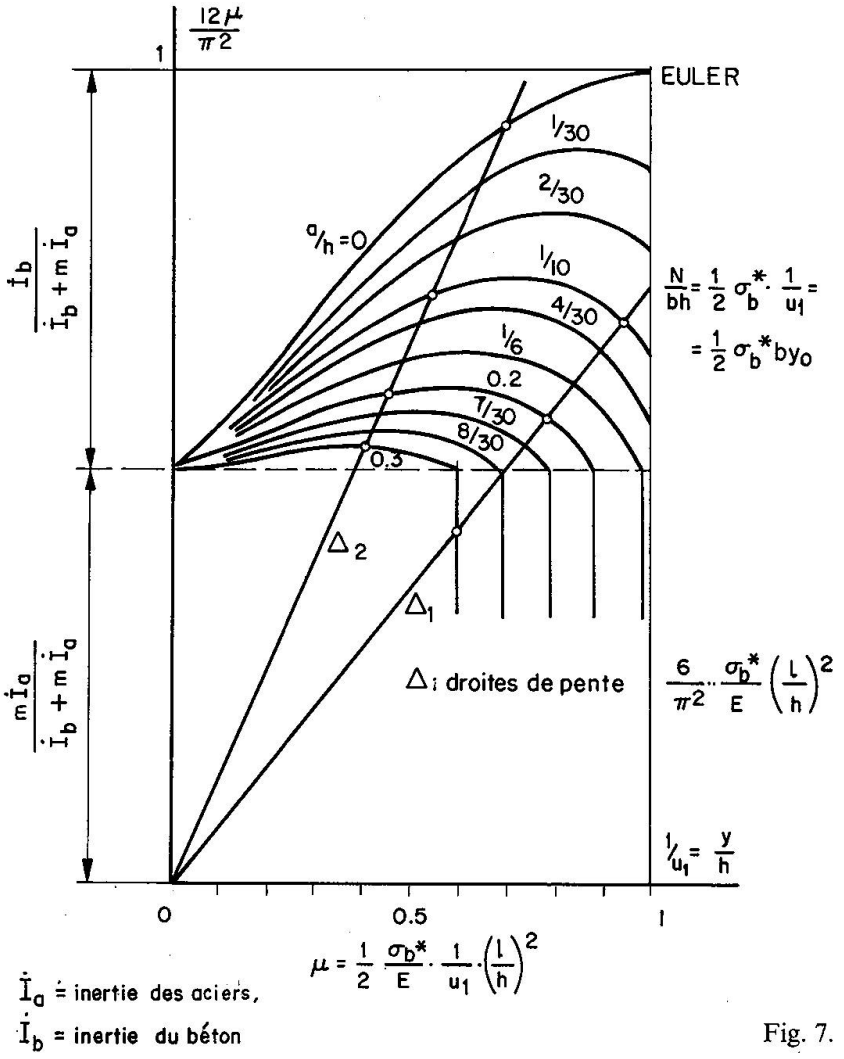

Fig. 7.

Prise en compte de la résistance du béton à la traction (Fig. 8)

Pour la colonne non armée, tout se passe comme si la charge était accrue du terme τby et que la contrainte limite dans la section la plus sollicitée était de $\sigma_b^* + 2|\tau|$ (au lieu de σ_b^*)[1].

[1] Voir à ce sujet: C. BOURDON, Problèmes d'élasticité et de poussée des terres. Le Génie civil, N° 7, de juillet-août 1967, pp. 541 à 544.

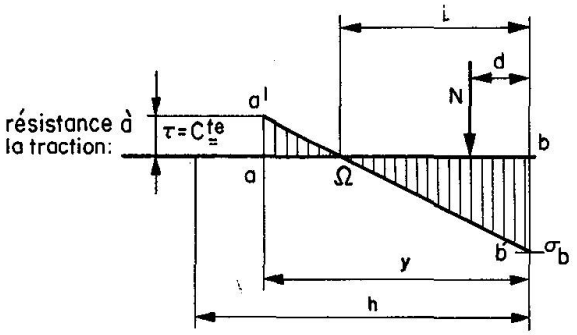

Fig. 8.

Poteaux «précontraints»

On vérifie qu'une précontrainte centrée ne modifie pas la loi de déformations de l'empilage. Mais les conditions aux limites sont évidemment changées. Pour $z = 0$ on a

$$\sigma^* = 2\frac{P+N}{by_0} \tag{21}$$

d'où, avec les notations déjà utilisées:

$$\frac{dz}{y_0} = \sqrt{\frac{E}{6\sigma^*}\left(1+\frac{P}{N}\right)} \cdot \sqrt{\frac{u}{u-1}} \cdot du \tag{22}$$

Tout se passe comme si la contrainte limite du béton dans la section la plus sollicitée était réduite dans le rapport $N/N+P$.

La précontrainte sera favorable pour des charges modérées, notablement inférieures à la charge critique, mais elle deviendra nuisible si la charge de la colonne se rapproche de la charge ultime, la compression supplémentaire due à la précontrainte s'ajoutant évidemment à la contrainte de compression due à la charge.

Prise en compte du poids propre dans la théorie de la stabilité élastique des empilages

Pour un empilage élastique soumis seulement à son poids propre, l'équation différentielle de l'équilibre s'écrit (avec les mêmes notations que précédemment):

$$y^2 \cdot y'' = \varepsilon \frac{6\bar{\omega}h}{E}(l-z) \tag{23}$$

où $\bar{\omega}$ est le poids volumique du matériau.

En remplaçant les différentielles dz et dp par des accroissements finis Δz et Δp, on peut déterminer facilement, de proche en proche, la forme de la déformée, puisque

$$x = \frac{h}{2} - \frac{y}{3}$$

Conclusion

La théorie des empilages élastiques permet d'analyser le comportement sous charge des poteaux en béton armé et de fournir des solutions approchées aux problèmes de flambement des poteaux, des murs, des plaques chargées dans leur plan, et des coques.

Conséquences pratiques pour le projet. Economie et sécurité des pièces comprimées élancées

Dans la pratique, les éléments de structure comprimés réels, et notamment les poteaux en béton armé, ne sont jamais soumis à une charge rigoureusement axiale. En outre, leur forme géométrique comporte des défauts d'origine, dont l'effet est également assimilable à une excentricité de chargement. La charge produit en outre une amplification des effets de ces diverses excentricités, que traduit bien dans le domaine élastique la formule de Perry, et dont les règlements de béton armé tiennent compte en faisant intervenir une flèche additionnelle. Le calcul est ensuite conduit comme en flexion composée.

Toutes ces méthodes, même les plus élaborées, tombent en défaut dans la plupart des cas pratiques, pour lesquels la «longueur de flambement libre» reste le plus souvent très mal connue. Nous renvoyons à ce sujet à notre étude parue en juillet et décembre 1972 dans le Bulletin technique de la Suisse romande.

Il résulte de la théorie des empilages élastiques, exposée ci-dessus, que pour les pièces comprimées très élancées, toute fissuration du béton annule pratiquement la force portante de ce composant et que l'on ne peut plus compter pour de telles pièces que sur celle de la cage d'armatures.

Du point de vue de la sécurité, il est préférable de concevoir une pièce comportant une bonne armature longitudinale plutôt qu'une pièce d'équarrissage plus grand, mais insuffisamment armée. A notre avis, l'économie ne doit pas être recherchée, comme elle l'est trop souvent en pratique, du côté des aciers, au prix d'une dépense de béton supplémentaire. Du point de vue réglementaire, nous pensons que, pour les pièces très élancées, il serait légitime de fixer un pourcentage minimal d'armatures longitudinales en fonction de l'élancement.

Une telle mesure ne grèverait en fait que très peu l'économie des projets. Elle contribuerait à éliminer un nombre croissant de risques d'effondrements dont le caractère soudain et brutal nous permet de dire qu'au regard de tels risques la sécurité n'a pas de prix.

Bibliographie

TIMOSHENKO: Théorie de la stabilité élastique.

BROMS, B. and VIEST, I.M.: Long Reinforced Concrete Columns. A Symposium, Transactions, ASCE V 126, 1961.

ROBINSON J.R. and MODJABI: La précision des charges de flambement des poteaux en béton armé par la méthode de M.P. Faessel. Annales ITBTP, N° 249, septembre 1968.

BOURDON, C.: Remarques pratiques sur le calcul des barrages-voûtes. Le Génie civil, 15 juillet 1961.

BOURDON, C.: Flambement des pieux en milieu élastique – Flambement des enveloppes coniques. Le Génie civil, mars 1969.
BOURDON, C.: Flambement des coques. Le Génie civil, décembre 1971.
BOURDON, C.: Discussion sur la stabilité élastique des poteaux, des pieux et des coques. Bulletin technique de la Suisse romande. N° 15, juillet 1972, N° 25, décembre 1972.
BOURDON, C.: Généralisation de la théorie d'Euler du flambement des pièces rectilignes comprimées. Le Génie civil, N^{os} 1 et 2, janvier-février 1973, et N° 4, avril 1973.

Résumé

En partant d'un modèle mécanique simple, constitué d'une colonne réalisée en empilant des tronçons, posés à joints secs, comme les éléments des colonnes antiques, il est possible de mettre en évidence des critères d'instabilité très éloignés de ceux de la théorie d'Euler, et d'en tirer des conclusions intéressantes pour les pièces en béton armé.

Pour les pièces en béton armé de grand élancement, il est prudent de ne pas descendre au-dessous d'un pourcentage minimal d'armatures longitudinales.

Zusammenfassung

Ausgehend vom einfachen mechanischen Modell der aus einzelnen Blöcken zusammengesetzten Säule (wie etwa die steinernen Säulen der Antike), werden Stabilitätskriterien abgeleitet, die von der Euler'schen Theorie beträchtlich abweichen. Auf Stahlbetondruckglieder angewandt, können hieraus interessante Folgerungen gezogen werden.

Bei schlanken Stahlbetondruckgliedern soll ein Mindestprozentsatz der Längsbewehrung nicht unterschritten werden.

Summary

On the basis of a simple mechanical model consisting of prismatic or cylindrical blocks put each on the top of the other, like the sections of an antique column, there can be found instability criteria, that differ fondamentally from Euler's solution. Interesting conclusions concerning reinforced concrete columns can be gathered.

For long concrete columns it is recommended to use adequate longitudinal reinforcement ratios.

Les normes structurales et l'inélasticité du béton armé

Die statisch konstruktiven Normen und das nicht elastische Verhalten des Stahlbetons

Structural Norms and the Inelasticity of Reinforced Concrete

M.Z. COHN
Professeur de génie civil à l'Université de Waterloo, Ontario, Canada

Introduction

Le comportement inélastique des structures en béton armé a été reconnu depuis la première guerre mondiale [1], [2]. Un demi-siècle de recherches très poussées [3], [4], [5] a contribué à la clarification d'un nombre important de problèmes. Pourtant, malgré la richesse des données théoriques et expérimentales disponibles, on est encore assez loin d'une adoption générale des concepts inélastiques dans le dimensionnement des structures. Par ailleurs, ceci est reflété dans le progrès très timide de ces concepts dans l'élaboration des normes et règlements des structures en béton armé.

Comment expliquer cet état de choses? Il est possible qu'un mélange de résistance aux évolutions, difficultés apparentes des nouvelles méthodes inélastiques, ainsi que certains doutes dans les hauts milieux professionnels, en soient, au moins en partie, responsables. Des discussions intéressantes ont été menées sur les avantages et les inconvénients des méthodes inélastiques sur lesquelles il n'y a pas lieu d'insister ici, mais le lecteur intéressé trouvera des arguments et contre-arguments révélateurs sur la question dans certains documents [6], [9].

Il paraît assez évident à l'auteur qu'il n'y a pas de raison majeure pour renoncer à la généralité, la simplicité relative et la tradition des méthodes élastiques, si ce n'est peut-être le besoin fondamental d'une considération plus correcte de tous les facteurs du dimensionnement des structures en béton.

En effet, une étude des normes et recommandations les plus connues [10], [16] peut illustrer abondamment les divergences des critères, des limites de sécurité, de l'effet des charges, de l'action inélastique, etc. Une méthode rationnelle devrait raffiner et harmoniser *tous* les facteurs mentionnés. Malgré son importance, la considération des phénomènes inélastiques dans les structures en béton armé ne représente qu'un premier pas vers l'élaboration d'une théorie plus rationnelle, à savoir la meilleure utilisation des propriétés réelles du matériau. De plus, une théorie idéale aura à considérer des valeurs plus réalistes des charges, leurs combinaisons et variations

statistiques, des facteurs de pondération des charges correspondant à ces variations, des facteurs de sécurité vis-à-vis des matériaux et enfin des conditions de service, etc.

En nous référant seulement au facteur matériau et à son comportement élastique ou inélastique, on peut distinguer quatre groupes de théories de calcul des structures, selon l'hypothèse admise sur le comportement au niveau des sections individuelles ou des structures en ensemble. Ceci est résumé dans le tableau 1 ci-dessous:

Tableau 1: Théories de calcul des structures en béton armé

Théorie	Section	Structure	Norme	Réf.
1. Contraintes admissibles	Elastique	Elastique	CC BA 68	(13)
2. A rupture (états limites)	Inélastique	Elastique	ACI 318-71	(10)
3.	Elastique	Inélastique	DS 411-49	(16)
4. Charges limites	Inélastique	Inélastique	NTU 123-55	(11)

Avec l'adoption dans les normes américaines [10], russes [11] et européennes [12] des principes des états limites et des phénomènes inélastiques dans les sections, il reste à franchir le pas suivant: celui d'accepter aussi le comportement inélastique des structures et d'en tirer les conséquences pratiques correspondantes.

Même les normes actuelles en bénéficient en partie en permettant une redistribution partielle des moments élastiques sous des conditions bien spécifiques. Mais tout ce potentiel offert par l'inélasticité des structures en béton armé ne peut être exploité que par les méthodes de calcul «inélastique». Les principaux types de méthodes sont résumés dans le tableau 2, avec à leurs limites les méthodes parfaitement «élastiques» ou «plastiques». La classification est basée sur la satisfaction explicite (+) des conditions *d'équilibre limite, de compatibilité et d'utilisation normale* (conditions de service), par chaque type de méthode.

Tableau 2: Méthodes de calcul des structures en béton armé

Méthodes	Critères de calcul		
	Equilibre limite	Compatibilité	Conditions de service
Elastique	+	−	+
Historique	+	+	+
Compatibilité	+	+	−
Equilibre	+	−	+
Plastique	+	−	−

L'objet de la présente étude est d'examiner la pratique actuelle des normes officielles au sujet du comportement inélastique des structures ainsi que les perspectives ouvertes par le développement des méthodes inélastiques, à savoir les méthodes de «compatibilité» et d'«équilibre».

Les méthodes «historiques» qui, dans l'approche manuelle [17], [18] ou par ordinateur [19], [20] consistent en une chaîne d'analyses élastiques, présentent un

intérêt spécial dans la recherche, mais ne seront pas envisagées ici; on estime qu'elles ne pourront être appliquées en pratique qu'après des simplifications considérables qui restent à développer.

Nous allons examiner les diverses déviations des méthodes élastiques permises par les normes en vigueur les plus connues. Ensuite, nous passerons en revue les principes des normes et recommandations possibles, basés sur les méthodes de «compatibilité» et d'«équilibre». Quelques exemples numériques seront présentés afin d'illustrer et de comparer les solutions basées sur les normes en vigueur ainsi que sur les recommandations possibles, déduites des méthodes inélastiques.

On trouvera dans l'annexe de cette étude les clauses concernant la redistribution plastique en diverses normes.

Méthode élastique

Dans notre contexte, la méthode «élastique» consiste à déterminer les sollicitations des structures fléchies en partant des hypothèses des théories élastiques et à dimensionner les sections en acceptant l'inélasticité du béton armé, selon, par exemple, la théorie des «états limites» (deuxième ligne du tableau 1).

Moments élastiques

Les méthodes d'analyse élastique fournissent les enveloppes des moments sous charges de service, sous la forme:

$$M = aG1 + bP1 \tag{1}$$

où a et b sont des constantes qui définissent les valeurs extrêmes des moments dans la section considérée, dus respectivement aux charges permanentes (G) et aux surcharges (P). Ces constantes dépendent de la géométrie, des conditions d'appuis et des types de charges de la structure. Les valeurs 1 sont définies par la géométrie de la structure.

Par exemple, pour une poutre continue à cinq portées égales, sous charge uniformément distribuée et aux appuis simples aux extrémités, les valeurs a et b résultant des théories élastiques et plastiques sont indiquées dans la fig. 1. Dans la même figure sont données les valeurs approximatives selon les différentes normes nationales (les valeurs b sont placées entre parenthèses sauf dans les cas où les recommandations prévoient $a = b$).

On peut remarquer que, dans la mesure où les coefficients a et b adoptés dans ces normes ne correspondent pas aux valeurs élastiques, celles-ci supposent implicitement une certaine redistribution plastique des moments dans les poutres continues en béton armé.

Cependant, le choix des coefficients a et b n'est pas seul à déterminer la nature d'une solution «élastique» ou «presque élastique». En effet, le critère de dimensionne-

ment consiste à assurer que les moments résistants M_u sont au moins égaux aux moments élastiques développés sous les combinaisons les plus défavorables des charges ultimes F_u:

$$M_u > M(F_u) \tag{2}$$

A la limite, l'équation (2) produit une solution si F_u est défini, c'est-à-dire lorsque la relation entre les moments aux états limites d'utilisation et aux états limites ultimes est précisée conformément aux critères de sécurité adoptés.

Critères de sécurité

En général, la sollicitation correspondant à l'état limite ultime S_u est définie en diverses normes comme une fonction linéaire des sollicitations dues aux charges appliquées S_k, soit:

$$S_u = \Sigma_k \gamma_k S_k \tag{3}$$

où γ_k est le facteur de pondération (ou de sécurité), correspondant à la Kième charge ou sollicitation considérée. Dans les normes, on recommande un certain nombre de combinaisons de sollicitations de type (3), les valeurs de γ_k adoptées pour chaque cas se trouvant dans une certaine relation à la probabilité de la combinaison respective et ses conséquences sur la sécurité de la structure.

Par exemple, en nous référant à la combinaison fondamentale des charges permanentes et imposées, les facteurs de pondération respectifs sont:

$\gamma_g = 1.4$ et $\gamma_p = 1.7$ dans les normes américaines [10];
$\gamma_g = 1.1$ et $\gamma_p = 1.4$ dans les normes soviétiques [11];
$\gamma_g = 1.5$ et $\gamma_p = 1.5$ dans les recommandations CEB [12];
$\gamma_g = 1.4$ et $\gamma_p = 1.6$ dans le code de pratique britannique [14].

Un concept souvent utile est le facteur de sécurité d'ensemble (ou facteur moyen de charge) γ_0, qui est une extension directe de la définition de la sécurité dans les méthodes des «contraintes admissibles», à savoir le rapport des charges ultimes S_u et en service S:

$$\gamma_0 = \Sigma_k \gamma_k S_k / \Sigma_k S_k = S_u/S \tag{4}$$

Dimensionnement des sections

Pour le cas typique de dimensionnement d'une section fléchie, le critère de base (2) peut être exprimé en fonction de (1) et (3) ou (4), et en affectant la résistance théorique de la section d'un facteur de minoration Φ comme suit:

$$\Phi M_u \geqslant a\gamma_g G1 + b\gamma_p P1 \tag{5}$$

Le facteur Φ tient compte de la variabilité des propriétés des matériaux et des conditions de service sous divers types de contraintes. Pour les éléments fléchis,

dont la rupture a lieu en traction $\Phi = 0{,}9$, selon les normes américaines [10] et russes [11], $\Phi = 1/1.15$ selon les recommandations CEB [12] et $\Phi = 1$ dans d'autres normes officielles.

Il est bien évident que pour une structure donnée, les résultats des calculs peuvent, en suivant les normes des différents pays, être comparés seulement en considérant tous les aspects concernant:

1. la théorie de résistance adoptée pour l'état limite ultime (évaluation de M_u);
2. la théorie statique pour l'analyse des sollicitations dues aux charges permanentes et aux surcharges (évaluation de a et de b);
3. la prise en compte de la dispersion des propriétés des matériaux (choix de Φ);
4. la manière d'envisager la sécurité (choix des facteurs γ_k).

Redistribution des moments

L'exemple de la poutre continue à portées égales de la fig. 1 indique que les normes permettent une déviation limitée par rapport à la théorie conventionnelle élastique, en raison des effets structuraux de l'inélasticité du béton armé.

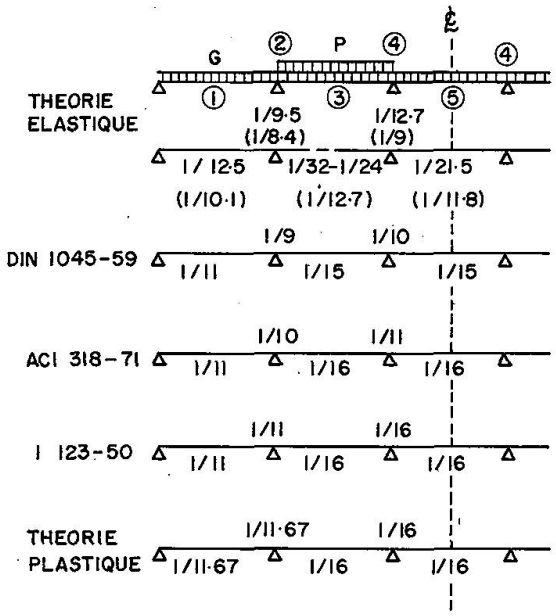

Fig. 1. Coefficients des moments élastiques $[(M/G + P)L^2]$ selon différentes normes.

D'une manière plus générale, les normes permettent aussi des redistributions des moments élastiques dans les structures ayant des cas de charges, de géométries et de conditions d'appui quelconques. Ces provisions sont reproduites pour la convenance du lecteur dans la première annexe à cette présentation.

On remarque les tendances suivantes:

1. Le degré maximal admissible de *redistribution arbitraire* des moments élastiques varie de 15% dans les recommandations CEB [12] et de 20% dans le code américain [10], jusqu'à 30% dans les standards russes [21] et britanniques [14], ou même jusqu'à 67% dans le standard danois [16].

2. Pour chaque condition de charge, la redistribution des moments, dans les limites mentionnées ci-dessus, est permise, si les conditions d'équilibre restent assurées partout dans la structure, c'est-à-dire si les réductions convenables des moments imposés en certaines sections sont compensées par des augmentations suffisantes dans le reste de la structure.
3. Dans certaines normes, la redistribution des moments n'est permise que sous limitation des quantités maximales d'armatures (nettes en traction) des sections critiques: $\bar{\omega} - \bar{\omega}' \leqslant 0{,}3$ en I 123-50 [21]; $\bar{\omega} - \bar{\omega}' \leqslant 0{,}5\,\bar{\omega}_b$ en ACI 318-71 [10], où $\bar{\omega}_b$ est le pourcentage mécanique d'armature compensée (correspondant à la rupture simultanée en traction et compression). Les normes britanniques [14] prévoient la limitation équivalente de la hauteur relative de l'axe neutre, soit: $0{,}3 \leqslant \alpha \leqslant 0{,}6$ lorsque la redistribution admise varie de 30% à 0%.

Les provisions principales sur les redistributions admissibles des moments sont résumées clairement dans les diagrammes de la fig. 2 dont les zones hachurées définissent les *domaines des redistributions admissibles* pour les normes américaines, russes et britanniques par rapport à ceux des règles CEB.

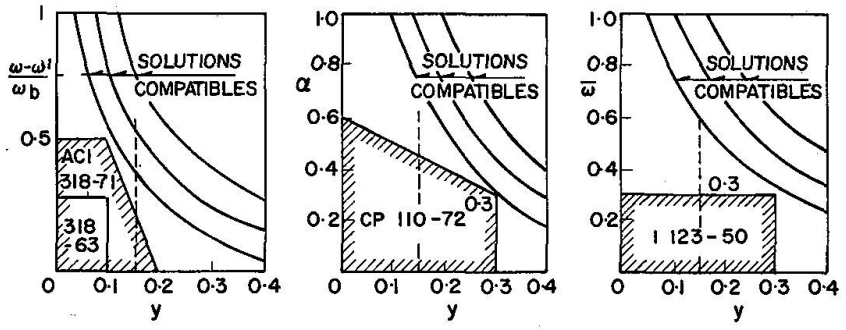

Fig. 2. Domaines des redistributions admissibles des moments élastiques extrêmes, selon différentes normes.

Evaluations des normes actuelles

Les normes actuelles, basées sur les concepts élastiques, ont constitué des outils satisfaisants dans la pratique des projets en béton armé.

Certaines normes reconnaissent la présence des phénomènes inélastiques et permettent, d'une manière assez simpliste, d'en tirer avantage. Néanmoins, leur application donne lieu à un nombre de contradictions internes et de problèmes de principe qui restent à résoudre:

1. Les sollicitations à l'état limite ultime S_u, calculées par une analyse élastique sous les charges ultimes (c'est-à-dire avec les facteurs de pondération respectifs) correspondent à un état limite fictif, puisque au-delà d'une valeur relativement faible des charges le comportement du béton armé cesse d'être élastique.
2. Le procédé consistant à égaliser la résistance à la rupture des sections avec les sollicitations élastiques correspondantes sous charges ultimes conduit en général à des solutions du côté de la sécurité. Néanmoins, le traitement élastique des structures, tout en acceptant la plasticité de ses sections, reste une approche strictement conventionnelle dont on peut mettre en doute la rationalité.

3. Les recommandations officielles sur la redistribution arbitraire des moments élastiques (sous certaines conditions) posent comme principe que, sauf accident, la structure possède une ductilité suffisante pour permettre l'adaptation plastique par rapport aux états de sollicitations désirées. Malheureusement, les limitations imposées (armature en traction ou hauteur de l'axe neutre) visent à la satisfaction de la compatibilité, en ignorant totalement les conditions de service, ainsi que l'influence d'autres facteurs affectant la redistribution plastique, notamment le rapport des charges permanentes et utiles, la géométrie de l'ossature, les conditions d'appui, la distribution des résistances (ou des rigidités en flexion) etc.
4. Certaines normes qui permettent la redistribution arbitraire (ou les moments du type $c(G+P)1$, en fig. 1) peuvent conduire à des solutions où des zones plastiques se développent sous conditions de service, si on impose des redistributions poussées lorsque les charges permanentes sont dominantes ($G/P \to 0$). Ceci est encore plus grave lorsque la redistribution permise va jusqu'à 67% des moments élastiques [16]. Une application irréfléchie de cette clause doit conduire inévitablement à des flèches et fissures exagérées, ainsi qu'à des contraintes au-delà de la limite élastique.

Nous allons maintenant démontrer que le respect d'une marge de sécurité spécifique vis-à-vis de l'état limite d'utilisation impose des limites précises à la redistribution inélastique admissible.

Pour simplifier la discussion, supposons qu'on fasse un projet selon les normes américaines, donc avec $\gamma_g = 1.4$ et $\gamma_p = 1.7$. Choisissons également la valeur $\gamma_1 = 1.2$ pour le facteur vis-à-vis de l'écoulement initial d'une section critique (rotule plastique). Il n'est pas difficile alors de montrer [22] que le rapport x_j entre les moments de calcul M_{pj} d'une section j (qui est à déterminer par le processus de dimensionnement) et son moment élastique maximal sous les charges limites M_j est à peu près égal au rapport du facteur de sécurité vis-à-vis de l'écoulement de la section j, γ_{1j}, au facteur de sécurité l'ensemble de la structure γ_0, soit:

$$x_j = M_{pj}/\overline{M}_j \doteq \gamma_{1j}/\gamma_0 \tag{6}$$

Pour assurer des conditions normales d'utilisation dans le contexte des hypothèses admises, il suffit que la condition $\gamma_{1j} \geqslant \gamma_1$ soit satisfaite, ou:

$$x_j \geqslant x_{\min} = \gamma_1/\gamma_0 \tag{7}$$

En notant $y = 1 - x$, la valeur $100y$ représente le pourcentage du moment élastique extrême redistribué et $y_{\max}$, qui est la valeur de la redistribution admissible devient, en tenant compte de (4):

$$y_{\max} = 1 - \gamma_1/\gamma_0 \tag{8}$$

$$\text{mais } \gamma_0 = (\gamma_g G + \gamma_p P)/(G+P) \tag{9}$$

et après substitution et transformation simples, l'équation (8) devient:

$$y_{\max} = 1 - \gamma_1 [(G/P)+1]/[\gamma_g (G/P) + \gamma_p] \tag{10}$$

L'équation (10) montre que la redistribution maximale des moments élastiques dépend des facteurs de pondération admis γ_1, γ_g et γ_p, ainsi que du rapport G/P

des charges permanentes et surcharges appliquées. Pour les valeurs adoptées, les variations de γ_1, γ_0, et $y_{max} = 1 - \gamma_1/\gamma_0$ sont illustrées en fonction du rapport G/P dans la fig. 3.

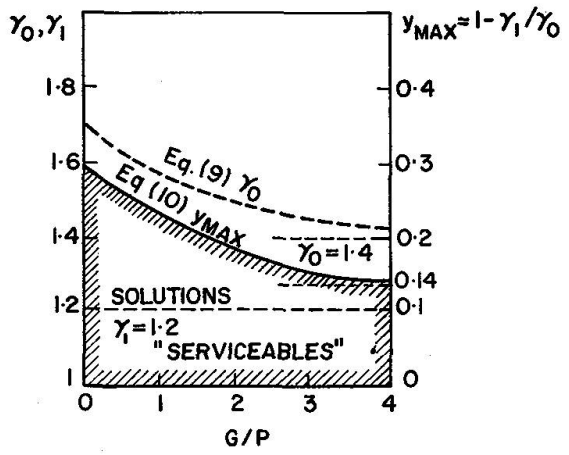

Fig. 3. Domaines des «solutions serviçables» et limites des redistributions maximales des moments élastiques en fonction du rapport G/P.

Il est visible que la redistribution maximale permise pour les facteurs de pondération varie de $1 - \gamma_1/\gamma_p = 29\%$ pour le cas $G=0$ à $1 - \gamma_1/\gamma_g = 14\%$ pour le cas $P=0$.

Ceci montre que pour des structures dont la surcharge est négligeable ($P=0$) et possédant des sections faiblement armées, on peut arriver aisément à l'état limite d'utilisation, si on admet les redistributions maximales des moments élastiques permises par les normes américaines (20%) ou britanniques (30%), tandis que l'adaptation réelle sous conditions normales de service ne permettra pas une réduction des enveloppes élastiques de plus de 14%.

Méthodes de «compatibilité»

Les méthodes de «compatibilité» ont un caractère commun: elles satisfont les conditions d'équilibre limite (sous les charges ultimes) et de compatibilité des rotations (des sections critiques). Ces méthodes ont pour but de vérifier la capacité de déformation de la structure correspondant à son état limite ultime sous les combinaisons les plus défavorables des surcharges. Par ailleurs, elles diffèrent dans les détails d'application sur deux hypothèses fondamentales, notamment le modèle mathématique du béton armé et la définition de l'état ultime.

A.L.L. Baker [7], [23], [24] adopte pour le diagramme moments-courbures l'idéalisation bilinéaire de la fig. 4a, avec les points L_1 et L_2 correspondant respectivement au début de l'écoulement de l'armature en traction et à la ruine de la zone comprimée du béton. Selon cette conception, l'état limite ultime d'une structure est atteint lorsqu'elle est rendue isostatique par la formation progressive d'un nombre suffisant de rotules plastiques, c'est-à-dire lorsque le comportement de n sections critiques (n étant le degré d'hyperstatisme) est défini par les valeurs des courbures se situant entre les limites L_1 et L_2 des diagrammes correspondants.

SAWYER [25], [26] adopte le modèle bilinéaire de la fig. 4b, avec les points E et U correspondant respectivement à la limite élastique et à l'état limite ultime de la section. Dans sa méthode, SAWYER considère que la capacité de résistance de la structure est épuisée dès que l'état limite ultime est atteint dans la section la plus sollicitée.

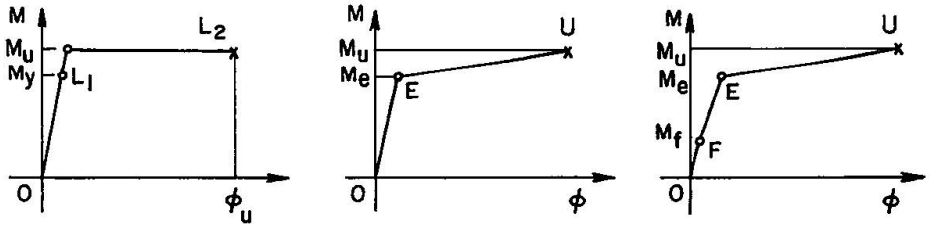

a) A.L.L. Baker [24]. *b)* Sawyer [25]. *c)* Macchi [27].

Fig. 4. Modèles du matériel élastique dans les méthodes de «compatibilité».

MACCHI [5], [27] adopte le modèle trilinéaire de la fig. 4c pour le diagramme moments-rotations des sections critiques. Les points E et U correspondent aux mêmes états que ceux de la fig. 4b, le point F correspond à l'état limite de fissuration.

En général, la forme des équations de compatibilité, pour les sections j, est celle indiquée dans les recommandations CEB [12]:

$$\int \frac{M_j M_0}{E' I'} ds + \sum X_k \int \frac{M_i M_k}{E' I'} ds + M_j \theta'_j + \sum M_j \Psi_n = {}^0 \tag{11}$$

Les trois premiers termes de cette équation expriment les rotations des sections des appuis j, dues respectivement à l'action des charges appliquées, aux effets des inconnues hyperstatiques X_k et à l'inélasticité de la section considérée. Le dernier terme exprime l'influence de l'action inélastique des zones situées entre les sections critiques d'appui.

Si on adopte les hypothèses de A.L.L. BAKER et si on choisit comme inconnues hyperstatiques un nombre de n moments aux nœuds de l'ossature, X_k deviennent des moments plastiques connus: M_{pk}, et en négligeant les effets de l'inélasticité entre les sections critiques ($\Psi = 0$, l'équation (11) peut être simplifiée sous la forme:

$$\int \frac{M_j M_o}{EI} ds + \sum M_{pk} \int \frac{M_j M_k}{EI} ds + \cdot \theta_j = 0 \tag{12}$$

Les exemples de calcul publiés dans la littérature paraissent démontrer que les techniques respectives des méthodes de «compatibilité» sont assez élaborées [24], [25], [27]. Quelques résultats numériques des études comparatives avec les méthodes d'«équilibre» sur un nombre de structures typiques seront présentés plus loin [28], [29].

Une des difficultés des méthodes de «compatibilité» dérive de leur nature itérative. Les solutions peuvent être obtenues seulement à la suite d'un processus plus ou moins complexe d'approximations successives. Ces difficultés sont éliminées, du moins pour la méthode des «rotations imposées» de MACCHI, moyennant les techniques de la programmation quadratique, comme cela a été démontré dans les études de MAIER et de ses collaborateurs [30], [31].

Du point de vue pratique, les méthodes «de compatibilité» ont abouti à peu de recommandations en général [6], [12], [24], [26] et à aucune encore officiellement adoptée dans les normes en vigueur.

Les ingénieurs européens, moins familiers avec les publications américaines, pourraient être intéressés par le projet de recommandations sur le calcul à limite élaboré par le Comité 428 de l'ACI et de l'ASCE [32].

En bref, le modèle de recommandations du Comité 428 permet l'utilisation libérale de toute distribution des moments inélastiques des poutres et portiques qui est basée sur des hypothèses logiques et qui satisfait les conditions suivantes:

a) les moments et les forces axiales ultimes sont calculés selon les normes en vigueur;
b) la rigidité élastique peut être calculée pour la section effective du béton ou la section fissurée transformée, en admettant des valeurs à $\pm 25\%$ près de celles des normes;
c) le moment à la limite élastique est fixé à au moins 80% de la valeur du moment ultime;
d) les courbures inélastiques ϕ_m peuvent être évaluées par tout diagramme se situant entre des segments *EBU* et *EU* de la fig. 5;
e) les longueurs des zones inélastiques sont limitées en fonction de la géométrie et des charges des éléments fléchies ainsi que des propriétés mécaniques des matériaux.

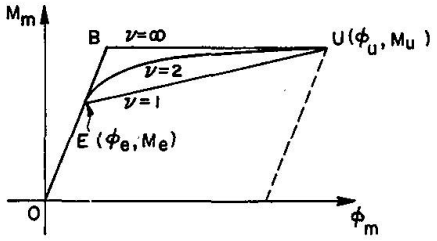

Fig. 5. Modèles de comportement inélastique des sections fléchies en béton armé [32].

Méthodes d'«équilibre»

Les méthodes d'«équilibre» constituent une classe de procédures basées sur la satisfaction exacte des critères d'équilibre limite et de serviçabilité [33], [34] et seulement sur une vérification du critère de compatibilité [35]. Les méthodes d'«équilibre» sont donc des méthodes qui assurent des marges de sécurité convenables vis-à-vis de deux états limites, à savoir γ_1 contre la ruine locale d'une section (supposée constituer l'état limite d'utilisation et avoir lieu au moment de l'écoulement de l'armature) et γ_0 contre la ruine plastique de l'ensemble de la structure (supposée avoir lieu à la formation d'un mécanisme à un degré de liberté).

Une caractéristique intéressante des méthodes d'«équilibre» est qu'elles permettent par extension d'obtenir des techniques d'optimisation mathématique formelle par l'addition des fonctions objectives convenables des variables au problème de dimensionnement.

En bref, les aspects principaux de ces méthodes sont les suivants:

1. Les moments de calcul M_{pj} sont définis comme des pourcentages x_j des moments correspondants de l'enveloppe élastique $\overline{M}_j$ sous les charges ultimes.

2. Les pourcentages x_j sont les variables des problèmes et représentent les indices de plasticité des sections j, qui synthétise l'essence même des méthodes: l'adoption des marges de sécurité γ_{1j} et γ_0 vis-à-vis des deux états limites considérés.
3. Choix des critères satisfaisants pour l'état limite ultime, c'est-à-dire contre tout mode possible de ruine plastique.
4. Choix des critères satisfaisants pour l'état limite d'utilisation, c'est-à-dire prévoir des marges de sécurité à plastification suffisante, lorsque chaque section critique est soumise à la plus défavorable combinaison des surcharges.

La combinaison des critères alternatifs vis-à-vis des deux états limites considérés permet une gamme assez large de solutions à sécurité spécifiées γ_1 et γ_0 [33], [36], [37]. A la limite de ce spectre, on a les solutions parfaitement élastiques (aux réserves de sécurité ainsi que les quantités de matériaux les plus importants) et les solutions optimales (aux réserves de sécurité minimales spécifiées et des économies maximales des matériaux).

Sans entrer dans les détails des techniques de calcul qui ont été résumées récemment en deux textes français [38], [39], la nature des diverses solutions possibles peut être évaluée par rapport aux diagrammes de la fig. 6 qui présentent la solution graphique d'un problème à seulement deux variables. Dans le plan, ou plus généralement l'espace de dimensionnement, un point (x_1, x_2) définit une solution au problème satisfaisant les critères ci-dessous, fig. 6a, b, c, qui sont des fonctions linéaires des variables:

a) service (*S*): $\gamma_{1j}(x_j) \geqslant \gamma_1$ ou $x_j = \gamma_{1j}/\gamma_0 \geqslant \gamma_1/\gamma_0$ (13)

b) équilibre limite (*E.L.*): $\gamma_i(x_j) \geqslant \gamma_0$ (14)

c) optimalité (*O*): $V(x_j) = \min.$ (15)

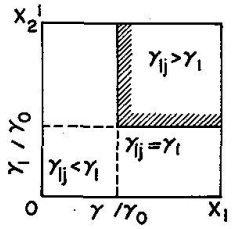

a) Critère de service.

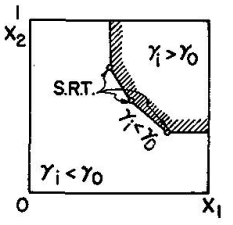

b) Critère d'équilibre limite.

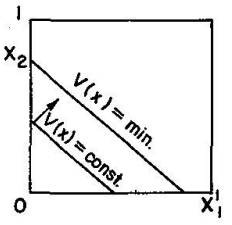

c) Critère d'optimalité.

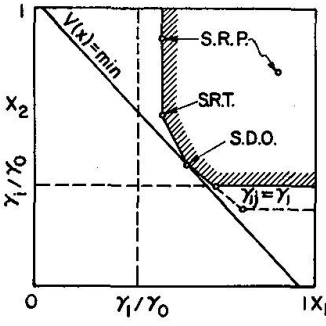

d) Solutions SRT, SRP, SDO.

Fig. 6. Solutions typiques des méthodes d'«équilibre».

La fig. 6d représente des solutions possibles, c'est-à-dire satisfaisant simultanément aux deux premiers critères ci-dessus, ou optimales, c'est-à-dire qui satisfont tous les trois critères. Les solutions possibles correspondent à des points se trouvant

à l'intérieur ou à la frontière du domaine admissible; les points représentant des coins du polygone «admissible» correspondent à des *solutions à redistribution totale* (SRT), pour lesquelles tout mode de ruine i se produit sous le facteur de charge spécifié ($\gamma_i = \gamma_0$); les autres points correspondent à des *solutions à redistribution partielle* (SRP), pour lesquelles les modes de ruine i se produisent à des facteurs de charges en général supérieurs aux valeurs spécifiées ($\gamma_i > \gamma_0$).

Si une solution possible satisfait aussi à la condition d'optimalité, le point correspondant est représenté par le lieu où une droite parallèle au critère d'optimalité est tangente au polygone des solutions possibles: c'est une *solution de dimensionnement optimal* (SDO), fig. 6d. On voit bien que SDO est toujours une SRT.

Par ailleurs, il n'est pas difficile de remarquer qu'en général le rendement économique mesuré en volume d'armature nécessaire des SRT est seulement de quelques % inférieurs des SDO [36], [37]. C'est une conclusion importante du point de vue pratique, puisqu'elle suggère qu'en tendant à maximiser la redistribution permissible des moments élastiques (afin d'aboutir à une SRT) on est très près des solutions optimales mathématiques.

Ceci nous a permis de préparer un projet de recommandations pratiques en partant des principes des méthodes d'«équilibre» [40].

En résumé, l'application des recommandations est limitée aux poutres et dalles continues, ainsi qu'aux portiques aux nœuds non déplaçables si les surcharges ont des valeurs entre ¼ et 4 des charges permanentes, les portées ne varient pas plus que de 50%, les aciers n'ont pas une résistance supérieure à 60 Ksi, le pourcentage mécanique ne dépasse pas 0.3 et enfin, si les armatures sont correctement détaillées et ancrées.

Le projet de recommandations énonce explicitement les critères fondamentaux vis-à-vis des états limites d'utilisation et ultimes, ainsi que la compatibilité des rotations sous charges ultimes.

Les moments de calcul recommandés ont la forme $M_{pj} = x_j \overline{M}_j$ et la considération de tout mode de ruine possible conduit aux inégalités linéaires dans les variables x_j.

Pour les solutions à redistribution totale, SRT[1], les valeurs des x_j doivent être choisies de manière à satisfaire identiquement toutes les équations d'équilibre limite. Dans ce but, des critères de service convenable peuvent être adoptés, par exemple l'égalité des valeurs x_j, ou $\overline{M}_j$ sur les sections d'appui ou de quelques portées, etc.

Pour les solutions à redistribution partielle, SRP[2] les valeurs de x_j recommandées pour les sections de portée sont de 0.85 à 0.90, correspondant à des redistributions de 10-15% par rapport au calcul élastique. Les pourcentages de redistributions permises aux sections d'appui seront déterminés de telle sorte que l'équilibre statique soit respecté partout.

Pour le dimensionnement à limite des portiques, on recommande que les valeurs de x_j pour les sections des poteaux, des appuis et des portées ne soient pas inférieures respectivement à 0.9, 0.85 et $1.2/\gamma_0$.

[1] En anglais, FRD, pour *Full Redistribution Design.*
[2] En anglais, LRD, pour *Limited Redistribution Design.*

Le calcul approché de la compatibilité n'est requis que pour les sections d'appui dont le x_j est inférieure à 0.85. Dans ce cas la satisfaction de la condition suivante doit être vérifiée:

$$x_j \geqslant x_0 = [1 + (\Phi_u/\Phi_e - 1)/12]^{-1} \tag{16}$$

où x_0 est la valeur minimale de x_j pour laquelle la compatibilité des rotations est satisfaite; Φ_u et Φ_e sont les courbures ultimes et à la limite élastique de la section j.

Exemples d'application

Afin d'évaluer comparativement les solutions obtenues par les différentes méthodes de calcul inélastique ou les normes en vigueur, nous présentons trois applications et les indices correspondants.

Application N° 1: Poutre continue [41]

Soit une poutre continue à cinq travées et appuis extrêmes libres, sous charge uniformément distribuée à dimensionner, selon les principes de l'élasticité et avec les coefficients permis par les normes des divers pays. On utilise une théorie à rupture pour le calcul des sections et on adopte: $G/P = 1/2$, $\gamma_1 = 1.1$, $\gamma_g = 1.4$ et $\gamma_p = 1.7$.

Les moments de l'enveloppe élastique sont donnés par l'équation (1) et ceux des normes par la relation $M_j = c_j(G + P)L^2$ avec les coefficients a_j, b_j, c_j, de la fig. 1.

Si on calcule pour toutes les solutions les valeurs des indices $x_j = M_{pj}/\gamma_0 M_j$, des sections $j = 1.1...5$, $u_i = \gamma_i/\gamma_0$ des mécanismes des portées $i = 1$, 2, 3 et $v_k = V_k/V_e = \Sigma_j M_{pj} 1_j / \Sigma_j M_{uj} 1_j = \Sigma_j x' 1_j / \Sigma_j x' 1_j$ (où $x'_j = M_{uj}/\gamma_0 M_j$ et 1_j sont les longueurs relatives des armatures construites, supposées $1_1/L = 1_5/L = 2/3$ et $1_2/L = 1_4/L = 1/2$), on obtient les résultats du tableau 3.

Tableau 3: Comparaison des solutions par différentes normes

Solution	Service					Equilibre limite			Rendement
	x_1	x_2	x_3	x_4	x_5	u_1	u_2	u_3	v_k
Théorie élastique	1.01	1.00	1.02	1.01	1.02	1.26	1.44	1.40	1.00
DIN 1045-59	0.98	0.98	1.00	1.00	0.93	1.24	1.37	1.33	0.98
ACI 318-71	0.98	0.88	0.94	0.91	0.87	1.09	1.26	1.23	0.90
I 123-50	0.98	0.80	0.94	0.63	0.87	1.06	1.11	1.00	0.84
Théorie plastique	0.93	0.75	0.94	0.69	0.87	1.00	1.09	1.00	0.82

Le tableau 3 confirme que les théories les plus conservatives (aux x_j plus larges) ont les plus grandes réserves de résistance vis-à-vis de la ruine plastique (u_i) mais sont aussi les moins économiques (valeurs de v_k plus près de l'unité). Les coefficients permis par les diverses normes conduisent à des solutions plus économiques que la théorie ($v_k < 1$), en déviant de celle-ci dans une certaine mesure.

Nour remarquons que la théorie plastique conduit à des ruines plastiques des portées marginales et centrales pour précisément les facteurs de surcharge spécifiée ($u1 = u3 = 1$) et à une économie de l'armature en traction de 18% par rapport au calcul élastique ($v_k = 0.82$). Nous remarquons également que toutes les normes conduisent à des solutions qui varient entre les solutions parfaitement élastiques et plastiques.

Application N° 2: dalle continue [41]

Soit une dalle armée dans une seule direction, continue sur cinq travées et aux appuis extrêmes libres, sous charges uniformément distribuées à dimensionner selon le principe de redistribution arbitraire des moments élastiques, permissible selon les normes des divers pays. Supposons $G/P = 1/2$, $\gamma_g = 1.4$, $\gamma_p = 1.7$, $\bar{\omega} < 1\%$ et $\bar{\omega} < 9{,}5\%$.

Pour toutes les solutions, nous adoptons les mêmes concepts sur les redistributions favorables des moments élastiques, à savoir:

a) la redistribution maximale permise est effectuée sur les sections d'appui afin de réduire la congestion d'armature des sections critiques;

b) la redistribution des moments dans les sections de portée est effectuée seulement si une augmentation correspondante des moments d'appui n'est pas nécessaire, afin d'obtenir une économie maximale par rapport à la méthode élastique.

Les résultats obtenus sont résumés au tableau 4 où on a noté par (3) et (5) les zones négatives respectivement des sections 3 et 5 fig. 1.

Tableau 4: Redistribution arbitraire des moments élastiques

Norme	Redistribution maximale $100(1-x)\%$	x min.	Mpj/PL^2							
			$j=(1)$	(2)	(3)	$(3)^-$	(4)	(5)	$(5)^-$	
			$\frac{l_j}{L}=\frac{2}{3}$	1/2	2/3	1/2	1/3	1/3	1/3	
Théorie élastique . .	0	1.00	0.225	0.280	0.157	0.056	0.243	0.177	0.036	1.000
ACI 318-63	10	0.90	0.225	0.252	0.141	0.056	0.218	0.177	0.036	0.940
CEB 70.	15	0.85	0.225	0.238	0.144	0.056	0.206	0.177	0.036	0.920
ACI 318-71	18	0.82	0.225	0.230	0.149	0.056	0.199	0.177	0.036	0.915
I 123-50 KCP 110-70. . . .	30	0.70	0.225	0.213	0.156	0.056	0.170	0.177	0.036	0.890

Nous remarquons que, cf. au critère *b* ci-dessus, les moments élastiques des sections (1) (3) – (5) et (7) – n'ont pas été redistribués. La dernière colonne indique l'indice de rendement, $v_k = V_k/V_e$, des solutions par rapport au dimensionnement élastique, pour lequel $v = 1$.

On voit bien que les redistributions arbitraires permises par les normes conduisent à des économies relatives d'armature jusqu'à 11%, en proportion aux taux maximaux des redistributions admissibles.

Application N° 3: Poutres et portiques [28], [29]

Soit les six structures de la fig. 7, avec les géométries, les sections de béton, les charges et les surcharges indiquées, à dimensionner et à comparer les solutions obtenues par les approches suivantes:

a) méthode élastique (avec les actions calculées à rupture);
b) méthode de «compatibilité» (de SAWYER [25] et de BAKER [23];
c) méthode d'«équilibre» (SRP et SRT [33], [34]);
d) méthode optimale (SDO [36]).

Sans insister sur les détails de calcul et les hypothèses communes du processus de dimensionnement développés en [28] et [29], nous reproduisons dans les tableaux 5, 6 et 7 les moments plastiques M_{pj} et les indices de plasticité x_j des sections j pour les six exemples.

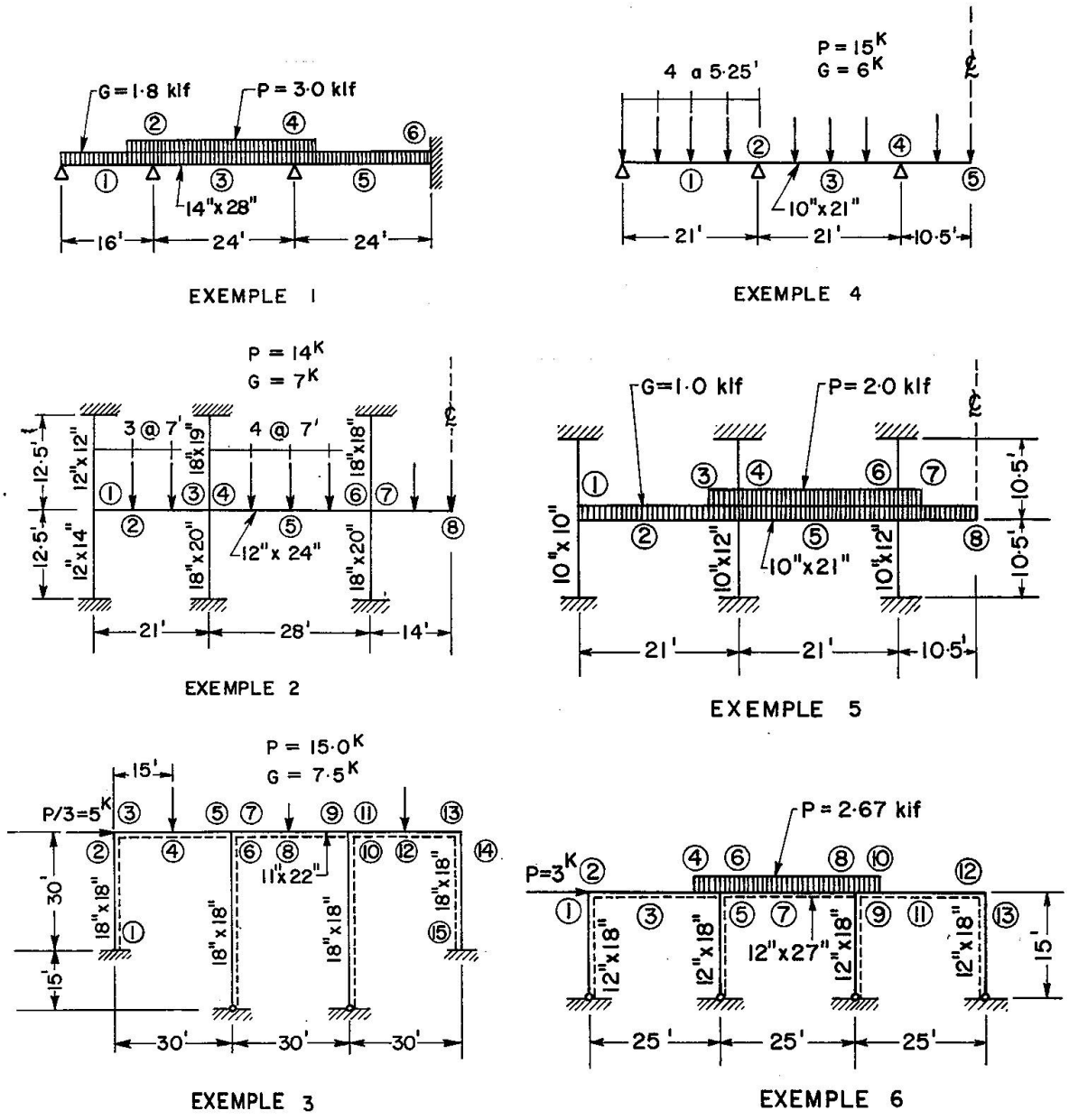

Fig. 7. Géométries et conditions de chargement pour les exemples d'application des méthodes inélastiques.

Tableau 5: Solutions de dimensionnement pour les exemples 1 et 4

Exemple	Section (j)	Th. élast.		Sawyer		Baker		S.R.P.		S.R.T.		S.D.O.	
		M_{pj}	x_j	M_{pj}	x_j	M_{pj}	x_j	M_{pj}	x_j	M_{pj}	x_j	M_{pj}	x_j
1	1	189.4	1.000	175.0	0.923	143.0	0.755	170.5	0.900	135.0	0.712	135.0	0.712
	2	368.7	1.000	335.0	0.910	270.0	0.732	310.0	0.840	289.0	0.785	271.3	0.736
	3	284.3	1.000	247.0	0.870	297.0	1.045	256.0	0.900	271.0	0.950	234.3	0.824
	4	426.4	1.000	385.0	0.905	331.0	0.777	358.0	0.840	334.0	0.785	426.4	1.000
	5	233.1	1.000	235.0	1.008	265.0	1.138	210.0	0.900	233.0	1.000	166.0	0.712
	6	465.5	1.000	385.0	0.826	331.0	0.710	392.0	0.840	366.0	0.785	408.1	0.877
4	1	284.0	1.000	—	—	275.5	0.970	255.5	0.900	260.5	0.916	253.0	0.889
	2	330.0	1.000	—	—	244.5	0.700	244.5	0.740	235.0	0.712	251.0	0.760
	3	215.0	1.000	—	—	193.3	0.782	193.3	0.900	157.0	0.732	150.3	0.700
	4	291.0	1.000	—	—	205.0	0.704	215.5	0.740	207.0	0.712	203.0	0.700
	5	240.5	1.000	—	—	181.5	0.756	216.5	0.900	171.0	0.712	172.3	0.726

Tableau 6: Solutions de dimensionnement pour les exemples 2 et 5

Exemple	Section (j)	Th. élast.		Baker		S.R.P.		S.R.T.		S.D.O.	
		M_{pj}	x_j	M_{pj}	x_j	M_{pj}	x_j	M_{pj}	x_j	M_{pj}	x_j
2	1	51.4	1.000	48.0	0.940	47.0	0.915	46.0	0.890	51.4	1.000
	2	153.9	1.000	155.0	1.010	141.0	0.915	143.0	0.930	153.9	1.000
	3	256.9	1.000	210.0	0.820	235.0	0.915	229.9	0.890	185.6	0.723
	4	317.1	1.000	275.0	0.870	290.9	0.915	282.0	0.890	317.1	1.000
	5	220.6	1.000	236.0	1.070	202.0	0.915	208.0	0.940	170.5	0.773
	6	340.7	1.000	275.0	0.810	312.0	0.915	303.0	0.890	340.7	1.000
	7	340.6	1.000	275.0	0.810	312.0	0.915	303.0	0.890	340.6	1.000
	8	219.5	1.000	236.0	1.070	202.0	0.915	197.0	0.890	159.6	0.727
5	1	70.6	1.000	70.0	0.992	63.3	0.897	56.7	0.803	70.6	1.000
	2	157.6	1.000	169.2	1.074	141.4	0.897	155.8	0.988	125.1	0.794
	3	241.2	1.000	170.0	0.706	216.2	0.897	194.0	0.803	241.2	1.000
	4	230.7	1.000	170.0	0.737	207.0	0.897	185.3	0.803	230.7	1.000
	5	126.2	1.000	124.6	0.986	113.2	0.897	102.8	0.814	89.1	0.706
	6	213.1	1.000	155.0	0.727	191.2	0.897	171.4	0.803	153.9	0.722
	7	216.0	1.000	155.0	0.717	193.9	0.897	173.7	0.803	183.1	0.866
	8	133.5	1.000	132.5	0.993	119.8	0.897	107.5	0.803	94.3	0.706

Tableau 7 : Solutions de dimensionnement pour les exemples 3 et 6

Exemple	Section (j)	Th. élastique				Sawyer				Baker				S.R.T.				S.D.O.			
		M_{pj}^+	x_j^+	M_{pj}^-	x_j^-	M_{pj}^+	x_j^+	M_{pj}^-	x_j^-	M_{pj}^+	x_j^+	M_{pj}^-	x_j^-	M_{pj}^+	x_j^+	M_{pj}^-	x_j^-	M_{pj}^+	x_j^+	M_{pj}^-	x_j^-
3	1	138.0	1.200	138.0	1.970	120	1.043	120	1.715	110.0	0.955	110.0	1.572	107.0	0.930	107.0	1.530	97.2	0.847	97.2	1.392
	2	138.0	3.450	138.0	1.000	120	3.000	120	0.870	110.0	2.750	110.0	0.797	107.0	2.680	107.0	0.776	97.2	2.436	97.2	0.706
	3	40.0	1.000	138.0	1.000	40	1.000	120	0.870	40.0	1.000	110.0	0.797	40.0	1.000	107.0	0.776	28.3	0.706	97.2	0.706
	4	198.0	1.000	28.0	1.000	180	0.910	28	1.000	167.0	0.843	28.0	1.000	164.0	0.828	28.0	1.000	164.0	0.828	19.8	0.706
	5	38.0	1.000	203.0	1.000	38	1.000	180	0.887	38.0	1.000	160.0	0.788	38.0	1.000	155.0	0.763	26.8	0.706	172.0	0.847
	6	59.0	1.000	59.0	1.135	66	1.118	66	1.270	50.0	0.847	50.0	0.961	42.0	0.712	42.0	0.807	41.7	0.706	41.7	0.801
	7	38.0	2.235	203.0	1.182	38	2.235	180	1.045	38.0	2.235	160.0	0.929	38.0	2.235	155.0	0.901	26.8	1.578	172.0	1.000
	8	168.0	1.000	32.0	1.000	140	0.833	32	1.000	140.0	0.833	32.0	1.000	148.0	0.882	32.0	1.000	118.5	0.706	22.6	0.706
6	1	42.9	1.000	106.6	1.000	—	—	—	—	25.8	0.600	83.3	0.782	25.8	0.600	95.8	0.900	25.8	0.600	93.2	0.875
	2	42.9	1.000	106.6	1.000	—	—	—	—	25.8	0.600	83.3	0.782	25.8	0.600	95.8	0.900	25.8	0.600	93.2	0.875
	3	268.8	1.000	56.2	1.000	—	—	—	—	260.0	0.966	33.8	0.600	228.5	0.850	33.8	0.600	177.5	0.660	33.8	0.600
	4	41.0	1.000	387.0	1.000	—	—	—	—	24.6	0.600	260.0	0.672	24.6	0.600	282.5	0.729	24.6	0.600	387.0	1.000
	5	109.3	1.000	61.2	1.000	—	—	—	—	66.0	0.603	36.8	0.600	74.0	0.677	36.8	0.600	65.6	0.600	36.8	0.600
	6	55.1	1.000	353.0	1.000	—	—	—	—	33.1	0.600	260.0	0.736	33.1	0.600	212.0	0.600	33.1	0.600	353.0	1.000
	7	221.5	1.000	111.6	1.000	—	—	—	—	180.0	0.812	66.8	0.600	180.5	0.815	66.8	0.600	142.0	0.642	66.9	0.600
	8	45.6	1.000	362.5	1.000	—	—	—	—	27.4	0.600	260.0	0.717	27.4	0.600	264.5	0.729	27.4	0.600	362.5	1.000
	9	85.7	1.000	84.8	1.000	—	—	—	—	57.5	0.600	50.9	0.600	51.5	0.600	50.9	0.600	51.5	0.600	50.9	0.600
	10	56.0	1.000	372.0	1.000	—	—	—	—	33.6	0.600	260.0	0.698	33.7	0.600	267.5	0.718	33.6	0.600	272.0	1.000
	10	266.1	1.000	58.9	1.000	—	—	—	—	260.0	0.976	35.4	0.600	226.5	0.850	35.4	0.600	168.0	0.631	35.4	0.600
	12	22.4	1.000	127.1	1.000	—	—	—	—	13.5	0.600	83.3	0.656	13.5	0.600	114.5	0.900	13.5	0.600	127.1	1.000
	13	22.4	1.000	127.1	1.000	—	—	—	—	13.5	0.600	83.3	0.656	13.5	0.600	114.5	0.900	13.5	0.600	127.1	1.000

Une évaluation des solutions obtenues peut être effectuée sur la sécurité à ruine plastique et sur les volumes d'armature de flexion nécessaire.

Pour un facteur minimal de charge à plastification $\gamma_1 = 1.2$ et pour les facteurs moyens de charge, γ_0 correspondant pour chaque exemple aux rapports G/P de la fig. 7, on obtient les valeurs minimales admissibles $xj \geqslant \gamma_1/\gamma_0$ du tableau 9.

Tableau 8: Valeurs minimales de $x_j(\geqslant \gamma_1/\gamma_0)$ admissibles

Exemple	1	2	3	4	5	6
γ_0	1.685	1.700	1.700	1.714	1.700	2.000
min. x_j	0.712	0.706	0.706[1]	0.700	0.706	0.600

[1] Pour la méthode de Sawyer min $x_j = 0.825$ et 0.818 à cause de la valeur $\gamma_1 = 1.39$ qu'il recommande.

Les mécanismes de ruine plastique des six structures sont identifiés en fig. 8. Les solutions des tableaux 5 à 7 sont utilisées pour déterminer les facteurs de surcharge à ruine γ_i pour chaque mode possible i. Ces valeurs permettent de calculer l'indice de sécurité à la ruine $u_i = \gamma_i/\gamma_0$ du tableau 10 avec les facteurs γ_0 du tableau 8.

Tableau 9: Sécurité à la ruine: indices u_i

Exemple	Mécanisme (i)	Théorie élastique	Sawyer	Baker	S.R.P.	S.R.T.	S.D.O.
1	1	1.381	1.269	1.029	1.205	1.000	1.000
	2	1.170	1.042	1.025	1.000	1.000	1.000
	3	1.164	1.063	1.022	1.000	1.000	1.000
2	1	1.095	—	1.028	1.000	1.000	1.000
	2	1.100	—	1.022	1.008	1.000	1.000
	3	1.122	—	1.022	1.028	1.000	1.000
3	1	1.285	1.150	1.052	1.028	—	1.075
	2	1.292	1.116	1.045	1.055	—	1.000
	3	1.975	1.810	1.618	1.542	—	1.396
	4	1.170	1.130	1.030	1.000	—	1.020
	5	1.160	1.100	1.012	1.000	—	1.000
	6	1.170	1.118	1.025	1.000	—	1.000
4	1	1.189	—	1.035	1.000	1.000	1.000
	2	1.389	—	1.022	1.121	1.000	1.000
	3	1.405	—	1.023	1.143	1.000	1.000
5	1	1.116	—	1.029	1.000	1.000	1.000
	2	1.240	—	1.021	1.112	1.000	1.000
	3	1.247	—	1.023	1.118	1.000	1.000
6	1	1.235	—	1.034	1.000	—	1.000
	2	1.387	—	1.054	1.003	—	1.000
	3	1.235	—	1.034	1.000	—	1.000
	4	4.060	—	2.520	2.950	—	3.000
	5	1.241	—	1.018	1.000	—	1.000
	6	1.258	—	1.004	1.000	—	1.050
	7	1.273	—	1.056	1.002	—	1.019
	8	1.325	—	1.020	1.031	—	1.110

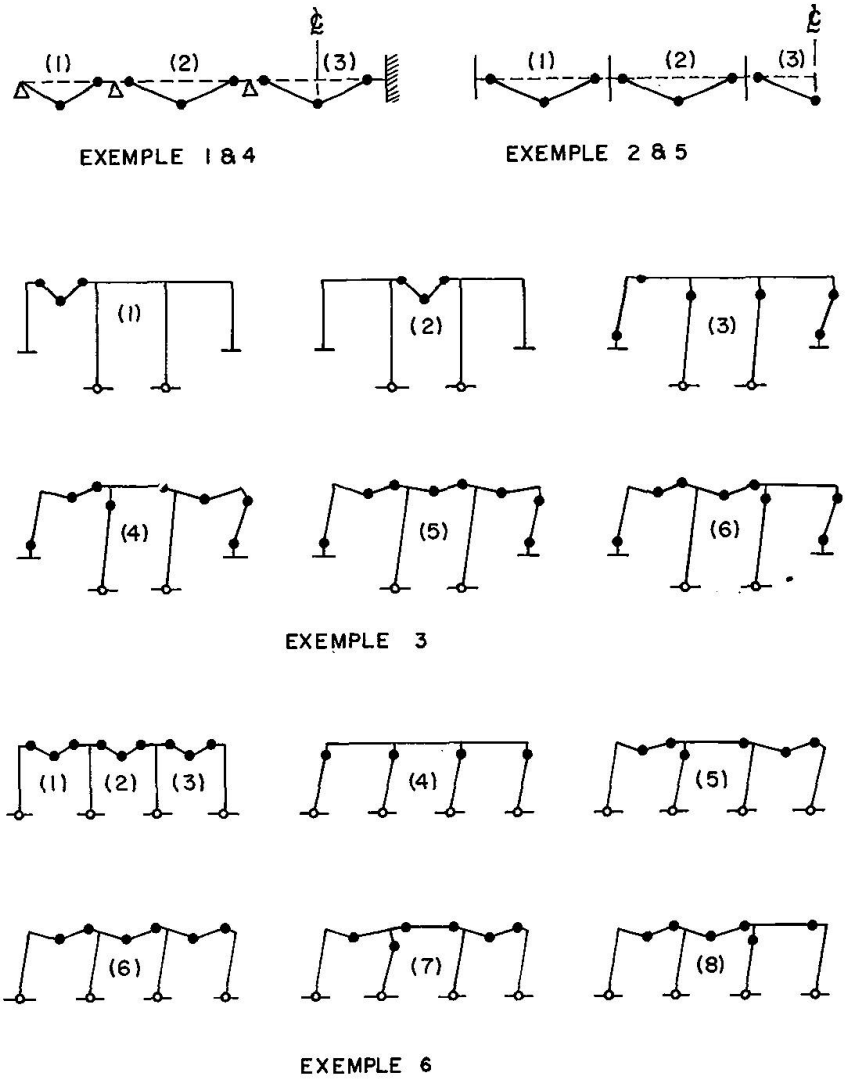

Fig. 8. Mécanismes de ruine plastique des structures de la fig. 7.

Le tableau 9 montre que les méthodes considérées dans la première ligne conduisent à des solutions dont les réserves de sécurité — par rapport aux spécifications des normes – diminuent vers la partie droite du tableau. A l'extrémité gauche, le calcul élastique assure au moins 10% de plus que le minimum de sécurité requis, tandis qu'à l'extrémité droite les solutions de redistribution totale (et optimales) conduisent à des modes de ruine plastiques aux charges ultimes spécifiées ($u_i = 1$).

La comparaison des quantités d'armatures nécessaires pour diverses méthodes a été effectuée en supposant que les sections de béton sont identiques pour toutes les solutions, que l'armature en flexion est proportionnelle au moment plastique de la section, et qu'elle est détaillée (pour toutes les solutions); cf. aux schémas typiques de la fig. 9.

Les valeurs des indices de rendement $v_k = V_k/V_e$ ainsi obtenues sont indiquées dans le tableau 10.

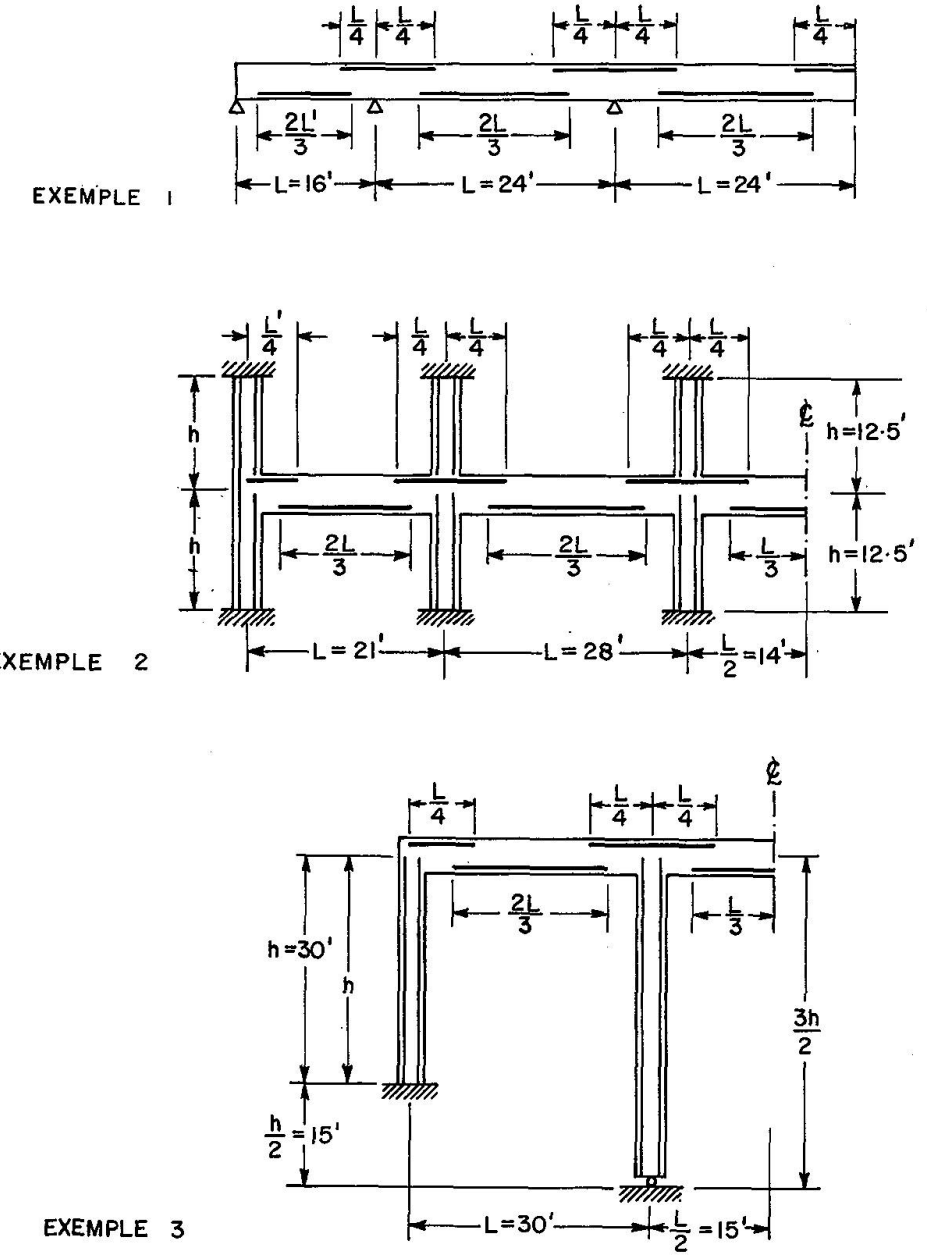

Fig. 9. Détails d'armature des structures de la fig. 7.

Tableau 10: Indice de rendement v_k

Exemple	Méthode élastique	Compatibilité		Equilibre		Méthode optimale
		Sawyer	Baker	Red. part.	Red. tot.	
1	1.000	0.907	0.877	0.868	0.850	0.825
2	1.000	—	0.948	0.927	0.922	0.890
3	1.000	0.926	0.934	0.790	—	0.760
4	1.000	—	0.793	0.831	0.768	0.766
5	1.000	—	0.897	0.909	0.866	0.829
6	1.000	—	0.772	0.757	—	0.756

Bien entendu, nous remarquons que, sur l'aspect économique, les diverses méthodes se placent dans le sens inverse aux réserves de sécurité qu'elles produisent: les méthodes optimales et à redistribution totale ont les indices de rendement les plus réduits et donc permettent les plus importantes économies de matériau par rapport à la méthode élastique.

Néanmoins, pour les six exemples de cette application, les méthodes inélastiques permettent des économies d'acier relatives allant de 5.2 à 25%.

Pour tous les exemples et les méthodes considérés (sauf les solutions extrêmes élastique et optimale), l'indice de rendement moyen est $v = 0.852$, ce qui suggère une économie de 15% vis-à-vis de la méthode élastique conventionnelle.

Il ne paraît pas trop optimiste à suggérer que des réductions de l'ordre de 15 à 20% des quantités d'acier soient parfaitement réalisables par l'utilisation des solutions à redistribution partielle ou totale, en préférence aux solutions élastiques présentes.

Conclusions

1. De nombreuses normes structurales existantes permettent la prise en compte des phénomènes inélastiques en béton armé, moyennant une redistribution plus ou moins arbitraire des sollicitations élastiques.

2. Le taux de redistribution autorisé par diverses normes varie de 0 à 66% des valeurs élastiques et ne peut pas être justifié par une base rationnelle. A la limite, il peut violer sévèrement les critères de serviçabilité.

3. Quelques normes (comme celles de l'URSS, des Etats-Unis et de la Grande-Bretagne) font dépendre les redistributions admissibles à la seule satisfaction de la compatibilité des rotations inélastiques, exprimée par une limitation de la fragilité des sections critiques (pourcentage d'armature en traction ou hauteur de l'axe neutre).

4. Parmi les méthodes plus exactes de calcul non élastique, les méthodes de «compatibilité», qui vérifient l'admissibilité des déplacements plastiques, sont assez complexes dans leurs applications et demandent une étude spéciale des conditions de service.

5. Les méthodes d'«équilibre» permettent un dimensionnement direct et paraissent plus aptes pour la pratique, ce qui est dû au fait qu'elles opèrent sur des sollicitations et tiennent compte implicitement de la satisfaction des critères de service.

6. L'utilisation des fonctions objectives convenables permet d'optimiser les solutions, de manière qu'elles préservent les marges de sécurité choisies, tant vis-à-vis de la ruine totale de la structure que de l'effondrement local de ses sections critiques.

7. Des études parallèles de dimensionnement des poutres et portiques par les méthodes d'équilibre et d'optimisation mathématique démontrent que des solutions quasi optimales peuvent être obtenues en maximisant l'adaptation plastique compatible avec les données du problème.

8. Il est déjà possible d'énoncer des recommandations simples et pratiques pour le calcul non élastique des poutres, dalles à armature unidirectionnelle et portiques en béton armé, en partant des concepts des méthodes d'équilibre. L'introduction et l'application graduelle de ces méthodes dans la pratique des

projets rétablira leur prestige, car elles présenteront un réel profit sur le plan économique et, d'autre part, elles établiront les limitations inhérentes à l'utilisation des phénomènes inélastiques en béton armé.

Annexe

RÈGLES POUR LA REDISTRIBUTION DES MOMENTS PRÉSENTÉES DANS DIFFÉRENTES NORMES

Recommandations C.E.B. – R.33.11 [12]

Dans les ossatures en béton armé (et seulement dans ce cas), on peut admettre, sans contrôle de la compatibilité de la déformation, une redistribution des moments calculés élastiquement: les moments maximaux de certaines sections peuvent être affectés d'une réduction maximale de 15%, à condition de prendre en compte l'augmentation des moments dans les autres parties de l'ossature, qui est nécessaire pour assurer l'équilibre.

ACI 318-71 – Cl. 8.6 [10]

Sauf dans le cas où l'on emploie des valeurs approchées des moments fléchissants, les moments négatifs calculés par la théorie élastique sur les appuis des éléments fléchis continus (sans précontrainte) pour toute combinaison de charges peuvent être augmentés ou réduits sans dépasser $20\,[1-(\omega-\omega')/\omega_b]\%$.

Ces moments négatifs modifiés doivent être utilisés pour le calcul des moments dans les sections de portée. La redistribution ne sera effectuée qu'à condition que la section dont le moment est réduit est détaillée, de telle sorte que w ou $w-w'$ ne dépasse pas $0{,}5\ w_b$, soit:

$$\omega_b = \frac{0{,}85\ \beta_1 f_c'}{f_y} \cdot \frac{87000}{87000 + f_y}$$

(et $\beta_1 = 0{,}85$ est une constante variant avec la qualité du béton, f_c' est la résistance cylindrique du béton et f_y la limite d'écoulement de l'acier en traction exprimées en psi).

I 123–50 [21]

Cl. 24

Pour l'analyse plastique des poutres continues principales à portées égales ou inégales et des portiques, il est nécessaire d'effectuer d'abord une analyse élastique conventionnelle.

Cl. 25

La redistribution des moments doit être limité à un maximum de 30% par rapport à l'analyse élastique conventionnelle.

Cl. 26

La redistribution des efforts doit être effectuée pour chaque cas de combinaison défavorable de surcharges.

BSI CP 110 Cl. 3.2.2.3 [14]

La redistribution des moments obtenue par une analyse élastique rigoureuse ou par les méthodes simplifiées indiquées en 3.2.2.1. et 3.2.2.2. peut être effectuée sous les conditions suivantes:

1. L'équilibre entre les sollicitations internes et les charges appliquées doit être maintenu sous chaque combinaison des charges ultimes.
2. Les moments de résistance limite des sections ne doivent pas être inférieurs à 70% des moments correspondants obtenus à partir de l'enveloppe des moments élastiques pour les combinaisons les plus défavorables des charges limites.
3. Le moment élastique en toute section d'un élément, dû à une combinaison particulière des charges limites, ne doit pas être réduit de plus de 30% de la valeur du moment maximal de l'enveloppe élastique.
4. Lorsque, comme suite de la redistribution, le moment de résistance limite d'une section est réduit, la hauteur relative de l'axe neutre ($\alpha = c/h$) de la section ne doit pas dépasser la valeur $\alpha_{max} = 0{,}6 - y$, où y est le rapport entre le moment réduit et le moment de l'enveloppe élastique calculée pour les combinaisons les plus défavorables des charges limites.
   Dans les structures à plus de quatre étages, où la stabilité latérale est assurée par l'ossature, la réduction des moments permise par la condition (3) ci-dessus sera limitée à 10%. En général, la condition (4) exclut la possibilité de redistribution et de réduction des moments dans les poteaux, sauf pour le cas où la force axiale est petite.

DS 411-49 Cl. 21 [16]

Les structures hyperstatiques peuvent être projetées sur la base des principes de l'élasticité, de la plasticité ou de l'encastrement partiel. En utilisant la théorie plastique, les moments élastiques peuvent être réduits jusqu'au tiers de leur valeur.

Remerciements

Les résultats présentés dans cette étude font partie d'un programme de recherches sur «le comportement inélastique des structures en béton armé» conduit par l'auteur au Département de génie civil de l'Université de Waterloo, avec l'assistance du Conseil national de la recherche du Canada (subvention A.4789) et de la Direction des Affaires scientifiques de l'OTAN (subvention N° 693).

L'auteur tient à remercier M. le professeur Giulio Maier, qui l'a invité à présenter cette étude dans le cadre du cours de spécialisation sur le Calcul à rupture des structures, qui a eu lieu à Politecnico di Milano, 24-26 juin 1974.

Bibliographie

1. BACH, C., GRAF, O.: Etudes expérimentales sur les Poutres encastrées (en allemand). Deutscher Ausschuss für Eisenbeton, H. 45, W. Ernst & Sohn, Berlin, 1920.
2. KAZINCZY, G.: La Plasticité du béton armé (en allemand). Beton und Eisen, V. 32, H. 5, 1973, pp. 74–80.
3. COHN, M.Z.: Limit Design for Reinforced Concrete Structures; an Annotated Bibliography. ACI Bibliography, No. 8, Detroit, Mich., 1970.
4. BRUMFITT, E.: Bibliography 1968-1972 in Inelasticity and Non-Linearity of Structural Concrete. (M.Z. Cohn Editor), SM Study No. 8, Univ. of Waterloo Press, 1972, pp. 513–522.
5. MACCHI, G.: Limit States Design of Statically Indeterminate Structures Composed of Linear Members. Costruzioni in Cementi Armato, Studi i Rendiconti, V. 6, 1969.
6. CEB COMMISSION XI HYPERSTATIQUE: Rapport sur la Session de Monaco. Bulletin d'Information CEB, N° 34, oct. 1961, pp. 32–73.
7. ICE RESEARCH COMMITTEE: Report on Ultimate Load Design of Concrete Structures. Proc. Inst. of Civ. Eng., V. 21, fev., oct., nov., 1962, V. 22, juin 1963.
8. WINTER, G., COHN M.Z.: Contributions to the International Symposium on Flexural Mechanics of Reinforced Concrete. Miami, Flo., nov. 1964, ACI SP-12, 1965, pp. 581–590, 591–594.
9. LEONHARDT, F., LEVI, F., RÜSCH, H.: Contributions au Bulletin d'Information CEB, N° 55: mai 1966, pp. 60–71, 131–153 et 154–158.
10. ACI 318-71: Building Code Requirements for Reinforced Concrete. ACI Publications, Detroit, 1971.
11. NTU 123-55: Normes techniques pour le dimensionnement des éléments en béton et béton armé (en russe). Grosstrojizdat, Moscou, 1955.
12. C.E.B.: Recommandations internationales pour le calcul et l'exécution des ouvrages en béton. Bulletin d'information CEB, N° 84, mai 1972.
13. CCBA 68: Règles techniques de conception et de calcul des ouvrages et constructions en béton armé. Soc. Dif. Tech. du Bâtiment et des Travaux publics, mai 1968.
14. BSI, CP 110-72: Code of Practice for the Structural Use of Concrete. British Standard Institution, London, 1972.
15. DIN, 1045-1972: Béton et béton armé, calcul et exécution (en allemand). Com. all. pour le béton armé, Berlin, 1972.
16. DS, 411-49: Danish Engineering Norms for Civil Engineers, Concrete and Reinforced Concrete Structures (en danois). Danish Standard Institution, Copenhagen, 1948.
17. HANGAN, M.D.: Le Calcul des structures hyperstatiques dans le domaine plastique. Annales de l'ITBTP, V. 16, N° 183-184, mars-avril 1963, pp. 299–324.
18. BERWANGER, C.: Limit Design by Successive Moment Distribution. Journal ASCE Struct. Div., V. 92, No. ST. 1, fév. 1966, pp. 405–430.
19. FERRY-BORGES, J., ARANTES, E., OLIVEIRA, E.R.: Non-Linear Analysis of Reinforced Concrete Structures. IBSE Publications, V. 23, 1963, pp. 51–70.
20. CRANSTON W.: Computer Method for Inelastic Analysis of Plane Frames. CCA Technical Report, TRA 386, mars 1965.
21. I 123-50: Instructions concernant le calcul des Structures hyperstatiques en béton armé, compte tenu de la redistribution des efforts. N.1.1.Zh.B., Moscou, 1961, traduction française dans le Bulletin d'information CEB, N° 28, Paris, oct. 1960.
22. COHN, M.Z.: Limit Design Solutions for Concrete Structures. Proc. ASCE, Journal Struct. Div. V. 93, No. ST.1, fév. 1967, pp. 37–58.
23. BAKER, A.L.L.: Limit State Design of Reinforced Concrete. Cement and Concrete Association, London, 1971.
24. BAKER, A.L.L.: Calcul des structures hyperstatiques par la méthode simplifiée bilinéaire de la Charge ultime. Annexes aux Recommandations CEB pour le calcul et l'exécution des ouvrages en béton, tome 3, AITEC, Rome 1972, pp. 219–312.
25. SAWYER, H.A.: Design of Concrete Frames by two Failure Stages. Proc. International Symposium on «Flexural Mechanics of Reinforced Concrete», Miami, Flo. nov. 1964, ACI SP. Publications SP-12m 1945, pp. 405–438.
26. SAWYER, H.A.: Comprehensive Design of Reinforced Concrete Frames by Plasticity Factors. Bulletin d'information CEB, No. 53, janvier 1966, pp. 299-316.

27. MACCHI, G.: Calcul des structures hyperstatiques par la méthode des rotations imposées. Annexes aux Recommandations Internationales CEB pour le calcul et l'exécution des ouvrages en béton, tome 3, AITEC, Rome, 1972, pp. 315–368.
28. COHN, M.Z., BURNETT, E.F., GRIERSON, D.E.: Safety, Serviceability and Efficiency of Reinforced Concrete Beams and Frames. Publications IABSE, V. 29-2. 1969, pp. 17–32.
29. COHN, M.Z., BURNETT, E.F., GRIERSON, D.E., DUTT, O., FRANCIS, R., PARAMESWAR, H.C., TALWAR, S.: Application of Limit Design to Reinforced Concrete Building Structures. Proc. ICE (London) 1970, Suppl. XVII, Paper 7335 S. pp. 375–414.
30. DE DONATO, O., MAIER, G.: Mathematical Programming Methods for the Inelastic Analysis of Reinforced Concrete Frames Allowing for Limited Rotation Capacity. Int. Jour. Numerical Methods in Engng., V. 4, 1972, pp. 307–329.
31. MAIER, G., DE DONATO, O., CORRADI, L.: Inelastic Analysis of R.C. Frames by Quadratic Programming in Inelasticity and Non-Linearity in structural Concrete. SM. Study No. 8, Univ. of Waterloo Press, pp. 265–288.
32. ACI-ASCE Joint Committee 428: Progress Report on Code Clauses for Limit Design et Comments on Model Code Clauses, par H.A. Sawyer, ACI Journal, No. 9, sept. 1968, pp. 713–719.
33. COHN, M.Z.: Optimum Limit Design for Reinforced Concrete Continuous Beams. Proc. ICE (London), V. 30, avril 1965, pp. 17–32.
34. COHN, M.Z.: Limit Design of Reinforced Concrete Frames: Journal Struct. Div. ASCE, V. 94, No. ST.10, oct. 1968, pp. 2467–2483.
35. COHN, M.Z.: Rotation Compatibility in the Limit Design of Reinforced Concrete Continuous Beams. Proc. Int. Symposium on «Flexural Mechanics of Reinforced Concrete», Miami, Flo., nov. 1964, ACI Publications SP-12, 1965, pp. 359–382.
36. COHN, M.Z., GRIERSON, D.E.: Optimal Design of Reinforced Concrete Beams and Frames. Final Publication 8th IABSE Congress, N.Y., sept. 1968, pp. 215–226.
37. COHN, M.Z., GRIERSON, D.E.: Further Results on the Equilibrium Method for Limit Design. Proc. ICE (London), V. 6, juin 1970, pp. 143–168.
38. COHN, M.Z.: Dimensionnement à l'état limite des ossatures en Béton armé. Costruzioni in Cemento Armato, Studi i Rendiconti, V. 11, 1974.
39. COHN, M.Z.: Optimisation des structures en béton et optimisation en construction. Colloque au Collège international de la science des constructions, Saint-Rémy-lès-Chevreuse, 6-9 nov. 1973.
40. COHN, M.Z.: Equilibrium (Serviceability) Methods of Limit Design for Concrete Frames. Proc. ICE (London), Paper 7514 S, Supplement XIV, 1972, pp. 263–275.
41. COHN, M.Z.: Analysis and Design of Inelastic Structures. SM Text G1, V. 2, Applications, Univ. of Waterloo Press, 1972.
42. COHN, M.Z. (editor): Inelasticity and Non-Linearity in Structural Concrete. SM Study No. 8, Univ. of Waterloo Press, 1973.

Résumé

L'article passe en revue la pratique actuelle des normes officielles sur le comportement inélastique des poutres et portiques en béton armé et les perspectives d'application des principales méthodes inélastiques, à savoir les méthodes dites de «compatibilité» et d'«équilibre».

Après la présentation de propositions concernant la redistribution arbitraire des moments élastiques selon divers règlements européens et américains, on examine les principes des méthodes de compatibilité et d'équilibre.

Quelques exemples d'application aux poutres, dalles et portiques permettent une comparaison des résultats obtenus selon diverses méthodes du point de vue de la résistance, de la sécurité à la ruine, des conditions de service, ainsi que du rendement de ces solutions par rapport à la méthode élastique traditionnelle.

Zusammenfassung

Der Artikel behandelt der Reihe nach die verschiedenen heute gültigen offiziellen Normen in Bezug auf das nicht elastische Verhalten von Stab- und Rahmentragwerken aus Stahlbeton sowie die verschiedenen Gesichtspunkte einer Anwendung der wesentlichen nicht elastischen Methoden, d.h. der „Verträglichkeitsmethode" und der „ Gleichgewichtsmethode".

Nach einer Übersicht der Normenbestimmungen bzgl. willkürlicher Neuverteilung der elastisch ermittelten Momentenverteilung gemäss verschiedenen europäischen und amerikanischen Regeln werden die Prinzipien der Verträglichkeits- und Gleichgewichtsmethoden untersucht.

Einige Anwendungsbeispiele an Balken, Platten und Rahmentragwerken gestatten einen Vergleich der anhand verschiedener Methoden erhaltenen Ergebnisse für Widerstand, Bruchsicherheit und Gebrauchsbedingungen, sowie der Auswirkung dieser Ergebnisse in Bezug auf die traditionelle elastische Methode.

Summary

The paper reviews the current practice considering the inelastic action in reinforced concrete beams and frames, as allowed by some standard codes of practice. Also, it discusses the prospect of applications of the main inelastic methods, in particular the "compatibility" and "equilibrium" methods.

After the provisions on arbitrary redistribution of elastic moments in various european and american standards are presented, the principles of the compatibility and equilibrium methods are briefly examined.

Some examples of application to beams, one-way slabs and frames allow comparisons of solutions obtained by various methods from the viewpoint of collapse safety, serviceability and efficiency versus the traditional, elastic (ultimate strength) design solutions.

Panel Method for Multistorey Flat Plate Structures

Calcul de structures en dalles plates à plusieurs étages

Berechnung von mehrstöckigen aus Flachdecken und Stützen bestehenden Bauwerken

S. FRENCH
Teaching Fellow

D.C. BLACK
Research Fellow

V.A. PULMANO
Senior Lecturer

A.P. KABAILA
Associate Professor

School of Civil Engineering, The University of New South Wales, Kensington, Australia.

Introduction

The continuing search for economy in buildings has led to the recognition of the contribution made by flat plate floors to the overall lateral structure stiffness. Current practice is to approximate each floor by equivalent beams spanning between the columns, in the direction of the lateral load. These may be used in the analysis of an equivalent frame as mentioned in most building codes, e.g. the ACI Code 1971 [1] and the SAA Code 1480-1974 [2]. This approach produces a very inadequate representation of the three dimensional behaviour of each floor. Transverse behaviour is only approximated by adding a torsional component to the column stiffness, whilst diagonal interaction is neglected completely. CARPENTER [3] found that the moment carried over longitudinally from one column to the next by the floor is less than that predicted by the ACI equivalent beam approximation. The ACI method, when estimating the effective width of the equivalent beam, takes no account of the effects of the dimensions of the column, or the plate. In addition, the equivalent frame method is generally applicable only to the internal bents in a structure.

To overcome these problems, this paper presents an alternative method of analysis, referred to here as the "Panel Method". This method considers a structural system consisting of columns and floor slab panels, which are defined by the grid of lines through the column centres in both directions. Once the bending stiffnesses of the panels are known, the structure is analysed by the stiffness procedures used for ordinary frame structures.

The bending stiffness of regular square column supported plates has been investigated by FAULKES [4] and SMITH [5], using non-conforming finite elements. They found that appreciable moments did not carry over more than one bay away

from the point of moment application. They were thus able to produce (8×8) matrices representing the moment stiffnesses of the three types of floor panels, namely the corner, edge and internal panels, as shown in Fig. 2.

In this paper the panel stiffnesses have been recalculated using compatible quadrilateral elements [6]. The scope has been expanded to include rectangular panels with an aspect ratio of 1.5:1 and also to include the vertical freedom at each node (Fig. 1). This inclusion is essential where column axial deformation effects are significant. The three freedoms at each node are thus $\left(w, \frac{\partial w}{\partial x}, \frac{\partial w}{\partial x}\right)$.

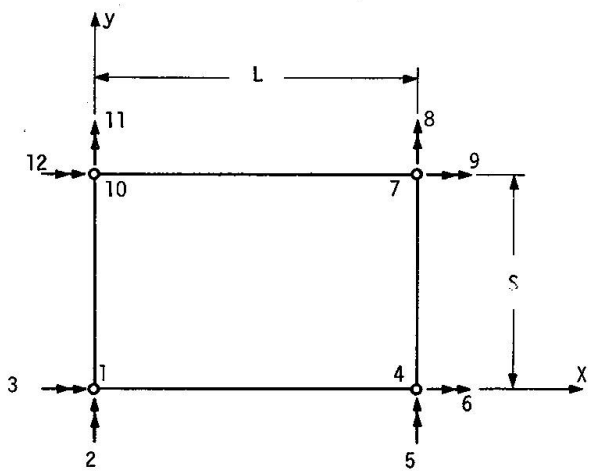

Fig. 1. 12 Degree of freedom panel.

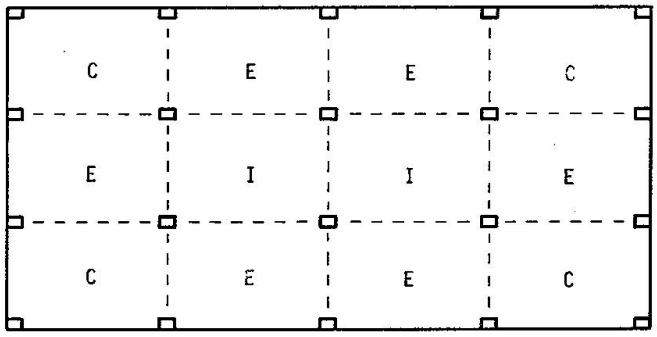

Fig. 2. Flat plate floor comprised of corner edge and internal panels.

The evaluation and the application of these stiffness matrices are described in this paper. Results have been obtained for three values of column/span (c/L), covering the normally used range. The stiffnesses of both rectangular and square panels are tested in multistorey building analyses. To provide a performance comparison, analyses of the buildings were also carried out using a complete finite element representation and the equivalent frame method.

Stiffness of Panel Element

Method of Obtaining Panel Stiffness

A finite element analysis was carried out for each of the panel configurations investigated. The plates considered were 4 × 4 bays. However, by utilizing symmetry only one quarter of each plate had to be analysed. Boundary conditions specified along the lines of symmetry represented either symmetry or antisymmetry.

Stiffness values at the columns were obtained by applying in turn unit displacements at each column freedom, the resultant forces at each freedom being the stiffness terms for that displacement.

Finite Elements Used in Obtaining Panel Stiffness

Compatible quadrilateral elements, as described by KABAILA *et al.* [6], were chosen for the analysis. Their superior performance has been demonstrated by BLACK *et al.* [7]. The meshes used for the square and rectangular cases are shown in Fig. 3b and c. To provide accurate modelling in regions of high curvature, the mesh grading technique of SOMERVAILLE [8] was used extensively.

Column axes were connected to the boundaries of abutting elements by "rigid arm".

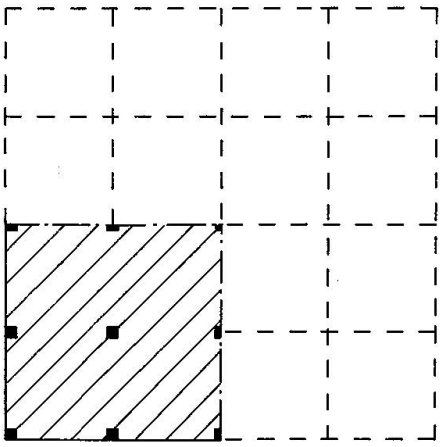

a) Quarter plate analysed.

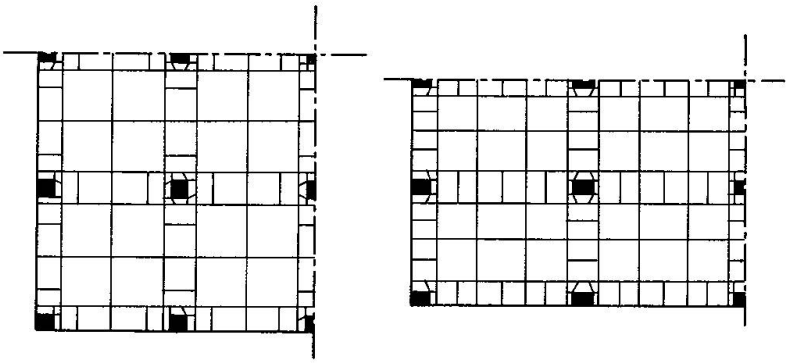

b) Square plate mesh. *c)* Rectangular plate mesh.

Fig. 3. 4 × 4 Bay plates used in stiffness generation.

Extraction of Panel Stiffnesses

Output from the finite element program consisted of the (27×27) stiffness matrix of the quarter plate for each value of c/L and each set of boundary conditions. Suitable combination of the boundary conditions produced the stiffness which would result from an analysis of the complete plate. The (12×12) stiffnesses of the corner, edge and internal panels were extracted from these results. The numerical value of each panel stiffness coefficient had to be divided by the number of panels through which that action was transmitted.

The non-dimensionalization of each panel stiffness followed the method of tabulation used by PRZEMIENIECKI [9]. First, the whole stiffness matrix was divided by D/LS, where $D = Et^3/12(1 - \mu^2)$ and L and S are the side lengths of the panel. This left factors of S and L in all rows and columns relating to the freedoms $\frac{\partial w}{\partial x}$ and $\frac{\partial w}{\partial y}$ respectively. The appropriate rows and columns were then divided by S or L as indicated in the tables. This procedure, on reversal, gives the stiffness of any size panel with that aspect ratio.

Tables 1 to 3 give the non-dimensionalized stiffness coefficients for corner, edge and internal square panels respectively. The three values in each square of the tables are the stiffness values for column/span ratios of 1/8, 1/16 and 1/20 respectively. Similarly, Tables 4 to 7 give the stiffness matrices for rectangular panels which have an aspect ratio of 1.5:1 and the same column/span ratio in both directions. Four tables are required in this case because the edge panels may have either their long or short sides along the free edge.

Illustrative Examples

To use the tabulated stiffnesses it is necessary only to reintroduce values of the appropriate parameters as described in the Appendix. Stiffness values for c/L ratios other than those tabulated may be obtained by interpolation. The matrices thus formed may then be used directly as input data for a three dimensional stiffness program. Assembly of the structure stiffness follows the same procedure as for other structural elements.

The performance of the panel method is demonstrated by the analysis of the two structures given below. A description of these buildings is followed by an outline of the two methods used for comparison.

Example 1: Interior Bay of a Ten Storey Building

To check the performance of the stiffness matrices of rectangular panels, one bay of the building shown in Fig. 4 was analysed by the panel method for a distributed lateral load. The structure has three bays in the transverse direction and is assumed to have many bays in the longitudinal direction. The columns have a uniform cross-section and are proportioned so that the column/span ratio (c/L) is 1/8 in each direction.

The building was also analysed using a full finite element solution and by the equivalent frame method. Displacement and column moment diagrams are given in Figs. 6, 7 and 8. The values are given in Table 8.

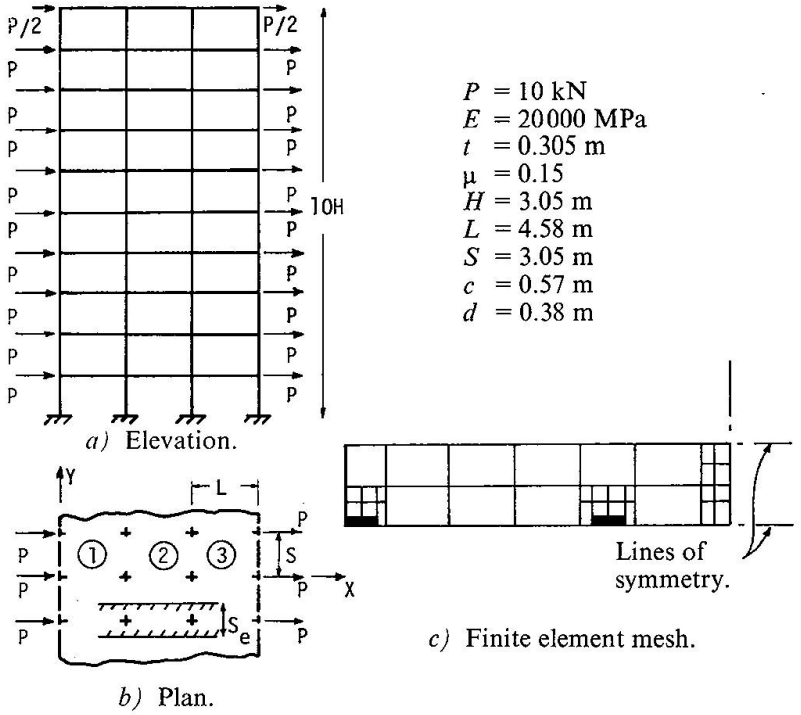

Fig. 4. Example 1: Interior bay of a 10 storey building.

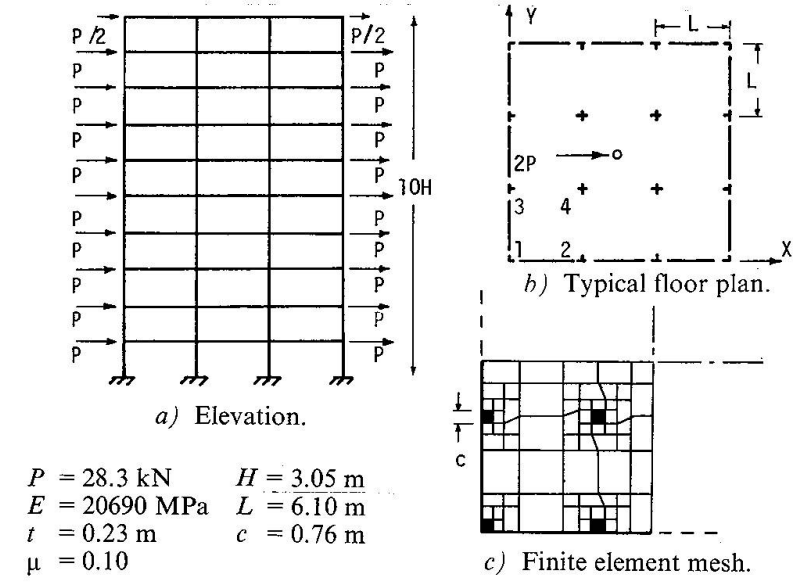

Fig. 5. Example 2: 3 × 3 bay 10 storey building.

Example 2: 3 × 3 Bay Ten Storey Building

This example demonstrates the manner in which horizontal shear loads are distributed within a structure. The building, whose details are given in Fig. 5 spans

three bays in each direction. The tabulated stiffnesses for $c/L = 1/8$ and aspect ratio = 1 were used. The results (Figs. 9a, 9b and Table 9) show the horizontal deflection and column shear forces for a uniformly distributed lateral load.

The power of the method over equivalent frame methods is also demonstrated by the analysis of the structure subjected to a distributed twist load. The rotations produced by this loading are plotted in Fig. 9c. For each loading case the full finite element solution results are also given.

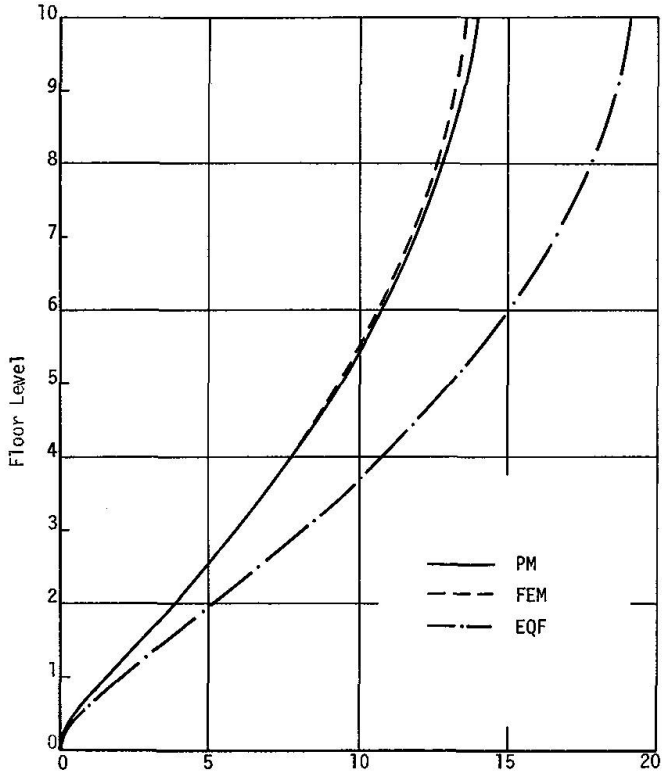

Fig. 6. Example 1: lateral deflection (mm).

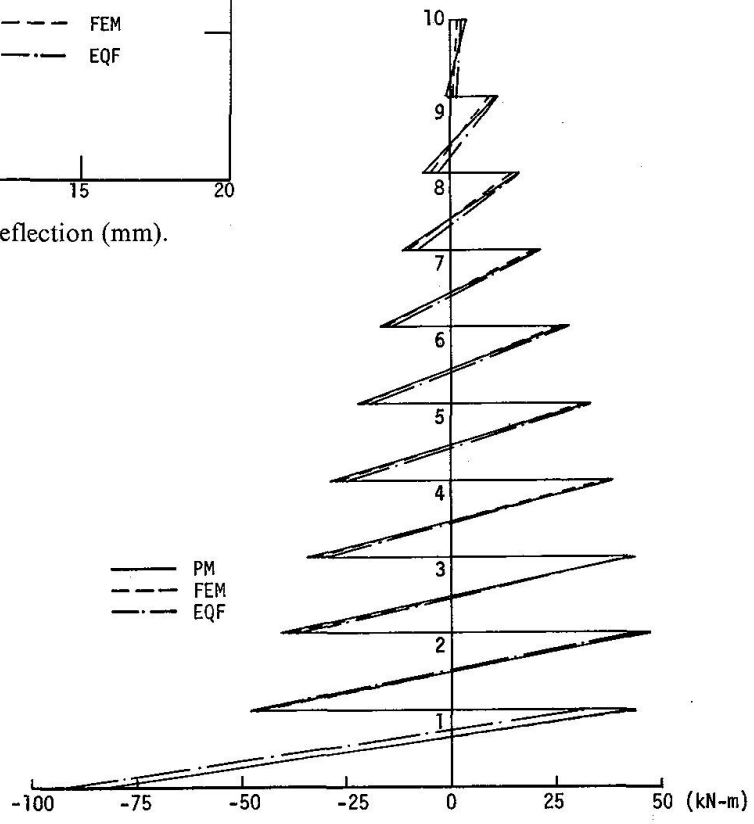

Fig. 7. Example 1: bending moment diagram of exterior column.

Finite Element Method (FEM)

Both structures were analysed using finite element meshes to represent the floor plate. Compatible quadrilateral elements were used in the substructure program described by PULMANO *et al.* [10]. The division of the floor plates into finite elements is shown in Figs. 4c and 5c. This method provides the closest available approximation to the elastic solution and its results are used as reference values.

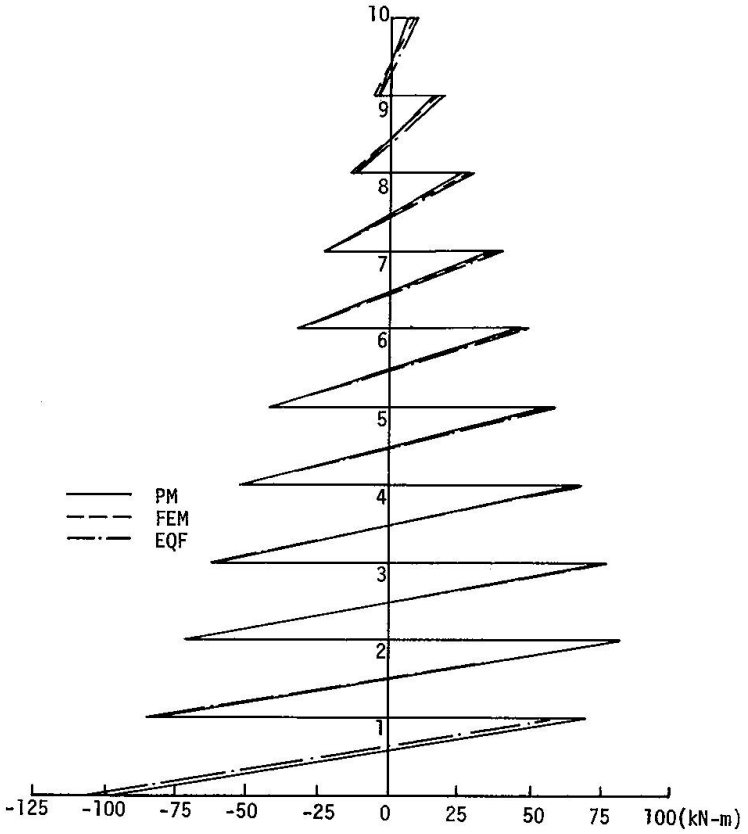

Fig. 8. Example 1 : bending moment diagram of interior column.

Equivalent Frame (EQF)

A two dimensional equivalent frame representation of the first example was analysed for the applied lateral loads. Several investigators have suggested various parameters with which to estimate a reliable value of the effective width (S_e) of the slab. QADEER and STAFFORD SMITH [11], by simultaneously rotating two columns of an internal panel using finite difference methods, produced a family of curves for effective width. In a discussion of this paper, MICHAEL [12] produced a single graph for effective width. From this graph the value of $S_e = 0.59S$ was obtained for example 1.

Note that the recommendations of both papers are only strictly valid for internal panels of an internal bay. In a structure such as that of example 2 the distribution of shear forces differs significantly from the assumed conditions thus rendering the effective width recommendations inapplicable.

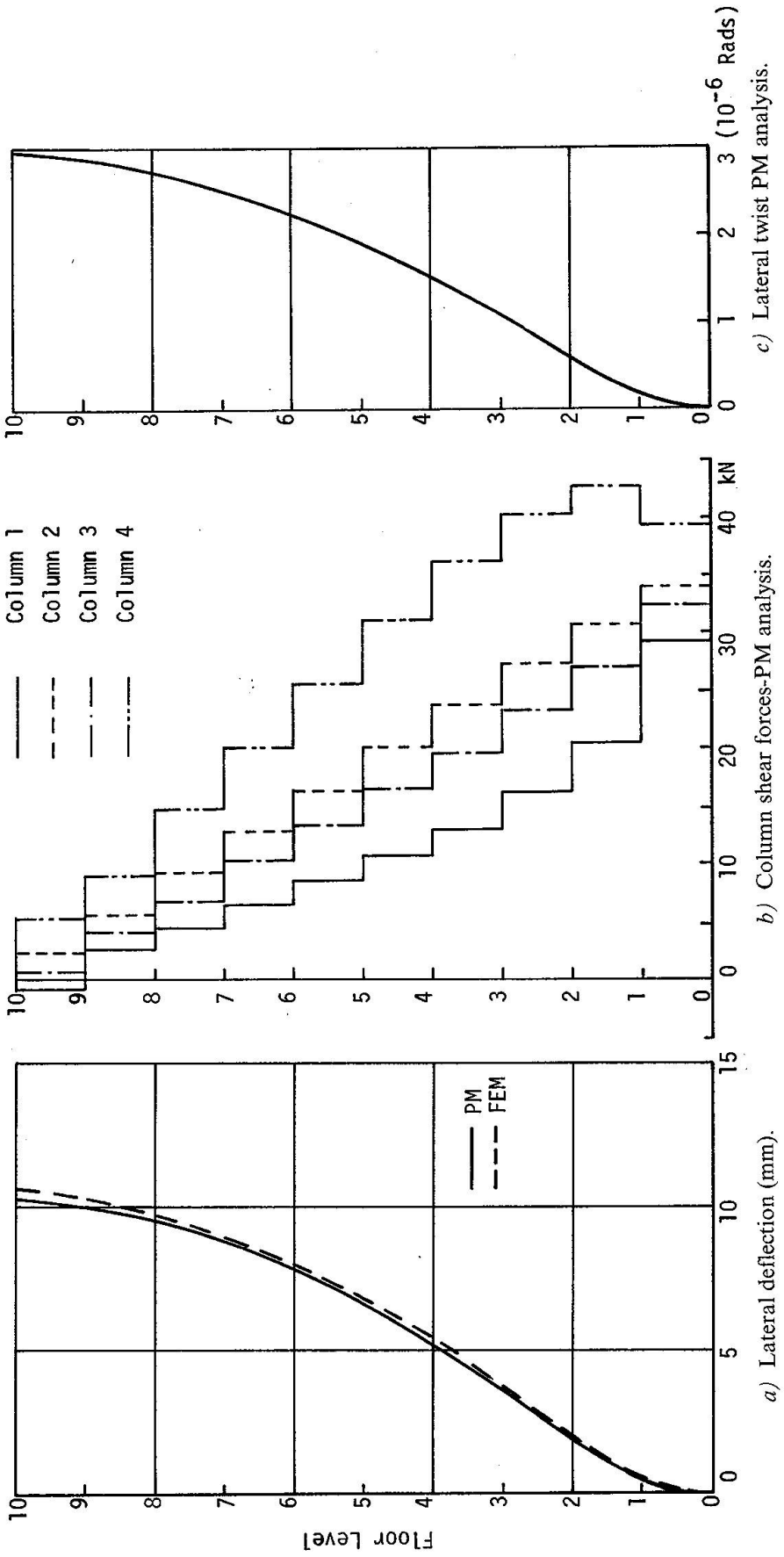

a) Lateral deflection (mm). *b)* Column shear forces-PM analysis. *c)* Lateral twist PM analysis.

Fig. 9. Example 2: lateral deflection, column shear and lateral twist diagrams.

Discussion of Results

The lateral deflection curves for both examples show close correlation between the panel method and the finite element method. The maximum difference, which is less than 2½%, is due to the difference between the finite element meshes used in the FEM solution and those used in generating the panel method (PM) stiffnesses. From the deflection and column moment results it can be concluded that both the square and rectangular PM stiffnesses provide a close approximation to the more sophisticated methods of analysis. The reduction in the number of unknowns and hence of storage requirements and computation cost savings, is an attractive feature.

In contrast with these results, the deflection at the top of the equivalent frame is 40% greater than the FEM value. This results from the failure of the method to properly reflect all the relevant parameters. Although the deflection predictions for this case are on the safe side, there is no guarantee that this will be maintained for other column and panel configurations.

The column shear force diagram for example 2, shown in Fig. 9b indicates the way in which shear forces are distributed within a flat plate building. Although the horizontal displacement of all columns is the same at each floor level, the interior columns carry the largest shear loads. This is due to the greater slab bending stiffness at these joints causing them to attract a greater share of the load. An equivalent frame analysis could not take this transverse redistribution into account.

Excellent correlation is achieved between the FEM and PM results for the second example when it is subjected to a distributed twist load. The analysis of non-symmetric structures or non-symmetric loading is not possible using the equivalent frame method.

Applications

Until the present time, the situation relating to the lateral analysis of flat plate structures has been one of conflict and uncertainty. The ACI Committee 442 on Response of Buildings to Lateral Forces [13] noted that little research has been done to represent the stiffness of flat plates which connect columns. In fact, available test results have shown that values for effective width of less than the full slab width [11], equal to the full width [14], and greater than full width [15] are valid under different circumstances.

This situation is greatly clarified by the application of the Panel Method to the analysis of these buildings. As the method accounts for all the dimensional parameters of the plate, the resultant stiffness is more accurate, thus giving greater reliability to the results. The danger of significantly over or underestimating the plate stiffness is effectively eliminated. The economy inherent in the concept of flat plate structures may thus be expected to be enhanced.

For regular structures, the implementation of the Panel Method is straightforward. The column centre to centre spans in each direction define the size of the panels and their aspect ratios (L/S). By following the method outlined in the Appendix,

the stiffness matrix of each panel may be tabulated. This data, plus the column stiffness matrices would then form the overall structure stiffness to which vertical and lateral loads may be applied. The analysis would then follow the stiffness analysis procedures of ordinary frame structures. Such an analysis would yield the moment transferred, and the movement of each column/slab joint. Any of several available mthods could then be used to design or check the details of the structural members.

Conclusions

In this paper, the proposed panel method of analysis for multistorey flat plate buildings under lateral and/or vertical loads has been presented. The method assumes a structural system which consists of columns and floor slab panels which are defined by adjacent column lines in both directions. The method has been shown to model plate behaviour with comparable accuracy to a refined finite element analysis. It achieves this with a smaller number of equations and hence with less computation cost.

The proposed structural system requires the least approximation of the actual structure whilst allowing for vertical, horizontal and twist loadings. The problems of determining the stiffness and carry over factors of conventional equivalent beams are eliminated whilst all the necessary parameters, particularly the column/span ratio, are included. Finally, the proposed method of analysis allows the moment resultants in the floor slabs to be defined more accurately, thereby enabling engineers to achieve greater economy and safety in the design of buildings with flat plate floors.

In each square, Row 1: c/L = 1/8
Row 2: c/L = 1/16
Row 3: c/L = 1/20

symmetric

	1	S	L	1	S	L	1	S	L	1	S	L
1	14.80 10.05 9.23											
S	3.68 2.23 1.98	2.38 1.49 1.33										
L	3.68 2.23 1.98	0.48 0.24 0.20	2.38 1.49 1.33									
1	-8.45 -6.15 -5.78	-3.17 -2.00 -1.80	-0.46 -0.25 -0.22	14.30 10.48 9.85								
S	2.99 1.84 1.63	0.91 0.47 0.40	0.15 0.07 0.06	0.02 0.03 0.04	2.23 1.44 1.29							
L	-0.56 -0.40 -0.38	-0.21 -0.14 -0.12	-0.27 -0.12 -0.10	3.35 2.30 2.11	0.00 0.00 0.00	2.11 1.43 1.30						
1	1.22 1.19 1.19	-0.26 -0.19 -0.17	-0.26 -0.19 -0.17	-7.31 -5.72 -5.46	0.02 0.03 0.03	-2.58 -1.76 -1.61	13.70 10.82 10.38					
S	0.22 0.17 0.16	0.15 0.09 0.08	0.10 0.06 0.06	0.02 0.03 0.03	-0.18 -0.10 -0.09	0.00 0.00 0.01	0.02 0.04 0.04	1.99 1.44 1.33				
L	0.22 0.17 0.16	0.10 0.06 0.06	0.15 0.09 0.08	2.41 1.62 1.47	0.00 0.00 0.00	0.69 0.39 0.34	0.02 0.04 0.04	0.00 0.00 0.00	1.99 1.43 1.33			
1	-8.45 -6.15 -5.78	-0.46 -0.25 -0.22	-3.17 -2.00 -1.80	1.11 1.06 1.06	0.14 0.07 0.06	-0.32 -0.25 -0.23	-7.31 -5.72 -5.46	2.41 1.62 1.47	0.02 0.03 0.03	14.30 10.48 9.85		
S	-0.56 -0.40 -0.38	-0.27 -0.12 -0.10	-0.21 -0.14 -0.12	-0.32 -0.25 -0.23	0.14 0.08 0.07	-0.15 -0.10 -0.09	-2.58 -1.76 -1.61	0.69 0.39 0.34	0.00 0.00 0.01	3.35 2.30 2.11	2.11 1.43 1.30	
L	2.99 1.84 1.63	0.15 0.07 0.06	0.91 0.47 0.40	0.14 0.07 0.06	-0.06 -0.02 -0.02	0.14 0.08 0.07	0.02 0.03 0.03	0.00 0.00 0.00	-0.18 -0.10 -0.09	0.02 0.03 0.04	0.00 0.03 0.00	2.23 1.44 1.29

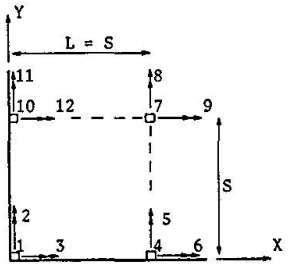

Table 1: Lower Triangular Stiffness Matrix for Square Corner Panel
[All values to be multiplied by $Et^3/12\,(1-\mu^2)\,LS$]

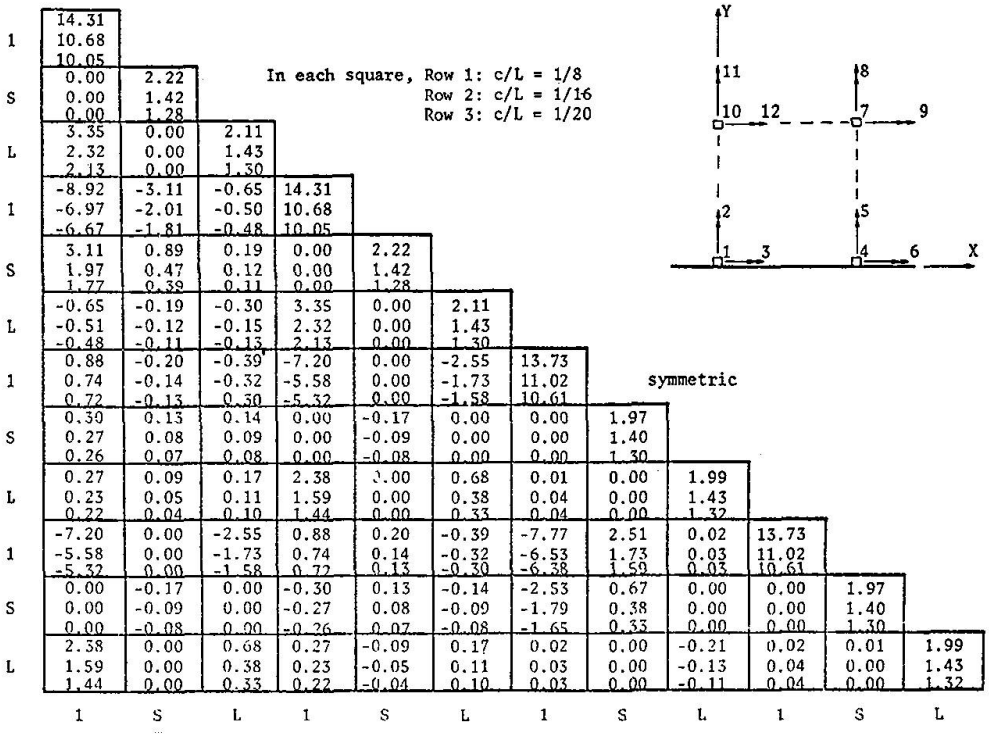

	1	S	L	1	S	L	1	S	L	1	S	L
1	14.31 10.68 10.05											
S	0.00 0.00 0.00	2.22 1.42 1.28										
L	3.35 2.32 2.13	0.00 0.00 0.00	2.11 1.43 1.30									
1	-8.92 -6.97 -6.67	-3.11 -2.01 -1.81	-0.65 -0.50 -0.48	14.31 10.68 10.05								
S	3.11 1.97 1.77	0.89 0.47 0.39	0.19 0.12 0.11	0.00 0.00 0.00	2.22 1.42 1.28							
L	-0.65 -0.51 -0.48	-0.19 -0.12 -0.11	-0.30 -0.15 -0.13	3.35 2.32 2.13	0.00 0.00 0.00	2.11 1.43 1.30						
1	0.88 0.74 0.72	-0.20 -0.14 -0.13	-0.39 -0.32 -0.30	-7.20 -5.58 -5.32	0.00 0.00 0.00	-2.55 -1.73 -1.58	13.73 11.02 10.61					
S	0.30 0.27 0.26	0.13 0.08 0.07	0.14 0.09 0.08	0.00 0.00 0.00	-0.17 -0.09 -0.08	0.00 0.00 0.00	0.00 0.00 0.00	1.97 1.40 1.30				
L	0.27 0.23 0.22	0.09 0.05 0.04	0.17 0.11 0.10	2.38 1.59 1.44	0.00 0.00 0.00	0.68 0.38 0.33	0.01 0.04 0.04	0.00 0.00 0.00	1.99 1.43 1.32			
1	-7.20 -5.58 -5.32	0.00 0.00 0.00	-2.55 -1.73 -1.58	0.88 0.74 0.72	0.20 0.14 0.13	-0.39 -0.32 -0.30	-7.77 -6.53 -6.38	2.51 1.73 1.59	0.02 0.03 0.03	13.73 11.02 10.61		
S	0.00 0.00 0.00	-0.17 -0.09 -0.08	0.00 0.00 0.00	-0.30 -0.27 -0.26	0.13 0.08 0.07	-0.14 -0.09 -0.08	-2.53 -1.79 -1.65	0.67 0.38 0.33	0.00 0.00 0.00	0.00 0.00 0.00	1.97 1.40 1.30	
L	2.38 1.59 1.44	0.00 0.00 0.00	0.68 0.38 0.33	0.27 0.23 0.22	-0.09 -0.05 -0.04	0.17 0.11 0.10	0.02 0.03 0.03	0.00 0.00 0.00	-0.21 -0.13 -0.11	0.02 0.04 0.04	0.01 0.00 0.00	1.99 1.43 1.32

Table 2: Lower Triangular Stiffness Matrix for Square Edge Panel
[All values to be multiplied by $Et^3/12\,(1-\mu^2)LS$]

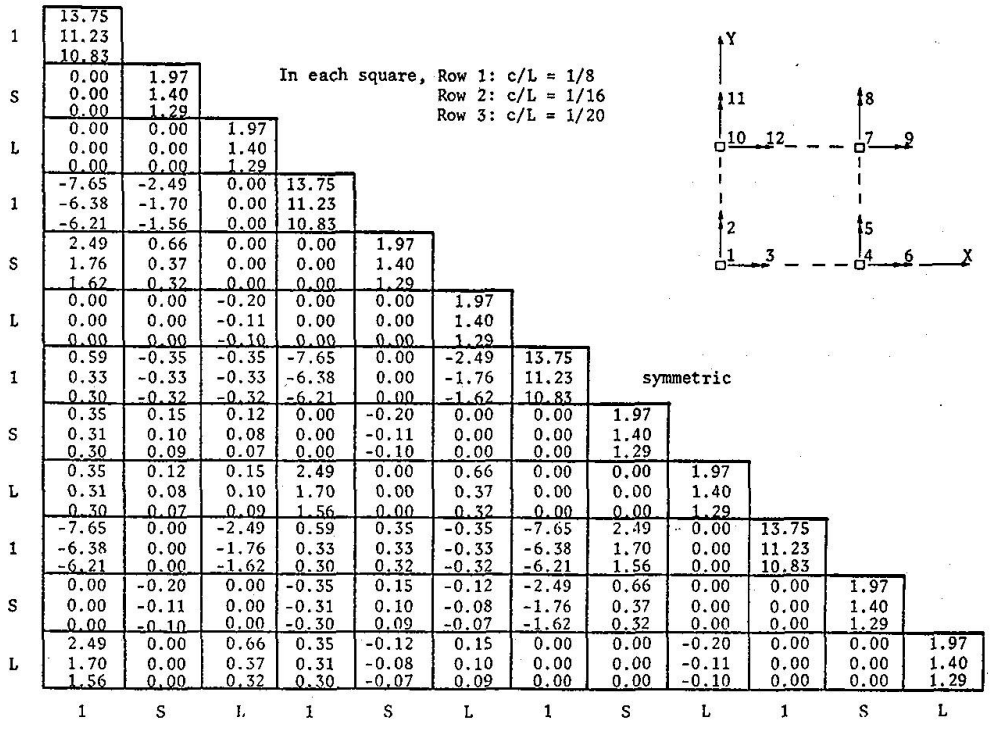

	1	S	L	1	S	L	1	S	L	1	S	L
1	13.75 11.23 10.83											
S	0.00 0.00 0.00	1.97 1.40 1.29										
L	0.00 0.00 0.00	0.00 0.00 0.00	1.97 1.40 1.29									
1	-7.65 -6.38 -6.21	-2.49 -1.70 -1.56	0.00 0.00 0.00	13.75 11.23 10.83								
S	2.49 1.76 1.62	0.66 0.37 0.32	0.00 0.00 0.00	0.00 0.00 0.00	1.97 1.40 1.29							
L	0.00 0.00 0.00	0.00 0.00 0.00	-0.20 -0.11 -0.10	0.00 0.00 0.00	0.00 0.00 0.00	1.97 1.40 1.29						
1	0.59 0.33 0.30	-0.35 -0.33 -0.32	-0.35 -0.33 -0.32	-7.65 -6.38 -6.21	0.00 0.00 0.00	-2.49 -1.76 -1.62	13.75 11.23 10.83					
S	0.35 0.31 0.30	0.15 0.10 0.09	0.12 0.08 0.07	0.00 0.00 0.00	-0.20 -0.11 -0.10	0.00 0.00 0.00	0.00 0.00 0.00	1.97 1.40 1.29				
L	0.35 0.31 0.30	0.12 0.08 0.07	0.15 0.10 0.09	2.49 1.70 1.56	0.00 0.00 0.00	0.66 0.37 0.32	0.00 0.00 0.00	0.00 0.00 0.00	1.97 1.40 1.29			
1	-7.65 -6.38 -6.21	0.00 0.00 0.00	-2.49 -1.76 -1.62	0.59 0.33 0.30	0.35 0.33 0.32	-0.35 -0.33 -0.32	-7.65 -6.38 -6.21	2.49 1.70 1.56	0.00 0.00 0.00	13.75 11.23 10.83		
S	0.00 0.00 0.00	-0.20 -0.11 -0.10	0.00 0.00 0.00	-0.35 -0.31 -0.30	0.15 0.10 0.09	-0.12 -0.08 -0.07	-2.49 -1.76 -1.62	0.66 0.37 0.32	0.00 0.00 0.00	0.00 0.00 0.00	1.97 1.40 1.29	
L	2.49 1.70 1.56	0.00 0.00 0.00	0.66 0.37 0.32	0.35 0.31 0.30	-0.12 -0.08 -0.07	0.15 0.10 0.09	0.00 0.00 0.00	0.00 0.00 0.00	-0.20 -0.11 -0.10	0.00 0.00 0.00	0.00 0.00 0.00	1.97 1.40 1.29

Table 3: Lower Triangular Stiffness Matrix for Square Internal Panel
[All values to be multiplied by $Et^3/12\,(1-\mu^2)LS$]

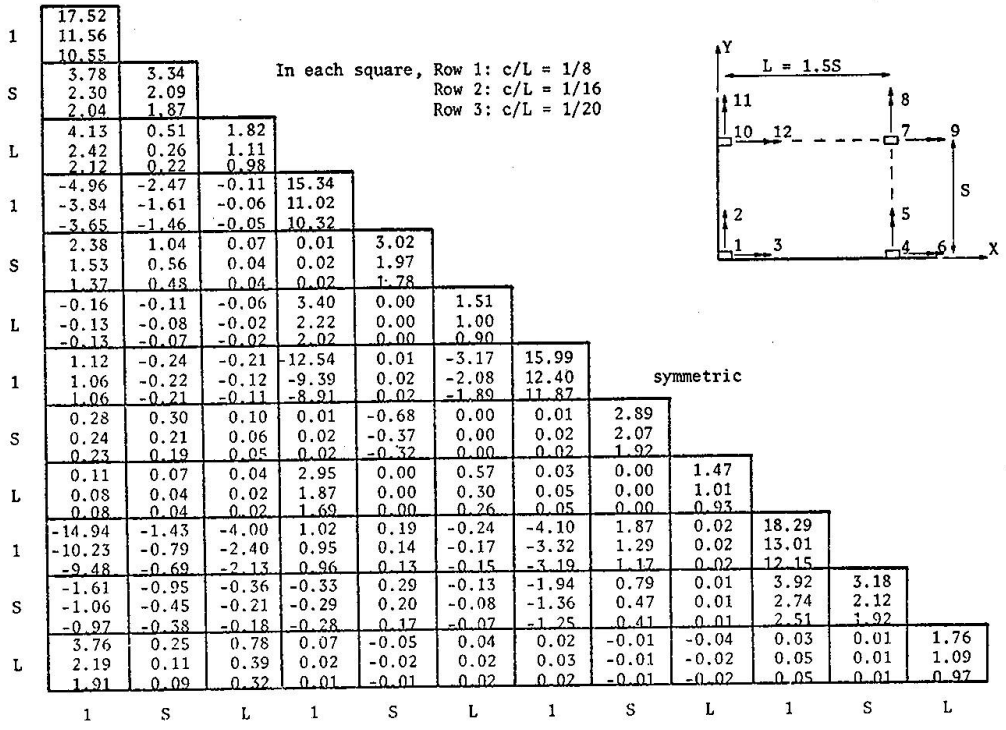

	1	S	L	1	S	L	1	S	L	1	S	L
1	17.52 11.56 10.55											
S	3.78 2.30 2.04	3.34 2.09 1.87										
L	4.13 2.42 2.12	0.51 0.26 0.22	1.82 1.11 0.98									
1	-4.96 -3.84 -3.65	-2.47 -1.61 -1.46	-0.11 -0.06 -0.05	15.34 11.02 10.32								
S	2.38 1.53 1.37	1.04 0.56 0.48	0.07 0.04 0.04	0.01 0.02 0.02	3.02 1.97 1.78							
L	-0.16 -0.13 -0.13	-0.11 -0.08 -0.07	-0.06 -0.02 -0.02	3.40 2.22 2.02	0.00 0.00 0.00	1.51 1.00 0.90						
1	1.12 1.06 1.06	-0.24 -0.22 -0.21	-0.21 -0.12 -0.11	-12.54 -9.39 -8.91	0.01 0.02 0.02	-3.17 -2.08 -1.89	15.99 12.40 11.87					
S	0.28 0.24 0.23	0.30 0.21 0.19	0.10 0.06 0.05	0.01 0.02 0.02	-0.68 -0.37 -0.32	0.00 0.00 0.00	0.01 0.02 0.02	2.89 2.07 1.92				
L	0.11 0.08 0.08	0.07 0.04 0.04	0.04 0.02 0.02	2.95 1.87 1.69	0.00 0.00 0.00	0.57 0.30 0.26	0.03 0.05 0.05	0.00 0.00 0.00	1.47 1.01 0.93			
1	-14.94 -10.23 -9.48	-1.43 -0.79 -0.69	-4.00 -2.40 -2.13	1.02 0.95 0.96	0.19 0.14 0.13	-0.24 -0.17 -0.15	-4.10 -3.32 -3.19	1.87 1.29 1.17	0.02 0.02 0.02	18.29 13.01 12.15		
S	-1.61 -1.06 -0.97	-0.95 -0.45 -0.38	-0.36 -0.21 -0.18	-0.33 -0.29 -0.28	0.29 0.20 0.17	-0.13 -0.08 -0.07	-1.94 -1.36 -1.25	0.79 0.47 0.41	0.01 0.01 0.01	3.92 2.74 2.51	3.18 2.12 1.92	
L	3.76 2.19 1.91	0.25 0.11 0.09	0.78 0.39 0.32	0.07 0.02 0.01	-0.05 -0.02 -0.01	0.04 0.02 0.02	0.02 0.03 0.02	-0.01 -0.01 -0.01	-0.04 -0.02 -0.02	0.03 0.05 0.05	0.01 0.01 0.01	1.76 1.09 0.97

Table 4: Lower Triangular Stiffness Matrix for Rectugular Corner Panel
[All values to be multiplied by $Et^3/12\,(1-\mu^2)LS$]

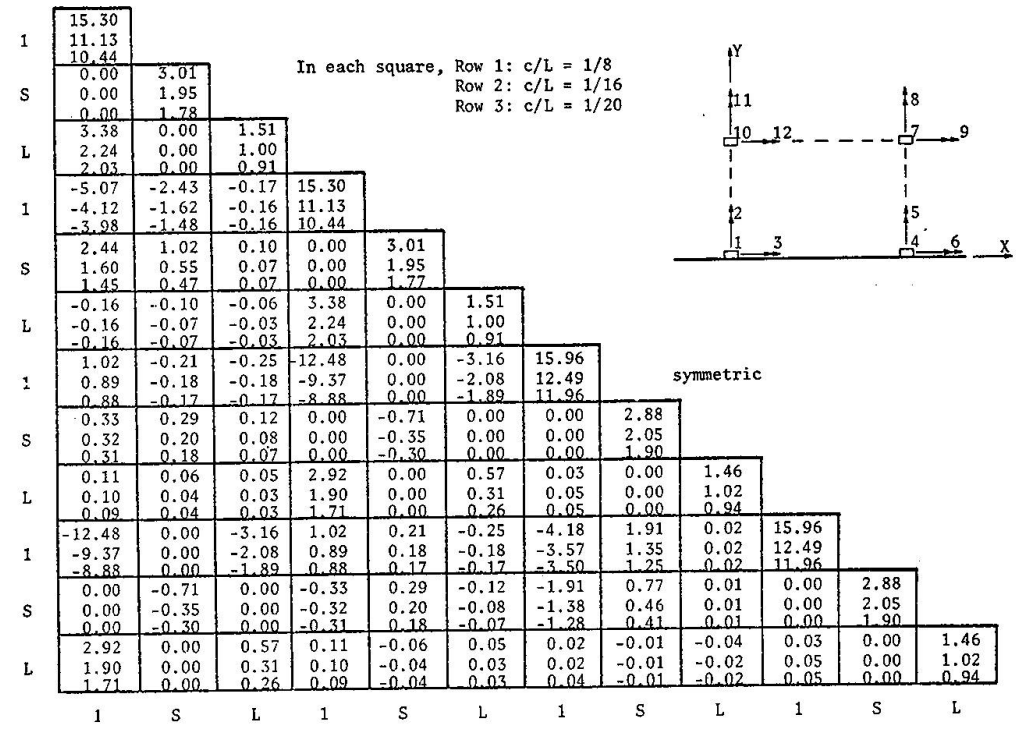

	1	S	L	1	S	L	1	S	L	1	S	L
1	15.30 11.13 10.44											
S	0.00 0.00 0.00	3.01 1.95 1.78										
L	3.38 2.24 2.03	0.00 0.00 0.00	1.51 1.00 0.91									
1	-5.07 -4.12 -3.98	-2.43 -1.62 -1.48	-0.17 -0.16 -0.16	15.30 11.13 10.44								
S	2.44 1.60 1.45	1.02 0.55 0.47	0.10 0.07 0.07	0.00 0.00 0.00	3.01 1.95 1.77							
L	-0.16 -0.16 -0.16	-0.10 -0.07 -0.07	-0.06 -0.03 -0.03	3.38 2.24 2.03	0.00 0.00 0.00	1.51 1.00 0.91						
1	1.02 0.89 0.88	-0.21 -0.18 -0.17	-0.25 -0.18 -0.17	-12.48 -9.37 -8.88	0.00 0.00 0.00	-3.16 -2.08 -1.89	15.96 12.49 11.96					
S	0.33 0.32 0.31	0.29 0.20 0.18	0.12 0.08 0.07	0.00 0.00 0.00	-0.71 -0.35 -0.30	0.00 0.00 0.00	0.00 0.00 0.00	2.88 2.05 1.90				
L	0.11 0.10 0.09	0.06 0.04 0.04	0.05 0.03 0.03	2.92 1.90 1.71	0.00 0.00 0.00	0.57 0.31 0.26	0.03 0.05 0.05	0.00 0.00 0.00	1.46 1.02 0.94			
1	-12.48 -9.37 -8.88	0.00 0.00 0.00	-3.16 -2.08 -1.89	1.02 0.89 0.88	0.21 0.18 0.17	-0.25 -0.18 -0.17	-4.18 -3.57 -3.50	1.91 1.35 1.25	0.02 0.02 0.02	15.96 12.49 11.96		
S	0.00 0.00 0.00	-0.71 -0.35 -0.30	0.00 0.00 0.00	-0.33 -0.32 -0.31	0.29 0.20 0.18	-0.12 -0.08 -0.07	-1.91 -1.38 -1.28	0.77 0.46 0.41	0.01 0.01 0.01	0.00 0.00 0.00	2.88 2.05 1.90	
L	2.92 1.90 1.71	0.00 0.00 0.00	0.57 0.31 0.26	0.11 0.10 0.09	-0.06 -0.04 -0.04	0.05 0.03 0.03	0.02 0.02 0.04	-0.01 -0.01 -0.01	-0.04 -0.02 -0.02	0.03 0.05 0.05	0.00 0.00 0.00	1.46 1.02 0.94

Table 5: Lower Triangular Stiffness Matrix for Rectugular Edge Pannel, Free Edge on Long Side
[All values to be multiplied by $Et^3/12\,(1-\mu^2)LS$]

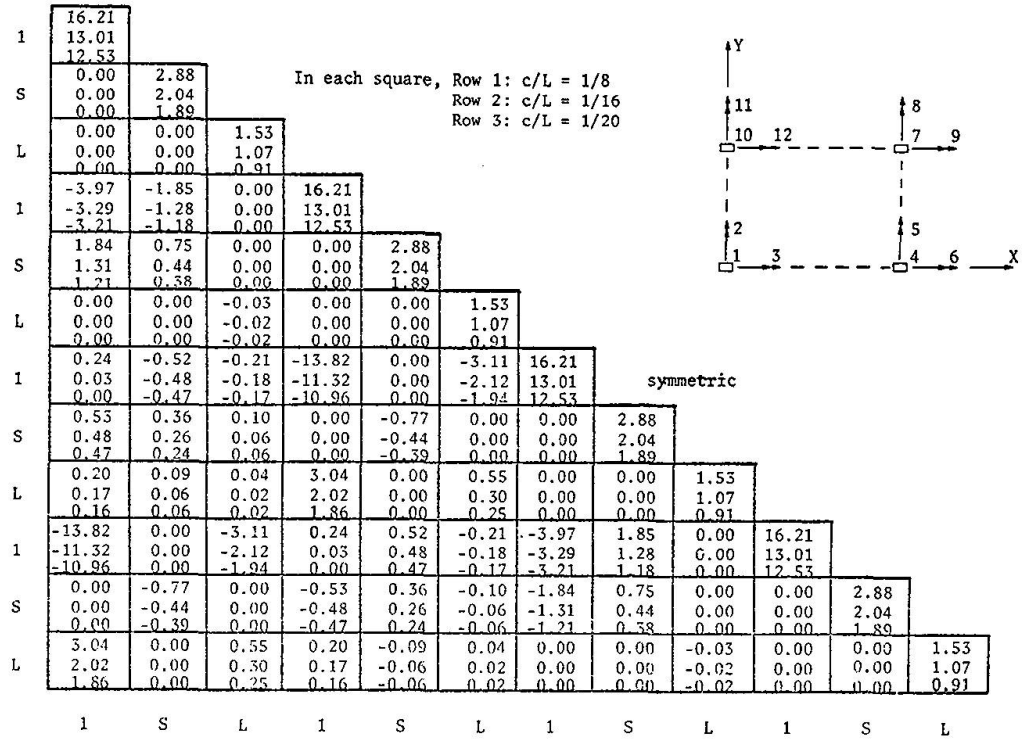

Table 6: Lower Triangular Stiffness Matrix for Rectugular Internal Panel
[All values to be multiplied by $Et^3/12\,(1-\mu^2)LS$]

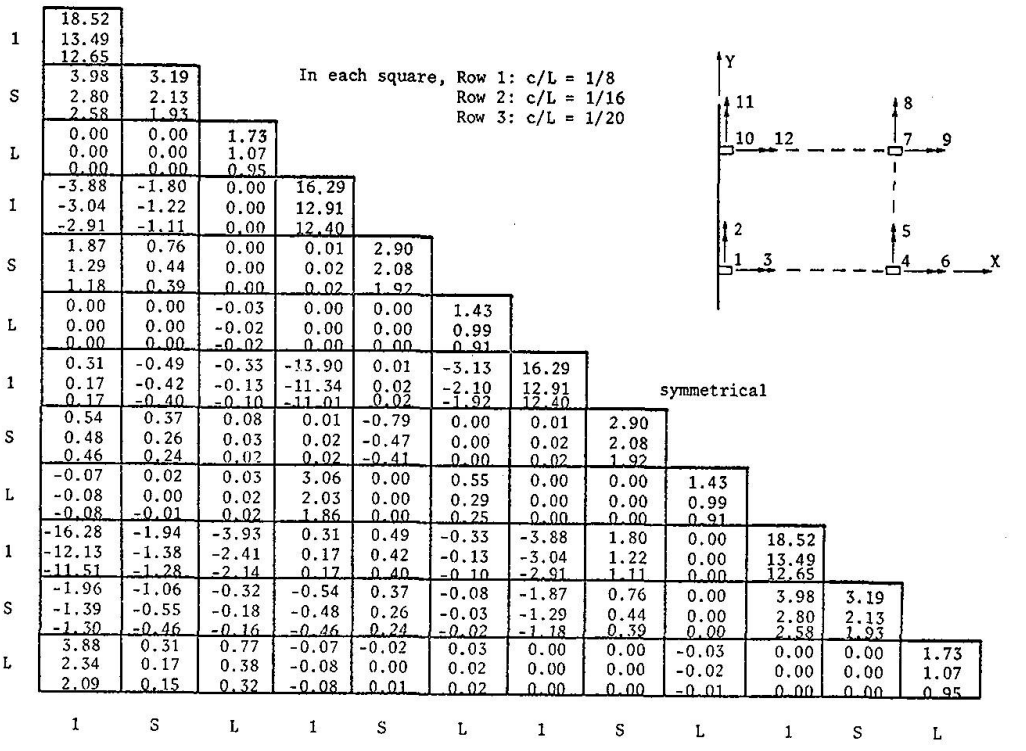

Table 7: Lower Triangular Stiffness Matrix for Rectangular Edge Panel, Free Edge on Short Side
[All values to be multiplied by $Et^3/12\,(1-\mu^2)LS$]

FLOOR	LATERAL DEFLECTION (mm)			COLUMN END MOMENTS (kN-m)					
				EXTERIOR COLUMN			INTERIOR COLUMN		
LEVEL	FEM	PM	EQF	FEM	PM	EQF	FEM	PM	EQF
10	13.63	13.96	19.12	1.72 -0.82	4.11 0.96	2.72 -1.73	8.55 5.80	6.13 3.82	9.56 4.68
9	13.24	13.52	18.63	9.39 4.72	10.73 6.22	11.02 3.24	17.35 14.26	15.84 12.73	18.74 12.72
8	12.63	12.85	17.81	14.79 10.22	16.24 11.74	16.31 8.46	27.22 23.97	25.57 22.46	28.94 22.48
7	11.76	11.94	16.62	20.36 15.86	21.71 17.31	21.77 13.92	36.81 33.65	35.23 32.24	38.68 32.30
6	10.65	10.78	15.05	25.90 21.56	27.14 22.92	27.13 19.42	46.37 43.34	44.88 42.05	48.43 42.17
5	9.29	9.37	13.10	31.47 27.35	32.56 28.57	32.50 25.04	55.85 52.97	54.49 51.85	58.08 52.02
4	7.68	7.74	10.79	37.09 33.22	38.01 34.28	37.80 30.78	64.00 62.59	64.02 61.65	67.54 61.94
3	5.84	5.88	8.12	42.76 39.73	43.48 40.59	42.78 37.70	74.16 71.94	73.18 71.25	76.14 71.93
2	3.79	3.81	5.13	47.01 47.02	47.48 47.59	44.60 47.88	81.69 83.36	80.98 82.97	80.95 85.59
1	1.61	1.61	2.03	42.87 82.92	43.04 83.10	31.60 93.63	68.20 95.57	67.87 95.52	57.62 106.62

Table 8, Example 1: Lateral Deflections and Column End Moments

FLOOR	LATERAL DEFLECTION (mm)		COLUMN END MOMENTS (kN-m)								ROTATION DUE TO APPLIED TWIST (10^{-6} RADS)	
			COLUMN 1		COLUMN 2		COLUMN 3		COLUMN 4			
LEVEL	FEM	PM	FEM	PM	FEM	PM	FEM	PM	FEM	PM	FEM	PM
10	10.65	10.42	5.37 -8.40	5.43 -8.41	10.88 -4.22	10.26 -4.71	7.70 -6.06	8.67 -5.85	16.38 0.34	16.11 0.12	2.98	2.99
9	10.31	10.11	16.27 -8.59	16.32 -8.64	20.20 -3.48	19.98 -3.90	18.41 -5.74	18.92 -5.32	25.08 2.61	25.06 2.54	2.88	2.89
8	9.80	9.63	20.75 -7.40	20.84 -7.50	27.62 0.15	27.33 -0.35	24.65 -2.96	25.35 -2.52	35.87 9.27	35.87 9.12	2.74	2.75
7	9.07	8.93	24.50 -4.80	24.60 -4.95	33.50 5.05	33.22 4.49	29.95 1.25	30.62 1.64	44.60 17.19	44.70 17.04	2.53	2.54
6	8.09	7.99	27.00 -1.24	27.15 -1.44	38.41 10.97	38.17 10.34	34.05 6.43	34.84 6.78	52.60 26.17	52.80 25.99	2.26	2.27
5	6.88	6.81	28.40 3.84	28.59 3.56	42.00 18.17	41.81 17.47	37.05 13.00	37.82 13.27	59.00 36.02	59.38 35.95	1.92	1.93
4	5.45	5.40	27.64 11.87	27.90 11.52	43.10 27.85	42.98 27.10	37.60 22.20	38.43 22.41	62.60 48.00	63.00 47.78	1.52	1.52
3	3.85	3.82	22.43 26.58	22.75 26.20	38.80 42.80	38.76 42.12	33.15 37.22	33.93 37.32	59.50 63.50	60.00 63.29	1.07	1.07
2	2.19	2.17	7.16 55.20	7.50 54.80	22.55 69.80	22.60 69.17	17.30 64.60	18.03 64.81	42.10 88.20	42.59 88.06	0.60	0.61
1	0.72	0.71	-29.68 118.70	-29.35 118.50	-20.47 123.30	-20.29 123.00	-23.55 121.70	23.06 121.61	-8.95 129.10	-8.44 128.92	0.20	0.20

Table 9, Example 2: Lateral Deflections, Column End Moments and Lateral Twist

Appendix

Data Preparation

To illustrate the procedure for evaluating a panel stiffness matrix, a typical panel, shown in Fig. 10b will be examined. In this example $c/L = 1/8$ in each direction and the aspect ratio (L:S) is 9m:6m. Stiffness values for the panel are therefore taken from the top rows (since $c/L = 1/8$) of Table 7.

Using as data E = 25000 *MPa*, $t = 0.2$m and $\mu = 0.15$ the value of $Et^3/12(1-\mu^2)LS$ is 316 *kN/m*.

To establish the value of K(8,3), for instance, we note that the values of row 8 are multiplied by L, and the values of column 3 are multiplied by S.

$K(8,3)$ would therefore be $(316 \times 10^3) \times 9 \times 6 \times 0.084 = 1433$ *kN/m*.

In like manner, the full matrix may be evaluated.

As this panel is oriented differently from the reference diagram of Table 7, the stiffness matrix must be rotated. This is performed by a congruent transformation which has the form:

$$\overline{K} = RKR^T$$

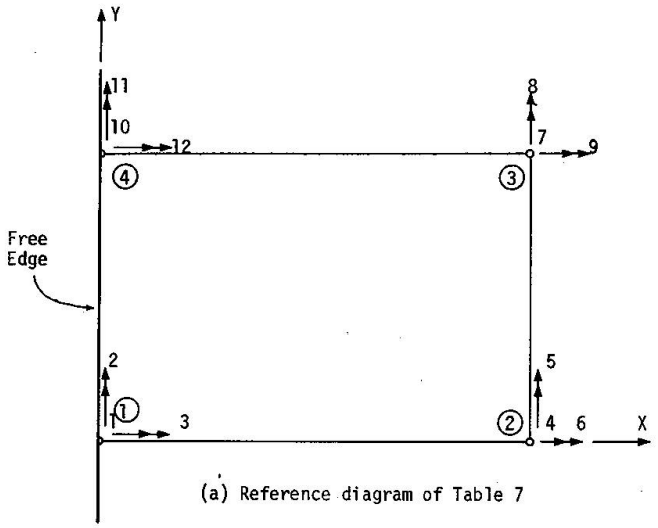

(a) Reference diagram of Table 7

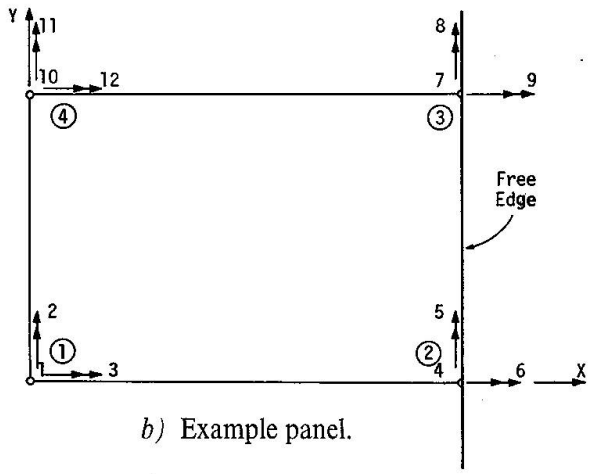

b) Example panel.

Fig. 10. Panel rotation to suit boundary conditions.

where $\overline{K}$ is the resultant stiffness matrix.

Matrix R contains four submatrices r, which perform the axis rotation of the three freedoms at each node.

In terms of generalised forces, the matrix r forms the relation:

$$\begin{bmatrix} \overline{P}_1 \\ \overline{P}_2 \\ \overline{P}_3 \end{bmatrix} = \underbrace{\begin{bmatrix} C_{11} & C_{12} & C_{13} \\ C_{21} & C_{22} & C_{23} \\ C_{31} & C_{32} & C_{33} \end{bmatrix}}_{r} \begin{bmatrix} P_1 \\ P_2 \\ P_3 \end{bmatrix}$$

where C_{ij} are direction cosines.

For the example panel, the rotation is 180°, therefore:

$$r = \begin{bmatrix} 1 & 0 & 0 \\ 0 & -1 & 0 \\ 0 & 0 & -1 \end{bmatrix}$$

The moment sign convention used is that positive rotations cause a positive slope in the direction of the axis.

The final step is to move the nodes to their new positions. In this example, node 1 is interchanged with node 3, which is achieved by placing submatrix r in $R(3,1)$. Likewise the other nodes are interchanged as indicated in the matrix:

$$R = \begin{bmatrix} 0 & 0 & r & 0 \\ 0 & 0 & 0 & r \\ r & 0 & 0 & 0 \\ 0 & r & 0 & 0 \end{bmatrix}$$

Notations

The following symbols are used in this paper:

C_{ij}	direction cosines.
c	column thickness in x direction.
D	flexural rigidity of plate.
d	column thickness in y direction.
E	Young's Modulus.
EQF	equivalent frame method.
FEM	finite element method.
K	panel stiffness matrix.
$\overline{K}$	transformed panel stiffness matrix.
L	column centre to centre span in x direction.
P	lateral point load.
P_i	generalized nodal forces.
$\overline{P}_i$	transformed forces.
PM	panel method.
R	rotation transformation matrix.
r	transformation submatrix.
S	column centre to centre span in y direction.

S_e effective width in y direction.
t plate theckness.
w nodal deflection orthogonal to plate.
μ Poisson's Ratio.

Acknowledgement

The work reported in this paper forms part of a research project on the three dimensional analysis of multistorey flat plate buildings and is supported in part by the Australian Research Grants Commission. This support is gratefully acknowledged.

References

1. ACI Code 318-1971: Building Code Requirements for Reinforced Concrete.
2. SAA Code 1480-1974: Concrete Structures Code.
3. CARPENTER, J.E. (1965): Flexural Characteristics of Flat Plate Floors in Buildings Subjected to Lateral Loads. PhD Thesis, Purdue University.
4. FAULKES, K.A. (1974): Bending Moments in Flat Plate Structures. PhD Thesis, The University of New South Wales, Kensington, Australia.
5. SMITH, E.T. (1974): Flexural Characteristics of Flat Plate Structures. PhD Thesis, The University of New South Wales, Kensington, Australia.
6. KABAILA, A.P., PULMANO, V.A., and SOMERVAILLE, I.J. (1972): A Compatible Quadrilateral Plate Bending Element. UNICIV Report No. R-86, The University of New South Wales, Kensington, Australia.
7. BLACK, D.C., PULMANO, V.A., and KABAILA, A.P. (1974): Certain Finite Elements for Plate Bending Problems. UNICIV Report No. R-126, The University of New South Wales, Kensington, Australia.
8. SOMERVAILLE, I.J. (1972): A general Procedure for Grading the Mesh in Arrays of Finite Elements. UNICIV Report No. R-85, The University of New South Wales, Kensington, Australia.
9. PRZEMIENIECKI, J.S. (1968): Theory of Matrix Structural Analysis. McGraw-Hill.
10. PULMANO, V.A., BLACK, D.C., and KABAILA, A.P. (1974): Substructure Analysis of Multistorey Flat Slab Buildings. Proceedings of the ASCE-IABSE Regional Conf. on Tall Buildings, Bangkok, Thailand.
11. QADEER, A., and STAFFORD SMITH, B. (1969): The Bending Stiffness of Slabs Connecting Shear Walls. ACI Journal, Proceedings, Vol. 66, No. 6, pp. 464–473.
12. MICHAEL, D. (1969): Discussion of the Bending Stiffness of Slabs Connecting Shear Walls by Qadeer, A., and Stafford Smith, B. ACI Journal, Proceedings, Vol. 66, No. 12, pp. 1021–1022.
13. ACI Committee 442 Report (1971): Response of Buildings to Lateral Forces. ACI Journal, Proceedings, Vol. 68, No. 2, pp. 81–106.
14. BARNARD, R.P., and SCHWAIGHOFER, J. (1967): Interaction of Shear Walls Connected Solely Through Slabs. Tall Buildings, Pergamon Press Ltd., London, pp. 157–173.
15. COULL, A. (1966): Tests on a Model Shear Wall Structure, Civil Engineering and Public Works Review (London), Vol. 61, No. 722, September, pp. 1129–1133.

Summary

Presented herein are the stiffness matrices of flat plate floor panels in non-dimensional form for use as input data for a three dimensional frame analysis computer program. The tabulated stiffness values take into account the parameters involving the size of the floor panel and the cross sectional dimensions of the supporting columns.

Two multistorey buildings are analysed to demonstrate the application of the method and its advantages over alternative methods.

Résumé

Les auteurs étudient les matrices de rigidité de dalles plates — dans une présentation sans dimension — en tant que données pour un programme de calcul à l'ordinateur de cadres tridimensionnels. Les valeurs de ridigité indiquées en forme de tableaux tiennent compte de paramètres relatifs aux dimensions des dalles ainsi qu'aux sections des colonnes.

Deux bâtiments à plusieurs étages sont calculés et montrent l'application de la méthode ainsi que ses avantages par rapport à d'autres procédés.

Zusammenfassung

In der vorliegeden Arbeit werden die Steifigkeitsmatrizen für die Felder von Flachdecken in dimensionsloser Form zum Gebrauch als Eingabedaten für ein dreidimensionales Computerprogramm dargestellt. Die tabellarisch angegebenen Steifigkeitswerte berücksichtigen die Abmessungen der Deckenplatten sowie die Querschnittsabmessungen der Stützen.

Zwei mehrstöckige Bauten werden berechnet, um die Anwendung der Methode und ihre Vorzüge gegenüber anderen Verfahren zu belegen.

An Incremental Collapse Model for Metal Fatigue

Un modèle incrémental de rupture à la fatigue d'un métal

Ein inkrementales Bruchmodell zur Prüfung der Metallermüdung

S.A. GURALNICK
Professor of Civil Engineering
Illinois Institute of Technology, Chicago

Introduction

A number of attempts [1, 2, 3 and 4] have been made in the past to explain by means of mechanical models, or other analog systems the puzzling, and apparently even contradictory, set of phenomena which are comprised in metal fatigue. Previous attempts have been largely unsatisfactory because the models used were chosen in order to display a response which was analogous to a few gross macroscopic aspects of metal fatigue but could not be "stretched" to simulate the entire spectrum of observable phenomeny. These deficiencies may be largely overcome if the model (or analogue) chosen is the hyperstatic portal frame shown in Fig. 1. This structure has been treated by conventional analytical methods by NEAL [5] and experimentally by Neal and SYMONDS [6].

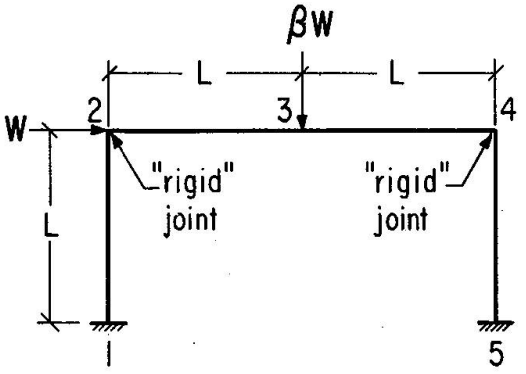

Fig. 1. Three-bar hyperstatic portal frame.

The Model

If the flexural members of the structure of Fig. 1 are uniform in cross section, are made of an elasto-plastic material whose stress-strain behavior is similar to that

diagrammed in Fig. 2a, they display the bending moment versus curvature response (linear-perfectly plastic) shown in Fig. 2b; and if the structure is subjected to repeated cycles of loading, the first sequence of which is shown in Fig. 3; then, for $\beta = 1$, the alternating plasticity load is,

$$W_a = 2.759 \frac{M_p}{L}; \tag{1}$$

the shakedown load is,

$$W_s = 2.857 \frac{M_p}{L}; \tag{2}$$

and, the plastic collapse load is,

$$W_c = 3 \frac{M_p}{L}. \tag{3}$$

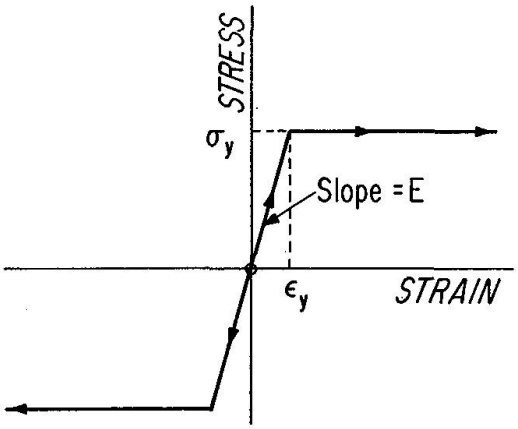

Fig. 2a. Stress Versus Strain.

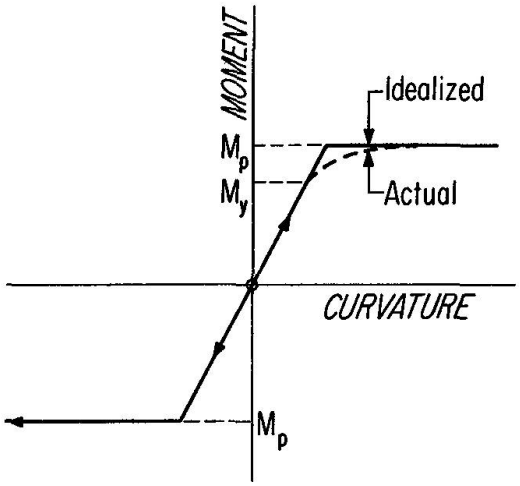

Fig. 2b. Bending moment versus curvature.

The mechanism of collapse corresponding to a monotonic increase in the loads to the collapse level is shown in Fig. 4. Additional values of W_a, W_s, and W_c are given in Table 1 for $\beta = 0.5$, 1, 1.5, and 2.

Table 1

Load	β	0.5	1.0	1.5	2.0
Alternating Plasticity	$\frac{W_a L}{M_p}$	2.750	2.425	2.049	1.665
Shakedown	$\frac{W_s L}{M_p}$	3.478	2.857	2.264	1.875
Plastic Collapse	$\frac{W_c L}{M_p}$	4.00	3.00	2.40	2.00

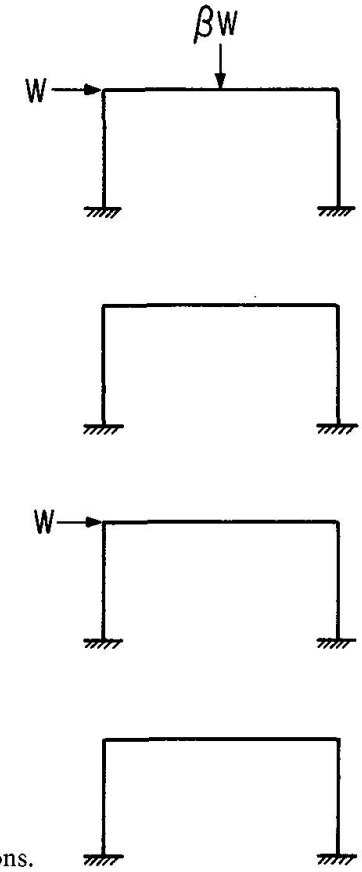

Fig. 3. One cycle of load applications.

If the more generalized cyclic load pattern of Fig. 5 is applied to the model and if the hysteresis energy ΔU generated in each cycle at various load ranges is computed, then the results may be displayed in graphs such as those shown in Fig. 6 for $\overline{W} = 0.5\ W_s$ and $\beta = 1.0$. Similar graphs may be obtained for all relevant values of $\overline{W}$ and β. An examination of all such graphs reveals that, depending on load range and mean load, one of two types of cyclic hysteresis may occur: If for a particular mean load $\overline{W}$ the load range R *lies* below a certain limiting value R^*, then the hysteresis energy ΔU decreases to zero as N increases. This form of hysteresis is sometimes called "elastic hysteresis". On the other hand, if for a particular mean load $\overline{W}$ the load range R exceeds the limiting value R^*, then the hysteresis is called "asymptotic hysteresis." GURALNICK [7] has shown that R^* is a continuous

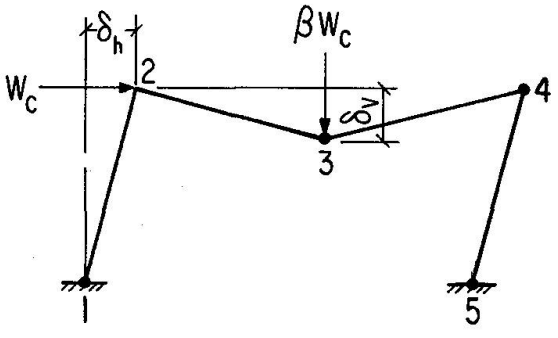

Fig. 4. Collapse mechanism.

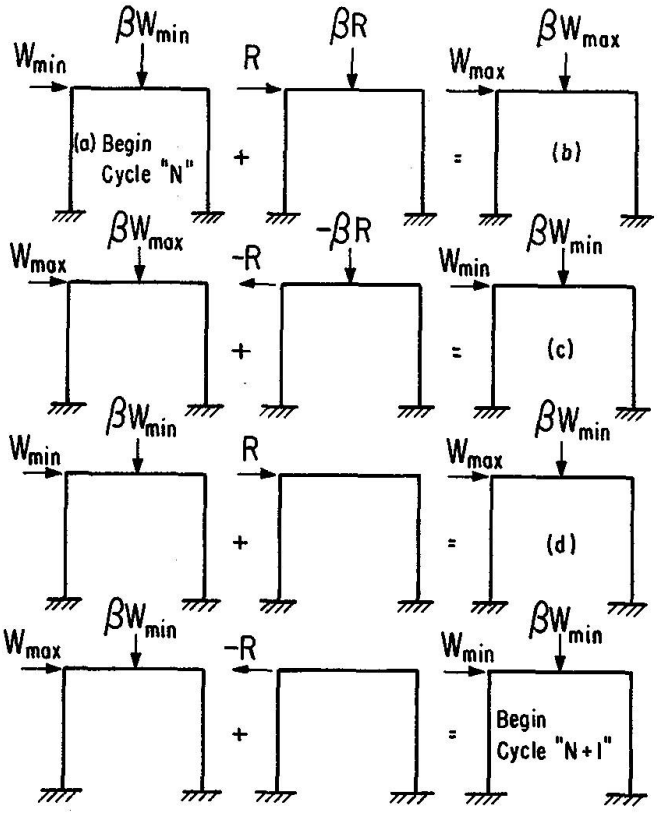

Fig. 5. The N^{th} cycle of load applications.

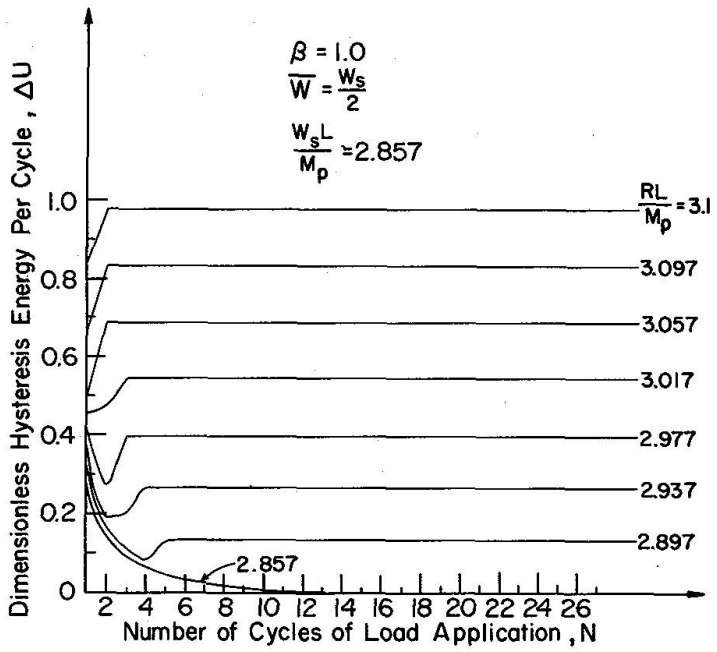

Fig. 6. Hysteresis energy per cycle versus number of cycles of load application.

function of the mean load $\overline{W}$. The results of a simple computerprogram which determines ΔU at the end of each cycle of load levels for prescribed mean loads may be used to construct graphs of the type displayed in Fig. 7. Because maximum and minimum loads are defined in terms of range R and mean load $\overline{W}$, the results displayed in Fig. 7 may be expressed as a family of envelopes, called "extended incremental collapse envelopes," as shown in Fig. 8 for various values of β in the range $0.5 < \beta < 2$. In Figs. 7 and 8 the curves corresponding to $\beta = 1$ have been emphasized for clarity. It may be observed from the $\beta = 1$ curve in Fig. 8, that values of W_a, W_s and W_c may be inferred which are in perfect agreement with the respective values given by Eqs. 1, 2, and 3 even though these latter three values were obtained by using conventional methods of "plastic analysis" rather than a computational process involving a consideration of hysteresis energy occurring during each cycle of load applications.

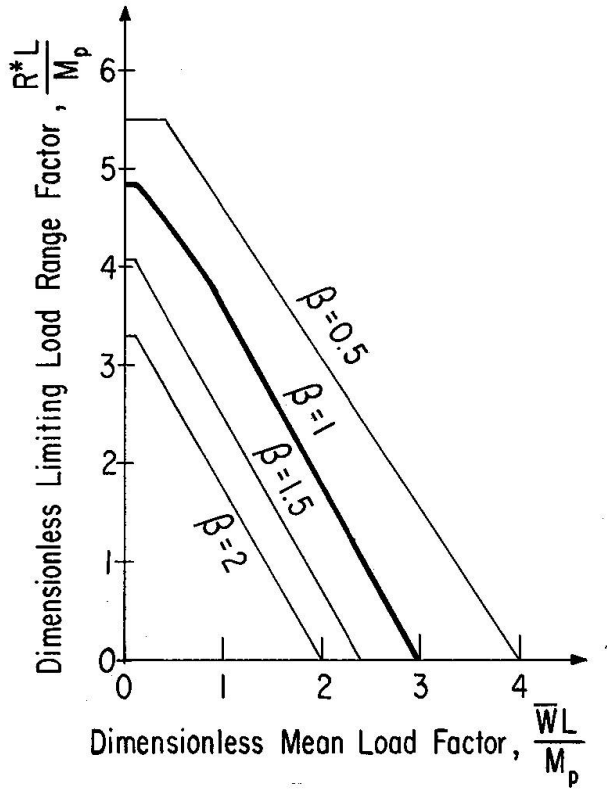

Fig. 7. Load range factor versus mean load factor diagrams.

If the initial direction of loading shown in Fig. 5 is reversed and if this reversed pattern of loading is applied to the model, then diagrams geometrically similar to those of Fig. 8 may be constructed except that algebraic signs will be reversed. If such diagrams for reversed loading are combined with those of Fig. 8 then the "complete" maximum or minimum load factor versus load factor diagrams of Fig. 9 will result. These diagrams, of course, are completely analogous to the conventional GOODMAN [9] — GERBER [8] diagram for metal fatigue. The diagrams of Fig. 9 are completely symmetrical whereas it is well known that such diagrams for real materials are unsymmetrical.

The graphs of cyclic hysteresis energy versus number of cycles of load application shown in Fig. 6 are particularly interesting because both strain softening and strain

hardening behavior is exhibited in the asymptotic hysteresis spectrum in addition to the aforementioned elastic hysteresis. Curiously enough, graphs similar to those of Fig. 6 for other values of $\overline{W}$ and β do not always display elastic hysteresis. Hence, it may be inferred that elastic hysteresis is a function of mean load as well as load range. This is indeed true as may be seen in Fig. 10 in which the loads producing the onset of elastic hysteresis are defined by the innermost set of lines which appear on the partial Goodman-Gerber type diagrams. This behavior of the model helps to clear up an aspect of the relationship between hysteresis and fatigue in materials that has puzzled many investigators ever since FÖPPL [10] noted that it is possible in some instances to observe hysteresis in a cyclic test even though the material does not fail in fatigue. This observation may now be clearly placed in its proper perspective by distinguishing between elastic hysteresis and asymptotic hysteresis. Furthermore, it is clear from the diagrams of Fig. 10 that elastic hysteresis may be present under some conditions (fluctuating or pulsating loads) and not appear in others (fully reversed alternating loads) even though the same material is being stress cycled.

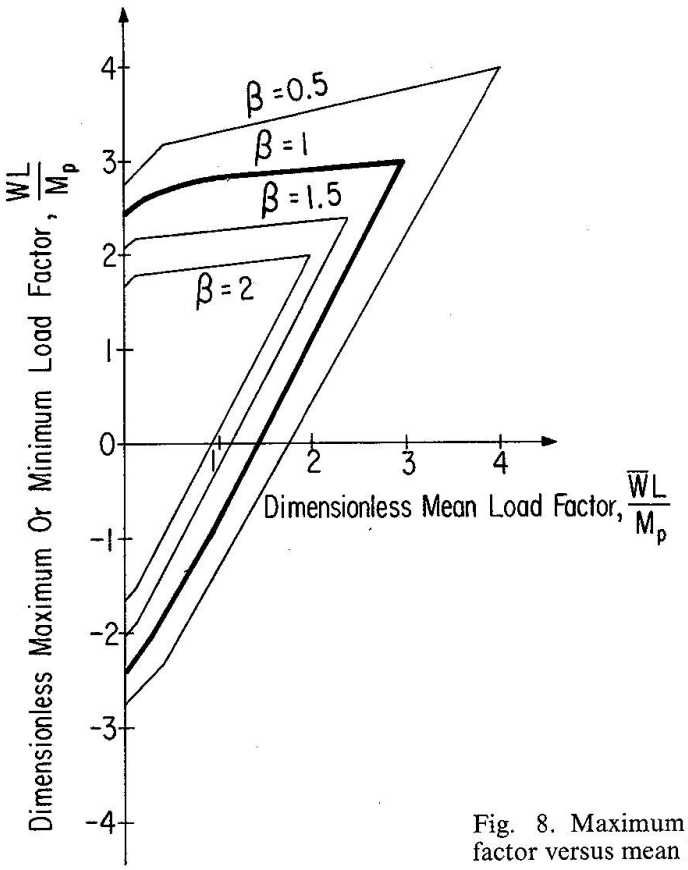

Fig. 8. Maximum or minimum load factor versus mean load factor diagrams.

The hysteresis energy dissipated in each cycle of load applications may be summed to obtain the cumulative hysteresis energy imparted to the structure at the end of the Nth cycle according to the relationship,

$$U = \sum_{i=1}^{N} \Delta U_i \tag{4}$$

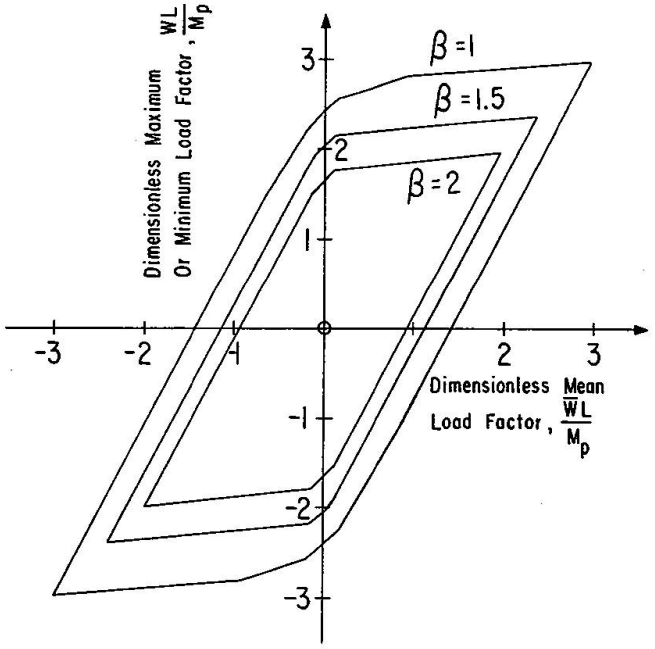

Fig. 9. Complete load factor versus mean load factor diagrams.

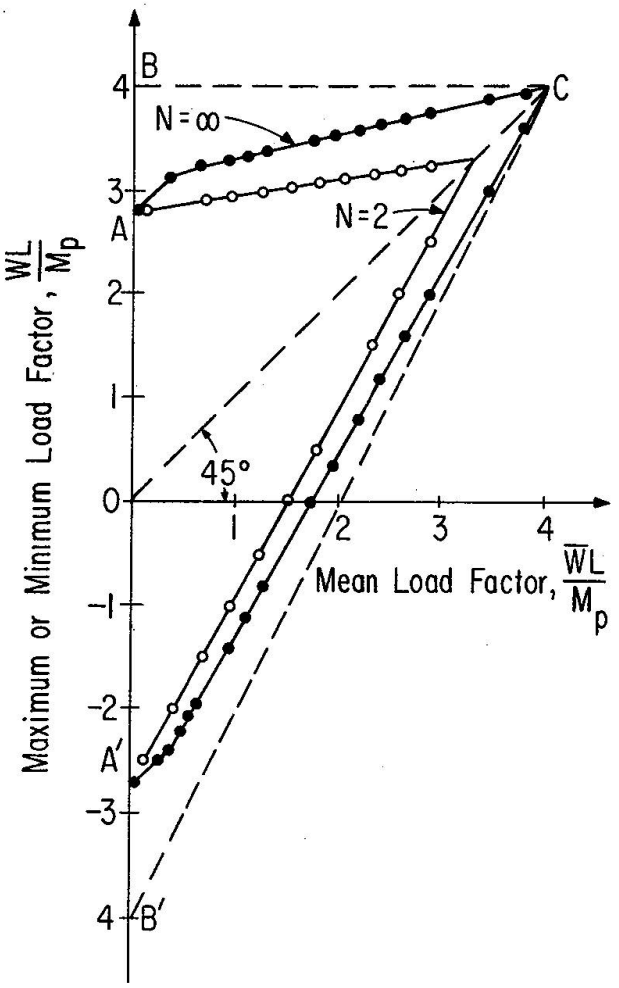

Fig. 10. Load factor versus mean load factor diagrams, $\beta = 0.5$.

in which ΔU_i is the hysteresis energy appearing in the ith cycle. A typical set of graphs of cululative hysteresis energy versus number of cycles of load application are shown in Fig. 11 for $\overline{W} = 0.5\ W_s$ and $\beta = 1.0$.

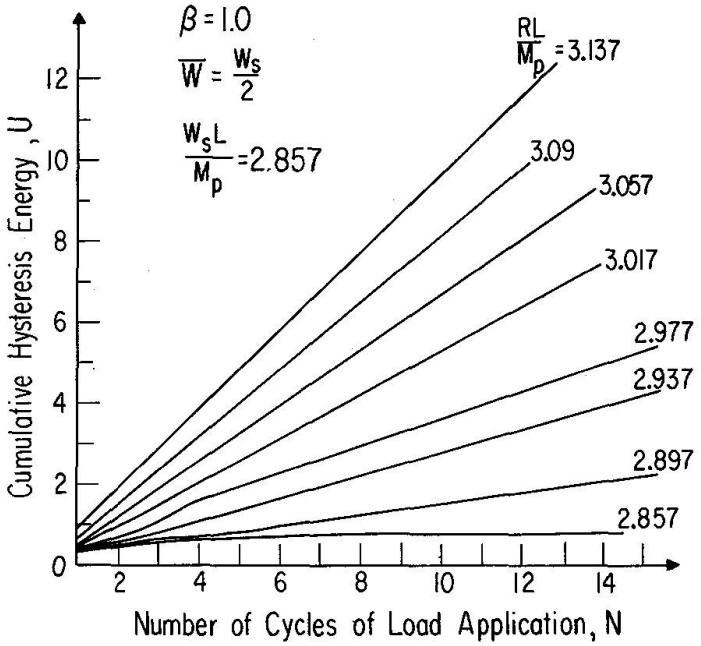

Fig. 11. Cumulative hysteresis energy versus number of cycles of load application.

The ability of any real structure to absorb hysteresis energy is finite and, hence, it may be argued that failure occurs when,

$$\sum_{i=1}^{N_F} \Delta U_i = U_F, \tag{5}$$

in which N_F is the extended incremental collapse life and U_F is the extended incremental collapse toughness. There is an obvious analogy between Eq. 5, representing the behavior of the model, and the behavior of metals in fatigue where U_F of the model is analogous to Ω_f, the "fatigue toughness" (c.f. HALFORD [11]).

Returning to the graphs of Fig. 10, it is known that if load range is confined to the region of the diagram bounded by the curves AC and $A'C$, then failure will not occur no matter how many cycles of load are applied to the model. If load range is allowed to exceed these boundary curves[1] and the loads penetrate into the regions ABC and $A'B'C$, then failure occurs when a finite number of load cycles have been applied.

Asymptotic hysteresis prevails in the regions ABC and $A'B'C$ in Fig. 10 and failure will occur, as argued above, when the cumulative hysteresis energy reaches the value U_F. Additional information may be derived if it is assumed that U_F is a linear function of the number of cycles to failure, or,

$$U_F = U_0 + MN, \tag{6}$$

[1] Of course, cyclic loads with a load range which exceeds the bounds defined by the lines BC and $B'C$ cannot be applied to the model because collapse in a single cycle would occur.

in which M is a constant. If the graph of Eq. 6 is plotted on the same diagram as a set of U versus N curves for a particular mean load and a particular value of β then a diagram such as that sketched in Fig. 12 results. Each curve of U versus N for a particular load range R_j may be approximated by a straight line of the form,

$$U = b_j + m_j N \tag{7}$$

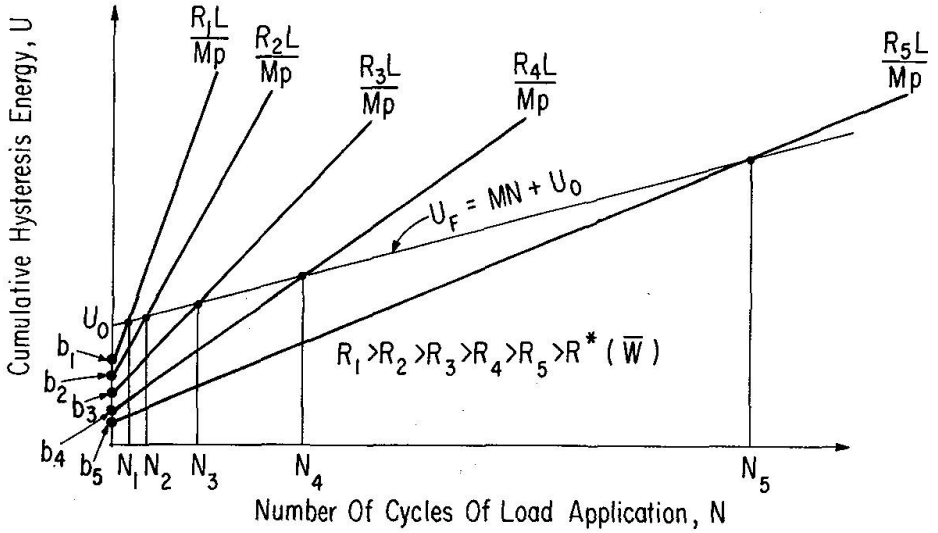

Fig. 12. Cumulative hysteresis energy versus number of cycles of load application.

in which b_j and m_j are constants defined for the corresponding load range R_j. For any particular load range R_j, the point of intersection of a line representing Eq. 7 with the line representing Eq. 6 has an N-coordinate on Fig. 12 which is the extended incremental collapse life N_{Fj}. The collection of R_j and N_{Fj} values for a particular value of mean load $\overline{W}$ and load ratio β is a set of ordered pairs and, hence, it may be argued that load range at failure and extended incremental collapse life are connected by a functional relationship which, for any particular set of values for $\overline{W}$ and β, may be written in the form,

$$\left.\frac{RL}{M_p}\right|_{\substack{\overline{W} \\ \beta}} = f(N_F). \tag{8}$$

Typical graphs of Eq. 8 for $\beta = 0.5$ and $\overline{W} = 0$ and $\overline{W} = 0.5\ W_s$ are shown in Fig. 13. The resemblance of the curves shown in Fig. 13 to conventional $S - N$ diagrams for the fatigue of ferrous metals is remarkable. In this regard, it may be observed that the limiting load range R^* (cf. Fig. 13) of the model is completely analogous to the endurance limit or fatigue limit displayed by cyclically stressed ferrous metals. Of course the graphs shown in Fig. 13 are merely contour lines projected on the load range versus life plane of the entire extended incremental collapse surface expressed in the coordinates of load range, mean load and life.

Such a surface for $\beta = 0.5$ is shown in Fig. 14. It is, of course, the analogue of the Fatigue Strength versus Mean Stress and Fatigue Life diagram proposed by STÜSSI [12].

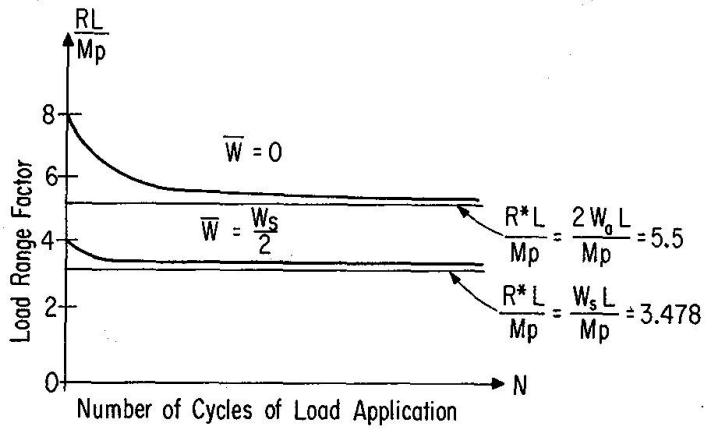

Fig. 13. Load range factor versus number of cycles of load application for $\beta = 0.5$.

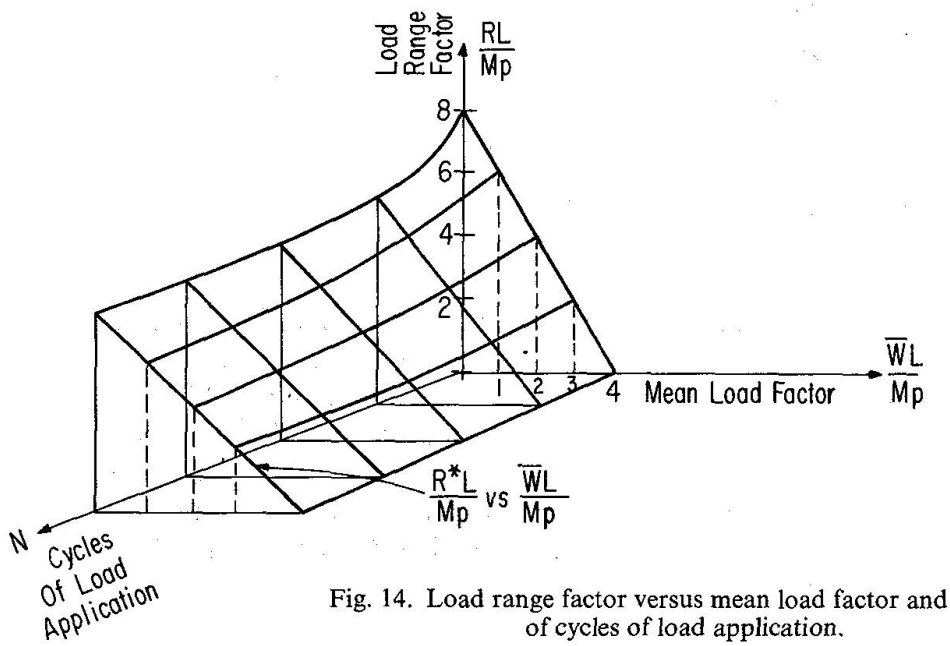

Fig. 14. Load range factor versus mean load factor and number of cycles of load application.

Among the several important observations made by HORNE [13] concerning the shakedown condition, he stated that,

(*i*) "The shakedown condition is unaffected by initial stresses however caused, so that these have no effect on whether or not a structure can shake down under a given set of loads. Initial stresses may, however, affect the number of load variations which have to take place before a condition of shakedown is actually reached."

and

(*ii*) "The order in which loads are applied has no effect on whether a structure can shake down, although again the order of loading may influence the rapidity with which a shakedown state is reached."

These two observations apply equally well to the entire extended incremental collapse envelope (cf. Fig. 9) instead of merely to one point on this envelope (i.e. the point defined by a cyclic load pattern with maximum load equal to the shakedown load W_s) and they may be restated as a principle.

Principle 1. The shape of the extended incremental collapse envelope for any particular value of β is neither affected by previous load history nor by the order in which loads are applied.

For all load patterns with a range which lies outside of the incremental collapse envelope, asymptotic hysteresis occurs. This means that, except for slight perturbations which occur during the first few cycles, the hysteresis energy per cycle rapidly approaches a constant value which depends only on load range, mean load and β and is independent of previous load history. These observations may also be stated as a principle.

Principle 2. If a cyclic pattern of loads is imposed on a structure such that the mean load and load range are constant and the load range lies outside of the corresponding incremental collapse envelope (or, load range $R > R^*$), then the hysteresis energy per cycle ΔU rapidly approaches a constant which depends only on load range, mean load and β and is independent of prior load history.

It may be inferred from Principles 1 and 2 that if the model is subjected to a sequence of load regimes each having a particular constant mean load and constant load range such that $R > R^*$, then the total hysteresis energy U is merely the sum of the hysteresis energies accumulated during each individual load regime and may be written as,

$$U = \sum_{i=1}^{n_1} \Delta U(R_1, \overline{W}_1)_i + \sum_{j=1}^{n_2} \Delta U(R_2, \overline{W}_2)_j + \sum_{k=1}^{n_3} \Delta U(R_3, \overline{W}_3)_k + \ldots \tag{9}$$

in which the typical term $\Delta U(R_p, \overline{W}_p)_q$ is the increment of hysteresis energy, for a particular set of values R_p and $\overline{W}_p$, accumulated during the 8th cycle of load applications. If the $\Delta U(R_p, \overline{W}_p)_q$ are independent of the number of cycles (i.e. independent of q) then Eq. 9 may be written as,

$$U = n_1 \Delta U(R_1, \overline{W}_1) + n_2 \Delta U(R_2, \overline{W}_2) + n_3 \Delta U(R_3, \overline{W}_3) + \ldots \tag{10}$$

Of course if the sequence of load applications is continued until failure by incremental collapse occurs, then U in Eq. 9 becomes U_F and,

$$n_1 + n_2 + n_3 + \ldots = N_F, \tag{11}$$

in which N_F is the extended incremental collapse life.

Fig. 11 clearly indicates that for any constant value $\overline{W}_p$ and R_p in excess of $R^*(\overline{W}_p)$, the graph of U versus N is, for all practical purposes, a straight line which may be written in the form,

$$U = m_i N + b_i, \tag{12}$$

as shown in Fig. 12. If the model is subjected to a sequence of load regimes each having a particular mean load $\overline{W}_p$ and load range R_p such that $R_p > R^*(\overline{W}_p)$, then according to Eq. 10 the total hysteresis energy U is merely the sum of the hysteresis energies accumulated during each individual load regime. This statement

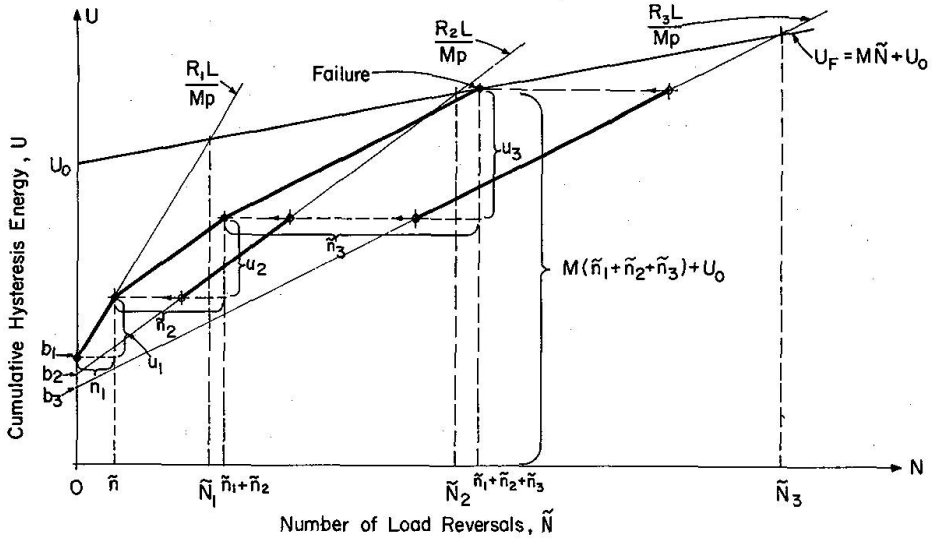

Fig. 15. Growth of hysteresis energy with number of load reversals.

may be represented by the three connected line segments starting at the point $(0, b_1)$ in Fig. 15. Failure occurs when the third line segment intersects the U_F – line[1]. Considering the geometry of the diagrams shown in Fig. 15, together with the equations of the lines, one may write,

$$\frac{\tilde{n}_1}{\tilde{N}_1}+\frac{\tilde{n}_2}{\tilde{N}_2}\left(\frac{U_0-b_2}{U_0-b_1}\right)+\frac{\tilde{n}_3}{\tilde{N}_3}\left(\frac{U_0-b_3}{U_0-b_1}\right)=1$$

or, in general, for a total of p load sequences,

$$\frac{\tilde{n}_1}{\tilde{N}_1}+\frac{\tilde{n}_2}{\tilde{N}_2}\left(\frac{U_0-b_2}{U_0-b_1}\right)+\ldots+\frac{\tilde{n}_p}{\tilde{N}_p}\left(\frac{U_0-b_p}{U_0-b_1}\right)=1 \tag{13}$$

in which the tilde mark denotes load reversals rather than load cycles. Since the number of load reversals is simply twice the number of load cycles, Eq. 13 may be rewritten as,

$$\frac{n_1}{N_{F1}}+\frac{n_2}{N_{F2}}\left(\frac{U_0-b_2}{U_0-b_1}\right)+\ldots+\frac{n_p}{N_{Fp}}\left(\frac{U_0-b_p}{U_0-b_1}\right)=1 \tag{14}$$

in which N_{Fp} is the fatigue life corresponding to a particular set of values $\overline{W}_p$ and R_p. If the quantities $b_1, b_2, \ldots, b_p$ are roughly equal to one another and/or they are very small compared to U_0, Eq. 14 reduces to the considerably simpler form:

$$\frac{n_1}{N_{F1}}+\frac{n_2}{N_{F2}}+\ldots+\frac{n_p}{N_{Fp}}=1. \tag{15}$$

It is clear that Eq. 15 is the exact analogue of the well-known "Cumulative Damage" or Palmgren-Miner Law for metal fatigue (cf. PALMGREN [14],

[1] The equation of this line is given by Eq. 6.

MINER [15], GROVER [16], KAECHELE [17] and LEVE [18]). Furthermore, insofar as the model is concerned, Eq. 15 is applicable regardless of the magnitude of $\overline{W}$ (provided that it is smaller than W_c) and regardless of the exact sequence of load applications (i.e. high loads followed by low loads or low loads followed by high loads). The only information one needs to have in order to use Eq. 15 for the model is the information contained in Fig. 14 and a specification of all but one of the values of $n_1, n_2, ..., n_p$. It is also worth noting that Eqs. 14 and 15 are apparently independent of the slope M of the U_F-line given by Eq. 6. Insofar as the derivation of these equations is concerned, there would be no difference in the result if it were assumed that $M = 0$. On the other hand, as was shown earlier, the values of $N_{F1}, N_{F2}, ..., N_{Fp}$ are clearly influenced by the character of the U_F versus N relationship.

Discussion and Conclusions

A consideration of the response of a simple portal frame model to cyclically applied loads reveals that localized plastic yielding alone is sufficient to cause behavior which simulates practically all of the gross macroscopic phenomena (in the purely deterministic sense) associated with metal fatigue. Hysteresis strain energy is widely recognized as an important macroscopic manifestation of the fatigue process in metals. The work of FELTNER [19], MARTIN [20], MORROW [21], CHANG [22] and LANDGRAF [23] is particularly noteworthy in this regard. It has been repeatedly (c.f. BAUSCHINGER [24], BAIRSTOW [25] and SANDOR [26]) observed, however, that the hysteresis which occurs when there are predominately tensile stresses differs considerably from that which occurs when the stresses are predominately compressive. In the former case, the micromechanisms of slip and microcracking contribute to fatigue behavior while in the latter case, slip alone may be the only significant micromechanism which is operative in the fatigue process.

While fatigue behavior in general may be investigated by means of hysteresis strain energy studies, it has been shown elsewhere [27] that hysteresis itself deserves study apart from its obvious implications with respect to fatigue. The goal of many investigations concerning the fatigue of metals is to produce a workable theory which will make an accurate prediction of fatigue behavior possible based upon data taken from tests of a relatively small number of samples. As a result of the analysis presented herein, it appears that such a goal can be attained, using hysteresis strain energy as the basic quantity measured, only if behavior in tension and behavior in compression can be properly differentiated and the resulting differences adequately treated.

Security and Economy

Metal fatigue is a catastrophic failure condition that has the potentiality to affect almost any bridge. This potentiality for disaster certainly justifies the many measures adopted by bridge engineers to minimize the dangerous effects of fatigue on their constructions. Yet, despite more than a century of research into the causes of fatigue in metals, much remains to be learned.

There are many questions regarding fatigue behavior that urgently require answers if engineers are to continue to provide improvements in the security and economy of bridge constructions. Some of the most urgent of these questions are: First, why do metals exhibit different fatigue characteristics when subjected on the one hand to purely compressive stresses and on the other hand to purely tensile stresses? Second, what is the relationship between hysteresis strain energy and fatigue strength? Third, and last, to what extent do fatigue effects cumulate in a metal structure subjected to a long history of cyclicallyvarying stresses? When satisfactory answers to these and other important questions are obtained, it will, of course, become possible to make more accurate predictions of the fatigue strength of bridge constructions than is now the case.

The mechanism of local plastic deformation or "slip" and the mechanism of microcracking or "fracture" are widely believed to be the microscopic phenomena which cause the wellknown macroscopic manifestations of fatigue to appear. It is shown in this paper, by means of an incremental collapse model, that the micro-mechanism of local plastic deformation alone is sufficient to account for practically all of the macroscopic manifestations of fatigue behavior in compression and that the fracture micro-mechanism is useful to explain the additional macroscopic aspects of fatigue which are associated with tensile stresses. Furthermore, it is shown that if properly treated, hysteresis strain energy is a useful macroscopic indicator of the fatigue process in metals. It is believed that the very careful categorization and elucidation of hysteresis strain energy described in this paper will lead to further progress in the quest for an adequate, and scientifically satisfactory basis for the prediction of fatigue strength of metal structures under service conditions.

Notation

E Modulus of Elasticity or Young's Modulus.
I Second static moment of cross-sectional area of flexural member.
L Length of Flexural member.
M_p Bending moment at which a plastic hinge will form in flexural member.
N_f Fatigue life or number of cycles to rupture in fatigue.
N_F Extended incremental collapse life or number of cycles to failure of the model.
W_a The alternating plasticity load.
W_c The plastic collapse load.
W_s The incremental collapse load or "shakedown" load.
$W_{\max}$ Maximum load intensity applied to the structure.
$W_{\min}$ Minimum load intensity applied to the structure.
$\overline{W}$ Mean load intensity applied to the structure.
R Range of loads applied to the structure (equal to absolute value of difference between $W_{\max}$ and $W_{\min}$).
S General notation for strength (i.e. stress level) in fatigue strength versus fatigue life graphs.
S_{EL} Endurance limit or Fatigue limit.
δ_h Horizontal displacement of end 2 of member 1-2 relative to end 1 during the application of a horizontal load to the frame at location 2.

δ_v Vertical displacement of member 2-4 at the point 3 relative to its end during the application of a vertical load to frame at location 3.

ΔU_i Irrecoverable energy or hysteresis energy imparted to the model during the ith cycle of load application and removal.

U Cumulative hysteresis energy imparted to the model at the end of the Nth cycle of load application and removal.

U_F Extended incremental collapse toughness or the sum of all hysteresis energy increments occurring during a sequence of cycles of stress application carried on until failure by incremental collapse occurs.

β Ratio of vertical load to horizontal load applied to the portal fram structure.

σ Stress.

σ_a Stress amplitude.

σ_m Mean stress = $1/2\ (\sigma_{max} + \sigma_{min})$.

σ_{max} Maximum stress level.

σ_{min} Minimum stress level.

σ_R Range of stress (equal to absolute value of difference between σ_{max} and σ_{min}).

Ω_f Fatigue toughness or the sum of all hysteresis strain energy increments occurring during a sequence of cycles of stress application carried on until fatigue rupture.

Acknowledgements

I am grateful to Professors Thomas Erber and Kuang-Han Chu of IIT for their many helpful suggestions and encouragement and to Mr. Surendra Singh for writing a computer program to carry out many of the extensive computations involved in this work.

The support of the National Science Foundation provided through Grant No. GH-34664 was of benefit during the final phase of the research.

References

1. TIMOSHENKO, S.P.: Strength of Materials. Vol. II, Third Edition, D. Van Nostrand Company, Inc., Princeton, N. J., 1956, pp. 413 and 514.
2. JAECKEL, H.R.: Simulation, Duplication and Synthesis of Fatigue Load Histories. Sound and Vibration, Vol. 4, March, 1970, pp. 18 to 29.
3. MARTIN, J.F., TOPPER, T.H., AND SINCLAIR, G.M.: Computer-Based Simulation of Cyclic Stress-Strain Behavior with Applications to Fatigue. Materials Research and Standards, Journal ASTM, Vol. 11, No. 2, February 1971.
4. WETZEL, R.M.: A Method of Fatigue Damage Analysis. Ford Motor Company Scientific Research Staff Technical Report, September, 1971, privately published.
5. NEAL, B.G.: The Plastic Methods of Structural Analysis. Chapman and Hall, London, 1956, Chapter V.
6. NEAL, B.G., and SYMONDS, P.S.: Cyclic Loading of Portal Frames, Theory and Tests. Publ. Intern. Assoc. of Bridge and Structural Engineer, Vol. 18, 1958, pp. 171–199.
7. GURALNICK, S.A.: Incremental Collapse Under Conditions of Partial Unloading. Publ. Intern. Assoc. of Bridge and Structural Engineers, Vol. 33, part II, September, 1973.
8. GERBER, W.: Bestimmung der zulässigen Spannungen in Eisenkonstructionen. Z. bayer. Architekten u. Ing. - Ver., 1874.

9. GOODMAN, J.: Mechanics Applied to Engineering. Longmans, Green and Company, London, 1899.
10. FÖPPL, O.: The Practical Importance of the Damping Capacity of Metals, Especially Steels. Journal of the Iron and Steel Institute, Vol. 134, 1936.
11. HALFORD, G.R.: The Energy Required for Fatigue. Journal of Materials. Vol. 1, No. 1, March 1966, pp. 3–18.
12. STÜSSI, Fritz: Die Dauerfestigkeit und die Versuche von August Wöhler. Mitt. der T.K.V.S.B., No. 13, Verlag V.S.B., Zurich, 1955.
13. HORNE, M.R.: Plastic Theory of Structures. MIT Press, Cambridge, Mass., 1971, p. 126.
14. PALMGREN, A.: Die Lebensdauer von Kugellagern. Zeitschrift des Vereins Deutscher Ingenieure, Vol. 68, 1924.
15. MINER, M.A.: Cumulative Damage in Fatigue. Journal of Applied Mechanics, Vol. 12, No. A-159, 1945.
16. GROVER, H.J.: An Observation Concerning the Cycle Ratio in Cumulative Damage. Symposium on Fatigue of Aircraft Structures. American Society for Testing and Materials, Special Technical Publication No. 274, 1960.
17. KAECHELE, L.: Review and Analysis of Cumulative Fatigue Damage Theories. The RAND Corp. Report RM-3650-PR, August 1963.
18. LEVE, H.L.: Cumulative Damage Theories. Chapter 6, Metal Fatigue, Edited by A.F. Madayag, John Wiley and Sons, Inc., New York, 1969.
19. FELTNER, C.E.: Strain Hysteresis, Energy and Fatigue Fracture. Report No. 146 of the Department of Theoretical and Applied Mechanics, University of Illinois, Urbana, Ill., June, 1959.
20. MARTIN, D.E.: An Energy Criterion for Low-Cycle Fatigue. Trans. ASME, Journal of Basic Engineering, December 1961, pp. 565–570.
21. MORROW, J.D.: Cyclic Plastic Strain Energy. To be found in Special Technical Publication, No. 378, entitled, "Internal Friction, Damping, and Cyclic Plasticity", published by the American Soc. for Testing and Materials, Philadelphia, Pa., 1965.
22. CHANG, C.S., PIMBLEY, W.T. and CONWAY, H.D.: An Analysis of Metal Fatigue Based on Hysteresis Energy. Experimental Mechanics, Journal of the SESA, March 1968, pp. 133–137.
23. LANDGRAF, R.W., MORROW, J.D., and ENDO, T.: Determination of the Cyclic Stress-Strain Curve. Journal of Materials, Vol. 4, No. 1, March 1969, pp. 176–188.
24. BAUSCHINGER, J.: Über die Veränderungen der Elastizitätsgrenze und der Festigkeit des Eisens und Stahls durch Strecken, Quetschen, Erwärmen, Abkühlen und durch oftmals wiederholte Belastung. Mitt. Tech. Lab., Munich, Vol. 13, 1886.
25. BAIRSTOW, L.: The Elastic Limits of Iron and Steel Under Cyclical Variations of Stress. Philosophical Transactions of the Royal Society, London, Series A, Vol. 210, p. 35, 1911.
26. SANDOR, B.I.: Fundamentals of Cyclic Stress and Strain. University of Wisconsin Press, Madison, 1972.
27. ERBER, T., GURALNICK, S.A., and LATAL, H.G.: A General Phenomenology of Hysteresis. Annals of Physics, Published by Academic Press, Inc., Vol. 69, No. 1, January 1972, pp. 161–192.

Summary

Many of the phenomena observed in connection with fatigue of metal structures subjected to long-term, cyclically-varying loads remain unexplained. The stress-strain hysteresis exhibited by a metal structure or specimen when it is subjected to cyclically-varying loads has long been considered to be an important indicator of fatigue characteristics. Unfortunately, a means of satisfactorily linking stress-strain hysteresis with fatigue strength has hitherto been lacking. It is shown by means of an incremental collapse model that a process of localized plastic deformation (or "slip") is sufficient to cause fatigue rupture even under conditions where only purely compressive stresses exist. Hence, the differences in fatigue behaviour of the same material when subjected on the one hand to purely compressive stresses and the other hand to purely tensile stresses is explained.

Résumé

De nombreux phénomènes relatifs à la fatigue sous charges cycliques, variables et de longue durée, restent encore inexpliqués. L'hystérèse contrainte/allongement de structures ou d'éléments en métal sous une charge cyclique variable a été longtemps considérée comme une caractéristique importante de la fatigue. Mais il manquait une relation entre cette hystérèse et la résistance à la fatigue. Un modèle incrémental de rupture a permis de démontrer qu'un processus de déformation plastique limitée suffit à provoquer une rupture de fatigue, même en la seule présence de contraintes de compression. Les différences dans le comportement à la fatigue d'un même matériau sont ainsi expliquées, selon qu'il s'agit exclusivement de contraintes de compression ou de traction.

Zusammenfassung

Zahlreiche Phänomene der Metallermüdung unter lange wirkenden zyklisch variierenden Lasten bleiben ungeklärt. Die Spannungs/Dehnungs-Hysterese, die an Metallbauten oder -proben auftritt, wenn diese zyklisch variabler Belastung ausgesetzt sind, wurde lange als wichtiges Merkmal des Ermüdungsverhaltens betrachtet. Leider fehlte bisher eine befriedigende Beziehung zwischen der Spannungs-Dehnungs-Hysteresis und der Ermüdungsfestigkeit. An einem inkrementalen Modell wird gezeigt, dass ein Prozess örtlich begrenzter plastischer Verformungen (bzw. „Schiebungen") genügt, um Ermüdungsbrüche sogar unter Anwesenheit reiner Druckbeanspruchung herbeizuführen. Deshalb werden die Unterschiede im Ermüdungsverhalten desselben Materials erklärt, wenn dieses einerseits reiner Druckbeanspruchung, anderseits reiner Zugbeanspruchung ausgesetzt ist.

Leere Seite
Blank page
Page vide

Inelastic Response of Prestressed Concrete Beams

Comportement inélastique de poutres précontraintes en béton

Unelastisches Verhalten vorgespannter Betonbalken

J.M. KULICKI
Engineer, Modjeski and Masters, Harrisburg Pennsylvania (Formerly Visiting Assistant Professor of Civil Engineering, Lehigh University)

C.N. KOSTEM
Associate Professor
Fritz Engineering Laboratory
Lehigh University
Bethlehem, Pennsylvania, USA

Introduction

The purpose of the reported study was to develop an analytic technique to adequately describe the inelastic load-deflection behavior of prestressed concrete beams. The finite element method was used as the basis of solution. The stress distribution, and response to material nonlinearities such as the yielding of the reinforcement and the cracking and crushing of concrete are included. It was desired to produce a technique which would be efficient enough to be used as part of a larger nonlinear analysis problem, e.g., the overload analysis of beam-slab bridges. It will be seen that simplifying assumptions have been made in order to achieve the desired efficiency while continuing to allow a realistic treatment of beams subjected primarily to bending action. The emphasis of this paper will be on nonlinear analysis of prestressed concrete beams. Notation used herein will be defined when first encountered.

Basic Model

The basic model under consideration is a simply supported, essentially prismatic beam subjected to loading in a plane of symmetry. The formulation is general enough to allow for a wide range of materials and boundary conditions, but does not allow for the inclusion of local or lateral-torsional buckling of the beam. The nonlinear behavior of a beam is treated as a piecewise linear problem using an incremental loading path with iteration of each load step.

The beam is discretized as a series of beam type finite elements along its length. The elements are subdivided into layers. The node points at each end of the beam elements lie in an arbitrary plane of reference. Fig. 1 shows a beam element, coordinates and positive sign conventions. The plane sections assumed by the

Bernoulli beam theory is used to relate the strains in the layer to the displacements at the nodes. If a sufficient number of layers is used each layer may be assumed to be in a state of uniaxial tension or compression with the centroid of the layer assumed to be representative of the layer. These assumptions would become tenuous if high shearing stresses were present.

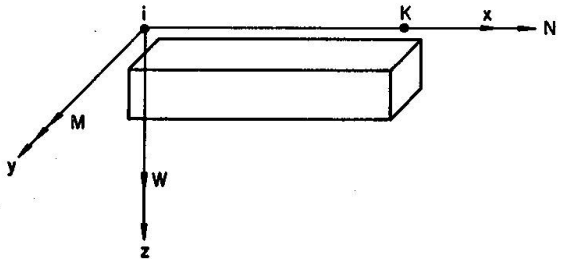

Fig. 1. Coordinate system and positive sign convention.

The effect of this simplified layered model on the economy of solution via the tangent stiffness approach is apparent from the following example. If 10 elements each having 15 layers is used with the proposed method there are 11 nodes each having 3 degrees of freedom. This results in 33 simultaneous equations. If, on the other hand, a continuum approach utilizing 300 triangular elements with 2 degrees of freeedom per node were used, there would be 352 simultaneous equations. Considering that incremental $\frac{1}{N}$ iterative approaches may require hundreds of solutions it is apparent that the savings in computational effort is enormous.

There are three degrees of freedom at each node of the beam element. They are the axial displacement, U, the lateral displacement, W, and the bending rotation, θ. The following polynomials are used to describe displacements within the element.

$$U = \alpha_1 + \alpha_2 X \tag{1}$$

$$W = \alpha_3 + \alpha_4 X + \alpha_5 X^2 + \alpha_6 X^3 \tag{2}$$

The α's are constants to be determined by using the boundary conditions at both ends of an element.

The generalized stresses are the normal force, N, and bending moment, M, at the plane of reference defined by $Z = 0.0$ in Fig. 1. The generalized strains are the axial strain and curvature at the plane of reference. The generalized stresses and strains are related by an elasticity matrix $[D]$. The assumption of plane sections makes it possible to generate the elasticity matrix using the usual equations of mechanics instead of the theory of elasticity. This is a trade-off of some accuracy and geometric generality for far greater computational efficiency. The result is:

$$\begin{Bmatrix} N \\ M \end{Bmatrix} = \begin{bmatrix} \bar{A} & \bar{S} \\ \bar{S} & \bar{I} \end{bmatrix} \begin{Bmatrix} dU/dX \\ -d^2W/dX^2 \end{Bmatrix} \tag{3}$$

in which for n layers per element:

$$\bar{A} = \sum_{i=1}^{n} E_i A_i, \; \bar{S} = \sum_{i=1}^{n} E_i A_i Z_i, \; \bar{I} = \sum_{i=1}^{n} E_i A_i Z_i^2 \tag{4}$$

The element stiffness matrix can then be established using the well defined procedures of the finite element method, e.g., [16]. A detailed derivation can be found in [8].

Incremental Iterative Analysis Scheme

The load is applied in increments. The increments of forces, $\{F\}$, and displacements, $\{\delta\}$, are related by Eq. 5.

$$\{F\} = [K]\{\delta\} \tag{5}$$

Matrix $[K]$ is the assembled and reduced tangent stiffness matrix for the beam. The displacement increment is used to compute new trial increments of stress and strain. Each incremental displacement component is then checked against the corresponding component of the last trial. If all are within a relative tolerance of the last trial the iteration is stopped and the stress and displacement fields are incremented to include the new contributions from this load step. Each layer is then checked for tensile cracking or compressive crushing.

If no cracking or crushing has taken place, another load increment is added and the process is repeated with the generation of a new stiffness matrix which reflects the current state of stress.

If convergence of the current load step has not been attained the incremental stresses are temporarily added to the total stresses to find new tangent moduli using the layer stress-strain laws. A new stiffness matrix is generated and new incremental displacements are computed and compared with the last set to check convergence. This process is repeated until either convergence is attained in a limited number of trials or the maximum number of trials is reached at which time the load increment is reduced and the whole process is repeated.

Stress-Strain Curves

The following types of stress-strain curves can be used: (1) elastic-brittle, (2) elastic-plastic, not just elastic-perfectly plastic, (3) elastic-plastic with linear strain hardening, (4) elastic-plastic with tensile cracking, and (5) elastic-plastic with tensile cracking and compressive crushing.

The Ramberg-Osgood formulation, [12], has been chosen to provide generality in the shape of the stress-strain curve while maintaining a continuous mathematical expression, and to allow for a common base for all stress-strain curves.

$$\varepsilon = \frac{\sigma}{E} + \frac{1-m}{m}\left(\frac{\sigma_1}{E}\right)\left(\frac{\sigma}{\sigma_1}\right)^n \tag{6}$$

σ = Stress at some load.
ε = Strain at a stress equal to σ.
E = Initial modulus of elasticity.
σ_1 = Secant yield strength equal to the ordinate of intersection of the $\sigma\frac{I}{N}\varepsilon$ curve and a line of slope $(m)\cdot(E)$.
n = A constant.
m = A constant defining a line of slope $(m)\cdot(E)$ on a plot of stress and strain.

The following approach has led to stress-strain curves for concrete in uniaxial compression which compare well with similar curves in the literature:

1. Assume a value for Young's modulus from any acceptable equation or from laboratory tests.
2. Assume $\sigma_1 = f'_c$.
3. Assume that the stress-strain curve must pass through the point $(\bar{\varepsilon}, f'_c)$. This leads to the following equation for the coefficient m. $\bar{\varepsilon}$ is typically 0.002 for normal weight concrete.

$$m = \frac{f'_c}{E\bar{\varepsilon}}$$

4. Assume the Ramberg-Osgood curve stops at a strain of $\bar{\varepsilon}$.
5. Assume a horizontal straight line from a strain of $\bar{\varepsilon}$ to a strain given in Table 1 below as ε_1.
6. Assume a straight line sloping downward from ε_1 to a stress of zero. Suggested values for this slope, "E_{down}", are also found in Table 1. "E_{down}" will be used to compensate for compressive crushing.

Table 1

f'_c(psi)	E_{down}(ksi)	ε_1
5600	3000	0.0022
4750	1800	0.0022
3900	1250	0.0023
<3000	700	0.0024

7. From trial and error comparisons a value of $n = 9$ was found to give consistently good results for all strengths tried.

The results of this method of approximating the concrete compressive stress-strain curve are shown in Fig. 2. The approximate curves are quite close to the

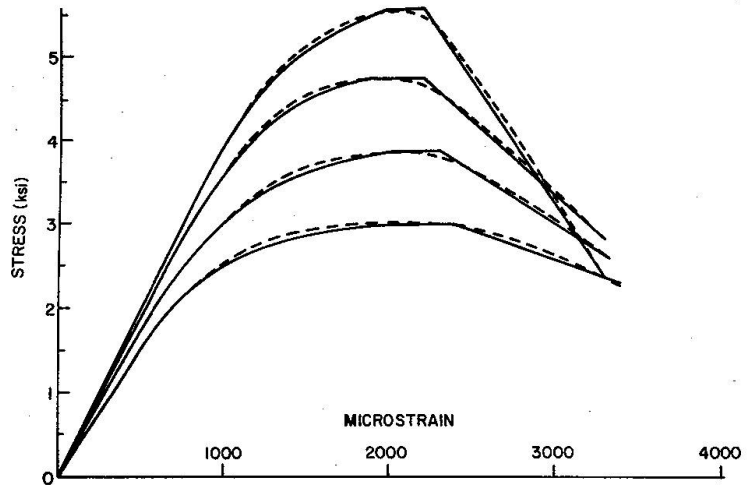

Fig. 2. Analytic and "actual" stress-strain curves.

typical smoothed concrete stress-strain curves as measured on the compressive side of flexural tests which are shown by the dotted lines. The overall shape is similar to that of Hognestad's stress-strain curve [5]. This curve has been compared with specific stress-strain curves for concrete [2 and 13]. The result is shown in Fig. 3.

The object of this analytic method is to produce the load-deflection curve of prestressed concrete beams. This implies that the strength and stiffness of concrete in tension cannot be neglected as is commonly done in ultimate strength type analyses. The inclusion of tensile concrete in this analysis procedure requires the employment of an appropriate tensile stress-strain curve for concrete. [3, 7 and 11] contain complete experimental tensile stress-strain curves for concrete. Fig. 4 represents the particular curves found in [3]. Unfortunately there is a small data base from comparative complete tensile and compressive stress-strain curves. This means that some assumptions about the tensile stress-strain curves are necessary. Fig. 5 shows the analytic tensile stress-strain curve actually used in the numerical examples to be presented as Curve *B*. The formulation has been left general enough to accept a curve as complex as Curve *A*, modeled after the curves in Fig. 4, so that the future developments in material behavior can be accomodated. The principle that concrete cracking does not create instantaneous unloading, as evidenced by the analytic tensile stress-strain curve used here, has also been employed by other investigators [1, 6, 10, 14]. The term tension stiffening stress-strain curve has also been used to describe similar phenomenon. Further information on the development of this tensile stress-strain curve can be found in [8].

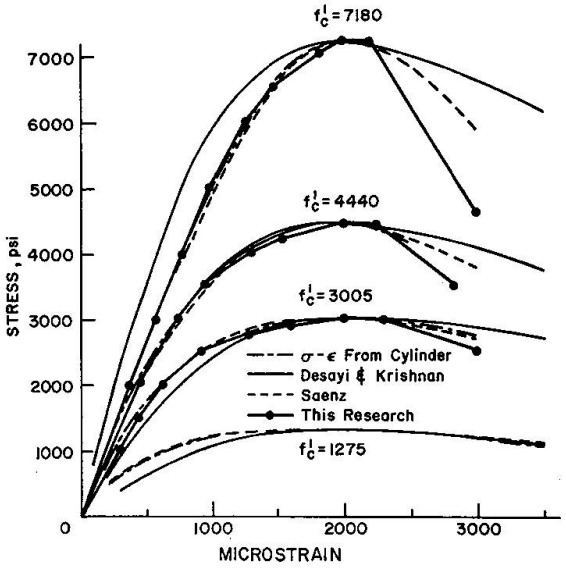

Fig. 3. Comparisons of concrete stress-strain curves.

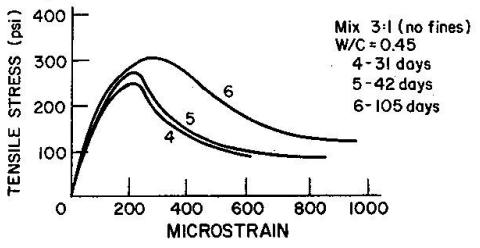

Fig. 4. Concrete tensile stress-strain curves.

The effect of various parameters used to define the tensile and compressive stress-strain curves on the resulting load-deflection behavior for under-reinforced prestressed concrete beams has been studied. This information as well as the effect of other geometric modeling parameters are contained in [9].

Application of Ramberg-Osgood formulation to reinforcing and prestressing steels is virtually exactly what it was intended for and deserves no more comment.

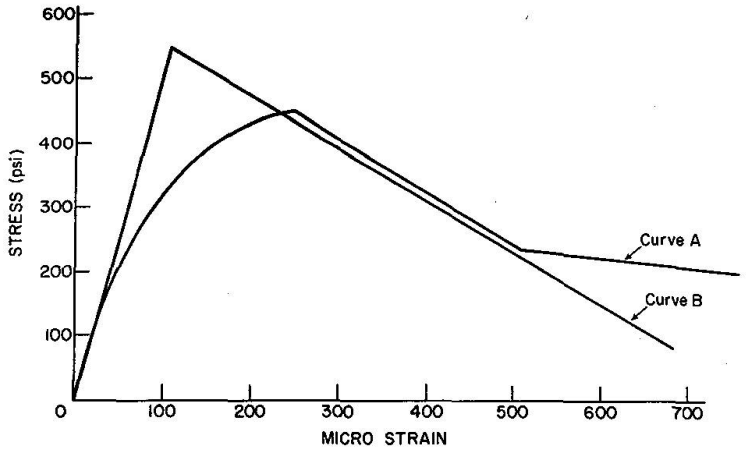

Fig. 5. Analytic tensile stress-strain curves.

A Technique for Cracking and Crushing Analysis

When the iterative procedure used to find the incremental displacements and stresses corresponding to a given load step has converged to an acceptable tolerance, the accumulated stresses and displacements are tentatively incremented. A prescanning and load reduction process is used to prevent large overstressing of the material for any load step. If no stresses exceed the compressive or tensile limit, another load step is taken.

If scanning reveals that the temporary accumulated stress is greater than the allowable tensile stress for any layer, then the layer is said to have cracked and steps are taken to set its modulus of elasticity to zero and redistribute the stresses in that layer.

The redistribution of stresses is accomplished by using the downward leg of the tensile stress-strain curves and a basic concept of the initial stiffness method. The amount of strain beyond that corresponding to cracking, or the incremental strain, whichever is appropriate, is multiplied by "E_{downt}" to produce a stress-like quantity called a fictitious stress. This is shown schematically in Fig. 6. This fictitious stress is applied to the layer which has cracked until the sum of the increments of fictitious stress and the accumulated tensile stress are zero. The redistribution to the rest of the beam is accomplished by using the layer area to convert stress into an eccentric force and thereby generating a fictitious load vector with axial force and corresponding moment terms. This is also shown in Fig. 6 in which element "i" is unloaded by the fictitious stress while the rest of the beam is being held in equilibrium.

Fig. 6. Ficticious stresses and forces.

During the same scanning operation a test is also made to see if a given layer exceeds a crushing criteria. The crushing criteria for a layer is the attainment of the maximum compressive stress or a strain greater than ε_1 as given in Table 1. If it is ascertained that crushing has occurred, the first stage is to set Young's modulus equal to zero. If the strain is less than the value of ε_1 given in Table 1 no unloading or redistribution is considered. If the strain exceeds ε_1, the excess strain is converted to fictitious stresses and hence fictitious loads analogously to the tensile cracking analysis.

Once all layers have been scanned, the fictitious load vector is used to compute an auxiliary stress and displacement increment. Essentially the same iterative process is used to find convergence for the auxiliary displacement increment as that used for the actual load step. Once convergence has been obtained, the layers are rescanned to check if the redistribution of cracking and/or crushing stresses has caused any more layers to reach a cracking or crushing criteria. If any layers have reached these criteria the process of assembling a fictitious load vector and iterating to convergence is repeated. If no additional layers have reached cracking or crushing there may still be additional fictitious load vector components as a result of the additional strains computed from the increments of displacements. Therefore, the entire process is repeated until the fictitious loads are smaller than some tolerance. At that time the cracking-crushing analysis is terminated and the accumulated stress and displacement field are permanently updated for the effects of this load increment.

Prestressed Concrete Beams

The additional steps used with prestressed concrete beams follow from the physical actions involved in prestressing. An initial stress field is read in for each layer. This provides the initial steel tension. An eccentric prestressing force is applied using the nodal force vector. It is advisable to compensate this prestressing force for the elastic loss which well occur when it is applied. It should be apparent that the object of applying the nodal forces used in prestressing is to produce the same thrust and moment diagrams in the reference plane as would be generated by replacing the prestressing elements at each point along the beam by an eccentric force at that location. This concept is important in generalizing the process for cases other than straight strands or for conditions other than prestressed concrete.

Consider a simply supported prestressed concrete beam pretensioned with a draped strand such that the end eccentricity was e_1 and the eccentricity at a distance L_2 from an end was e_2 and the strand was straight line segments in between. e_1 and e_2 are measured from the reference plane. The prestressing forces would then be modeled as follows:

1. An axial force, P, is applied at each end of the beam.
2. End moments are applied to each end of the beam to $(P)\,(e_1)$.
3. A concentrated load is applied to the point L_2 from an end such that $P(e_2 \frac{1}{N} e_1) = \bar{P}/L_2$.

In No. 3 $\bar{P}$ is the concentrated load, and L_2 is the distance from the end of the beam to drape point. If due consideration is given to algebraic sign this system of

forces will be equivalent to draped strand prestressing. The inclined strand should be simulated by a series of horizontal line segments to approximate its contribution to the global stiffness matrix.

The beam deflects under the influence of the nodal force and moment used to apply the prestressing force. The prestress camber must be included when displacements are converted to total strains to test against strain based behavior criteria.

Comparisons with Test Beams

The experimental results with which comparisons will be made were available in the literature. No experimental work was done as a part of this study. Comparisons will be made with rectangular and I-shaped prestressed concrete beams. All the beams were pretensioned with six 7/16 inch seven wire strands. The rectangular beams had two layers of three strands each, the I-beams had three layers of strands; the top layer having one strand, the middle two and the bottom three.

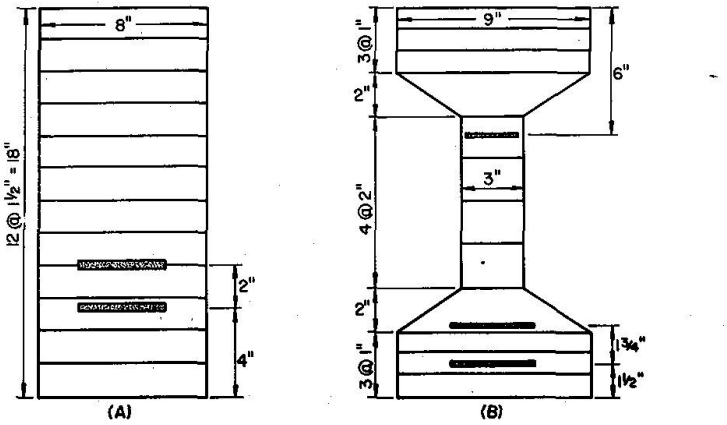

Fig. 7. Layering discretization.

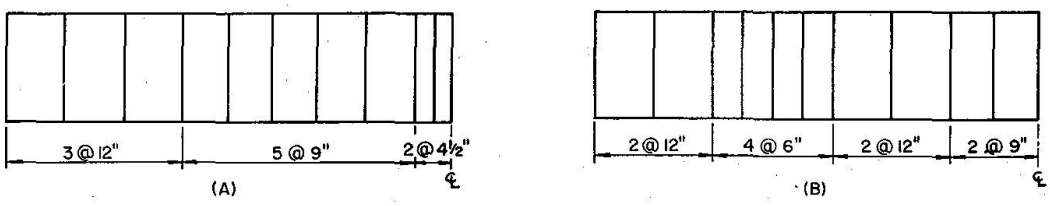

Fig. 8. Elemental discretization.

The prestressed concrete rectangular beams used for the comparative purposes in this study were tested by WALTHER and WARNER [15]. The cross-sectional layering and the elemental discritizations used to model this beam are shown in Figs. 7A and 8A. The cross-sectional dimensions and the half span lengths are also indicated in these figures. The rectangular beams were simply supported to produce a nine foot clear span and were subjected to third point loading within the span. Fig. 9 shows a comparison of the computed and measured load-deflection histories of the

beams. Each curve in Fig. 9 (and 10) starts with zero load and zero deflection. The horizontal axes are therefore shown with a "typical" distance rather than an enumerated annotation. The beams had cylinder strength ranging from 6.14 ksi to 6.32 ksi, the prestressing forces varied from 85.73 kips to 93.85 kips, on the day of testing. A comparison of analytic and experimental ultimate strength is given in Table 2.

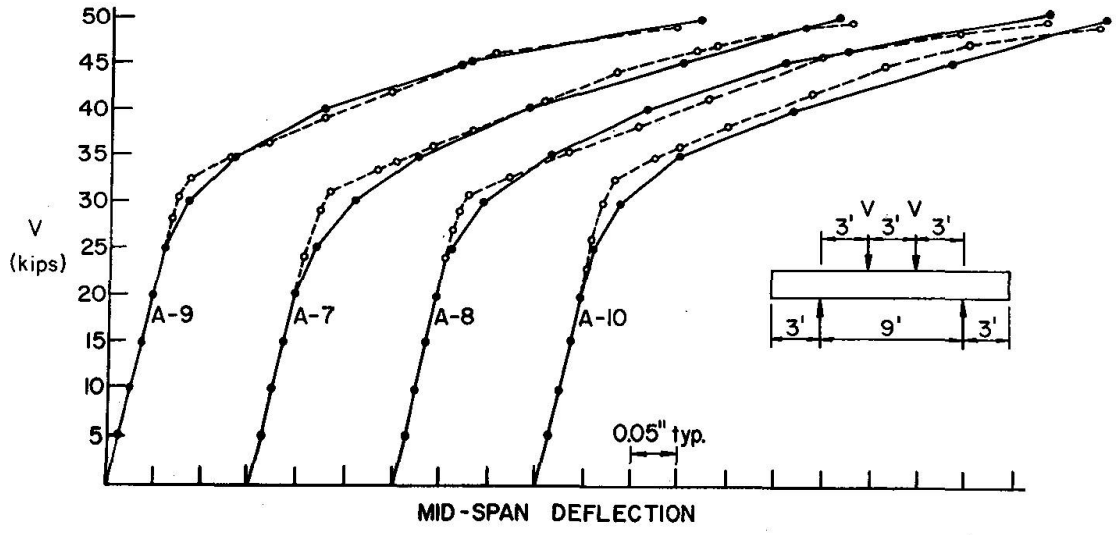

Fig. 9. Load-deflection-curves for prestressed concrete solid box beams.

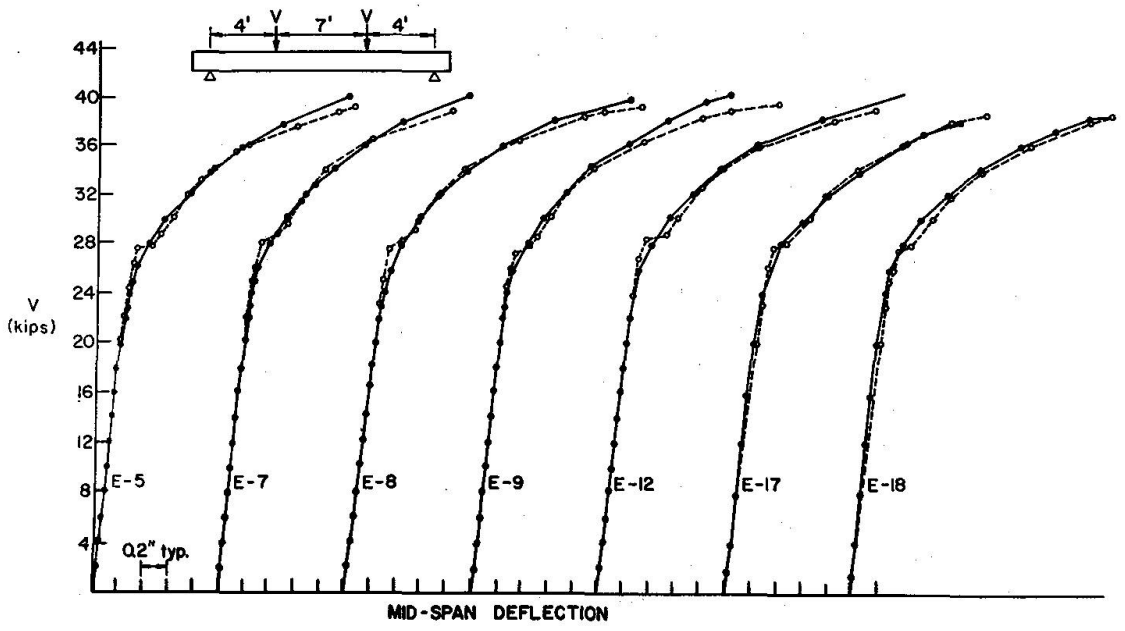

Fig. 10. Load-deflection curves for prestressed concrete I-beams.

The prestressed concrete I-beams were tested by HANSON and HULSBOS [4]. The discretization, layering and dimensions are shown in Figs. 7B and 8B. These beams were simply supported to produce a 15 ft. bending span and were loaded with a concentrated load 4 ft. from each end. Fig. 10 shows a comparison between

the analytical and experimental load-deflection curves for these beams. For this series of examples the cylinder strength varied from 6.58 ksi to 7.23 ksi, the prestressing force at the time of test varied from 90.6 kips to 92.6 kips. A comparison of analytic and experimental ultimate strength is given in Table 2.

Table 2: Ultimate Loads

Beam No.	Test (kips)	Calculated (kips)	Deviation (%)
A7	49.9	49.0	1.8
A8	50.2	48.9	2.6
A9	49.8	48.7	2.2
A10	49.9	49.0	1.8
E5	42.0	39.2	6.7
E7	41.1	39.8	3.2
E8	41.2	39.3	4.6
E9	41.2	38.9	5.6
E12	41.2	39.0	5.3
E17	38.0	38.2	0.5
E18	38.7	38.2	1.3

Other comparisons with reinforced concrete beams having considerably lower cylinder strength, uniformly distributed loading and the fixed ended steel beam, as well as more discussions of the test comparisons included herein can be found in [8 and 9].

Implementation

The analysis schemes, as applied to prestressed concrete beams, are primarily aimed either at the elastic regime or the ultimate strength of the member. The application of the reported study allows the prediction of the full inelastic behavior of these beams. Through the predicted response, the possible occurrence of overstressing, cracking, etc., can be predetermined for various load levels; which in turn will define the serviceability and safety characteristics of the structure. Conversely, economy in dimensioning can be assured for the beams that were overdimensioned in order to enhance their serviceability and strength, if the predicted response happens to be too conservative.

The reported scheme can, and in some cases has been, extended to the study of beam-columns, beam-slab bridge superstructures, gridwork, stiffened floors and similar structural systems. Due to the generality of the formulation, it can be applied to structural systems with or without prestressing. The structures can be constructed of any material with known stress-strain curve, or composites consisting of these materials.

Conclusions

A simple, efficient but effective model has been developed for the inelastic flexural analysis of beams. This method is based on a layered beam type finite element. An incremental iterative tangent stiffness analysis technique is used to solve the

nonlinear problem in a piecewise linear manner. The resulting load-deflection curves have been compared herein with experimental results obtained from tests of eleven prestressed concrete beams. Good correlation has been observed. This beam analysis technique has been developed for use in the analysis of bridge superstructures subjected to significant overloading.

References

1. CRANSTON, W.B., and CHATTERJI, A.K.: Computer Analysis of Reinforced Concrete Portal Frames with Fixed Feet, TRA/444. Cement and Concrete Association, London, England, 1970.
2. DESAYI, P., and KRISHNAN, S.: Equations for the Stress-Strain Curve of Concrete. Journal of American Concrete Institute, Vol. 61, No. 3, pp. 345–349, March 1964.
3. EVANS, R.H., and MARATHE, M.S.: Microcracking and Stress Strain Curves for Concrete in Tension. Matériaux et Constructions, No. 1, pp. 61–64, January-February 1968.
4. HANSON, J.M., and HULSBOS, C.L.: Overload Behavior of Prestressed Concrete Beams with Web Reinforcement. Fritz Laboratory Report, No. 223.25, Lehigh University, February 1963.
5. HOGNESTAD, E.: A Study of Combined Bending and Axial Load in Reinforced Concrete Members. Bulletin Series, No. 399, Engineering Experiment Station, University of Illinois, 1951.
6. HSU, C.-T., and MIRZA, M.S.: Structural Concrete-Biaxial Bending and Compression. pp. 285–290, ST2, Journal of the Structural Division, Proceedings of the American Society of Civil Engineers, February 1973.
7. HUGHES, B.P., and CHAPMAN, G.P.: The Complete Stress-Strain Curve for Concrete in Direct Tension. Bulletin RILEM, No. 30, March 1966.
8. KULICKI, J.M., and KOSTEM, C.N.: The Inelastic Analysis of Reinforced and Prestressed Concrete Beams. Fritz Laboratory Report, No. 378B.1, Lehigh University, November 1972.
9. KULICKI, J.M., and KOSTEM, C.N.: Further Studies on the Nonlinear Finite Element Analysis of Beams. Fritz Engineering Laboratory Report, No. 378A.5, Lehigh University, April 1973.
10. LIN, C.S.: Nonlinear Analysis of Reinforced Concrete Slabs and Shells. Report No. UC SESM 73-3, Structures and Materials Research Department of Civil Engineering, University of California, Berkeley, 1973.
11. NELISSEN, L.J.M.: Biaxial Testing of Normal Concrete. Heron, Vol. 18, No. 1, Stevin Laboratory of the Department of Civil Engineering, Delft Technological University, the Netherlands, 1972.
12. RAMBERG, W., and OSGOOD, W.R.: Description of Stress Strain Curves by Three Parameters. NACA, TN 902, July 1943.
13. SAENZ, L.P.: Discussion of Equations for the Stress-Strain Curve of Concrete. By P. DESAYI and S. KRISHNAN. American Concrete Institute Journal, Proceedings, Vol. 61, No. 9, pp. 1229-1235, September 1964.
14. SCANLAN, A., and MURRAY, D.W.: An Analysis to Determine the Effect of Cracking in Reinforced Concrete Slabs. pp. 841–868 of the Proceedings of the Specialty Conference on Finite Element Method in Civil Engineering, McGill University-Canadian Society of Civil Engineers-Engineering, Institute of Canada, 1972.
15. WALTHER, R.E., and WARNER, R.F.: Ultimate Strength Tests of Prestressed and Conventionally Reinforced Concrete Beams in Combined Bending and Shear. Prestressed Concrete Bridge Members Progress Report No. 18, Fritz Laboratory, Lehigh University, September 1958.
16. ZIENKIEWICZ, O.C.: The Finite Element Method in Engineering Science. McGraw-Hill Book Company, New York, 1971.

This work was sponsored by the Pennsylvania Department of Transportation; U.S. Department of Transportation, Federal Highway Administration; and the U.S. National Science Foundation. Their assistance is gratefully acknowledged. The contents of this paper reflect the view of the authors who are responsible for the facts and the accuracy of the data presented herein. The contents do not necessarily reflect the official views of the policies of the sponsors.

Summary

An analytical method is presented that describes the inelastic load deformation behaviour of prestressed concrete beams. Material nonlinearities such as cracking and crushing of concrete and yielding of steel are included. It is assumed that the response of the member is flexure dominated. Through simplifying assumptions maximum computational economy is achieved without any sacrifice in accuracy. The scheme is based on the finite element method.

Résumé

L'article présente une méthode analytique décrivant le comportement charge/déformation inélastique de poutres précontraintes en béton, tenant compte de non-linéarités, telles que fissuration et rupture du béton et écoulement de l'armature. Il est assumé que l'élément de construction est soumis essentiellement à la flexion. Des hypothèses simplificatrices permettent une économie de temps d'ordinateur sans diminution de la précision.

Zusammenfassung

Der Beitrag behandelt eine Methode zur Berechnung des unelastischen Last-Deformations-Verhaltens vorgespannter Betonbalken. Dabei sind Nichtlinearitäten, wie Rissebildung und Stauchung des Betons sowie das Fliessen der Bewehrung inbegriffen. Es wird angenommen, dass das Verhalten des Bauelementes vorwiegend auf Biegung zurückzuführen ist. Durch vereinfachende Annahmen wird eine grösstmögliche Einsparung an Rechenzeit ohne irgendwelche Beeinträchtigung der Genauigkeit erzielt. Das Verfahren stützt sich auf die Methode der finiten Elemente.

Experimental Study of Masonry Walls Strengthened by Reinforced Concrete Elements

Etude expérimentale de murs en maçonnerie renforcés d'éléments en béton armé

Experimentelle Untersuchung an durch Stahlbetonelemente verstärktem Mauerwerk

M. LEVY

D.Sc., Previously Research Fellow, Struct. Dept., Building Research Station, Technion - Israel Institute of Technology, Presently Chief Struct. Engineer in "Yotam" Advanced Design Consultants Ltd. Haifa, Israel.

E. SPIRA

Professor, Fac. of Civil Engineering, Technion - Israel Institute of Technology.

Introduction

The structural behaviour of a masonry wall bordered by reinforced concrete, which is a structural element of some importance, has not been analyzed in a satisfactory manner till now. It has been under intensive investigation during the last decades. In masonry infilled frames the influence of openings on the lateral rigidity [3] and the resistance against differential support settlements [6] was studied. The great majority of the theoretical studies, which either determine displacements by the Finite-Element method [3] or the Stress Function by Finite Differences techniques [2, 4, 8] are based on the assumption of linear elasticity. But in view of early cracking of the masonry, owing to the brittleness and separation of the components, the validity of the linear elastic analysis is rather limited in range as far as the structural behaviour is concerned.

In [8] the authors report on an experimental investigation of masonry walls bordered by r.c. elements. In the present paper the findings of the above experiments are examined in the light of a theoretical linear analysis. Special attention is paid to the question of the validity range of the theoretical analysis, and procedures for predicting cracking or failure loads are suggested.

General Description of Experiments

The objective was to study the structural behaviour of masonry walls bordered by r.c. elements and to compare it with the predicted results obtained by linear elastic analysis, cf. [2, 8].

Two test series are discussed:

Series A – Dealing with uniformly loaded and simply supported walls.

Series B – Dealing with continuous walls with openings, acted upon by differential support settlements.

Series *A* comprises 8 specimens with and without edge columns, which represent 1:2 scale models of actual wall panels, the masonry being either of 7.5 cm thick "Ytong" blocks (light weight aerated cellular concrete) or 10 cm thick hollow block concrete. They were tested in 1958-1960 in the Building Research Station of the Technion - Israel Institute of Technology, by Dr. S. Rosenhoupt, as reported in [5]. Some additional conclusions flowing from these experiments are brought here.

Details of the specimens are shown in Figs. 1-3 where the failure crack patterns are indicated.

Series *B* comprises two specimens (*B*1, *B*2), representing 1:2 scale models of hollow concrete block walls on three supports with door openings. Details are shown in Figs. 5-7.

The loading was by forces corresponding to differential support settlements.

Material Properties

Concrete (age 28 days):

Series	Cube strength (kg/cm^2) measured on 12 cm cubes		Modulus of elasticity (kg/cm^2) measured on 10/10/52 cm prisms	
A	142	191	175,000	235,000
B	206	228	230,000	270,000

Note: The higher values correspond to bottom beams, the smaller ones — to top beams and posts.

Concrete hollow blocks (two holes):

Series	Dimensions	Crushing strength (kg/cm^2) related to gross area	Modulus of elasticity (kg/cm^2) measured on masonry pier
A	10/10/20	32	20,000
B	10/10/20	78	75,000

"Ytong" blocks (Series *A*): – 7.5/15/25 cm, 650 kg/m^3 specific weight; crushing strength 14.5 kg/cm^2; modulus of elasticity 6900 kg/cm^2, measured on a 7.5/61.5/50.5 cm masonry.

Mortar for joints:

Series	Crushing strength (kg/cm^2) measured on 7 cm cube	Tensile strength in flexure (kg/cm^2) measured on prisms 7/7/28 cm
A	4.5	3.4
B	89	22

Reinforcement steel: modulus of elasticity 2,090,000 kg/cm^2:

Series	Diam (mm)	Yield joint (kg/cm^2)	Ultimate strength (kg/cm^2)
A	6	4,830	6,220
	8	3,150	4,100
	12	3,140	4,240
B	6	3,129	4,450
	8	3,770	4,830
	10	4,270	5,400

Loading, measurement and results

All specimens of series *A* were loaded on the top beam by means of an AMSLER hydraulic press.

Measurements read included:

— Vertical strains across the first masonry layer (on the bottom beam) and horizontal strains in 3 vertical sections, measured by mechanical strain gauges of 0.001 mm reading accuracy.

— Deflection of the bottom beams by means of deflectometers of 0.01 mm reading accuracy.

Figs. 1, 2 give the measured results versus their predicted values for specimens A4 and A7. Dotted lines and figures in brackets are values obtained by elastic analysis.

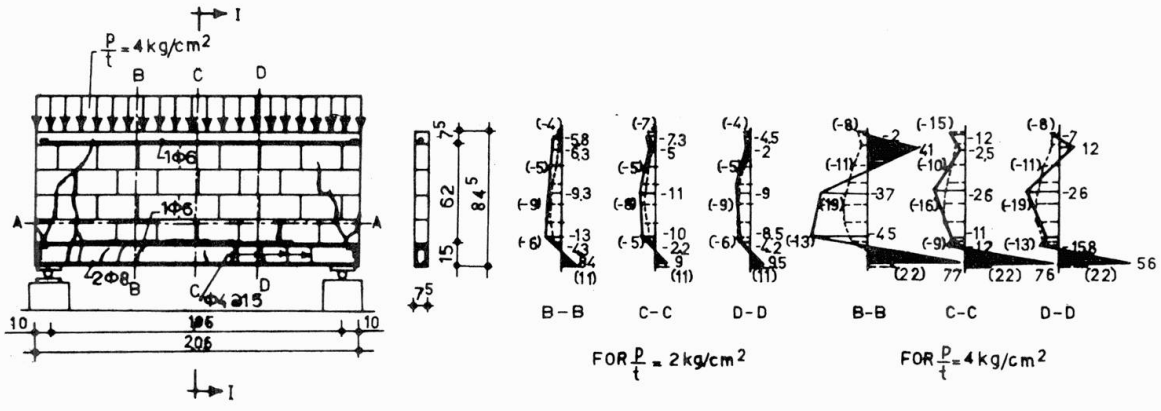

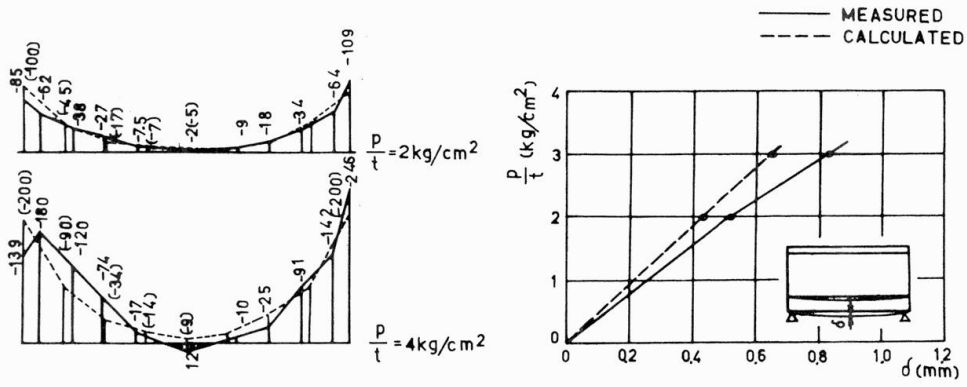

Fig. 1. Test A4.

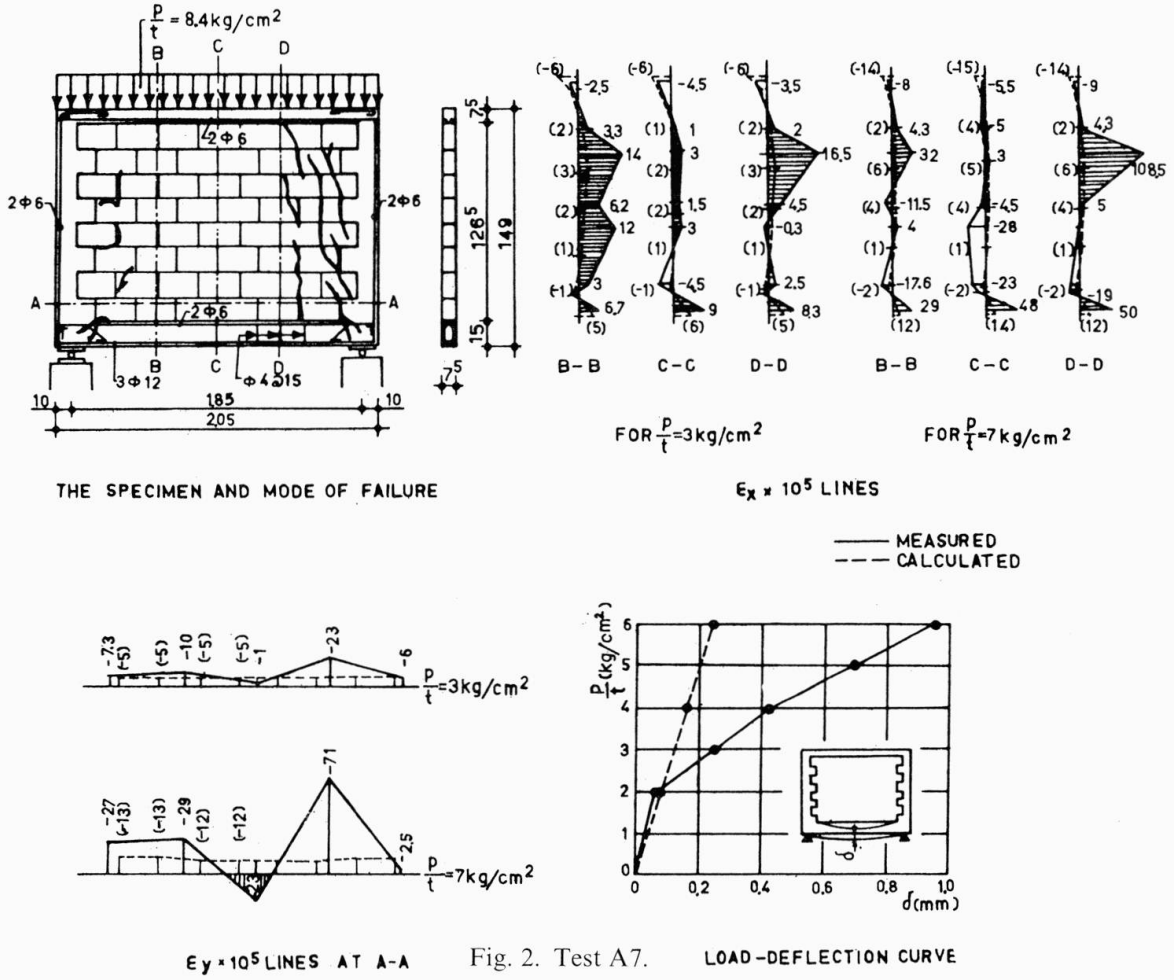

Fig. 2. Test A7. LOAD-DEFLECTION CURVE

Fig. 3 shows the crack patterns at ultimate load and in Fig. 4 the curves of mid span deflection of bottom beams.

Specimens B1 and B2 – (Figs. 5 to 7) which were erected as continuous units together with the base blocks and base columns, rest on 3 pairs of (base) columns, and were separated from them by paper layers, in order to eliminate tensile forces between them.

The loading included 2 parts:

— Uniformly distributed load at the top amounting to a total of 4.0 tons (i.e. = 1.0 t/m) supplied by 4 jacks of 17.0 tons capacity each.

— A variable concentrated load from below, supplied by a 10.0 ton jack (Fig. 6).

The load (from below) was applied in two manners:

— First at the central support, while the two edge columns were anchored in the testing floor up to ultimate load ("Convex bending").

— Then the load was applied at one of the edge supports, while the other 2 columns were anchored in the testing floor ("Concave bending").

"Convex bending" — The load was applied in rates of 200 to 500 kgs until incipient failure, while at each load level the upward displacement of the point of load application was measured by 3 deflectometers. In addition, the strains in the masonry were measured, once before applying the load from below, and a second time, when it had the value of 4.5 tons.

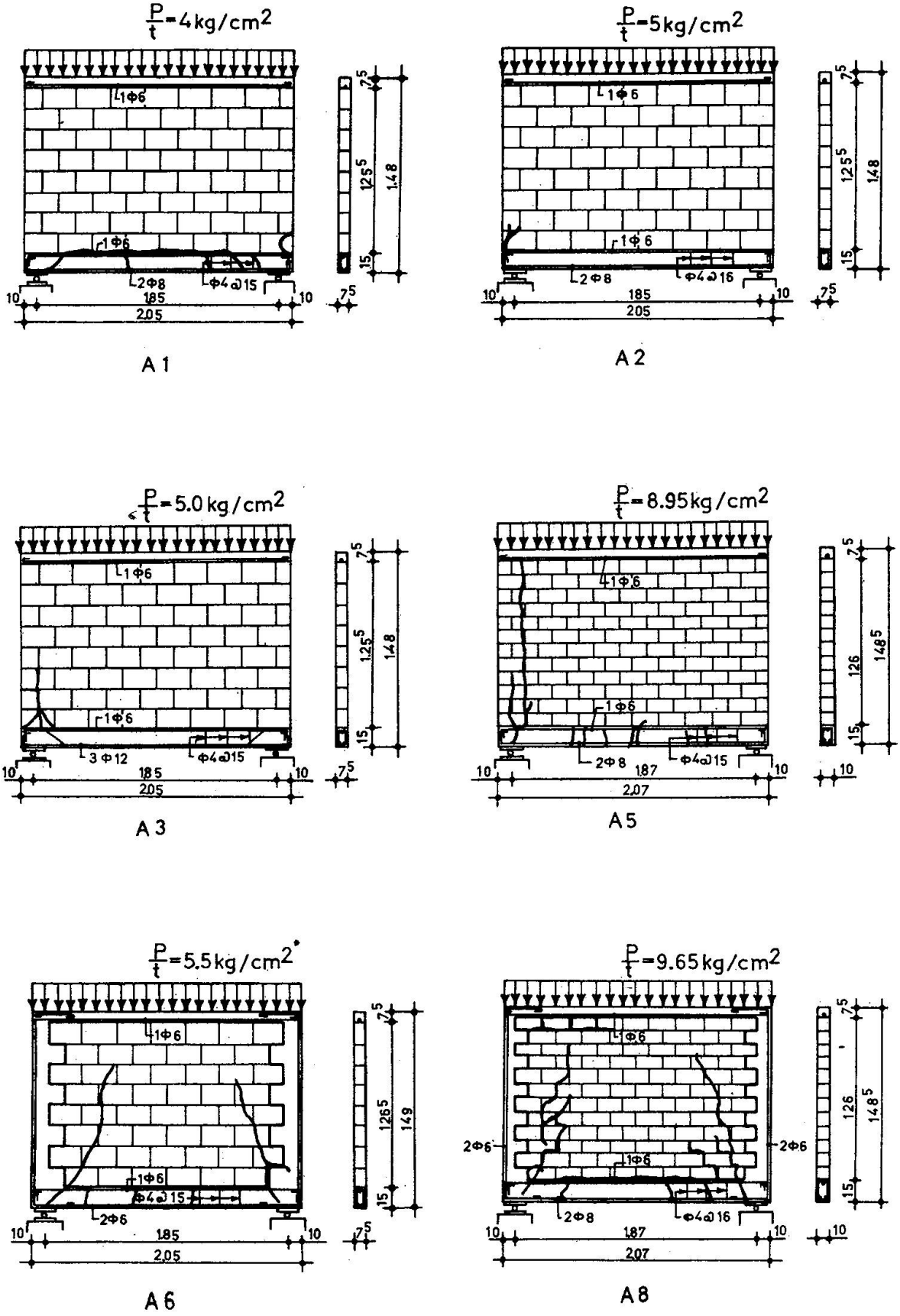

Fig. 3. Series A, Specimens and Modes of Failure.

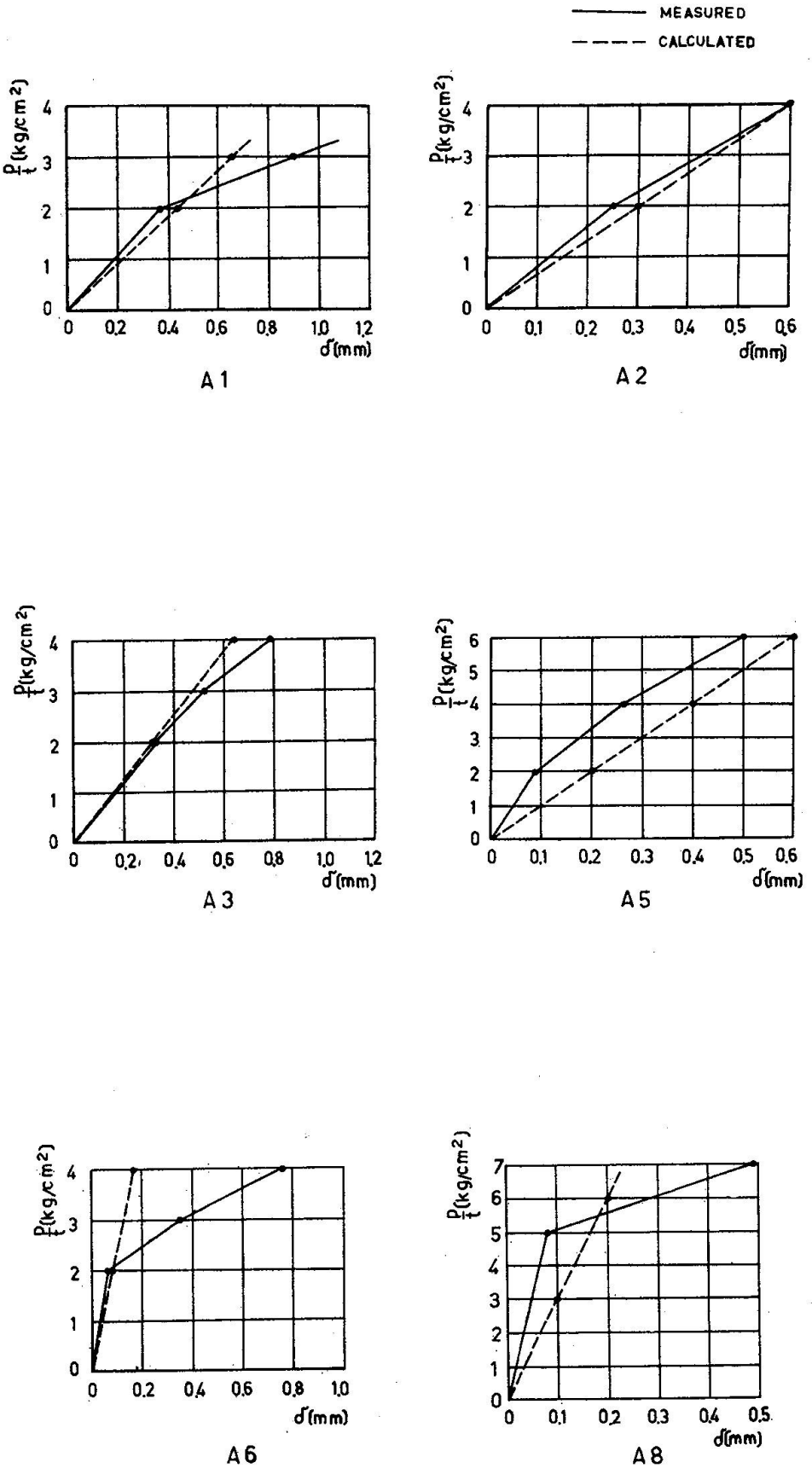

Fig. 4. Series A, Load Deflection Curves.

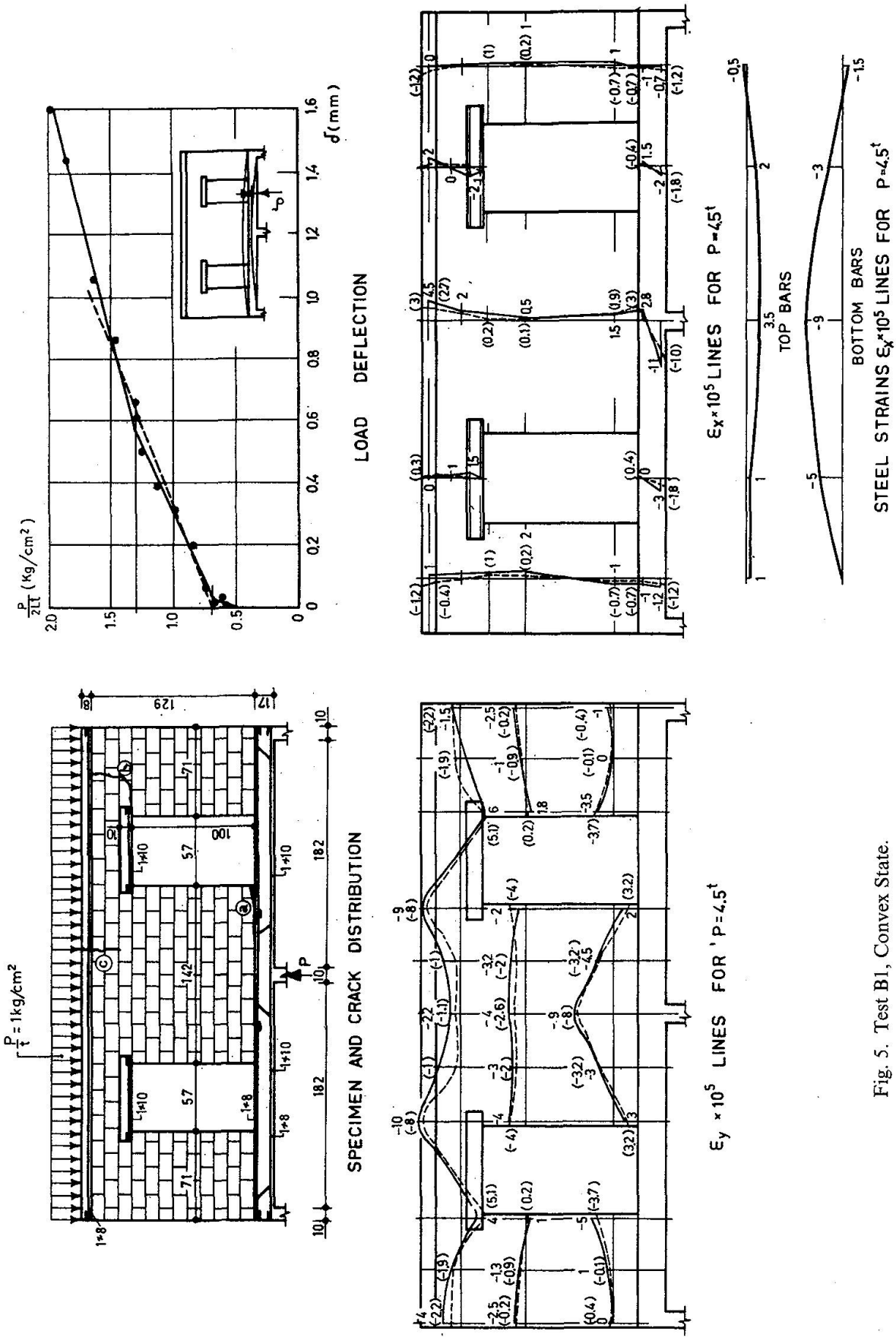

Fig. 5. Test B1, Convex State.

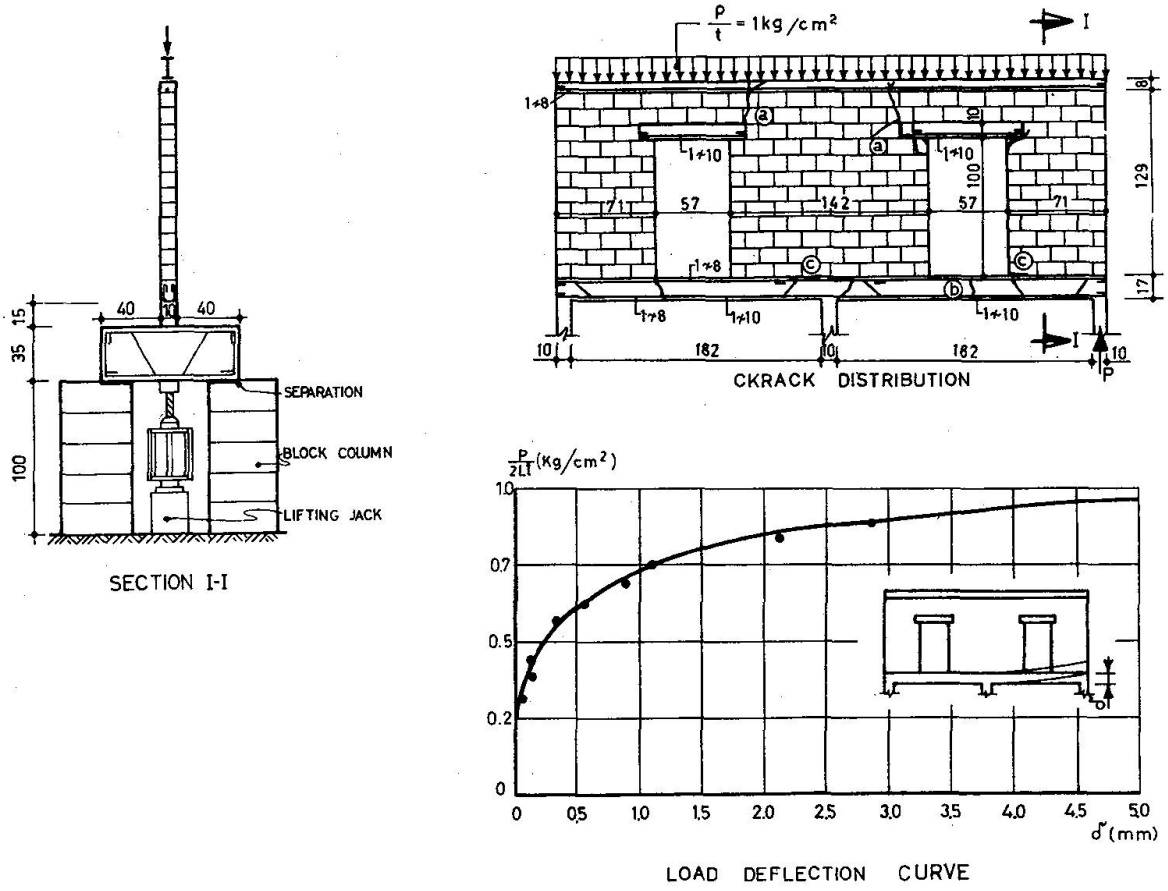

Fig. 6. Test B1, Concave State.

The reinforcement strains were measured by electric-resistance strain gauges. The crack formation was recorded at each load level.

"Concave bending" — The load was again applied in rates of 200 to 500 kgs until complete failure of the structures. The upward displacement of the point of load application was measured at each load level, and the formation of additional cracks was recorded.

Part of the test results, including $P/2Lt$ — δ graphs and cracks patterns, vertical and horizontal strains in B1 are shown in Figs. 5 to 7.

The theoretical analysis was performed for "Convex bending" only. For this purpose 2 separate load cases of the wall, considered supported at the 2 external footings only, were analyzed:

— Uniformly distributed external load.
— Concentrated upward load at the central support.

From the numerical results (omitted here), the midspan deflections and the strains in masonry were evaluated and indicated in Figs. 5, 7 by dotted lines and values in brackets.

A summary of loads causing visible cracking and failure and description of modes of cracking and failure is given in Table 1.

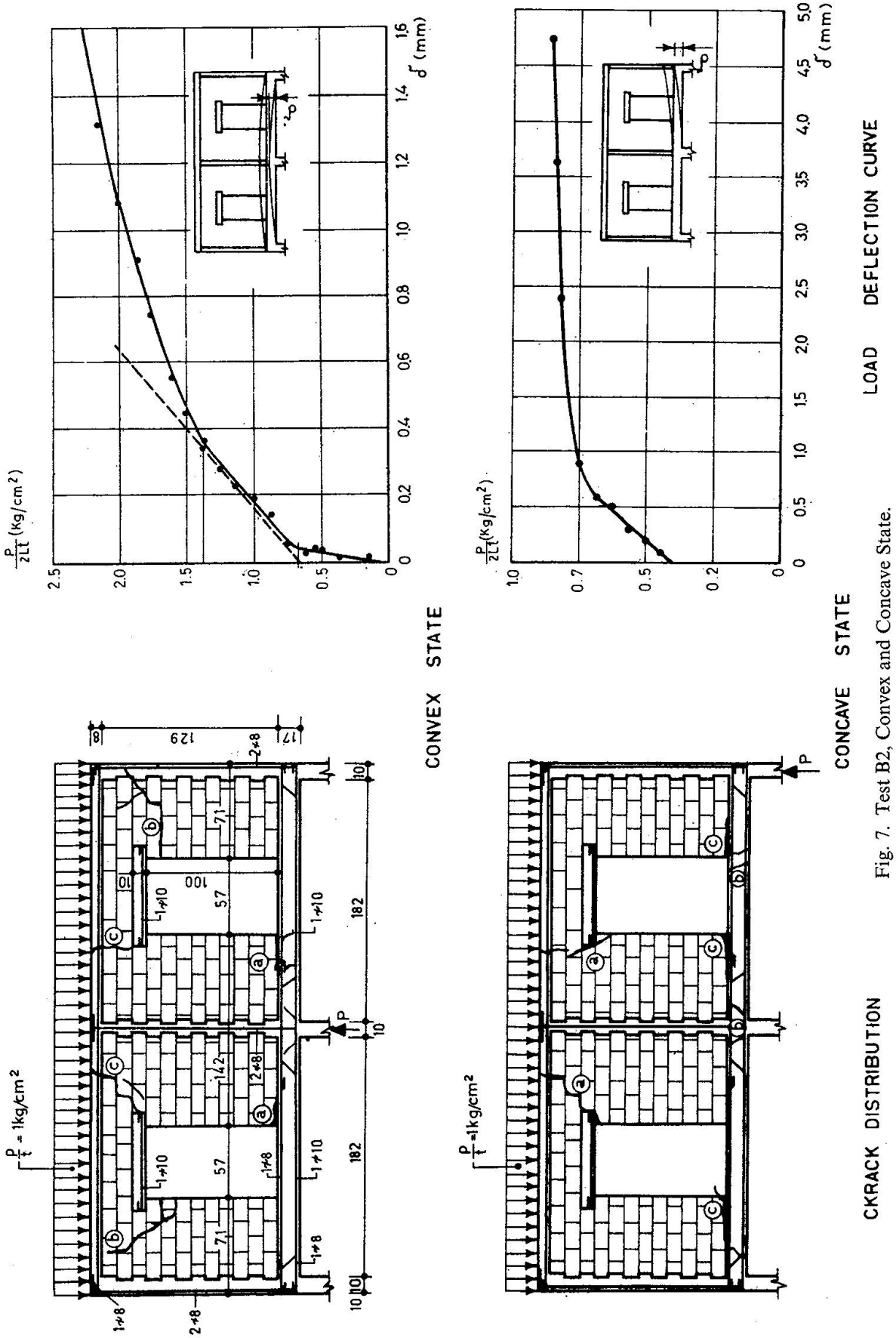

Fig. 7. Test B2, Convex and Concave State.

Table 1

Specimen, wall type	Masonry material	Cracking load (kg/cm^2) (1)	Mode of cracking	Failure load (kg/cm^2) (1)	Mode of failure (2)
A1, without edge columns	Ytong	3.0	Tension cracks in bottom beam	4.0	Rapidly increasing cracks and deflections of bottom beam, and crushing of outermost block above support
A2, without edge columns	Ytong	5.0	Cracks in outermost block above support	5.0	Crushing of outermost block above support
A3, without edge columns	Ytong	5.07	As in A2	5.07	As in A2
A4, without edge columns	Ytong	4.0	Tension cracks in bottom beam	4.0	Crushing of outermost block above support and diagonal cracks along the height of masonry
A5, without edge columns	Conc. hollow blocks	5.0	Tension cracks in bottom beam	8.95	Rapidly increasing cracks and deflections of bottom beam, vertical cracks along the height of masonry
A6, with edge columns	Ytong	3.0	Diagonal crack at the beampost joint	5.5	Rapidly increasing deflections and cracking of bottom beam, and diagonal cracks in beam and wall
A7, with edge columns	Ytong	4.0	As in A6	8.4	Crushing of masonry and diagonal cracks in wall near support
A8, with edge columns	Conc. hollow blocks	7.0	As in A6	9.65	As in A6
B1, without edge columns	Conc. hollow blocks	1.40	Separation of wall from bottom beam near the inner bottom corner of opening (a), cracking of wall near the top outer corner of opening (b) and tension cracks in top beam (c)	2.03	Disruption of wall continuity near the top outer corner of opening (b), and yield of top beam reinforcement (c) - fig. 5.
B2, with edge columns	Conc. hollow blocks	1.52	As in B1	2.20	As in A6 - fig. 7

[1] The cracking and the failure load is defined

for series A as $\frac{\text{uniformly dist. load}}{\text{wall thickness}}$ i.e. $\frac{p}{t}$ for series B as $\frac{\text{concent. load at central support}}{\text{wall length} \times \text{wall thickness}}$ i.e. $\frac{P}{2Lt}$

[2] The primary cause of failure indicated here represents the authors' opinion which does not necessarily conform with that stated in [5].

Discussion of Test Results, Proposed Procedures for Predicting Ultimate Loads

Series A – full masonry.

Perfect agreement between test results and those to be expected from (linear elastic) calculations was not achieved and could not be expected because of the following reasons:

a) The strength of the masonry, acting as a whole, seems to be considerably undervalued by the results of the preliminary tests. Possibly, this is due to the very low quality of the joint mortar in those preliminary test specimens. Also the crushing strength of "Ytong" blocks, stated to be 14.5 kg/cm^2, is very much lower than the minimum values known to the authors (18-24 kg/cm^2).

b) While the assumption of linear behaviour appeared to be justified for "Ytong" masonry, it did not appear to be so for concrete block masonry, even at very low load levels.

c) In infilled frames (A6, A7, A8) there is a geometrical difference between the model for analysis and the test specimens, in as much as the r.c. columns are connected with masonry by indentations.

d) In some cases difficulties were encountered in determining the primary cause of failure, because of the appearance of additional cracks at high load levels, which blurred the visibility of the primary cracks or the crushed part of the masonry.

1. Walls without edge columns

For "Ytong" masonry, for which a realistic estimate of modulus of elasticity was made, reasonable even quantitative agreement between measured and calculated results was obtained, up to cracking load.

For the majority of these specimens failure load was not much above cracking load so that the elastic analysis can be considered valid for almost the entire load range. On the other hand, for hollow block masonry, where the masonry showed non-linear behaviour throughout (therefore a realistic E_w could not be determined) the agreement between test and calculation was only a quantitative one.

The load carrying capacity of masonry walls without edge columns is determined mainly by two factors:

— The tensile strength of the bottom beam.
— The crushing strength of the masonry.

Masonry crushing is sometimes accompanied by spalling and flexural-shear failure of the bottom beam; this is because, with progressive masonry crushing an increasing part of the total shear acts on bottom beam, which is not designed for it.

The intrinsic reason for the predominance of the two above named factors can be seen in the arching effect typical of deep beams [1].

In order to demonstrate this, the principal compressive and tensile stresses in the masonry of specimen A4 were calculated and found to be $-4.6\frac{p}{t}$ and $0.35\frac{p}{t}$ respectively, which confirms the above statement. Although the appearance of (shear)

cracks, due to the principal tensile stresses is probable in most cases (as in A4 and A5) the wall will continue to transmit load as long as the crushing strength of the masonry, or the tensile strength of the bottom beam, has not been exceeded.

In view of the above said, prediction of the load carrying capacity of a wall without edge columns may be reduced to the evaluation of the maximal compressive stresses in the masonry and the inner forces of the bottom beam; for this purpose linear analysis or design aids (in the form of approximation formulae or graphs based on linear analysis) may be used. Design aids of this kind were given by the authors in [2].

For illustration, approximate analysis for A4 is shown in the following:

By formula (17) of [2]

$$K_1 = 2\left(\frac{E_c I}{E_w t}\right)^{1/3} = 2\left(\frac{235{,}000 \times 2{,}494}{6{,}800 \times 7.5}\right)^{1/3} = 45 \text{ cm}$$

$$\left(\bar{a} = \frac{a}{K_1} \cong 0.22;\ \frac{2L}{K_1} = \frac{206}{45} \cong 4.6\right)$$

The maximal values of compressive stress in the wall and the bending moment of the bottom beam are obtained from the graphs of Fig. 11 in [2] as follows: (values obtained by full numerical analysis are given in brackets)

$$\sigma_{y,\max} = 1.995\frac{R}{K_1 t} = -1.995 \times \frac{103}{45}\frac{p}{t} = -4.56\frac{p}{t}\left(-4.51\frac{p}{t}\right)$$

$$M_{x=2.3\,K_1} = 2 \times 0.0468\, RK_1 = 0.0934 \times \frac{45}{103} pL^2 = 0.0406\, pL^2\ (0.037\, pL^2)$$

Note: Multiplication by 2 takes account of action of concentrated loads (support reactions) at both ends.

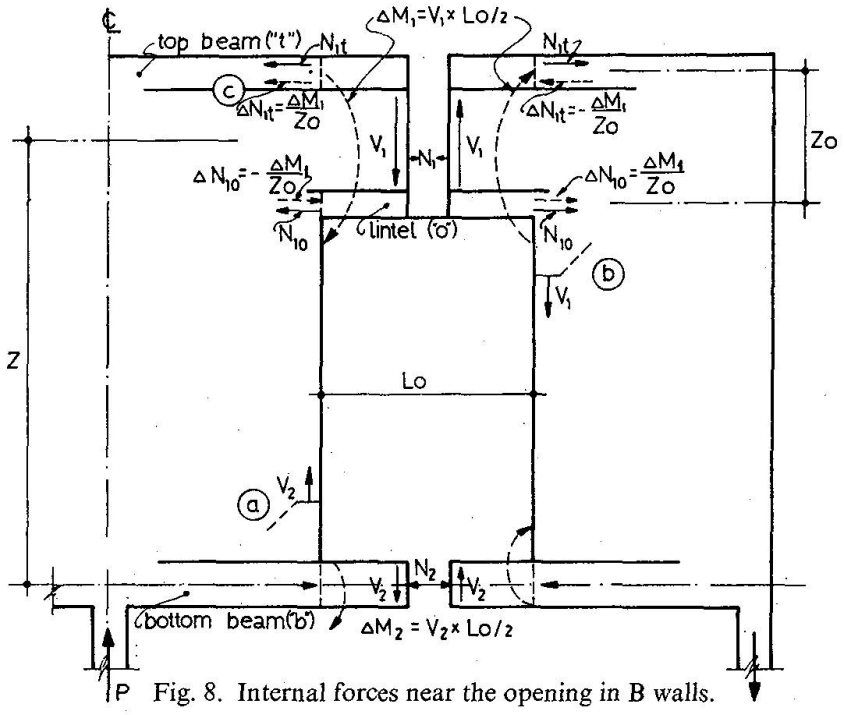

Fig. 8. Internal forces near the opening in B walls.

For the evaluation of the tensile force in the bottom beam use of this graph is not advisable because here $2L < 8K_1$; therefore expression (22) in [2] is recommended

$$\bar{N} = \frac{N}{R} = 2\left[\frac{4}{\pi^2 - 4}\left(\frac{\pi}{2} + \frac{2\frac{x}{K_1} - \pi}{2\left(\frac{x^2}{K_1{}^2} + 1\right)} - \operatorname{arc\,tan}\frac{x}{K_1}\right) - 2\frac{\frac{a}{K_1}\frac{x^2}{K_1{}^2}}{\left(\frac{x^2}{K_1{}^2} + 1\right)^2}\right]$$

$$= 2 \times 0.682\left(1.5708 + \frac{2 \times 2.3 - 3.1416}{2(2.30^2 + 1)} - \operatorname{arc\,tan} 2.3\right)$$

$$- 2 \times 2\frac{0.22 \times 2.3^2}{(2.3^2 + 1)} = 0.57\,R = 0.57\,pL(0.56\,pL)$$

Wall specimen A4 failed at $\frac{p}{t} = 4.0$ kg/cm^2 with computed a maximal compressive stress of 18 kg/cm^2.

Tensile cracks appeared on the bottom beam. The steel strain measured at this load level was $E_s = 890 \times 10^{-6}$ corresponding to a stress of 1870 kg/cm^2.

The computation yielded:

$M = 0.0406 \times 4.0 \times 7.5 \times 103^2 = 12{,}900$ kg/cm^2 (11,800 kg/cm^2)
$N = 0.57 \times 4.0 \times 7.5 \times 103 = 1{,}770$ kg (1760 kg)

These values produce, by customary r.c. section calculations, a stress of 1,950 kg/cm^2 (1,812 kg/cm^2) which is very close to the above measured value. So, even at a load level near failure load, linear theoretical analysis yields results which may be considered reliable.

To sum up the findings of these sub-series tests, most specimens failed by masonry crushing; In wall A1 cracks opened up in the weakly reinforced (3ϕ6) bottom beam (while the calculated reinforcement stress was 3,000 kg/cm^2); in A5 the compressive stress in the masonry approached the crushing strength but the load carrying capacity was determined by the exhaustion of the tensile strength of the bottom beam. There appeared cracks in masonry which were vertical, not inclined as would be expected, probably due to weakness of the vertical mortar joints.

2. *Walls with edge columns*

This series comprises 3 specimens. For two of them, namely A6 and A7, there is good agreement of test results with the calculations, up to a load level of $\frac{p}{t} = 2.0$ kg/cm^2. Beyond this, the measured deflections exceeded the calculated values (see Figs. 2 and 4) which seems to be due to the gradual loosening of the connection of the masonry to the edge columns.

Some measure of verification of this supposition can be had from the calculated values for $\frac{p}{t} = 2.0$ kg/cm^2.

$\tau_{max} = 0.64\frac{p}{t} = 1.28$ kg/cm^2
$\sigma_1 = 0.54\frac{p}{t} = 1.08$ kg/cm^2

The value of the principal tensile stress is close to the tensile strength of "Ytong" blocks. From this load level on, the wall appears to transmit loads by a changed

statical schema i.e. as if without edge columns. With the reorientation of the wall behaviour towards arch action, the strength of tension element (bottom beam) and that of the compression arches (masonry) become decisive for the carrying capacity of the wall.

In A6 the bottom was weak (reinforcement $3\phi6$); the carrying capacity of the wall was exhausted at $\frac{p}{t} = 5.5$ kg/cm^2, due to excessive tension of the bottom beam accompanied by diagonal cracks in the wall.

In A7 the tension beam was strong (reinforcement $2\phi6 + 3\phi12$) and the wall failure at $\frac{p}{t} = 8.4$ kg/cm^2 was due to crushing of the masonry accompanied by shear cracks.

To complete the record, it is noted that specimen A8 (in which the lack of agreement between tests and calculations is similar to that in A5) failed due to tension of the bottom beam (as in A6) accompanied by shear cracks in the wall and separation between bottom beam and masonry.

The described three tests may warrant the following conclusions concerning the behaviour under load of walls with edge columns:

The presence of the edge columns causes a drastic reduction of the compressive stresses in the masonry (cf. [2], p. 149); consequently the schema of internal action emphasizes the "cables" (as opposed to the "arch action"). This is illustrated by the relatively large value of the principal tensile stress $-\sigma_1 = 0.54\frac{p}{t}$ in A6 and A7 — (compared with $0.35\frac{p}{t}$ in A4). But this situation can remain unchanged only until these stresses reach the tensile strength of the masonry, which occurs usually at 20%–30% of the ultimate load.

From this load stage on, a gradual shear cracking develops, invisible at first and clearly seen at the last load stages. Due to the emphasized arch action the wall carrying capacity returns to the dictated by the crushing strength of the masonry and/or by the tensile strength of the bottom beam.

A satisfactory ultimate load theory for infilled frames has not yet been proposed; so, based on the above discussed test results and those reported in [1,7] the following procedure may be suggested:

We may first evaluate the load carrying capacity of a wall without edge columns — which corresponds to the given wall in every respect (measurements, strength of masonry and edge beams) — by the procedure described in the preceding paragraph.

Then the effect of edge columns will be expressed by addition (to the above value) of the following percentages:

If the carrying capacity of the corresponding wall is dictated by the bottom beam — approximately 10% ÷ 15%.

— If it is dictated by the strength of the masonry.

— 40% ÷ 60%, depending on the depth of the edge columns. For the greater part of the usual cases the depth is approximately one twentieth of the span, for these the lower value (40%) is recommended.

The test results of A7, A8 and A6 — which correspond to A3, A5 and A1 respectively, may now be reviewed as follows:

All three specimens of this subseries had deep edge columns. A3 failed through masonry crushing the ratio of ultimate loads for A7 and A3 amounts to $\frac{8.40}{5.07} = 1.66$, A5 failed by excessive tension of the bottom beam, the ratio of ultimate loads for A8 and A5 is $\frac{9.65}{8.95} = 1.08$. The failure of A1 was due to combination of

masonry crushing and bottom beam insufficiency and the ratio of ultimate loads for A6 and A1 was $\frac{5.5}{1.4} = 1.38$ which is an average of the values suggested for the two failure modes (1.10 and 1.60).

— Series B — walls with openings.

As can be seen from the description of the loading arrangement, the specimens of this series, B1 and B2, were loaded from below by a lifting jack at the middle support (Fig. 6).

Before describing the behaviour of the specimens under such loading beyond the value corresponding to the reaction force, it may be mentioned that the measured reaction (of 2,000 kg for both specimens) was in good agreement with the values calculated using the "Force Method" [2,8] and also to that obtained by the proposed approximate calculation in [2] (1,900 kg and 1,940 kg for B1 and B2 respectively).

Jacking loads beyond the value of the original support reaction caused "Convex bending" (see graphs $\frac{P}{2Lt} - \delta$) in Figs. 5, 7 and diminishing external reactions. At the moment of their becoming negative (i.e. anchoring forces) there appeared cracks (see Figs. 5, 7 and Table 1) at:

— Inner bottom corner of the opening (marked *a*).
— Top outer corner of the opening (marked *b*).
— Tension cracks at top beam (marked *c*).

The development of cracks *b* and *c* — from their appearance until failure load — was rapid, the load increase amounting to 50%. The load carrying capacity was dictated mainly by the tensile strength of top beam and the diagonal tensile strength of the outer regions of the masonry. No particular strengthening influence can be attributed to the presence of the r.c. posts in specimen B2. The agreement between the calculations and measurements taken during the experiments was satisfactory up to 70% of ultimate loads.

In the following an approximate design procedure is proposed, which supplements the qualitative indications given in [2].

The key question for walls with openings is the estimation of the integral inner forces in the vertical sections of the wall parts above and below the opening.

On the basis of the analysis of walls B and other walls with openings it may be assumed that these parts have points of Zero-curvature (inflection points), approximately at their centres; so, that the integral moment produces a couple of axial forces, obtained easily from lever arm considered as the distance between the middle lines.

Further, the shear force in each of these parts is approximately proportional to the relative equivalent stiffnesses of the top (subscript 1) and bottom (subscript 2) wall parts

$$V_i = V \frac{S_i}{\sum\limits_{j=1,2} S_j} \quad (i = 1, 2) \tag{1}$$

Where the equivalent stiffness is defined by

$$S_i = D_i + \sum_k K_{1k} \tag{2}$$

D_i = the depth of the masonry above (and sometimes below) the opening.
K_{1k} = the relative bending rigidity of the r.c. stiffening element as defined by expression (17) in [2], namely

$$K_{1k} = 2\left(\frac{E_c I_k}{E_w t}\right)^{1/3}$$

In Fig. 8 the disposition of the inner forces in the wall parts above ($j=1$) and below ($j=2$) the opening is shown. Now the tendency of cracking at *a*, *b* and *c* can easily be understood.

To ensure the load carrying capacity of the wall the vicinity of the opening should be strengthened. The authors' recommendations are as follows:

a) Vertical r.c. members at both sides of the opening should be arranged and designed for a tensile force equal to the greater of the shear forces acting in the parts above or below the opening. These elements should be well connected to edge beams.

b) The lintel and the edge beams should be designed for axial forces stemming from: 1) The integral moment — N_j and 2) The local moments due to the shearing forces at the sections in line with the vertical edges of the opening — ΔN_j (see Fig. 8). There is always a cumulative tension in edge of the lintel, therefore sufficient anchorage length should be provided.

These calculations, for designing the strengthening elements are shown in the following, for a wall whose measurements are as those of walls *B*; The loading is 1.4 t/m applied at the top (including self weight of 0.4 t/m) and uplifting force of 8.0 tons applied at the central support.

The integral moment at the centre of the opening

$$M = \left(4.00 - \frac{3.94}{2} \times 1.40\right) \times 0.95 + \frac{1.40}{2} \times 1.00^2 = 1.88 \text{ tm}$$

The lever arm is $Z = 1.28$ m

The axial forces due to the integral moment are:

$$N_1 = -N_2 = \frac{1.88}{1.28} = 1.47 \text{ t}$$

Assuming that the masonry does not transfer tensile forces the axial force N_1 — above the opening — shall be split between the lintel (subscript *o*) and the top beam (subscript *t*), proportionally to their axial stiffnesses

$$N_{1t} \cong 1.47 \times \frac{8}{8.0 + 10.0} = 0.65^t; \; N_{1o} \cong 1.47 \times \frac{10.0}{8.0 + 10.0} = 0.82^t$$

The integral shear at the middle of the opening is

$$V = 1.24 + 1.00 \times 4.40 = 2.64^t$$

The wall part above the opening is composed of the lintel (10 cm deep), top beam (8 cm deep) and a masonry strip 21 cm deep. The equivalent stiffness of this part is

$$S_1 = 2\left[\left(\frac{230{,}000 \times \frac{10.0 \times 10^3}{12}}{75{,}000 \times 10}\right)^{1/3} + \left(\frac{230{,}000 \times \frac{10.0 \times 8.0^3}{12}}{75{,}000 \times 10}\right)^{1/3}\right] + 21 =$$

$$= 23 + 21 = 44 \text{ cm}.$$

The wall part below the opening consists in this case of the bottom beam only (with $E_w = 270{,}000$ kg/cm^2) and its equivalent stiffness is

$$S_2 = 2\left(\frac{270{,}000 \times \frac{10 \times 17^3}{12}}{75{,}000 \times 10}\right)^{1/3} \cong 23 \text{ cm}$$

The shear forces are split between the two wall parts as follows

$$V_1 = \frac{44}{44+23} V \cong 0.66\ V = 0.66 \times 2.64 = 1.74^t$$

$$V_2 = \frac{23}{44+23} V \cong 0.34\ V = 0.34 \times 2.64 = 0.90^t$$

It should be noted that the numerical analysis gave results for $B_1 - 0.66\ V$, $0.34\ V$ and for $B_2 - 0.70\ V$, $0.30\ V -$ in good agreement with the above approximate calculations.

The vertical r.c. strengthening elements on both sides of the opening shall be designed for a tensile force of 1.74^t, to counteract the vertical cracking in *a* and *b* zones.

The local moment in the wall part 1 (above the opening) at the section in line with the vertical edges of the opening is:

$$\Delta M_1 = 1.740 \times 0.57/2 \cong 0.495 \text{ tm}$$

and is resolved into a couple of axial forces in the lintel (o) and the top beam (t) (with lever arm $Z_o = 0.29_m$)

$$\Delta N_1 = \frac{0.495}{0.29} \cong 1.71^t$$

The maximal tensile forces are produced 1) in the top beam above the top inner corner of the opening (zone *c*) and 2) in the lintel's edge at the top outer corner of the opening (zone *b*). These forces are

$$N_{1t} = 0.65 + 1.71 = 2.36^t;\ N_{10} = 0.82 + 1.71 = 2.53^t.$$

The required anchorage length of the lintel (assuming allowable bond stress of 2.0 kg/cm^2) is

$$\Delta 1_o = \frac{2{,}530}{2 \times 2.0 \times 10} \cong 64 \text{ cm}$$

The above calculations, besides showing in detail the proposed approximate numerical procedure, shows the importance of the strengthening of masonry in the vicinity of the opening, wherever large shear forces are present.

A similar conclusion was also reached in [6]. There it is stated that proper stiffenings by r.c. elements or prestressing may enhance the carrying capacity of walls with openings "to give equal or even higher strength than that of solid wall".

Conclusions for Practical Application

This paper deals with load-bearing masonry walls, which are structural elements frequently used owing to their relatively low cost and other properties. The *main purpose* is to provide the tools for rational design ensuring stability and soundness without overdimensioning or exaggerating strength requirements.

Estimation of the load carrying capacity is based on the elastic-linear analysis of the plane-stress problem, by means as of a digital computer [2], formulas (1)-(16), pp. 144–149. For the purpose of engineering design tables, graphs and approximation formulas were given which permit immediate calculation of the stresses in the critical parts of the wall ([2], pp. 149–163).

Masonry is an essentially brittle material, susceptible of cracking, devoid of tensile strength. It must be, therefore, seen to it that, for the dominant mode of load transfer, the masonry is in compression while the internal tensile forces are carried by r.c. stiffening elements. In fact, loading tests of full masonry walls without strengthening posts under vertical loading confirm the above indicated distribution of the internal forces, and furthermore, analytical determination of the load carrying capacity based on the crushing strength of the masonry and the tensile strength of the bottom beam ([2], formulas 17-22) give results in good agreement with the experiments. The experiments also show that strengthening posts (of reinforced concrete) cause some increase of carrying capacity, but their effect is particularly pronounced in weak masonry. The evaluation of the load-carrying capacity of such walls with stiffening posts was based on empirical adaptation of test results (see par. 2.: "Walls with edge columns").

Openings cause a substantial reduction of the load-carrying capacity, especially if they are large and situated in the region of large shear forces. (A theoretical analysis of the plane-stress problem of the multiply connected region was given in [2], pp. 146–148.) The results of the numerical and experimental investigation indicate tensile stress concentrations near the openings, which can lead to early failure. This can, of course, be prevented by appropriate strengthening elements, but, often designers do not pay the necessary attention to this problem, and content themselves with lintels. In this paper an approximate, but sufficiently reliable, calculation is shown for the horizontal and vertical forces near the openings and for the required strength of the stiffening elements. (See formulas (1), (2), and the numerical example in the section: Series B: "Walls with openings").

In conclusion, the present paper offers tools for the rational design of typical masonry, in consideration of the state of failure. But it must be said that even under service loads shear cracking and/or separation of the masonry from the stiffening elements can not be disregarded, as it may impair the proper performance. Control of such phenomena was not yet sufficiently covered by research.

Notation

a	distance of reaction from wall corner.
D	depth of masonry strip in wall part near opening Eq. (2).
K_1	relative flexural rigidity of stiffener.
E_c, E_w	modulus of elasticity of stiffener and wall, respectively.
L	half length of wall.
M	bending moment.
N	axial force.
ΔN	additional axial force (in walls with openings).
P	concentrated load.
p	distributed load.
V	shear force.
S_i	equivalent stiffness of wall part i above or below the opening.
t	wall thickness.
ε	normal strain.
σ	normal stress.
τ	shear stress.

Subscripts

b	of bottom beam.
c	of stiffener.
o	of opening.
t	of top beam.
w	of wall.
i, j, k	of wall part above or below the opening, or its components.

Acknowledgements

The experimental and theoretical work mentioned in this paper was carried out in the Building Research Station of the Technion, Israel Institute of Technology. The experiments of series A were carried out by Dr. S. Rosenhaupt.

Thanks are due to the U.S. National Bureau of Standards and to the Israeli Ministry of Housing, who sponsored the research.

Key words

Masonry walls, load, reinforced concrete, beam, strains, deflections.

References

1. LEONHARDT, F., and WALTER, R.: Wandartige Träger. Deutscher Ausschuss für Stahlbeton, Heft 178, Wilhelm Ernst & Sohn, Berlin, 1966.
2. LEVY, M., and SPIRA, E.: Analysis of Composite Walls with and without Openings. Publications I.A.B.S.E., Zurich, Vol. 33 (1973), I.
3. MALLICK, D.V., and GARG, R.P.: Effects of Openings on the Lateral Stiffness of Infilled Frames, Inst. Civ. Engrs. Proc. 49, June 1971, pp. 193–209.

4. ROSENHAUPT, S.: Stresses in Point Supported Composite Walls. ACI Journal 61, No. 7, 1964, pp. 795–810.
5. ROSENHAUPT, S.: Experimental Study of Masonry Walls on Beams. Journal of the Structural Division, ASCE, Vol. 88, No. ST3, June 1962, pp. 137–165.
6. ROSENHAUPT, S., and MÜLLER, G.: Openings in Masonry Walls on Settling Supports. Journal of the Structural Division, ASCE, Vol. 89, No. ST3, June 1963, pp. 107–131.
7. ROSENHAUPT, S., and SOKAL, Y.: Masonry Walls on Continuous Beams. Journal of the Structural Division, ASCE, Vol. 91, No. ST1, February 1965, pp. 155–171.
8. SPIRA, E., and LEVY, M.: Stress Analysis of Composite Walls and Walls with Opening. Final report to U.S. National Bureau of Standards, Building Research Station, Technion, Haifa, November 1970.
9. WOOD, R.H.: Studies of Composite Construction. Part 1, Natl. Building Study, Research Paper No. 13, London, H.M.S.O., 1952.

Summary

The paper presents the results of experimental studies on masonry walls, bordered by reinforced concrete elements.

Two series of wall specimens were loaded to destruction:

a) Simply supported solid walls, acted upon by uniformly distributed vertical load.

b) Two bay walls, with opening, subjected to support elements.

The test results were examined in the light of a theoretical linear stress analysis up to cracking load. An attempt was made to interprete the behaviour of the wall specimens after cracking until failure with the purpose of proposing design procedures for evaluating the load carrying capacity of such walls.

Résumé

Cette contribution présente les résultats expérimentaux sur des murs en maçonnerie bordés d'éléments en béton armé. Deux séries de murs ont été chargés jusqu'à rupture:

a) Des murs pleins supportés simplement, sous l'effet d'une charge verticale uniforme.

b) Des murs à deux panneaux, avec ouvertures, agissant sur poutres-support.

Les résultats d'essai ont été examinés du point de vue de l'analyse admettant une répartition linéaire des contraintes jusqu'à fissuration. Les auteurs ont étudié le comportement des murs de la fissure jusqu'à la rupture, afin de proposer une méthode de dimensionnement à la rupture pour de tels murs.

Zusammenfassung

Die Arbeit berichtet über die Ergebnisse von Versuchen mit Wänden aus Mauerwerk, die durch Stahlbetonelemente eingefasst sind. Dabei wurden zwei Versuchsreihen von Mauern bis zum Bruch belastet, und zwar:

a) Einfach gelagerte volle Mauerwerkscheiben unter Einwirkung gleichmässig verteilter Last.

b) Zweifeldrige Wände mit Öffnungen und Stützträgern.

Die Versuchsergebnisse wurden verglichen mit einer Berechnung unter Annahme einer linearen Spannungsverteilung bis zur Bruchlast. Im Hinblick auf vorgeschlagene Berechnungsmethoden zur Abschätzung der Traglast solcher Wände wurde versucht, das Verhalten der Wände nach dem Reissen bis zum Versagen zu interpretieren.

A Curved Plate Element for the Analysis of Thin, Thick and Sandwich Plates

Un élément de plaque courbe pour le calcul de plaques minces, épaisses et sandwich

Ein gekrümmtes Plattenelement zur Berechnung dünner, dicker und Sandwichplatten

A.S. MAWENYA
University of Dar-es-Salaam

Introduction

An extensive effort has been invested in the construction of plate bending finite elements which include shear [1-6]. This has been done in order to obtain more realistic elements for the analysis of structures which experience significant transverse shear deformations such as thick plates, sandwich plates and cellular plate structures.

The elements derived, however, are either rectangular, triangular or quadrilateral in shape; the triangular and quadrilateral shapes being very useful because of their ability to idealize more general shapes. General finite element formulations for the analysis of arbitrarily curved homogenous thick shells have also been presented [7-8].

Herewith is reported the formulation of a curved quadratic isoparametric plate element for the analysis of thin, thick and sandwich plates. It is assumed in the derivation that plane cross-sections of the plate remain plane during deformation, but not necessarily normal to the deformed reference surface of the plate. This assumption violates the Kirchoff's normality hypothesis used in classical thin plate theory, and permits the plate to experience transverse shear deformations. It is also assumed that the transverse normal stress is zero.

These assumptions are identical to the approximations made by AHMAD *et al.* [7], in formulating the curved quadratic superparametric thick shell element. The same approximations were adopted by Too [8] in his version of Ahmad's thick shell element, in which reduced numerical integration was used to eliminate spurious shear effects and to improve element performance.

However, being general thick shell elements, Ahmad/Too elements involve more degrees of freedom than are required for the complete specification of plate bending. Also, since they were derived from three-dimensional elements, they involve

numerical integration with respect to the thickness co-ordinate of the shell. This can be avoided by defining the constitutive relationship in terms of stress resultants as is done below, thereby saving considerably on the computing cost.

Formulation of the Quadratic Isoparametric Plate Element

The details of the formulation of the quadratic isoparametric plate element are given elsewhere [9], and only the essential steps are reiterated here.

Fig. 1 defines the deformation of the plate, which is described by the transverse deflection w and the rotations ϑ_x and ϑ_y of the normal to the reference xy-plane. Fig. 2 shows the quadratic isoparametric plate element with nodes numbered in a clockwise sense. The displacement of a typical node i has three components which comprise the transverse deflection w_i and normal rotations ϑ_{xi} and ϑ_{yi}. These may be listed as a vector

$$\{\delta_i\} = \{w_i, \vartheta_{xi}, \vartheta_{yi}\}^T \tag{1}$$

and the element displacements as a vector

$$\{\delta\} = \{\delta_1, \delta_2, \ldots \delta_8\}^T \tag{2}$$

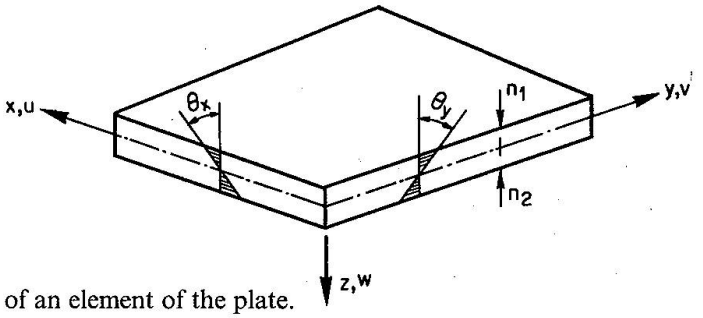

Fig. 1. Deformations of an element of the plate.

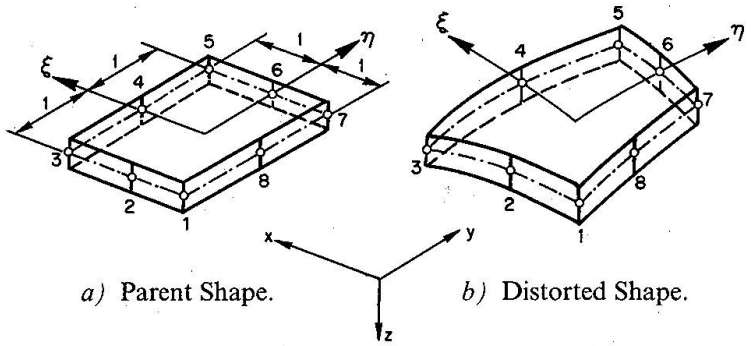

a) Parent Shape. *b)* Distorted Shape.

Fig. 2. The quadratic isoparametric plate bending element:

The displacements within the element are then defined in terms of the nodal displacements by the following equations

$$\begin{aligned} u &= -z\vartheta_x = -z\sum_{i=1}^{8} N_i\vartheta_{xi} \\ v &= -z\vartheta_y = -z\sum_{i=1}^{8} N_i\vartheta_{yi} \\ w &= \sum_{i=1}^{8} N_i w_i \end{aligned} \tag{3}$$

in which the shape functions N_i are:

$$N_i = \tfrac{1}{4}(1+\xi_0)(1+\eta_0)(\xi_0+\eta_0-1) \tag{4a}$$

at the corner nodes and

$$\begin{aligned} \xi_i &= 0,\ N_i = \tfrac{1}{2}(1-\xi^2)(1+\eta_0) \\ \eta_i &= 0,\ N_i = \tfrac{1}{2}(1-\eta^2)(1+\xi_0) \end{aligned} \tag{4b}$$

at the midside nodes;

$$\text{where} \quad \xi_0 = \xi\xi_i,\ \eta_0 = \eta\eta_i \tag{4c}$$

The same shape functions are used to define the x- and y-coordinates at any point within the element and the corresponding thickness of the plate at that point in terms of their nodal values. Thus

$$x = \sum_{i=1}^{8} N_i x_i,\ y = \sum_{i=1}^{8} N_i y_i,\ t = \sum_{i=1}^{8} N_i t_i \tag{5}$$

This definition enables the element to take up curved plan shapes and to have a parabolically varying thickness. Hence, any arbitrary geometry can be closely approximated.

The constitutive relationship for the element is given by [9]

$$\begin{Bmatrix} M_x \\ M_y \\ M_{xy} \\ Q_x \\ Q_y \end{Bmatrix} = [D] \sum_{i=1}^{8} \begin{bmatrix} 0 & -\dfrac{\delta N_i}{\delta x} & 0 \\ 0 & 0 & -\dfrac{\delta N_i}{\delta y} \\ 0 & -\dfrac{\delta N_i}{\delta y} & -\dfrac{\delta N_i}{\delta x} \\ \dfrac{\delta N_i}{\delta x} & -N_i & 0 \\ \dfrac{\delta N_i}{\delta y} & 0 & -N_i \end{bmatrix} \begin{Bmatrix} w_i \\ \vartheta_{xi} \\ \vartheta_{yi} \end{Bmatrix} \tag{6a}$$

$$\text{or } \{M\} = [D] \sum_{i=1}^{8} [B_i]\{\delta_i\} = [D][B]\{\delta\} = [S]\{\delta\} \tag{6b}$$

in which the matrix $[D]$ is the 5×5 property matrix, whose coefficients constitute the usual bending, twisting, shearing and coupling rigidities of the plate [9].

The stiffness matrix is obtained by numerical integration, using a 2×2 Gaussian integration grid, from the following equation [9]

$$[k] = \iint [B]^T [D][B]\,dx\,dy = \sum_{i=1}^{8}\sum_{j=1}^{8} \iint [B_i]^T [D][B_j]\,dx\,dy \tag{7}$$

It will be noted that for the exact integration of equation (7) a 3×3 Gaussian integration grid is required. But as explained in reference [9] a lower order 2×2 grid has been adopted in order to eliminate spurious shear effects and to improve element performance. This also offers a significant saving in computing effort.

Design Stresses

Equations (6) yield the stress resultants at any point within the element. But for the purposes of design equation (6) is usually evaluated at the nodal points to give the stress resultants at the nodes. This is the conventional approach of evaluating design stresses.

It has been observed that elements with reduced integration yield exceptionally accurate stresses at the Gaussian integration points, but that, in the case of thin plates, the shear stress resultants calculated at the nodes are poor [8-10]. However, in the case of the quadratic isoparametric plate element presented here, if the stress resultants at the nodes are bilinearly extrapolated from those calculated at the Gaussian integration points, then the shear stress resultants are always good irrespective of the magnitude of the shearing rigidity of the plate [9]. This important result follows from the fact that the lower order 2×2 Gaussian integration grid adopted actually implies smoothing of the components of the strain matrix $[B]$ by a least squares bilinear fit [9, 10]. Consequently, the unwanted spurious straining modes associated with the higher order shear strain terms appearing in equation (6) are filtered out, resulting in a more efficient element.

This method of obtaining nodal stresses from those already calculated at the Gaussian integration points will be referred to as the extrapolation method.

Numerical Results

In order to verify the accuracy of the formulation, a uniformly loaded square simply supported sandwich plate of side a, and having flexural and shear rigidities of D and $\frac{100\,D}{a^2}$ respectively, is analysed. Results of the maximum deflection, shearing

Table 1. Analysis of simply supported square sandwich plate having Poisson's ratio $\nu = 0.3$

FE mesh (symmetric quater)	Maximum central deflection	Maximum bending moment	Maximum twisting moment	Maximum edge shear
1×1	0.00464	0.0626 (0.0678)	0.0357 (0.0382)	0.625 (0.412)
2×2	0.00480	0.0495 (0.0516)	0.0337 (0.0351)	0.406 (0.339)
3×3	0.00480	0.0485 (0.0495)	0.0332 (0.0340)	0.371 (0.339)
4×4	00.0480	0.0482 (0.0488)	0.0330 (0.0335)	0.0358 (0.338)
5×5	0.00480	0.0481 (0.0484)	0.0328 (0.0332)	0.0351 (0.338)
Theory [11]	0.00480	0.0479	0.0325	0.338
Multiplier	$\frac{qa^4}{D}$	qa^2	qa^2	qa

force, bending and twisting moment are given in Table 1. The stress resultants given in Table 1 are calculated using both the conventional and extrapolation (shown in brackets) method. The close agreement between the two should be noted. It is seen that as the mesh is refined the results converge rapidly to the theoretical values given by PLANTEMA [11].

Table 2 gives the central deflection of a circular plate of variable thickness analysed using the finite element mesh shown in Figure 3. The results are in good agreement with theoretical values [12].

Table 2. Analysis of a simply supported circular plate of variable thickness. $\nu = 0.3$.

Thickness ratio (h_0/h_1)	Central deflection $\frac{wEh_0^3}{qa^4}$ for $\frac{a}{h_0} =$			
	5	20	40	Thin plate solution [12]
1.0	0.764	0.734	0.727	0.738
1.5	1.300	1.261	1.249	1.26

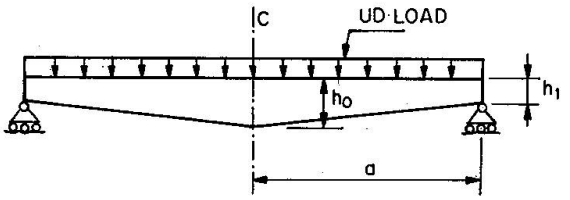

a) Plate cross-section.

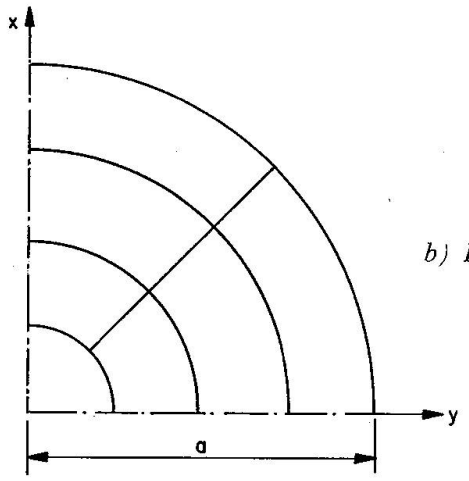

b) FE mesh in a symmetric quater.

Fig. 3. Circular plate of variable thickness:

Table 3 involves a study of the shear stress resultants in a uniformly loaded square simply supported plate and how they are influenced by the method of sampling them. It is seen that the shear stress resultants calculated using the extrapolation method are independent of the shear rigidity, which is consistent with theoretical findings [11]. However, those predicted by the conventional method are only satisfactory when the shear rigidity is small and deteriorate considerably as the shear rigidity increases. For this reason, the shear stress resultants should, as far as possible, be calculated by extrapolation.

Table 3. Shear stress resultants in a square simply supported plate analysed using 5 × 5 mesh. $\nu = 0.3$. Solution B is by extrapolation and *A* by the conventional method

Shear rigidity $\frac{Sa^2}{D}$	Method	Edge shearing force $\frac{Q_y}{qa}$ at $x=$					
		0	0.1*a*	0.2*a*	0.3*a*	0.4*a*	0.5*a*
20	*A*	0	0.172	0.253	0.304	0.331	0.339
	B	0.007	0.176	0.254	0.303	0.329	0.338
100	*A*	0	0.176	0.261	0.314	0.342	0.351
	B	0.007	0.176	0.254	0.303	0.329	0.338
500	*A*	0	0.200	0.301	0.364	0.399	0.410
	B	0.005	0.176	0.254	0.303	0.329	0.338
2500	*A*	0	0.317	0.501	0.618	0.685	0.706
	B	0.002	0.176	0.254	0.303	0.329	0.338
35000	*A*	0	2.229	3.727	4.740	5.325	5.518
	B	0.006	0.176	0.257	0.302	0.328	0.338
All values	Theory [11, 12]	0					0.338

Conclusion

A curved quadratic isoparametric plate bending element which involve shear has been presented for the elastic analysis of arbitrarily shaped plates. From the numerical solutions presented, it is evident that the element, which is formulated according to the isoparametric concept, offers demonstrated advantages in reproducing transverse shear deformability and in modelling curved geometries. The element is applicable to the analysis of not only thin, thick and sandwich plates, but also cellular and voided bridge decks that can be idealized by an equivalent homogeneous material.

Practical Application and Scope

The formulation presented extends the finite element method to plate structures which are arbitrarily curved in plan. Examples of such structures include the curved bridge decks which occur frequently in the design of modern highways and highway interchanges, where the designer has to fit his structure into the environment with the least disturbance to amenities and services.

Due to its accuracy, the quadratic isoparametric plate element presented is probably one of the best plate bending elements available. It is easy to formulate numerically and can represent curved plate boundaries and reproduce transverse shear deformations. It works well whether shear deformations are significant or not and can adequately simulate not only thin, thick and sandwich plates, but also

cellular and voided bridge decks that can be idealized by an equivalent homogeneous material. These features make the use of this element a very attractive proposition for bridge designers.

When compared with ordinary triangular or rectangular plate bending elements, which have no midside nodes, the quadratic isoparametric plate bending element involves a relatively high number of degrees of freedom. However, this is more than compensated for by its excellent performance and superior rate of convergence.

The application of the plate element presented is restricted to situations where there are no membrane forces acting in the plane of the plate. However, the formulation could be modified to include membrane action, and thereby extend its applicability to folded plates and flat shell structures.

Nomenclature

a	length of side of a square plate.
D	flexural rigidity of isotropic plate.
h, t	plate thickness.
M_x, M_y, M_{xy}	bending and twisting moments.
q	distributed transverse loading.
Q_x, Q_y	transverse shearing forces.
S	transverse shear rigidity of isotropic plate.
u, v, w	components of displacement parallel to x-, y- and z-axes.
x, y, z	rectangular co-ordinates.
$\vartheta_x \vartheta_y$	normal rotations of plate cross-section.
ξ, η	local natural dimensionless co-ordinates.
ν	Poisson's ratio.
$\{M\}$	stress resultants vector.
$\{\delta\}$	displacement vector.
$[B]$	matrix connecting strains and displacements of an element.
$[D]$	property matrix.
$[k]$	stiffness matrix.
$[N] = [N_1, N_2, \ldots]$	shape functions matrix.
$[S]$	stress matrix.

References

1. Smith, I.M.: A Finite Element Analysis for Moderately Thick Rectangular Plates in Bending. Int. J. Mech. Sci., 27, pp. 563–570, 1968.
2. Proyr Jr., C.W., Barker, R.M., and Frederick, D.: Finite Element Bending Analysis of Reissner Plates. Proc. ASCE, J. Engng. Mech. Div., 97, pp. 967–983, 1970.
3. Greimann, L.F., and Lynn, P.P.: Finite Element Analysis of Plate Bending with Transverse shear Deformation. Nucl. Engng. Design, 14, pp. 223–230, 1970.
4. Anderheggen, E.: Finite Element Plate Bending Equilibrium Analysis. Proc. ASCE, J. Engng. Mech. Div., 95, pp. 841–857, 1969.
5. Cook, R.D.: Two Hybrid Elements for Analysis of Thick, Thin and Sandwich Plates. Int. J. Num. Meth. Engng. 5, pp. 277–288, 1972.
6. Fried, I.: Shear in C^0 and C^1 Bending Finite Elements. Int. J. Solids Structures, 9, pp. 449–460, 1973.

7. AHMAD, S., IRONS, B.M., and ZIENKIEWICZ, O.C.: Analysis of Thick and Thin Shell Structures by Curved Finite Elements. Int. J. Num. Meth. Engng., 2, pp. 419–451, 1970.
8. TOO, J.M.: Two Dimensional, Plate, Shell and Finite Prism Isoparametric Elements and Their Application. Ph. D. Thesis, University of Wales, Swansea, 1971.
9. MAWENYA, A.S.: Finite Element Analysis of Sandwich Plate Structures. Ph. D. Thesis, University of Wales, Swansea, 1973.
10. RAZZAQUE, A.: Finite Element Analysis of Plates and Shells. Ph. D. thesis, University of Wales, Swansea, 1973.
11. PLANTEMA, F.J.: Sandwich Construction: The Bending and Buckling of Sandwich Beams, Plates and Shells. John Wiley, 1966.
12. TIMOSHENKO, S., and WOINOWSKY-KRIEGER, S.: Theory of Plates and Shells, 2nd Edition, McGraw-Hill, 1959.

Summary

A finite element formulation based on the isoparametric concept is presented for a curved plate element which includes shear, for the analysis of thin, thick and sandwich plates. Numerical examples are presented which demonstrate the applicability of the formulation to practical problems.

Résumé

L'auteur présente une méthode d'éléments fins basée sur le concept isoparamétrique et tenant compte du cisaillement, pour un élément de plaque courbe servant au calcul de plaques minces, épaisses et sandwich. Des exemples numériques montrent l'application de cette théorie à des problèmes pratiques.

Zusammenfassung

Für ein gekrümmtes Plattenelement, das auch Schubbeanspruchung einschliesst, wird eine auf isoparametrischem Konzept beruhende Methode der finiten Elemente zur Berechnung dünner, dicker und Sandwichplatten aufgezeigt. Numerische Beispiele zeigen die Anwendbarkeit der Formulierung auf praktische Probleme.

Influence of Joists on the Lateral Buckling of I Beams

Influence de poutres secondaires sur le déversement latéral de poutres en double té

Einfluss von Querbalken auf die Kippstabilität von I Trägern

D. VANDEPITTE
Professor at Gent University

Introduction

LEBELLE [1] has studied a large number of problems relating to lateral buckling of beams. When the connections between the joists and the main beams of a floor or roof system are such that an angle of twist of the main beams entails an equal angle of rotation of the ends of the joists, the flexural rigidity of the joists hampers lateral buckling of the beams.

The purpose of the present paper is to evaluate the resulting increase of the buckling load. Lebelle does not deal with this problem. TAYLOR and OJALVO [2] do; they present their results in the form of graphs, while in the present paper solutions are obtained in the form of equations; Taylor and Ojalvo do not mention the influence of the level of the point of application of the load with respect to the centroid on the magnitude of the critical load; although this effect is not large in most practical cases, it is not negligible.

We discuss the influence of rigidly connected transverse beams on the lateral stability of the main prismatic I beams of a rectangular grid system, which is supposed to be elastic. We assume that both ends of each main beam rotate freely about both principal axes of its cross-section, but that twisting of the ends is prevented by the supports.

We further assume that:

1. The restraining action of the transverse beams consists only in reactive couples and does not include horizontal forces perpendicular to the main beams. This situation obtains when two or more identical and identically loaded main beams have identical restraints and thus could buckle simultaneously.
2. Each main beam has a vertical plane of symmetry and its loading acts in that plane.
3. The moment of inertia of the cross-section of the main beam about the horizontal axis through its centroid is much greater than the moment of inertia about the vertical centre line. Hence we neglect vertical deflections with respect to horizontal displacements.

For the meaning of the notations used, see page 156.

Local Torsional Restraint at Mid-Span-Negligible Warping Rigidity-Pure Bending

The main beam is subjected to equal bending couples M at the ends (Fig. 2b). If, for a certain value of M, a slightly deflected and twisted form of equilibrium becomes possible, the rotation ϕ_0 of the cross-section of the beam at mid-span gives rise to a reactive couple $A\phi_0$. The cross-section shown in Fig. 2a is the one at mid-span. The couple $A\phi_0$, due to the existence of a transverse beam, is kept in equilibrium by two couples $\frac{A\phi_0}{2}$, applied by the forklike supports at the ends of the beam.

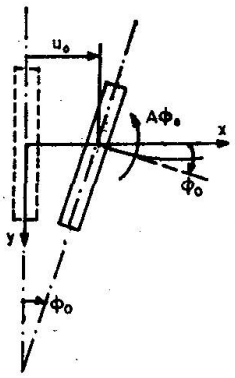

Fig. 2a.

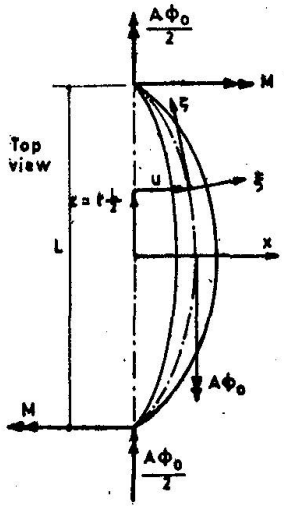

Fig. 2b.

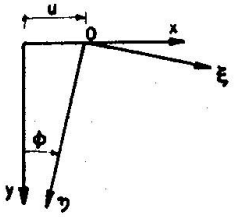

Fig. 2c.

The differential equations for horizontal bending and for twisting of the beam, as written by TIMOSHENKO [3] and taking account of the moment $\frac{A\phi_0}{2}$, are, for the half-beam with positive coordinates z:

$$B\frac{d^2u}{dz^2} = M_\eta = -M\sin\phi \cong -M\phi \tag{1}$$

$$C\frac{d\phi}{dz} = M_\zeta = \frac{A\phi_0}{2}\cos(z\zeta) + M\cos(x\zeta) = \frac{A\phi_0}{2} + M\frac{du}{dz} \tag{2}$$

By differentiating equation (2) with respect to z and eliminating $\frac{d^2u}{dz^2}$ by means of equation (1), we obtain:

$$C\frac{d^2\phi}{dz^2} = M\frac{d^2u}{dz^2} = -\frac{M^2}{B}\phi \text{ or } \frac{d^2\phi}{dz^2} + \frac{4\lambda^2}{L^2}\phi = 0 \tag{3}$$

The general solution of this differential equation is

$$\phi = K_1\sin\frac{2\lambda}{L}z + K_2\cos\frac{2\lambda}{L}z \qquad (z \geqq 0)$$

The conditions at the ends of the half-beam considered are:

1) $\phi = 0$ at $z = \frac{L}{2}$, which yields: $K_1 \sin\lambda + K_2 \cos\lambda = 0$ (4)

2) on account of the symmetry:

$\frac{du}{dz} = 0$ at $z = 0$, which is equivalent to

$$C\frac{d\phi}{dz} = \frac{A\phi_0}{2} \text{ at } z = 0, \text{ or to } C \cdot \frac{2\lambda}{L} K_1 = \frac{AK_2}{2}, \text{ or to } -K_1 \cdot \frac{2\lambda C}{L} + K_2 \cdot \frac{A}{2} = 0 \quad (5)$$

Lest equation (3) have only the trivial solution $\phi \equiv 0$ and the original shape of the beam be its only form of equilibrium, the determinant of the coefficients of K_1 and K_2 in (4) and (5) must be zero: $\frac{A}{2}\sin\lambda + \frac{2\lambda C}{L}\cos\lambda = 0$. The lowest value of λ satisfying this condition is the critical value of λ. Hence λ_c is the smallest root of the equation

$$tg\lambda_c = -\frac{4C}{AL} \cdot \lambda_c = -\frac{\lambda_c}{\alpha} \quad (6)$$

The critical value of the bending moment in pure bending then is

$$M_c = \frac{2\lambda_c}{L}\sqrt{BC} \quad (7)$$

A simple diagram (Fig. 3) shows that λ_c always lies in the interval $+\frac{\pi}{2}$, $+\pi$. When there is no torsional restraint of the main beam at mid-span, $A = 0$, $\lambda_c = \frac{\pi}{2}$ and $M_c = \frac{\pi}{L}\sqrt{BC}$. This is the well-known result for buckling of a beam of narrow rectangular cross-section, subjected to pure bending.

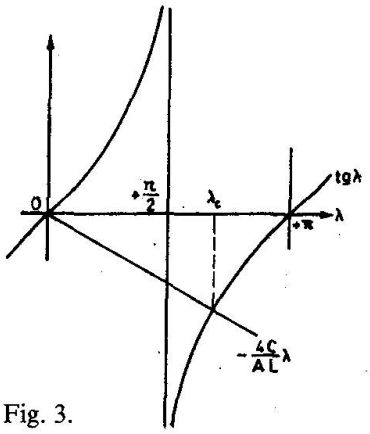

Fig. 3.

If, on the other hand, the rigidity of the transverse beam at the centre of the main beam increases indefinitely:

$A \to \infty$, $\lambda_c \to \pi$ and $M_c \to \frac{2\pi}{L}\sqrt{BC}$, as pointed out by TIMOSHENKO [3].

For all finite values of A or α, the solution is easily found by means of equations (6) and (7).

Comments about Equations 6 and 7

1. Equation (3) and hence equations (6) and (7) are strictly correct only in the case of cross-sections having two axes of symmetry. When there is only one axis of

symmetry, a fraction of the torque is taken up by the bending stresses, because these act in fibres that are twisted helicoidally. A term representing the derivative with respect to z of that part of the torque must be introduced into equation (3):

$$C\frac{d^2\phi}{dz^2} = -\frac{M^2}{B}\phi + c_y M\frac{d^2\phi}{dz^2}$$

(for the meaning of c_y, see ref. 4, p. 395).

$c_y = 0$ and formula (7) is not affected in the case of rolled I beams and of all other steel or concrete I beams having two planes of symmetry.

Steel or concrete beams that are symmetrical with respect to a vertical plane only have in most practical cases their widest flange acting in compression. Formula (7) should be conservative and may be applied with confidence for such beams, since, according to STÜSSI and DUBAS (ref. 4, p. 397) the term $c_y M\frac{d^2\phi}{dz^2}$ increases the critical load when the shear centre 0 is located in the compressive zone of the cross-section.

In the rare cases of beams having their shear centre in the tensile part of the cross-section, formula (7) overestimates the critical load, since, according to the same authors, the effect of the term $c_y M\frac{d^2\phi}{dz^2}$ that we have neglected is to decrease the critical load in those cases.

2. Neglecting the vertical deflections with respect to the horizontal displacements results in a slight underestimation of the critical load (ref. 4, p. 385).

3. The two above remarks also apply to the cases studied below and, more specifically, to the critical loads computed by means of (17) and of the appropriate equation among the equations (16), (21), (23), (26) and (28).

Local Torsional Restraint at Mid-Span-Negligible Warping Ridigity-Uniform Load

When the beam buckles, the deformation is again impeded by the restraining couple $A\phi_0$ at mid span (Fig. 4b), the shear centre 0 of the cross-section with coordinate z moves horizontally an amount u and lowers slightly, and the point of

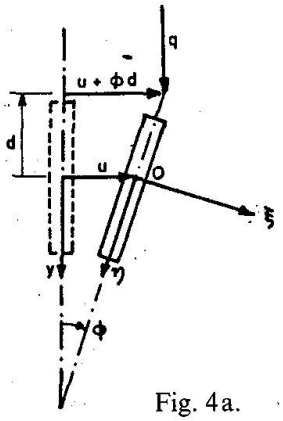

Fig. 4a.

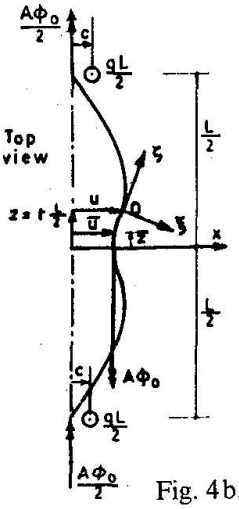

Fig. 4b.

application of the uniform load q moves horizontally an amount $u+\phi d$ and lowers a little more than 0 (Fig. 4a). Each end support again provides a torsional couple $\frac{A\phi_0}{2}$, but, besides, a couple of magnitude $c\cdot\frac{qL}{2}=q\int_0^{L/2}(u+\phi d)dz$ necessary to offset the horizontal deviation of the load q.

All bending and twisting moments appearing in the following equations are moments acting in the displaced cross-section with coordinate z and taken about an axis *through 0* whose direction is indicated by the subscript.

$$B\frac{d^2u}{dz^2}=M_\eta=-M_x\cdot\sin\phi\cong-M_x\cdot\phi=-\frac{q}{2}\left(\frac{L^2}{4}-z^2\right)\cdot\phi \tag{8}$$

$$C\tfrac{d\phi}{dz}=M_\zeta=M_x\cdot\cos(x\zeta)+M_z\cdot\cos(z\zeta)=M_x\cdot\sin(z\zeta)+M_z=M_x\cdot\tfrac{du}{dz}+M_z \tag{9}$$

We find M_z as the resulting moment about the z-axis shifted towards 0 of all the forces acting between 0 and the middle of the beam, and in the cross-section at mid-span, taking into account the following facts:

1) Half of the restraining couple $A\phi_0$ at mid-span acts on the part of the beam considered.
2) The bending moment at mid-span does not contribute to M_z.
3) There is no shear force at mid-span.
4) At any point $\bar{z}$ between 0 and mid-span, where the horizontal displacement of the shear centre is $\bar{u}$ and the angle of twist is $\bar{\phi}$, the load $q.d\bar{z}$ acts at a distance $u-\bar{u}-\bar{\phi}d$ to the left of 0.

$$M_z=\frac{A\phi_0}{2}+\int_0^z q(u-\bar{u}-\bar{\phi}d)d\bar{z}$$

Equation (9) becomes

$$C\frac{d\phi}{dz}=\frac{A\phi_0}{2}+q\int_0^z(u-\bar{u}-\bar{\phi}d)d\bar{z}+\frac{q}{2}\left(\frac{L^2}{4}-z^2\right)\frac{du}{dz} \tag{10}$$

We differentiate with respect to z:

$$C\frac{d^2\phi}{dz^2}=-q\phi d+qz\frac{du}{dz}+\frac{q}{2}\left(\frac{L^2}{4}-z^2\right)\frac{d^2u}{dz^2}-qz\frac{du}{dz}$$

and use (8) to eliminate $\frac{d^2u}{dz^2}$:

$$C\frac{d^2\phi}{dz^2}=-q\phi d-\frac{q^2}{4B}\left(\frac{L^2}{4}-z^2\right)^2\phi$$

This equation can be written in the form

$$\phi''+\phi[\varepsilon\delta+\varepsilon^2(1-t^2)^2]=0 \tag{11}$$

The solution must satisfy the following boundary conditions:

1) $\phi = 0$ at the support ($t = 1$)
2) $\frac{du}{dz} = 0$ at mid-span; (10) shows that this requires

$$C\frac{d\phi}{dz} = \frac{A\phi_0}{2} \text{ at } t = 0, \text{ or } C\phi'(0) = \frac{AL}{4}\cdot\phi(0), \text{ or } \phi'(0) = \alpha\cdot\phi(0)$$

Equation (11) further shows that $\phi''(1) = 0$.

Instead of trying to solve equation (11), we shall now use the Ritz energy method, as developed by TIMOSHENKO [3].

The increase ΔU in the strain energy of one half of the main beam and one half of the corresponding transverse beam(s) while the system moves from the loaded, unbuckled configuration to the loaded, buckled configuration is given by the expression

$$\Delta U = \frac{1}{2B}\int_0^{L/2} M_\eta^2\,dz + \frac{1}{2C}\int_0^{L/2} M_\zeta^2\,dz + \frac{1}{2}\left(A\phi_0\cdot\frac{\phi_0}{2}\right)$$

$$= \frac{1}{2B}\int_0^{L/2} M_x^2\phi^2\,dz + \frac{C}{2}\int_0^{L/2}\left(\frac{d\phi}{dz}\right)^2 dz + \frac{A}{4}\phi_0^2 \tag{12}$$

The original equilibrium configuration changes from stable to unstable when ΔU is equal to the work ΔT done by the load q during lateral buckling. As explained in LEBELLE'S paper (ref. 1, p. 792), the work done by the load whilst the shear centre 0 is lowered owing to the horizontal curvature combined with the twisting of the beam, would be

$\frac{1}{B}\int_0^{L/2} M_x^2\phi^2\,dz$, if the load acted at the shear centre 0. Because the load acts at distance d above the shear centre, there is an additional lowering (Fig. 5) by the amount $d(1-\cos\phi) \cong d\frac{\phi^2}{2}$, and the additional work is $q\int_0^{L/2} d\frac{\phi^2}{2}dz$. Hence

$$\Delta T = \frac{1}{B}\int_0^{L/2} M_x^2\phi^2\,dz + \frac{qd}{2}\int_0^{L/2}\phi^2\,dz \tag{13}$$

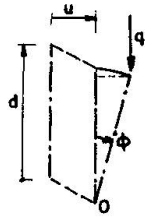

Fig. 5.

The energy equation $\Delta T = \Delta U$ determining the critical load q_c becomes

$$\frac{1}{2B}\int_0^{L/2} M_x^2\phi^2\,dz + \frac{q_c d}{2}\int_0^{L/2}\phi^2\,dz = \frac{C}{2}\int_0^{L/2}\left(\frac{d\phi}{dz}\right)^2 dz + \frac{A}{4}\phi_0^2$$

Substituting $M_x = \frac{q_c}{2}\left(\frac{L^2}{4} - z^2\right) = \frac{q_c L^2}{8}(1 - t^2)$ and introducing other symbols defined under the heading "Notations" (page 156), we obtain the integral equation

$$\varepsilon_c^2 \int_0^1 (1-t^2)^2 \phi^2 \, dt + \varepsilon_c \delta \int_0^1 \phi^2 \, dt = \int_0^1 \phi'^2 \, dt + \alpha \phi_0^2 \tag{14}$$

If all conceivable functions $\phi(t)$ that satisfy the boundary conditions were introduced into equation (14), the one yielding the lowest value of ε_c and hence of q_c would represent the true buckling configuration and would yield the correct value of ε_c and q_c. We will, however, obtain a fair approximation for ε_c by any reasonable choice for the function $\phi(t)$ that satisfies the boundary conditions.

We assume for ϕ the expression $\phi(t) = \phi_0(1 + at + bt^2 + ct^3)$. The boundary conditions $\phi(1) = 0$ and $\phi'(0) = \alpha . \phi(0)$, together with the condition $\phi''(1) = 0$ deduced from equation (11), enable us to find the coefficients a, b and c as functions of α. We introduce the expression

$$\phi(t) = \phi_0 \left[1 + \alpha t - \tfrac{3}{2}(1 + \alpha) t^2 + \tfrac{1}{2}(1 + \alpha) t^3\right] \; (0 \leqq t \leqq 1) \tag{15}$$

thus obtained into equation (14), and, after performing the calculations, find

$$\frac{\varepsilon_c^2}{132}(161\alpha^2 + 1620\alpha + 5287) + \varepsilon_c \delta (2\alpha^2 + 18\alpha + 51) - 21(\alpha + 1)(\alpha + 6) = 0 \tag{16}$$

This quadratic equation has a positive and a negative root. It is easy to compute the positive root ε_c and the buckling load

$$q_c = 16 \varepsilon_c \frac{\sqrt{BC}}{L^3} \tag{17}$$

The negative root of equation (16) gives the magnitude of the load which, applied upward at the same point, would produce lateral buckling of the beam. The negative root is, understandably, equal to minus the positive root of equation (16), written with the sign of δ reversed. The same comment applies to the negative root of similar quadratic equations to follow.

It is possible to refine the procedure that led to equation (16) by adding a fourth power term to the polynomial assumed for $\phi(t)$, by writing the coefficients as functions of a free parameter in order that $\phi(t)$ satisfy the three known conditions, by finding ε_c as a function of this parameter, and by adjusting the parameter in such a way as to make ε_c a minimum.

The computations would be very laborious and they would probably not be worth-while, as is indicated by the fact that replacement of the third power term by a fourth power term in expression (15) yields values of ε_c, which are hardly different from, but generally a fraction of 1% higher than the positive root of equation (16). That this equation may be used with confidence is further shown by its containing previously known results (ref. 1, p. 791) obtained by another method for the particular case

$$\alpha = 0, \; \delta = 0 \text{ or } \delta \neq 0$$

Local Torsional Restraint at Mid-Span-Uniform Load

Buckling in One Half-Wave

We refer again to Fig. 4, but now suppose that the beam has flanges and that the warping rigidity $C_1 = EC_w$ is not negligible.

Differential equation (8) remains valid. A term representing the part of the torque taken by the couple of shear forces in the flanges has to be added to the first member of equations (9) and (10):

$$C\frac{d\phi}{dz} - C_1\frac{d^3\phi}{dz^3} = M_\zeta = \frac{A\phi_0}{2} + q\int_0^z u\text{–}\bar{u}\text{–}\bar{\phi}d)\,d\bar{z} + \frac{q}{2}\left(\frac{L^2}{4} - z^2\right)\frac{du}{dz}$$

Differentiating with respect to z and using (8) to eliminate $\frac{d^2u}{dz^2}$, we find:

$$C\frac{d^2\phi}{dz^2} - C_1\frac{d^4\phi}{dz^4} = -q\phi d + \frac{q}{4}\left(\frac{L^2}{4} - z^2\right)\frac{d^2u}{dz^2} = -q\phi d - \frac{q^2}{4B}\left(\frac{L^2}{4} - z^2\right)^2\phi$$

which can be written in the form:

$$-\beta\phi'''' + \phi'' + \phi[\varepsilon\delta + \varepsilon^2(1-t^2)^2] = 0 \tag{18}$$

Four boundary conditions must be satisfied:

1) $\phi(1) = 0$.
2) At the support, the curvature $\frac{d^2u}{dz^2} + h_1\frac{d^2\phi}{dz^2}$ of the upper flange (Fig. 1) and the curvature $\frac{d^2u}{dz^2} - h_2\frac{d^2\phi}{dz^2}$ of the lower flange in the plane of the flanges are zero, and consequently $\phi''(1) = 0$.

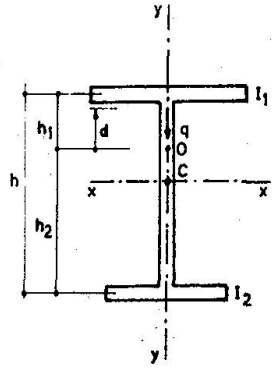

Fig. 1.

3) Owing to symmetry, buckling does not change the direction of the flanges at mid-span:

$$\frac{du}{dz} + h_1\frac{d\phi}{dz} = 0 \text{ and } \frac{du}{dz} - h_2\frac{d\phi}{dz} = 0; \text{ hence } \phi'(0) = 0$$

4) In the cross-section adjacent to the transverse beam, the torque

$$M_\zeta = C\frac{d\phi}{dz} - C_1\frac{d^3\phi}{dz^3} \text{ is } \frac{A\phi_0}{2}. \text{ Since } \frac{d\phi}{dz} = 0:$$

$$-\frac{8C_1}{L^3}\cdot\phi'''(0) = \frac{A}{2}\phi(0), \text{ or } -\beta\cdot\phi'''(0) = \alpha\cdot\phi(0)$$

Equation (18), together with the conditions 1) and 2), shows that $\phi''''(1) = 0$.

In order to apply the energy method, we must supplement expression (12) for ΔU with the strain energy resulting from the differential bending of the flanges in their plane. Excepting the general horizontal bending of the beam, the curvature of the upper and lower flanges is $h_1\frac{d^2\phi}{dz^2}$ and $-h_2\frac{d^2\phi}{dz^2}$ respectively. The corresponding strain energy for the half-beam is

$$\int_0^{L/2}\left|\frac{EI_1}{2}\left(h_1\frac{d^2\phi}{dz^2}\right)^2 + \frac{EI_2}{2}\left(h_2\frac{d^2\phi}{dz^2}\right)^2\right| dz = \frac{E}{2}\left(h_1^2 I_1 + h_2^2 I_2\right)\cdot\int_0^{L/2}\left(\frac{d^2\phi}{dz^2}\right)^2 dz =$$

$$= \frac{C_1}{2}\int_0^{L/2}\left(\frac{d^2\phi}{dz^2}\right)^2 dz$$

and the counterpart of expression (14) of the energy equation $\Delta T = \Delta U$ is here

$$\varepsilon_c^2\int_0^1 (1-t^2)^2\,\phi^2\,dt + \varepsilon_c\delta\int_0^1 \phi^2\,dt = \int_0^1 \phi'^2\,dt + \beta\int_0^1 \phi''^2\,dt + \alpha\phi_0^2 \tag{19}$$

We use a fifth power polynomial to describe approximately the unknown buckling configuration. The four boundary conditions, together with the fact that $\phi''''(1) = 0$, enable us to find the five coefficients in the polynomial as functions of $\mu = \frac{\alpha}{6\beta}$:

$$\phi(t) = \phi_0[1 - \tfrac{1}{4}(5-2\mu)t^2 - \mu t^3 + \tfrac{5}{16}(1+2\mu)t^4 - \tfrac{1}{16}(1+2\mu)t^5] \quad 0 \leqq t \leqq 1 \tag{20}$$

Introducing (20) into (19), we obtain after tedious calculations:

$$\frac{\varepsilon_c^2}{416}(1612\mu^2 + 88340\mu + 2243159) + 2\varepsilon_c\delta(4\mu^2 + 180\mu + 3455) =$$

$$= 22(4\mu^2 + 40\mu + 775) + 495\beta(1+2\mu)(85+2\mu) \tag{21}$$

One finds the buckling load q_c by substituting into equation (17) the one positive root of equation (21).

When $\mu = 0$, equation (21) is very nearly equivalent to the formula for ε_c given by LEBELLE (ref. 1, p. 791) for beams without torsional restraint at mid-span; there is a slight difference in the term representing the influence of the warping rigidity.

It is important to note that equation (21) is *not* valid when $\beta = 0$ (no warping rigidity), for the third boundary condition used in the process which led to equation (21) is not compatible with the second boundary condition obtaining when $\beta = 0$, unless $\phi(0)$ be zero, and there is no restraint that keeps $\phi(0)$ zero whenever $\beta = 0$.

Buckling in Two Half-Waves

Equation (21) gives the critical load that causes the main beam to buckle in one half-wave, which is symmetrical with respect to its mid-point, as sketched in Fig. 4. It is, however, conceivable that a transverse beam of great, but finite stiffness may prevent twisting of the main beam at mid-span during buckling.

In order to evaluate the critical load associated with the buckling mode sketched in Fig. 6 we describe this new buckling configuration approximately by means of the function

$$\phi(t) = a(8t - 20t^3 + 15t^4 - 3t^5) \tag{22}$$

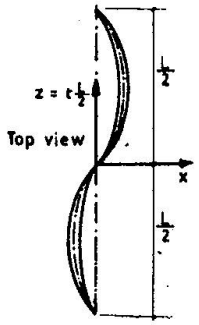

Fig. 6.

whose coefficients are such that:

1) as before: $\phi(1) = 0$; $\phi''(1) = 0$; $\phi''''(1) = 0$.
2) $\phi(0) = 0$; $\phi''(0) = 0$, thereby reflecting the absence of a twisting movement of the cross-section and the presence of inflection points in the flanges at mid-span.

When expression (20) is written with $\alpha\phi_0$ as a new, finite parameter while ϕ_0 vanishes, its second derivative is not zero at $t = 0$. Consequently, it does *not* represent the buckling mode pictured in Fig. 6, and expression (22) may therefore yield a lower critical load. We substitute it for ϕ in equation (19), in which $\alpha\phi_0^2$ is now zero. The positive root of the resulting quadratic equation is

$$16\varepsilon_c = 67{,}05\,(\sqrt{1 + 10\beta + 0{,}04479\delta^2} - 0{,}2116\,\delta) \tag{23}$$

For high values of α and small values of β, formula (23) turns out to give lower values of ε_c than equation (21). The transverse beam is then stiff enough to induce the main beam to buckle in two half-waves, and further stiffening of the transverse beam would not increase the buckling load. The ε_c to be used in (17) is always the lowest resulting either from (21) or from (23).

Remarks

Instead of assuming expression (22) to define the buckling configuration, we could use a sixth power polynomial that satisfies the same five conditions, and, moreover, the condition $\phi''''(0) = 0$ derived from equation (18). Although it accords

more completely with our information about the form of buckling, it yields, rather surprisingly, higher and therefore poorer values of the critical load.

When expression (15), which we used for beams with negligible warping rigidity, is rewritten with $\alpha\phi_0$ as a new, finite parameter while ϕ_0 is allowed to vanish, it does represent the buckling mode depicted in Fig. 6. Consequently, equation (16) remains valid even when the transverse beam is very stiff.

Local Torsional Restraint at Mid-Span-Effect of the Various Parameters

Table 1 illustrates the influence of the various parameters on the magnitude of the critical load. The numerical values appearing in the table may occur in practical cases. The values of $16\varepsilon_c$ in the column $\beta = 0$ were calculated by means of equation (16), the other ones by means of (21) or (23). The more heavily circumscribed figures are associated

Table 1

α	δ	$\beta = 0$	$\beta = 0{,}011$	$\beta = 0{,}1$
		$16\varepsilon_c$		
0	−0,2	30,5	31,0	33,9
	0	28,4	28,8	31,8
	+0,2	26,4	26,9	29,8
5	−0,2	54,2	70,8	66,4
	0	51,9	67,8	64,1
	+0,2	49,6	64,9	61,9
13	−0,2	61,9	73,5	90,7
	0	59,4	70,6	88,2
	+0,2	56,9	67,9	85,7
∞	−0,2	69,1	73,5	97,7
	0	66,4	70,6	94,8
	+0,2	63,8	67,9	92,0

with buckling in two half-waves. For instance, if $\beta = 0{,}011$, the critical load does not increase when α augments from 13 to infinity.

It is seen from the table that local torsional restraint at mid-span improves the stability substantially. Values of α of the order of magnitude of 10 are easily achieved in practice, and such restraint doubles or more than doubles the buckling load.

The critical load decreases from 4 to 7% when δ varies from 0 to +0,2. For a prestressed concrete I beam, $\delta = 0{,}2$ may mean, depending on the proportions of the cross-section, that the load acts on the upper flange.

Uniform Torsional Restraint-Negligible Warping Rigidity-Uniform Load

When the beam buckles, the deformation is hindered by a continuous restraining couple of magnitude $A_1\phi$ per unit length of the beam. The top view in Fig. 4b has to be replaced by Fig. 7. Each end support provides a torsional couple of magnitude $A_1\int_0^{L/2}\phi dz$ and a couple $c\cdot\frac{qL}{2}$.

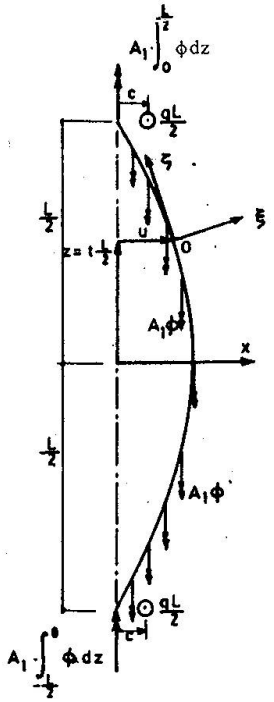

Fig. 7.

Equations (8) and (9) remain valid. Remembering that, owing to symmetry, there is no torque and no shear force in the cross-section at mid-span of the beam, we find M_z at 0 as the sum of the restraining moments $A_1\bar{\phi}d\bar{z}$ between 0 and mid-span, and of the moments $q(u-\bar{u}-\bar{\phi}d)d\bar{z}$ for the same portion of the beam:

$$M_z = A_1\int_0^z \bar{\phi}d\bar{z} + q\cdot\int_0^z (u-\bar{u}-\bar{\phi}d)\,d\bar{z}$$

Equation (10) becomes here:

$$C\frac{d\phi}{dz} = A_1\cdot\int_0^z \bar{\phi}\cdot d\bar{z} + q\cdot\int_0^z (u-\bar{u}-\bar{\phi}d)\,d\bar{z} + \frac{q}{2}\left(\frac{L^2}{4}-z^2\right)\frac{du}{dz} \tag{24}$$

Differentiation with respect to z and elimination of $\frac{d^2u}{dz^2}$ by means of (8) give the differential equation:

$$C\frac{d^2\phi}{dz^2} = A_1\phi - q\phi d + \frac{q}{2}\left(\frac{L^2}{4}-z^2\right)\frac{d^2u}{dz^2} = A_1\phi - q\phi d - \frac{q^2}{4B}\left(\frac{L^2}{4}-z^2\right)^2\phi$$

which is easily transformed into:

$$\phi'' + \phi[\varepsilon\delta - \alpha_1 + \varepsilon^2(1-t^2)^2] = 0 \tag{25}$$

The boundary conditions are:

1) $\phi(1) = 0$;
2) at mid-span: $\frac{du}{dz} = 0$; equation (24) shows that this implies $\frac{d\phi}{dz} = 0$ or $\phi'(o) = 0$.

Comparison of the differential equations (25) and (11), and of the boundary conditions pertaining to these equations shows that the mathematical formulation of the present problem is identical with that for the case of local torsional restraint at midspan, provided that in the latter we substitute the constant $\varepsilon\delta - \alpha_1$ for $\varepsilon\delta$, and zero for α. To obtain an approximate answer to the present problem, we need only make the same substitutions in equation (16). Hence we find the critical value of ε as the positive root of the equation

$$\frac{5287}{132}\varepsilon_c^2 + 51(\varepsilon_c\delta - \alpha_1) - 126 = 0$$

The value of $16\varepsilon_c$ to be used in expression (17) for the critical load q_c is

$$16\varepsilon_c = 28{,}4\,(\sqrt{1 + 0{,}405\alpha_1 + 0{,}1288\delta^2} - 0{,}359\delta) \tag{26}$$

Uniform Torsional Restraint-Uniform Load

If the warping rigidity $C_1 = EC_w$ is not negligible, we find the differential equation governing ϕ by adding the terms $-C_1\frac{d^3\phi}{dz^3}$ and $-\beta\cdot\phi'''$ to the first member of the equations (24) and (25), respectively. The new equation is

$$-\beta\cdot\phi'''' + \phi'' + \phi[\varepsilon\delta - \alpha_1 + \varepsilon^2(1-t^2)^2] = 0 \tag{27}$$

The boundary conditions are:

1) $\phi(1) = 0$; $\phi''(1) = 0$; $\phi'(o) = 0$, as in the case of local torsional restraint at mid-span.
2) $\phi'''(o) = 0$, resulting from the modified equation (24) and from the fact that $\frac{du}{dz} = 0$ at $t = 0$.

The differential equation (27) and the four boundary conditions are exactly the same as equation (18) and the appurtenant boundary conditions for the case of local torsional restraint at mid-span, if in the latter we replace $\varepsilon\delta$ by $\varepsilon\delta - \alpha_1$ and α by zero. Consequently we need only make the same changes in equation (21), which thus becomes:

$$\frac{2243159}{416}\varepsilon_c^2 + 6910(\varepsilon_c\delta - \alpha_1) - 17050 - 42075\beta = 0$$

Solving for ε_c we obtain

$$16\varepsilon_c = 28{,}4(\sqrt{1 + 0{,}405\alpha_1 + 2{,}468\beta + 0{,}1298\delta^2} - 0{,}36\delta) \tag{28}$$

For $\alpha_1 = 0$, this result is identical with known results referred to previously.

Formula (28) is valid also for $\beta = 0$ and indeed is then very nearly the same as formula (26), because this time the boundary conditions holding when $\beta \neq 0$ are not incompatible with those holding when $\beta = 0$.

Lateral buckling in two half-waves always requires a higher load than the load calculated with expression (28).

Value of A or A_1

One Transverse Beam at Mid-Span

When two main beams are connected by a single secondary beam of flexural rigidity $E_t I_t$ and length l (Fig. 8a), the stiffness of the restraint is

$$A = \frac{6E_t I_t}{l}$$

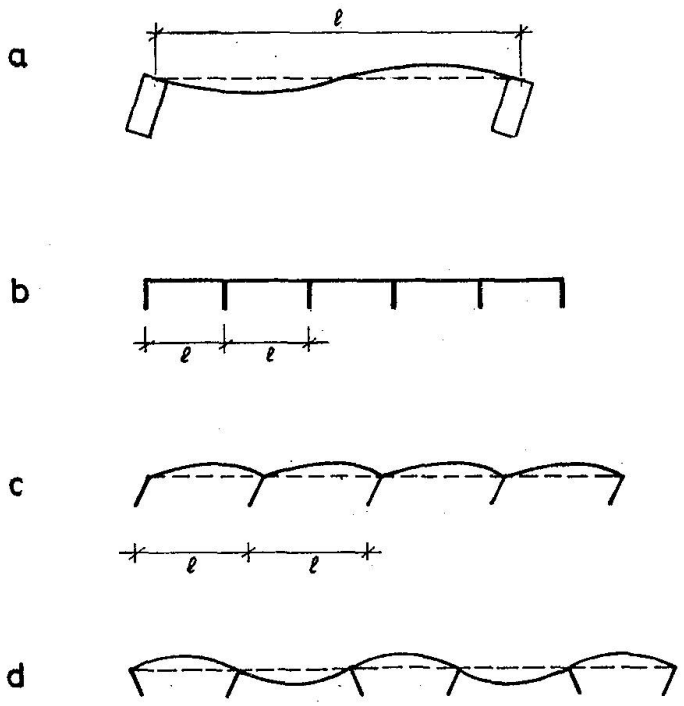

Fig. 8.

When a continuous cross-beam joins a number of principal beams (Fig. 8b), the stiffness of the restraint is

$A = \frac{12E_t I_t}{l}$ for all the intermediate main beams, and

$A = \frac{6E_t I_t}{l}$ for the first and the last one. The equations developed above give

correct values of ε_c or λ_c only if, L and d being the same for all the principal beams, q (or M in the case of pure bending), B, C and C_1 for the first and the last beam are each half as great as the common value of the corresponding parameter for the intermediate beams. If *all* the beams are identical, the first and last one carrying only half as much load as the other ones, the theory produces approximate, but safe values of the critical load.

Prof. P. Dubas has justly pointed out that lateral buckling of the main beams according to Fig. 8d is also possible, that in this case the values of A given above must be divided by 3 and the main beams do not deflect horizontally at the junctions with the secondary beams, and that the latter stabilizing effect may conceivably not quite compensate for the former unfavourable circumstance, thus leading to a lower critical load. Horizontal restraint of the beams delays lateral buckling quite efficiently, especially if the compressive flange is restrained. For instance, according to the German specifications (ref. 5, p. 24), lateral buckling is impossible when complete horizontal restraint without torsional restraint is applied at least half as high above the axis of the beam as the load. In actual practice, the joists are normally placed upon the upper flange of the main beams. Thus it seems highly unlikely that the mode of failure depicted in Fig. 8d would occur under a lower critical load than the one inducing all the main beams to rotate in the same direction.

The above expressions for A may be used to calculate α and ε or λ, provided that the connection between the transverse and each principal beam is such that any angle of twist, clockwise or counterclockwise, of the principal beam entails a rotation of the end of the secondary beam of exactly the same magnitude. If the beams are precast, reinforced or prestressed concrete beams, it may be more difficult to prevent opening than to prevent closing of the right angle between main and transverse beam (Fig. 8c). In that case, it is reasonable to estimate the stiffness of the restraint for the intermediate beams by means of the expression $A = \frac{3E_t I_t}{l}$, $E_t I_t$ again being the flexural rigidity of the cross-beam, and to assume that the first and the last principal beam are not restrained.

Joists Distributed Along the Span

The stiffness A_1 of the continuous torsional restraint is to be calculated with the appropriate expression given above for A, in which $E_t I_t$ now represents the flexural rigidity of the joists per unit length of the main beam.

Effect of Continuous Restraint and of Local Restraint at More Than One Point of the Span

Assuming, for example, that $\beta = 0$, we learn from table 1 that, for local torsional restraint at mid-span,

$16\varepsilon_c = 51{,}9$ when $\alpha = 5$, $\delta = 0$, and that
$16\varepsilon_c = 49{,}6$ when $\alpha = 5$, $\delta = 0{,}2$.

If the single cross-beam were replaced by numerous identical joists having together the same moment of inertia and uniformly distributed over the span of the principal beam, the new buckling load would be given by formula (26), with

$$A_1 = \frac{A}{L} \text{ or } \alpha_1 = \frac{A_1 L^2}{4C} = \frac{AL}{4C} = \alpha = 5.$$

The resulting values are

$$16\varepsilon_c = 49{,}4 \text{ when } \delta = 0,$$
$$16\varepsilon_c = 47{,}4 \text{ when } \delta = 0{,}2.$$

If, on the other hand, the stiffness of the single secondary beam were spread evenly over the central half of the main beam and if equivalent uniform torsional restraint were provided in the outer quarters of the span, A_1 in formula (26) would be $A_1 = \frac{A}{\frac{L}{2}}$ and α_1 would be $\alpha_1 = 2\alpha = 10$, with the following result:

$$16\varepsilon_c = 63{,}8 \text{ when } \delta = 0,$$
$$16\varepsilon_c = 61{,}8 \text{ when } \delta = 0{,}2.$$

Corresponding figures for a higher value of α are:

$16\varepsilon_c = 59{,}4$ when $\alpha = 13$, $\delta = 0$,
$16\varepsilon_c = 56{,}9$ when $\alpha = 13$, $\delta = 0{,}2$, torsional restraint being provided at mid-span only by a cross-beam with flexural rigidity $E_t I_t$, and
$16\varepsilon_c = 71{,}1$ when $\alpha_1 = 13$, $\delta = 0$,
$16\varepsilon_c = 69{,}1$ when $\alpha_1 = 13$, $\delta = 0{,}2$, $E_t I_t$ being distributed over many joists placed uniformly along the span.

Comparison of the above sets of figures suggests that when lateral buckling of the principal beam is counteracted by three or more joists, more or less equally spaced along the span, a fair approximation of the critical load will result from the assumption that the total stiffness of the joists is spread evenly over the span of the main beam.

Uniformly distributed joists stabilize the beam more efficiently than a single secondary beam at mid-span, whose moment of inertia is equal to the total moment of inertia of all the joists, when $\alpha = 13$; joists spread over the length of the span and of total rigidity $E_t I_t$ are almost as efficient as a single cross-beam of rigidity $E_t I_t$, when $\alpha = 5$.

The buckling load of beams without torsional restraint is multiplied by about 2,3 to 3, depending on β and δ, when an infinitely stiff transverse beam is rigidly connected to them at mid-span. It stands to reason, and expressions (26) and (28) confirm that the critical load increases indefinitely when the stiffness of uniformly distributed joists is increased indefinitely.

In prestressed concrete buildings, precast joists whose cross-section has the shape of a wide inverted U are often used. They are considerably stiffer horizontally than vertically. When their ends are connected to a flange of the principal beams in such a way that they participate in any horizontal rotation of the flange, the joists hamper lateral buckling of the main beams quite efficiently. The writer intends to elaborate on this subject in another paper.

Strength of the Rigid Connection Between Principal Beam and Cross-Beam

In stability problems, the question how strong — as opposed to how stiff — a restraining member has to be is always a moot point.

In the case of the joint between a cross-beam and a main beam, the simple answer that it must have the same moment capacity as the cross-beam itself is unsatisfactory. For one thing the positive moment capacity of the transverse beam may be considerably different from the negative moment capacity, at least for concrete beams. Actually there is no clear-cut answer. Some degree of arbitrariness is involved in every solution, including the procedure presented here. It pertains to the case of principal beams of narrow rectangular cross-section ($\beta = 0$), tied together by one secondary beam at mid-span.

Lebelle (ref. 1, p. 800) has obtained the differential equation for the angle of twist ϕ of a beam subjected to loads q and q_1, that act at the centroid $C \equiv 0$ of the rectangular cross-section in the plane of maximum and minimum flexural rigidity, respectively:

$$\phi'' + \frac{q^2 L^6}{4 \times 64 BC}(1 - t^2)^2 \phi + \frac{q q_1 L^6}{4 \times 64 BC}(1 - t^2)^2 = 0$$

$$\text{or } \phi'' + \varepsilon^2 (1 - t^2)^2 \phi + \varepsilon^2 \frac{q_1}{q}(1 - t^2)^2 = 0$$

This second order differential equation with variable coefficients and with a term not containing the unknown function ϕ obviously has $\phi = -\frac{q_1}{q}$ as a particular solution. Lebelle (ref. 1, p. 788) has obtained the general solution of the complete equation in the form of a power series in the independent variable t. When all terms whose coefficients of the powers of t contain ε^6 or higher powers of ε are neglected, the general solution is

$$\phi = K_1 \left| 1 - \frac{\varepsilon^2}{2} t^2 + \left(\frac{\varepsilon^2}{6} + \frac{\varepsilon^4}{24} \right) t^4 - \left(\frac{\varepsilon^2}{30} + \frac{7\varepsilon^4}{180} \right) t^6 + \frac{13\varepsilon^4}{840} t^8 - \frac{7\varepsilon^4}{2700} t^{10} + \frac{\varepsilon^4}{3960} t^{12} \right|$$

$$+ K_2 \left| t - \frac{\varepsilon^2}{6} t^3 + \left(\frac{\varepsilon^2}{10} + \frac{\varepsilon^4}{120} \right) t^5 - \left(\frac{\varepsilon^2}{42} + \frac{13\varepsilon^4}{1260} \right) t^7 + \frac{41\varepsilon^4}{7560} t^9 - \frac{31\varepsilon^4}{23100} t^{11} + \frac{\varepsilon^4}{6552} t^{13} \right|$$

$$- \frac{q_1}{q}$$

$$\text{or } \phi = K_1 \left| 1 + \varepsilon^2 \left(-\frac{t^2}{2} + \frac{t^4}{6} - \frac{t^6}{30} \right) + \varepsilon^4 \left(\frac{t^4}{24} - \frac{7t^6}{180} + \frac{13t^8}{840} - \frac{7t^{10}}{2700} + \frac{t^{12}}{3960} \right) \right.$$

$$\left. + K_2 \left| t + \varepsilon^2 \left(-\frac{t^3}{6} + \frac{t^5}{10} - \frac{t^7}{42} \right) + \varepsilon^4 \left(\frac{t^5}{120} - \frac{13t^7}{1260} + \frac{41t^9}{7560} - \frac{31t^{11}}{23100} + \frac{t^{13}}{6552} \right) \right| - \frac{q_1}{q} \right.$$

in which K_1 and K_2 are integration constants.

The boundary conditions of our problem are the same as those associated with equation (11):

$$\phi(1) = 0 \text{ and } \phi'(o) = \alpha \cdot \phi(o)$$

Since $\phi(o) = K_1 - \frac{q_1}{q}$ and $\phi'(o) = K_2$, the second boundary condition requires

$$K_2 = \alpha\left(K_1 - \frac{q_1}{q}\right).$$

The first condition becomes

$$\phi(1) = K_1\left(1 - \frac{11}{30}\varepsilon^2 + \frac{6617}{415800}\varepsilon^4\right) + \alpha\left(K_1 - \frac{q_1}{q}\right)\left(1 - \frac{19}{210}\varepsilon^2 + \frac{12161}{5405400}\varepsilon^4\right) - \frac{q_1}{q} = 0$$

Solving this equation for K_1, we are able to calculate the angle of twist at mid-span:

$$\phi(o) = K_1 - \frac{q_1}{q} = \frac{q_1}{q} \cdot \frac{\frac{11}{30}\varepsilon^2 - \frac{6617}{415800}\varepsilon^4}{1 + \alpha - \frac{\varepsilon^2}{210}(77 + 19\alpha) + \frac{\varepsilon^4}{5405400}(86021 + 12161\alpha)}$$

We now assume that the transverse load q_1 is due to an accidental out of plumb ω of the principal beam (Fig. 9) and hence is equal to $q_1 = q \sin\omega \cong q\omega$, so that $\frac{q_1}{q} = \omega$.

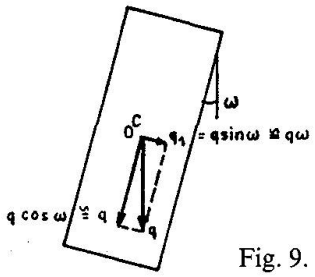

Fig. 9.

Noting that the moment applied by the cross-beam to the main beam is $A \cdot \phi(o)$, we obtain for this moment the expression:

$$A \cdot \phi(o) = \frac{11}{30}\omega A\varepsilon^2 \cdot \frac{1 - 0{,}0434\varepsilon^2}{1 + \alpha - \varepsilon^2(0{,}367 + 0{,}0905\alpha) + \varepsilon^4(0{,}0159 + 0{,}00225\alpha)} \tag{29}$$

In this formula $\varepsilon^2 = \frac{q^2 L^6}{256BC}$, in which q is not the critical load, but the working load, and, more specifically: the sum of dead load and superimposed load if the main beam did not carry its own weight when junction with the cross-beam was achieved, but the superimposed load only if the junction was achieved while the principal beam carried its own weight.

The designer has to assume a value for ω, for example 1% or 2%.

The joint between a cross-beam tying two principal beams together and each of these must have a positive and negative moment capacity calculated by means of expression (29). The joint between each span of a continuous transverse beam and each intermediate beam of a series of principal beams must be able to resist a negative as well as a positive moment, whose magnitude is half of that given by formula (29).

Formula (29) gives finite values, even when A and α are infinite.

Conclusions

(Subject to the reservations explained in the "Comments about equations 6 and 7")

Equations (6) and (7) give the critical moment for a beam of narrow rectangular cross-section, stiffened by local torsional restraint at mid-span and subjected to pure bending.

The uniform load causing lateral buckling is given by expression (17), in which ε_c is

— the positive root of equation (16) in the case of a beam of negligible warping rigidity, torsionally restrained by a cross-beam at mid-span;
— the positive root of equation (21), but never greater than the value resulting from expression (23), in the case of a beam with warping rigidity, torsionally restrained at mid-span;
— given by formula (28), when the beam has uniform torsional restraint.

Torsional restraint substantially increases the critical load.

The moment capacity required for the rigid connection between principal beams and secondary beams may be estimated with the help of formula (29).

Safety and Economy Aspects of the Problem

There have been failures of beams due to lateral buckling, most often during erection, while they were suspended from cranes and while their ends could rotate horizontally about the point of suspension, but also after erection, under the combined influence of their own weight and the superimposed load. In most cases the designers had not investigated the danger of lateral buckling; they simply had overlooked the problem.

If many other girders managed to carry their total load, in spite of not having been checked for lateral buckling, it is due undoubtedly to the fortunate circumstance that very few girders have no torsional restraint at all. Most principal beams are connected with each other by means of secondary beams or by joists or by a floor or by roof elements. Even when the designer does not consciously detail the connections with the purpose of providing torsional restraint to the principal beams, they normally possess some stiffness. This has probably saved many beams from failure, even though the designer was not aware of it.

Of course, a designer should not rely on chance and good luck to ensure the safety of a structure. The present paper provides a rational basis for the quantitative evaluation of the stabilizing influence of torsional restraint. Provided that the designer pays some attention to the details of the connections between slender main girders and secondary structural elements which are needed anyway, the formulas developed in this paper enable him to ascertain, without increasing the cross-section of the principal beams, that they are not in danger of buckling laterally, and thus to avoid the concomitant expenditure.

Notations

All Pertaining to the Main Beam

L span length.

I_x, I_y moment of inertia of the cross-section about the principal axes $x-x$ and $y-y$, respectively, through the centroid C (Fig. 1); $I_x >> I_y$.

I_1, I_2 moment of inertia of the upper and the lower flange, respectively, about the centre line $y-y$.

d vertical distance between the point of application of the uniform load q and the shear centre 0; d is positive when the load acts above the shear centre; the location of the shear centre results from the relation $h_1 I_1 = h_2 I_2$.

$B = EI_y$ horizontal flexural rigidity.

$C = GJ$ torsional rigidity; Poisson's ratio η in the relation $G = \dfrac{E}{2(1+\eta)}$ may be taken equal to 0,3 for steel and to 0,2 for prestressed or reinforced concrete.

$C_1 = EC_w$ warping rigidity; $C_w = \dfrac{h^2 I_1 I_2}{I_1 + I_2} = h_1^2 I_1 + h_2^2 I_2$; for a beam with two planes of symmetry: $h_1 = h_2 = \dfrac{h}{2}$ and $C_w = \dfrac{h^2}{2} I_1 = \dfrac{h^2}{2} I_2$.

A stiffness of the local torsional restraint at mid-span.

A_1 stiffness, per unit length of the main beam, of the continuous torsional restraint

$$\varepsilon = \frac{qL^3}{16\sqrt{BC}} \text{ or } \lambda = \frac{L}{2}\cdot\frac{M}{\sqrt{BC}}$$

$$\delta = 4\frac{d}{L}\sqrt{\frac{B}{C}} \quad \beta = \frac{4C_1}{L^2 C}$$

$$\alpha = \frac{AL}{4C} \text{ or } \alpha_1 = \frac{A_1 L^2}{4C}:$$

dimensionless parameters representing respectively: the intensity of the load, the level of its point of application, the warping rigidity of the cross-section, and the stiffness of the torsional restraint

$$\mu = \frac{\alpha}{6\beta}.$$

The subscript c denotes the critical value of the load q or M, or of the parameter ε or λ.

The superscript $'$ denotes differentiation with respect to t, with $z = t\frac{L}{2}$ (Fig. 2b).

u and ϕ horizontal displacement of the shear centre and angle of twist, respectively, of the cross-section with coordinate z (Fig. 2c).

References

1. LEBELLE, P.: Stabilité élastique des poutres en béton précontraint à l'égard du déversement latéral. Annales de l'Institut Technique du Bâtiment et des Travaux Publics, septembre 1959, pp. 780–831.
2. TAYLOR, A., and OJALVO, M.: Torsional Restraint of Lateral Buckling. Journal of the Structural Division, Proceedings of the American Society of Civil Engineers, April 1966, pp. 115–129.
3. TIMOSHENKO, S., and GERE, J.: Theory of Elastic Stability. McGraw-Hill Book Company, inc., New York, Toronto, London, 1961, Chapter 6.
4. STÜSSI, F., und DUBAS, P.: Grundlagen des Stahlbaues. Springer-Verlag, Berlin, Heidelberg, New York, 1971.
5. DIN 4114. Stabilitätsfälle (Knickung, Kippung, Beulung), Blatt 2: Richtlinien (Februar 1953).

Summary

Equations are developed which allow the easy calculation of the critical load causing lateral buckling of I beams without or with warping rigidity, which are stiffened either by local torsional restraint at mid-span or by uniform torsional restraint. The restraint may be provided by a cross beam or by joists, rigidly connected with the main beams. The strength necessary for the rigid connection is also discussed.

Résumé

L'auteur établit des équations qui permettent un calcul aisé de la charge critique provoquant le déversement latéral de poutres avec ou sans ailes, dont la stabilité est accrue par la présence d'une poutre secondaire à mi-portée ou de poutres secondaires disposées sur toute sa longueur et assemblée(s) rigidement à la poutre principale. L'auteur discute aussi la résistance requise pour le nœud rigide.

Zusammenfassung

Der Verfasser entwickelt Gleichungen, mit denen die Kippbelastung für I-Träger, deren Stabilität von einem Querbalken in der Mitte der Spannweite oder von über die ganze Länge der Spannweite angeordneten Querbalken gewährleistet wird, leicht zu berechnen ist. Querbalken und Hauptträger müssen steif miteinander verbunden sein. Der für diese steifen Knoten erforderliche Widerstand wird ebenfalls erörtert.

Leere Seite
Blank page
Page vide

Lateral Buckling Strength of Plate Girders

Tension de flambage latéral de poutres à âme pleine

Kippwiderstand von Vollwandträgern

H. YOSHIDA
Associate Professor of Civil Engineering
Kanazawa University, Kanazawa, Japan

Introduction

The lateral buckling strength of beams in the elastic and the inelastic range is governed by the flexural rigidity about the weak axis, St. Venant torsional rigidity and the warping rigidity of the cross section. The contributions of these rigidity of the elastic buckling strength are quite different for the compact section with large span length and for the thin-walled section with short span [1]. In the inelastic range, the problem is more complicate because the amount of yielding, and therefore the rigidities of the beam for the buckling, is dependent upon the applied critical moment. Even for I-shaped cross section usually used in structures, the direct relationship between the geometrical dimensions of the cross sections and the lateral buckling strength has not yet been established generally in the inelastic range.

First attempt to consider the effects of residual stresses was made by GALAMBOS [4] and he suggested an approximate method applicable to the lateral buckling of beams with general wide-flange cross sections under uniform moment. Nethercot also proposed an approximate design formula [11] in the inelastic range who investigated the various factors affecting the inelastic lateral buckling of beams. These formulae were inductively introduced from several typical cross sectional dimensions and thus the factors of the cross sectional dimensions affecting the lateral buckling of beams are not clear.

In this paper, the lateral buckling strength on the elastic and the inelastic ranges will be discussed for the I-shaped plate girders of which dimensions are with the thin web comparing with the flange thickness. For the plate girders with such dimensions, it will be shown that the lateral buckling strength can be expressed by only the ratio of the depth of the cross section to the web height with respect to the cross sectional geometry in both the elastic and the inelastic ranges and also the influence of such factors as cross sectional geometry, loading conditions, yield stress levels and residual stress distributions will be discussed in a general form.

Futhermore, the effect of the variations of cross sections with tapering flange widths or web depths on the elastic and the inelastic lateral buckling will be investigated.

Assumptions

The assumptions associated with the analysis are as follows:

1. The cross section of the plate girders is I-shaped doubly symmetric and the geometric center is horizontal and straight.
2. The effects of the web to the lateral flexural rigidity and the warping rigidity may be neglected and even to the St. Venant torsional rigidity may be neglected since $d_w w^3/2bt^3$ is less than 6% for the I-shaped plate girders usually used, in which d_w = the web height; w = the web thickness; b = the flange width and t = the flange thickness (see Fig. 1a). Furthermore, since after yielding of both flanges of I-shaped plate girders, the carrying capacity can not be expected, this assumption may be allowable.
3. The plate girders are perfectly straight before the buckling occurs and the cross section does not distort before and after the buckling.
4. The vertical displacement is small.
5. The stress-strain relation is for the elastic-perfectly-plastic.
6. The residual stress in the cross section distributes in the flanges only. The distribution of the residual stress is symmetric about axes of symmetry of the cross section. The residual stress in a cross section is in self-equilibrium and are ideally assumed as Figs. 1b and c for as-rolled and as-welded shapes, respectively.
7. The stiffnesses of lateral bending and warping in the inelastic range are calculated by the tangent modulus theory. The stiffness of the St. Venant torsion is by the incremental theory which predicts the same St. Venant torsional stiffness for the yielded portion as that of the elastic portion.
8. The variation of a cross section is not so steep that the assumptions associated with the so-called beam theory can not be available.

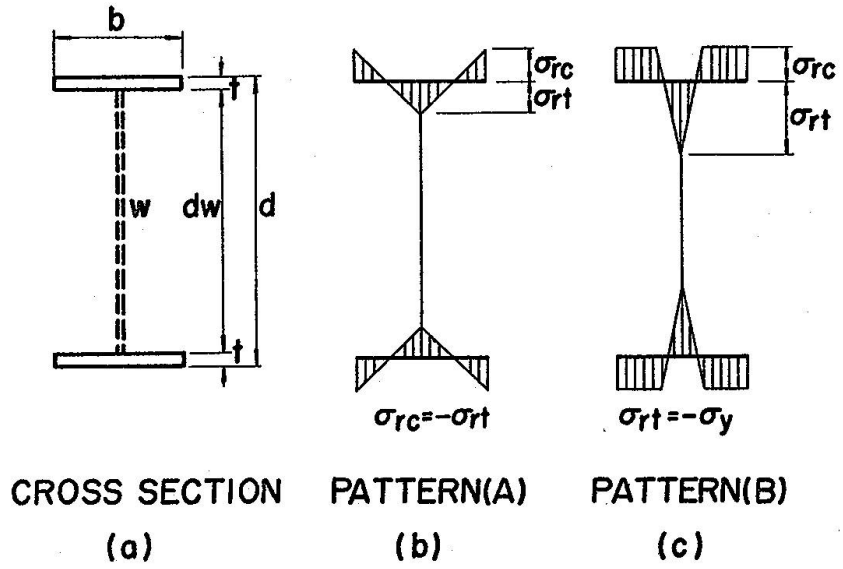

Fig. 1. Simplified cross section and idealized residual stresses.

As shown in Fig. 2, the x and y coordinates of the centroid of a small rectangular element in a flange divided by the horizontal and the vertical lines may be expressed by ξb and ηd of which origin locates at the center of the cross section, in which d = the depth of the cross section. The strain, ε, at the centroid of the element is the combination of the strain, ε_ϕ, due to the bending which is proportional to the distance from the center of the cross section, the strain, ε_o, which yields uniformly on the whole cross section and the strain, ε_r, due to the residual stress.

$$\varepsilon = \varepsilon_\phi + \varepsilon_o + \varepsilon_r = 2\varepsilon_y\left(\frac{\phi}{\phi_y}\right)\eta + \varepsilon_o + \varepsilon_r \tag{1}$$

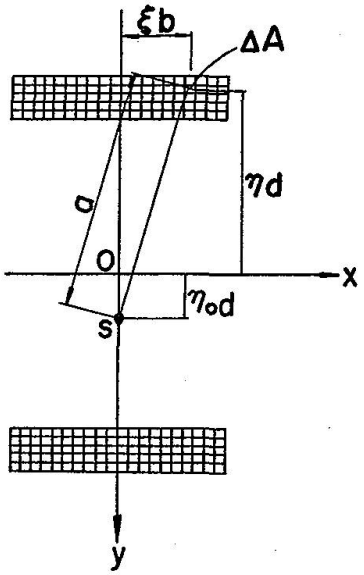

Fig. 2. Subdivided cross section.

in which ε_y = the strain corresponding to the yield stress; ϕ = the curvature and ϕ_y = the curvature corresponding to the yield in flexure.

Thus, the stress, σ, at the centroid of a small rectangular element becomes

$$\begin{aligned} \sigma &= E\varepsilon && |\varepsilon| \leqq \varepsilon_y \\ \sigma &= \sigma_y \cdot \mathrm{sgn}(\varepsilon) && |\varepsilon| > \varepsilon_y \end{aligned} \tag{2}$$

in which E = Young's modulus of elasticity; σ_y = the yield stress; $\mathrm{sgn}(\varepsilon) = 1.0$ when ε is positive and $\mathrm{sgn}(\varepsilon) = -1.0$ when ε is negative. From the equilibrium of longitudinal direction, $\int_A \sigma dA = 0$,

$$\sum_E \left(\frac{\varepsilon}{\varepsilon_y}\right) + \sum_P \mathrm{sgn}\left(\frac{\varepsilon}{\varepsilon_y}\right) = 0 \tag{3}$$

must be satisfied in which $\sum_E$ means the sum for the elastic elements only and $\sum_P$ means the sum for the yielded elements.

By the trial and error procedure, the strain, ε_o, in Eq. 1 which is satisfied by Eq. 3 can be obtained for a given curvature, ϕ/ϕ_y. Then, the strain and the stress at the centroid of the small rectangular element can be known.

The bending moment corresponding to the curvature, ϕ/ϕ_y, is

$$\frac{M}{M_y}=\frac{3}{mn(1+\beta+\beta^2)}\left\{\sum_E\left(\frac{\varepsilon}{\varepsilon_y}\right)\cdot\eta+\sum_P\mathrm{sgn}\left(\frac{\varepsilon}{\varepsilon_y}\right)\cdot\eta\right\} \tag{4}$$

in which m and n = the subdivided numbers of the flange thickness and the flange width with equal intervals, respectively; M_y = the yield moment without residual stress and $\beta=d_w/d$, the ratio of the web height, d_w, to the depth of the cross section, d.

The moment of inertia about the weak axis, I_y, and the warping moment of inertia, I_w, for the elastic core of the cross section corresponding to M/M_y are given by

$$I_y=\mu_{iy}\kappa_{iy}b^3d \tag{5a}$$

$$I_w=\mu_{iw}\kappa_{iw}b^3d^3 \tag{5b}$$

The equivalent St. Venant torsional stiffness, $G\bar{K}_T$, defined by the combination of the St. Venant torsional stiffness, GK_T, and the contribution to the torque caused by the normal stress, $\int_A\sigma a^2dA$, and the section modulus about the strong axis, S, are given by

$$G\bar{K}_T=GK_T+\int_A\sigma a^2dA=\mu_{kt}\kappa_{kt}bd^3 \tag{6a}$$

$$S=\mu_s bd^2 \tag{6b}$$

in which a = the distance between the point on a flange and the shear center, μ's in Eqs. 5 and 6 are functions with respect to only β defined by

$$\mu_{iy}=\tfrac{1}{12}(1-\beta) \tag{7a}$$

$$\mu_{iw}=\tfrac{1}{192}(1-\beta)(1+\beta)^3 \tag{7b}$$

$$\mu_{kt}=\tfrac{1}{12}(1-\beta)^2 \tag{7c}$$

$$\mu_s=\tfrac{1}{6}(1-\beta^3) \tag{7d}$$

and κ's are the reduction factors for the coefficients in the inelastic range given by

$$\kappa_{iy}=\frac{6}{mn}\sum_E\xi^2$$

$$\kappa_{iw}=\frac{6}{mn}\frac{\sum_{Eu}\zeta^2\sum_{El}\zeta^2}{\sum_E\zeta^2}\left\{\frac{\sum_{Eu}\zeta^2\eta}{\sum_{Eu}\zeta^2}-\frac{\sum_{El}\zeta^2\eta}{\sum_{El}\zeta^2}\right\} \tag{8a}$$

$$\kappa_{kt}=1.0-\frac{6}{mn(1+\beta+\beta^2)}\bar{\nu}\varepsilon_y\left[\left\{\sum_E\left(\frac{\varepsilon}{\varepsilon_y}\right)(\eta-\eta_o)^2+\sum_P\mathrm{sgn}\left(\frac{\varepsilon}{\varepsilon_y}\right)(\eta-\eta_o)^2\right.\right. \tag{8b}$$

$$\left.\left.+\alpha^2\left\{\sum_E\left(\frac{\varepsilon}{\varepsilon_y}\right)\xi^2+\sum_P\mathrm{sgn}\left(\frac{\varepsilon}{\varepsilon_y}\right)\xi^2\right\}\right]=1.0-\frac{6}{(1+\beta+\beta^2)}\bar{\nu}\varepsilon_y(\gamma_1+\alpha^2\gamma_2) \tag{8c}$$

In Eqs. 8, $\sum_{Eu}$ indicates the sum of the elastic small rectangular elements of the upper flange and $\sum_{El}$ indicates for the lower flanges, $\bar{\nu}=E/G$, the ratio of the Young's modulus to the shear modulus of elasticity; and $\alpha=b/d$, the ratio of the flange width to the depth of a cross section. Furthermore, $\eta_o d$ is the coordinate of the shear center of the elastic core on the y axis given by

$$\eta_o=\frac{\sum_E\xi^2\eta}{\sum_E\xi^2} \tag{9}$$

From Eq. 4 and Eqs. 8 and 9, the relationships between κ_{iy}, κ_{iw}, κ_{kt} and η_o in the inelastic range and M/M_y can be obtained under given residual stress level and pattern.

It can be observed from numerical calculations that these values are almost independent on β.

Analytical Method

The transfer matrix method in Ref. 15 may be applied in the analysis. Using the state vector given in Appendix, the 8×8 field transfer matrix can be formulated by the nondimensionalized forms which are independent on α.

For the calculation of the tapered beams, the point transfer matrix can be available at the nodal point and two parameters k_b and k_d are introduced which indicate the ratios of the flange width and the depth of a cross section at an arbitrary location to those at the reference point on a beam. The state vectors of both sides at nodal point i can be related by the point matrix given in Appendix which is independent on α and β.

The beam is divided by finite elements and it is assumed that the bending moment at the midpoint of an element is uniformly distributed in the element. Furthermore, for the tapered beams, it is assumed that the cross section is constant in an element and its dimension is represented by that at the midpoint of the element. Using the reduction factors and the sectional constants corresponding to the nondimensionalized bending moment by M_y and premultiplying the field transfer matrix of each element from left end to right, the state vectors at left and right ends can be related with each other. The buckling conditions in this case can be given by

$$|\mathbf{R}'\mathbf{F}_n\mathbf{P}_{n-1}\mathbf{F}_{n-1}\mathbf{P}_{n-2}\cdots\mathbf{P}_2\mathbf{F}_2\mathbf{P}_1\mathbf{F}_1\mathbf{R}| = 0 \tag{10}$$

in which $\mathbf{F}_1$, $\mathbf{F}_2$, $\cdots$ $\mathbf{F}_n$ = the field transfer matrices of elements 1, 2, $\cdots n$; $\mathbf{P}_1$, $\mathbf{P}_2$, $\cdots$ $\mathbf{P}_{n-1}$ = the point transfer matrices at nodes 1, 2, $\cdots$ $n-1$ and $\mathbf{R}$, $\mathbf{R}'$ = the boundary matrices at left and right ends. The critical moment may be determined as the smallest root of this determinantal equation.

Based upon this formulated equation, a computer program was developed to provide numerical results by trial and error procedure. First, the bending moment at the midpoint of each element is calculated for an arbitrary critical load factor then the reduction factors corresponding to the bending moment are numerically evaluated for each element. Second, the determinant of Eq. 10 is calculated. The calculation of these steps must be repeated using a new value of the critical load factor until a sufficient accuracy is obtained.

Buckling Strength under Pure Bending

Effects of Geometrical Shapes and Residual Stresses

As the factors to affect the lateral buckling strength of plate girders under pure bending, the ratio of the web height to the depth of a cross section, $\beta = d_w/d$, the magnitudes of a residual stress and the yield strain may be considerable from above discussion.

The nondimensionalized field transfer matrix discussed above is only a function of β as far as the dimensions of a cross sectional geometry are concerned and α is only

included in the coefficient of the equivalent St. Venant torsional rigidity given in Eq. 8c. But because γ_2 in Eq. 8c is considerably less than γ_1, the effect of α to the coefficient κ_{kt} is sufficiently small for usually used plate girders. For instance, the buckling strengths of $\alpha=0.1$ and 0.5 were compared for $\sigma_{rc}=0.3\sigma_y$ and $\varepsilon_y=0.0012$. From the numerical results, the difference between two cases is less than 1% in the elastic range and decreases further in the inelastic range. Thus, $\alpha=0.3$ may be used in the following numerical calculations.

Fig. 3 shows the effects of three magnitudes of the residual stress, $\sigma_{rc}=0.1\sigma_y$, $0.3\sigma_y$ and $0.5\sigma_y$, to the lateral buckling strength for three values of $1/\beta=1.03$, 1.05 and 1.07. The vertical line indicates M/M_y and the horizontal line indicates L/b. The boundary conditions are simply supported for the lateral displacement and the rotation at both ends and $\varepsilon_y=0.0012$ is used. From the figure, the buckling strength is greately affected by the parameter β in the elastic range but that effect decreases in the inelastic range with the reduction of L/b.

The elastic buckling moment of a doubly symmetric I-shaped beam without residual stress under pure bending can be expressed by [3],

$$(M_o)^e_{cr}=\frac{\pi}{L}\sqrt{EI_yGK_T\left(1+\frac{\pi^2EI_w}{GK_TL^2}\right)} \tag{11}$$

Substituting Eqs. 5, 6 and using Eqs. 7 and unity for κ_{iy}, κ_{iw}, κ_{kt}, the non-dimensionalized critical moment by the yield moment, $(m_o)^e_{cr}$ can be obtained by

$$(m_o)^e_{cr}=\frac{\pi}{2\sqrt{2(1+\nu)\varepsilon_y}}\frac{(1-\beta)^2}{(1-\beta^3)}\left(\frac{b}{L}\right)\sqrt{1+\tfrac{1}{8}(1+\nu)\pi^2\frac{(1+\beta)^2}{(1-\beta)^2}\left(\frac{b}{L}\right)^2} \tag{12}$$

in which $\nu=$ Poisson's ratio.

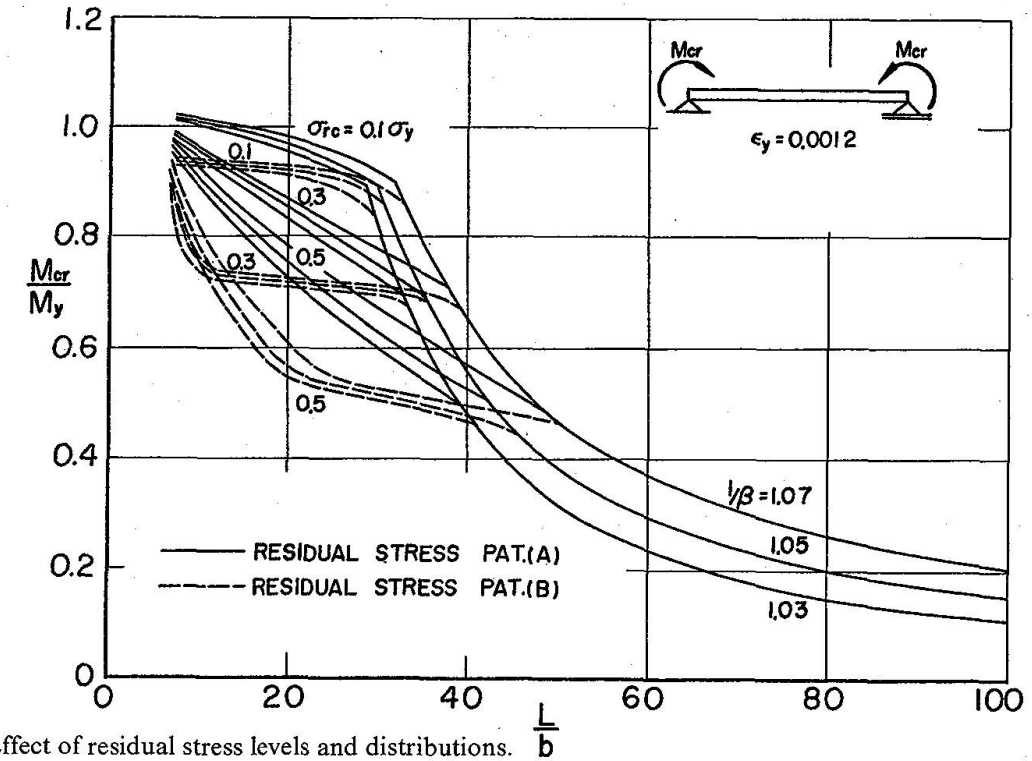

Fig. 3. Effect of residual stress levels and distributions.

Taking the vertical line the quotient of the nondimensionalized critical moment, M_{cr}/M_y, divided by $(m_o)^e_{cr}$ and the horizontal line the reciprocal of the square root of $(m_o)^e_{cr}$,

$$\lambda = 1/\sqrt{(m_o)^e_{cr}} \tag{13}$$

the buckling curves in the elastic range are horizontaly straight and these values are slightly less than unity because the residual stress reduces the elastic buckling strength.

The curves are independent on the geometrical shapes of the cross section but slightly depend on the residual stress levels and distributions. Thus, in this representation, the starting point of an inelastic buckling curve is independent on the geometrical shapes of the cross section. Fig. 4 shows the same buckling curves as Fig. 3 represented by such manner for the residual stress patterns (*A*) and (*B*), respectively. Fig. 5 shows the difference between both the residual stress patterns (*A*) and (*B*) for $\sigma_{rc}=0.3\sigma_y$.

In these figures, the solid curves and the dotted curves indicate for $1/\beta = 1.03$ and 1.07, respectively. It can be observed that the curves are also independent on the geometric dimensions and only depend on the residual stress levels and distributions in the inelastic range.

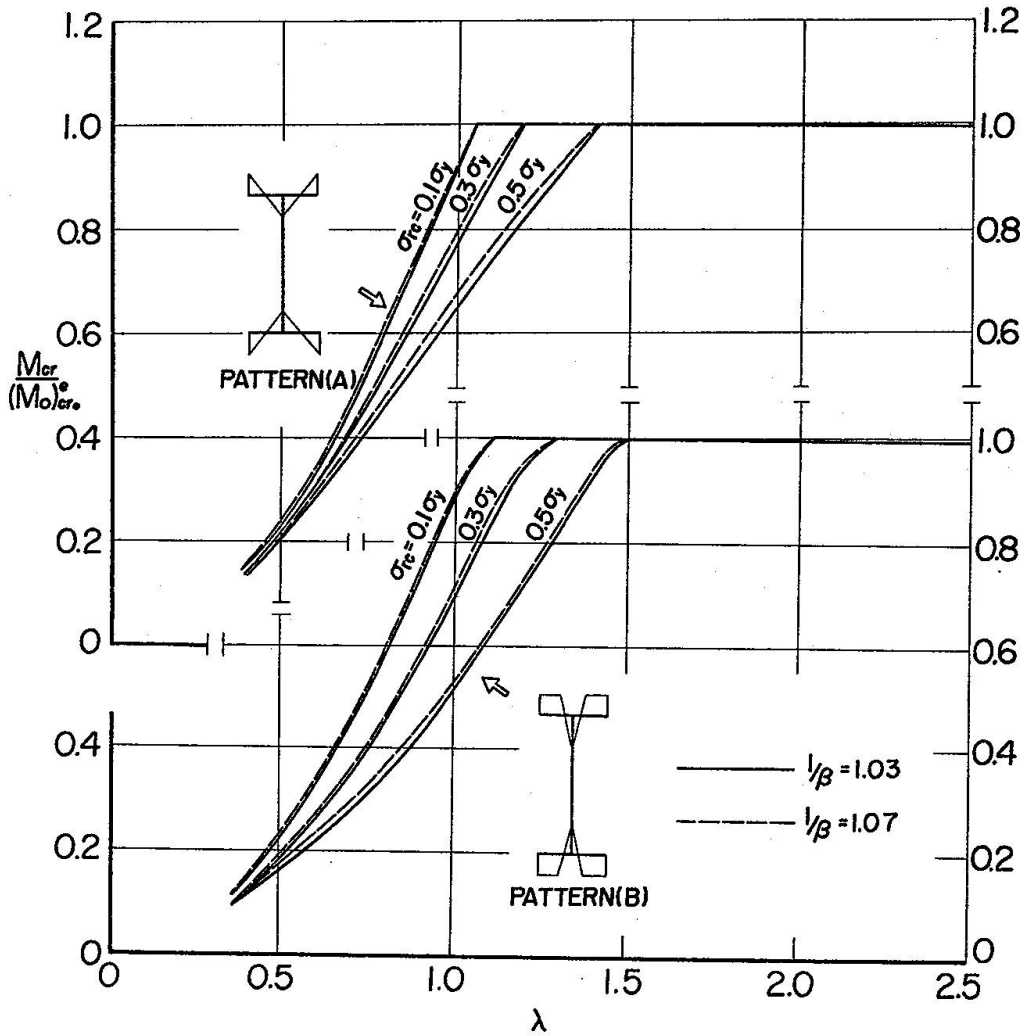

Fig. 4. A possible representation of buckling curves.

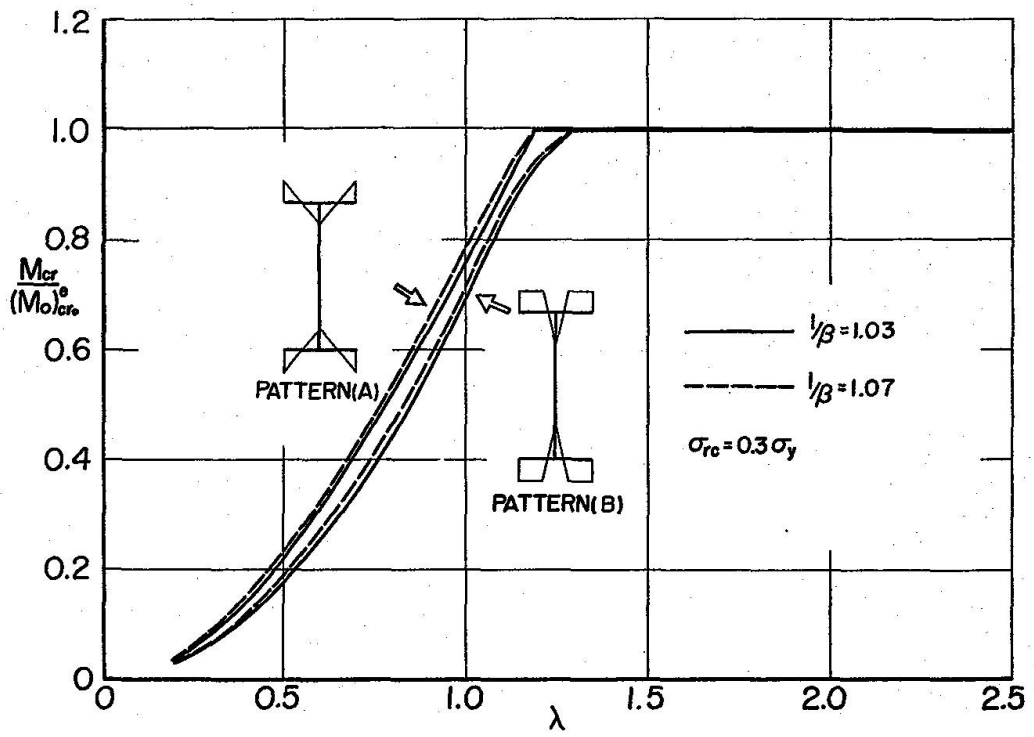

Fig. 5. Comparison between residual stress patterns.

Effect of the St. Venant Torsional Stiffness

It has been proposed that the lateral buckling strength calculated by neglecting the St. Venant torsional stiffness may be used for the plate girders with the relative short buckling length braced by cross beams or lateral bracings [1]. From this view point, both buckling curves for a uniform bending considering and neglecting the St. Venant torsional stiffness are compared in Fig. 6 by thick curves and thin curves, respectively.

The vertical line indicates the nondimensionalized critical bending moment, M_{cr}/M_y, and the horizontal line indicates the span length divided by the flange width, L/b.

The solid curves are for the residual stress pattern (A) and the dotted curves for the pattern (B) and $\sigma_{rc}=0.3\sigma_y$, $\varepsilon_y=0.0012$ are used. The values neglecting the St. Venant torsional stiffness are independent on the values of β in a long span length but slightly depend upon β in a relatively short span length.

The difference between the values considered and neglected the St. Venant torsional stiffness is small for $1/\beta=1.03$ but the strength calculated by neglecting the St. Venant torsional stiffness is on the safe side for $1/\beta=1.07$.

Effect of the Yield Stress Levels

The buckling curves in Fig. 3 are for the yield strain $\varepsilon_y=0.0012$. However, in the nondimensionalized representation of the buckling curves as Figs. 4 and 5, the effect of the yield strain will disappear because the yield strain only affects κ_{kt} and the influence on it is negligible.

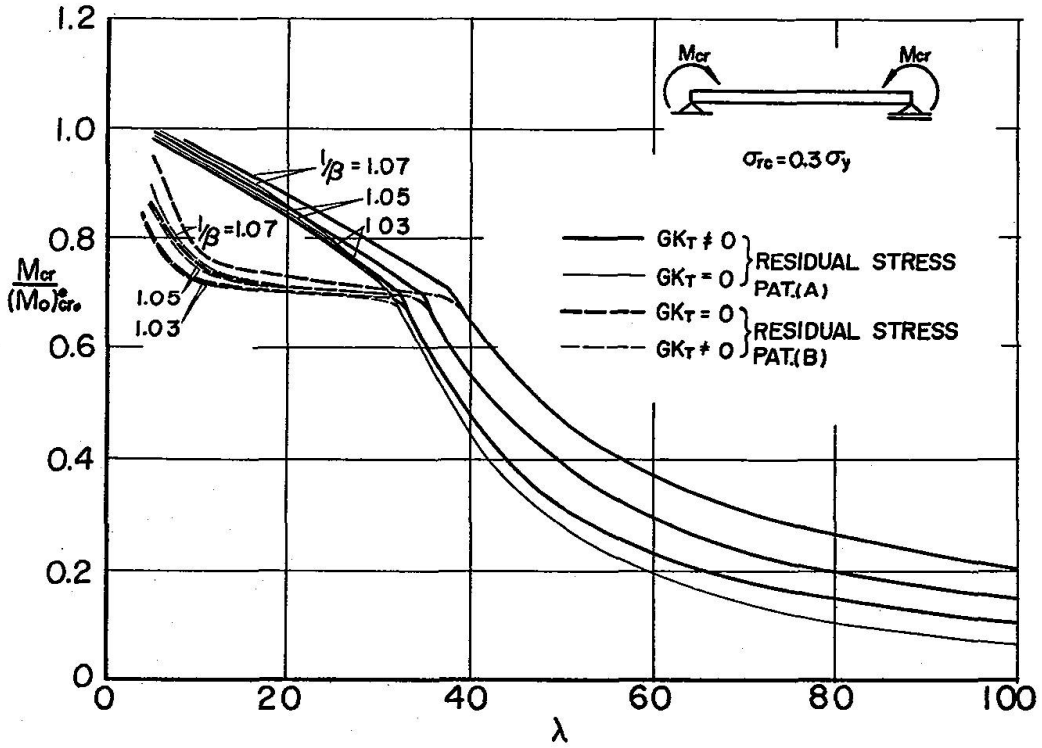

Fig. 6. Effect of St. Venant torsional stiffness.

Comparison with Test Results

In Ref. 2, Fukumoto *et al.* have carried out the tests of the plate girders. The experiments under the pure bending consisted of thirty-seven welded built-up beams and girders made from *SM*50 (*A*441) or *HT*80 (*A*514) steel. Some of them are annealed. The boundary conditions are fixed for the lateral displacements and the rotations at both ends.

The experimental values are plotted in Fig. 7. The vertical line indicates the nondimensionalized bending moment, $M_{cr}/(M_o^F)_{cr}^e$ and the horizontal line indicates $\lambda_F = 1/\sqrt{(M_o^F)_{cr}^e/M_y} = 1/\sqrt{(m_o^F)_{cr}^e}$ in which $(M_o^F)_{cr}^e$ = the elastic critical bending moment of the plate girder without the residual stress under the pure bending of which boundary conditions are fixed for the lateral displacements and the rotations at both ends. In the figure, the theoretical values are also shown by solid curve, dotted curve and one-dotted curve for plate girders without residual stress, with residual stress patterns (*A*) and (*B*) for $\sigma_{rc}=0.3\ \sigma_y$, respectively. In the representation, the effect of the geometrical shapes and the yield stress levels may not be included and only the effect of the residual stress levels and distributions is included.

The experimental results scatter in a relative small range and the theoretical curves for the residual stress pattern (*B*) with $\sigma_{rc}=0.3\sigma_y$ may give the lower bound.

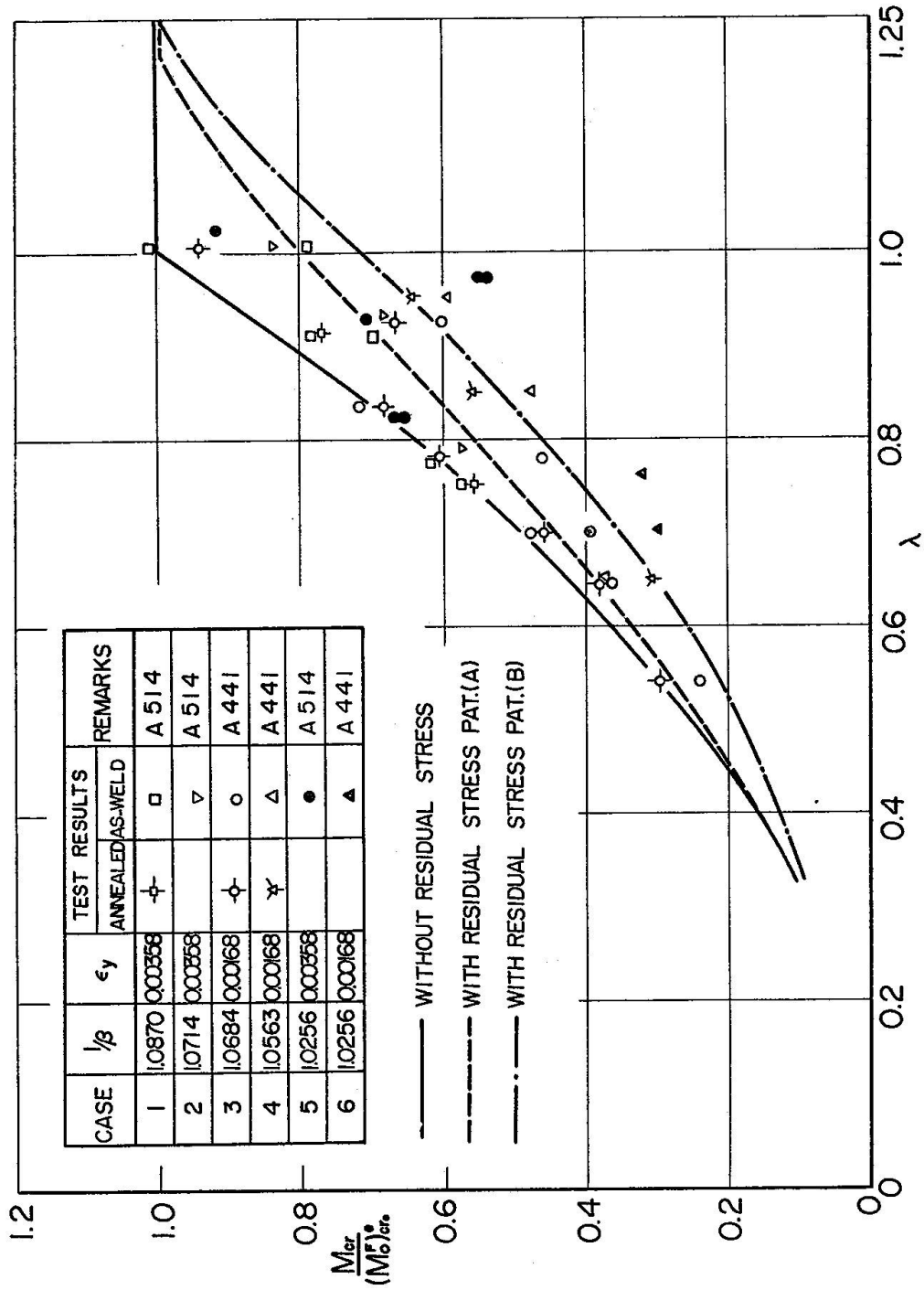

Fig. 7. Comparison with experimental results.

Buckling Strength under Various Loading Conditions

Fig. 8 shows the lateral buckling curves under three loading cases for $\sigma_{rc} = 0.3\sigma_y$. A uniform bending moment, a concentrated load applied at the midspan and a uniformly distributed load are considered. The uniform moment may be the most severe loading condition for the lateral buckling, the concentrated load at the midspan may be the most lenient condition and the uniformly distributed load lies midway.

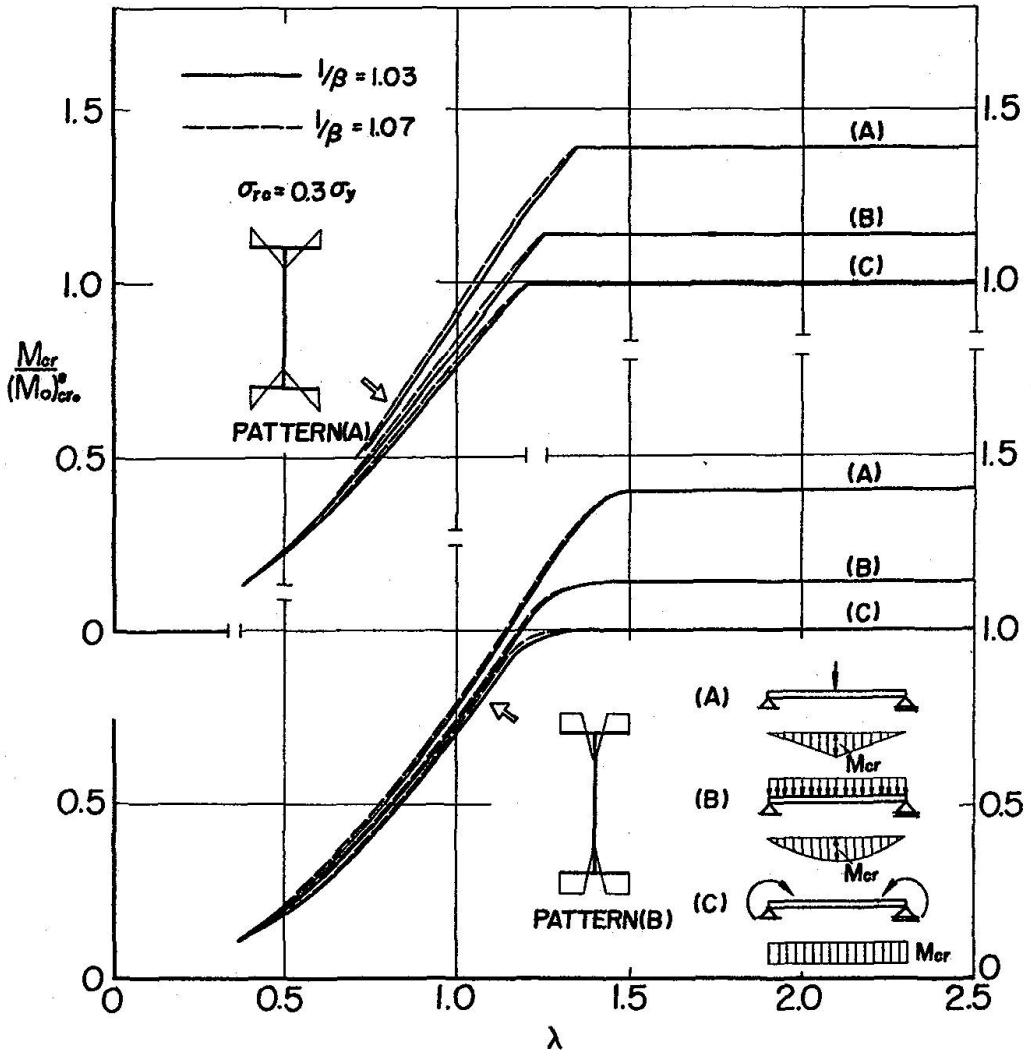

Fig. 8. Buckling curves for various loading conditions.

The horizontal line indicates λ given by Eq. 13 and the vertical line indicates the quotient of the nondimensionalized bending moment at the midspan corresponding to the buckling load, M_{cr}/M_y, divided by the elastic critical moment given by Eq. 12.

The effect of β to the buckling curves can be observed little in the elastic and the inelastic ranges for both the residual stress patterns.

Buckling Strength of Tapered Plate Girders

Effect of Variations of Cross Section and Loading Conditions

Three types of the variation of cross sections along the span length are considered. 1. The flange widths or depths of the cross section decrease linearly from the midspan (Type A); 2. remain a constant at a central one-third of the span length and decrease linearly at both outside one-thirds (Type B), and 3. decrease parabolically from the midspan (Type C).

For each type of the variation, the buckling strength under three loading cases of a uniform moment, a concentrated load at the midspan and a uniformly distributed load is calculated. The boundary conditions are simply supported for the lateral displacements and the rotations at both ends.

A few numerical examples are shown in Figs. 9 and 10. Fig. 9 shows the buckling curves for a concentrated loading case under a constant depth of the cross section, $k_d = 1.0$ and $/\beta = 1.05$. Only the flange widths vary such that the ratios of the flange width at the ends of the plate girder to that at the reference point of the midspan, k_{bo}, decrease from 1.0 to 0.2 with 0.2 pitch. The vertical line indicates the ratio of the nondimensionalized critical moment at the midspan, $M_{cr}/(M_y)_o$, for the varying cross section to the elastic critical moment, $(m_o)^e_{cro}$, in which $(M_y)_o$ and $(m_o)^e_{cro}$ are the yield moment and the elastic critical moment given in Eq. 12 for the uniform cross section of which dimensions are at the midspan of the varying cross section. The horizontal line indicates $\lambda_o = 1/\sqrt{(m_o)^e_{cro}}$ and the solid, dotted and one-dotted curves show for the types A, B and C, respectively.

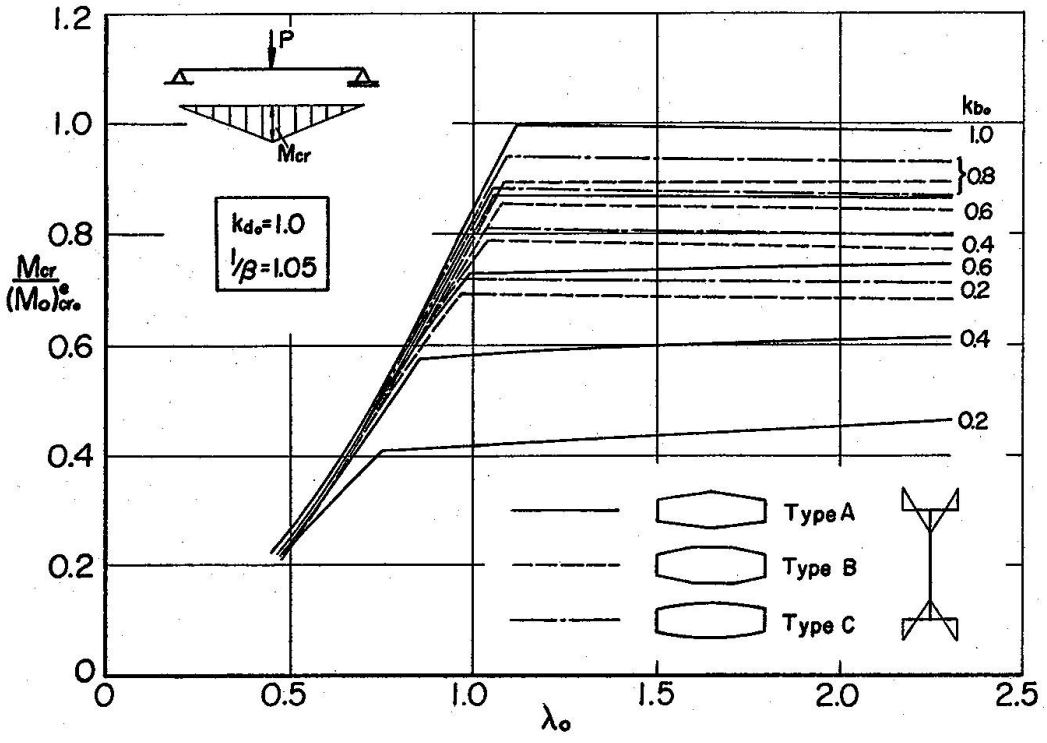

Fig. 9. Buckling curves of plate girders with tapering flange widths.

Fig. 10 shows the buckling curves under the same conditions except the depth of the cross section varies and the flange widths and $1/\beta$ remain constants. When the depths of the cross section and $1/\beta$ remain constants, the curves in the elastic range in Fig. 9 are almost straight and keep constants except for small values of k_{bo} of Type A but in the inelastic range, the curves decrease parabolically with the reduction of λ_o. When the widths of the flange and $1/\beta$ remain constants, the curves in the elastic range in Fig. 10 are ascending with the reduction of λ_o and this tendency becomes remarkable with the degree of taper. In the inelastic range, the curves decrease parabolically with the reduction of λ_o. From the numerical calculations, the buckling curves in Figs. 9 and 10 are independent on the values of β in both the elastic and the inelastic ranges when the value of β keeps a constant along the whole length of the plate girders. For other cases of the loading, the same tendency can be observed in the elastic and the inelastic ranges.

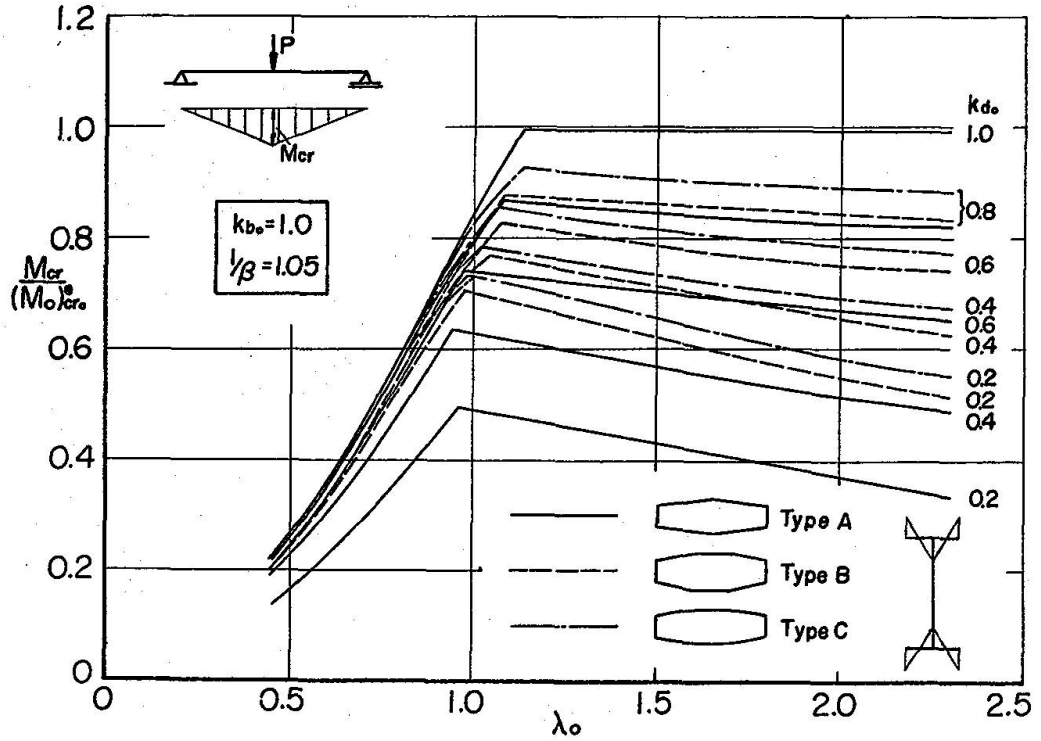

Fig. 10. Buckling curves of plate girders with tapering web depths.

Design Approximations for Plate Girders with Tapering Flange Widths or Web Depths

It is assumed that the flange widths or the web depths are linearly tapered between the restricted points of a plate girder by cross beams or lateral bracings and at these points the plate girder is simply supported for the lateral displacements and the rotations. The cross sectional dimensions of the plate girders are usually designed such that the stresses go near the margine under a applying bending moment. Thus, the bending moments at the restricted points in the plate girder may be proportional to the yield moments or the full plastic moments of the cross sections.

In the numerical calculations, it is assumed in addition to above assumptions that the bending moments at the restricted points are proportional to the yield moments of the cross sections and the bending moment distribution is linear between these points.

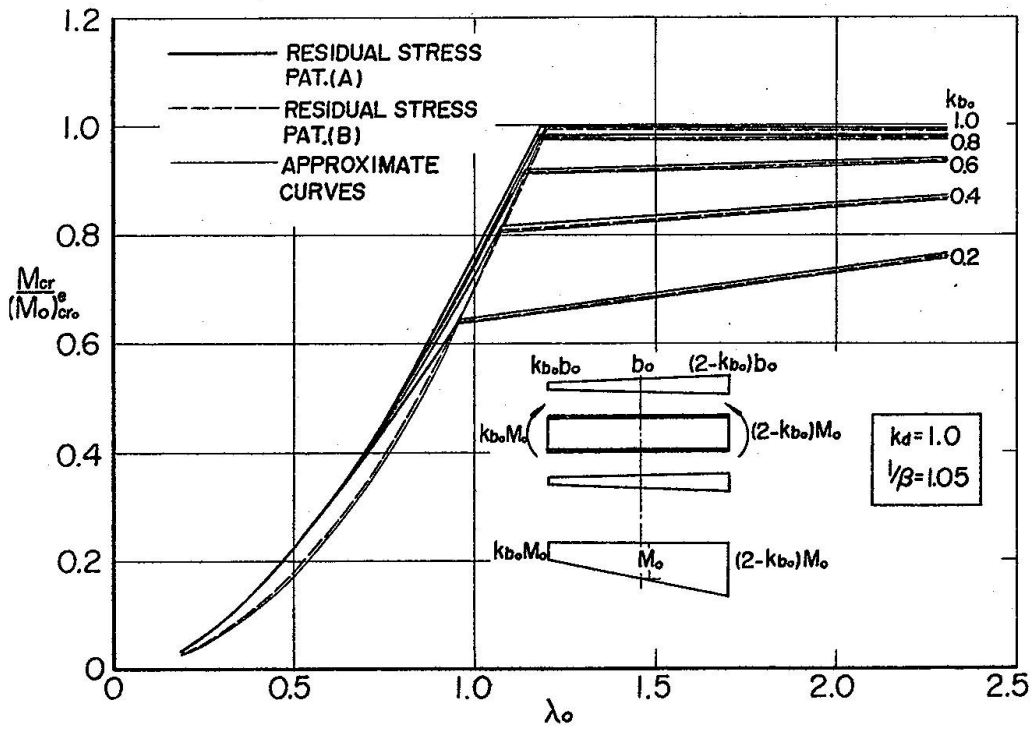

Fig. 11. Buckling curves of plate girders with linearly tapered flange widths.

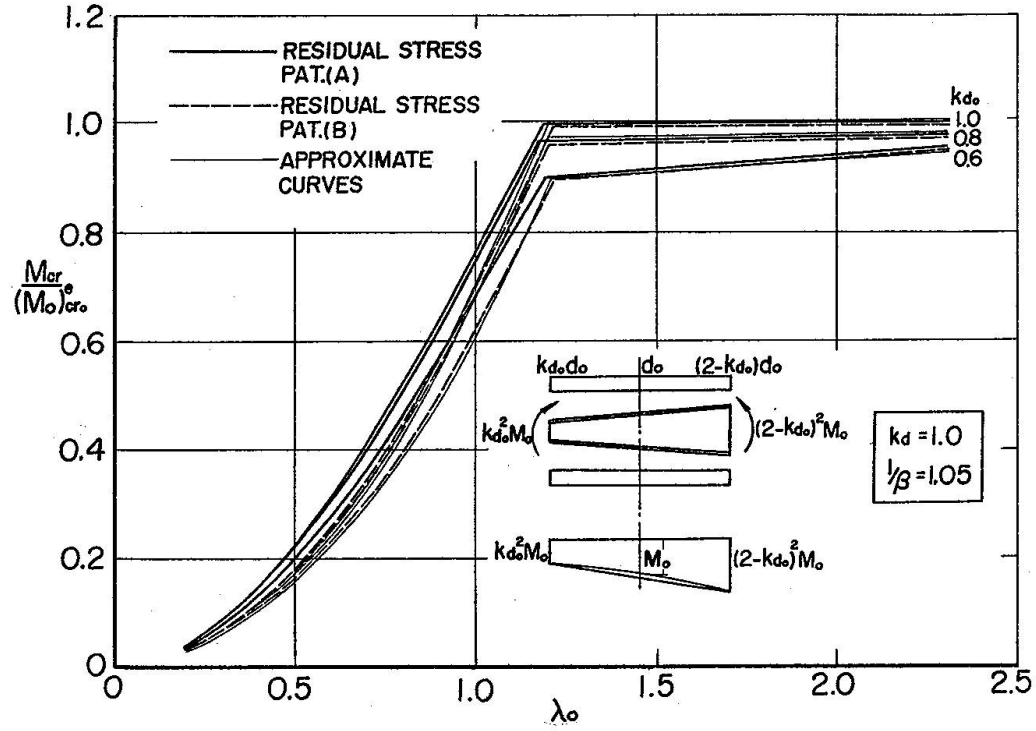

Fig. 12. Buckling curves of plate girders with linearly tapered web depths.

Fig. 11 shows the buckling curves of the plate girders with linearly tapering flange widths. The horizontal line indicates λ_o and the vertical line indicates the critical moment at the midspan nondimensionalized by the same manner as Figs. 9 and 10.

The degrees of the taper of the flange widths, k_{bo}, are the ratios of the smaller flange width at the supports to the flange width at the midspan. In the numerical calculations, $1/\beta = 1.05$ is used and the buckling curves in the figures are shown by solid curves for the residual stress pattern (A) and by dotted curves for the pattern (B). The same illustration for the plate girders with linearly tapering web depth is given in Fig. 12. It should be noted that the yield moment of the cross section is not vary linearly along a span in this case.

The curves in the elastic ranges in Figs. 11 and 12 are almost straight and keep constants under a gentle taper of cross sections. However, when the degrees of taper become steep, the curves are descending with the reduction of λ_o. In the inelastic range, the curves decrease parabolically with the reduction of λ_o.

The discrepancy between the buckling curves in Fig. 11 or 12 for $1/\beta = 1.05$ and for the values of $1/\beta = 1.03$ or 1.07 cannot be recognized.

In the figures, the thin lines show the approximate design formulae proposed herein by

$$\frac{M_{cr}}{(M_o)^e_{cro}} = C_1 + (1.0 - C_1)\,(2.0 - k)k \tag{14}$$

in the elastic range and

$$\frac{M_{cr}}{(M_o)^e_{cro}} = C_2\lambda_o^2 \tag{15}$$

in the inelastic range in which $C_1 = 0.15\lambda_o + 0.3$ and $C_2 = 0.7$ for the tapering flange widths and $C_1 = 0.3\lambda_o$, $C_2 = 0.7 - 0.5 \times (1.0 - k_{do})^2$ for tapering web depths, respectively and k is the degree of the taper of flange width or web depth.

Remarks on Practical Application

In this paper, the effects to the rigidities of the web of plate girders were neglected in the analysis. It is well known that the model neglected the effects of web gives a good approximation to the lateral flexural and the warping rigidities. However, the error accompanied by the calculation of the axial forces of the flanges may not be small. A few actual plate girders were examined considering and neglacting the web effects in this view point. As the result, it is found that the representation of the buckling curves as shown in Fig. 4 gave a satisfactory agreement for both cases.

The buckling strength of the plate girders with tapering flange wides or web depths decreases comparing the strength of those with a uniform cross section for all loading conditions of a uniform bending moment, a concentrated load and a uniformly distributed load. The economy of the flange or the web weight of the plate girders with tapering constant k_{bo} or k_{do} can be given by $(1-k)/2$ and $(1-k)/3$ for the Type A and Type B, C, respectively, in which k = a tapering constant k_{bo} or k_{do}.

The reduction of the buckling strength of plate girders with a tapering cross section exceeds the decrease of the flange or the web weight in the elastic range. This tendency is most remarkable under a loading case of a uniform bending moment and least under a concentrated loading case. However, in the inelastic range, the reduction of the strength can not be almost recognized under both the cases of a concentrated load and a uniformly distributed load.

The results shown in Figs. 11 and 12 may contribute to the rational design of plate girders.

Conclusions

The elastic and the inelastic lateral buckling strength of I-shaped plate girders were studied theoretically and a general method of analysis was developed by the transfer matrix method in the nondimensional form. First, it was shown that the sectional properties in the inelastic range could be calculated numerically by only β as a parameter of cross sectional dimensions. Secondly, the field transfer matrix was derived in the nondimensional form and the point transfer matrix which took the variation of the cross section into account was expressed.

A new representation of the buckling curves which was independent on the cross sectional geometry of plate girders and only depend on the residual stress levels and distributions. Using this representation, the numerical examples were presented for the simply supported plate girders with uniform and tapered cross sections under various loading conditions. It was also shown that the experimental results could be adjusted by this method.

The method should find a particular application in the design of plate girders.

Appendix - Transfer Matrices

State Vector

Using the same notations as in Ref. 15, the following nondimensionalized state vector may be used.

$$V = \left\{\frac{u}{b}\ \theta\ \frac{\phi}{\alpha}\ \frac{\rho b}{\alpha}\ \frac{S}{\alpha\sigma_y d^2}\ \frac{M_\eta}{\alpha^2\sigma_y d^3}\ \frac{M_z}{\alpha\sigma_y d^3}\ \frac{M_w}{\alpha^2\sigma_y d^4}\right\} \tag{16}$$

in which u and θ = the lateral displacement and its slope at shear center; ϕ = the angle of twist; ρ = the angle of twist per unit length; S = the lateral shear force; M_η = the bending moment about weak axis; M_z = the torsional moment and M_w = the bimoment produced by warping.

Point Transfer Matrix

The compatibility and the equilibrium conditions at the nodal point i where the cross section is discontinuous are obtained as follows [14] considering the movement of the locations of shear center:

$$
\begin{aligned}
u_i^L &= u_i^R - \Delta s \phi_i^R \\
\theta_i^L &= \theta_i^R - \Delta s \rho_i^R \\
\phi_i^L &= \theta_i^R \\
\rho_i^L &= \rho_i^R \\
S_i^L &= S_i^R \\
M_{\eta i}^L &= M_{\eta i}^R \\
M_{zi}^L &= M_{zi}^R - \Delta s (m_{oi}^R M_{yi}^R \rho_i^R - S_i^R) \\
M_{wi}^L &= M_{wi}^R + \Delta s M_{\eta i}^R
\end{aligned} \tag{17}
$$

in which Δs = the movement of the shear center downward.

The elements of the 8×8 point transfer matrix can be expressed by the non-dimensional form as follows:

$$
\begin{aligned}
(1,1) &= \left(\frac{k_b^L}{k_b^R}\right) & (1,3) &= \Delta\eta\left(\frac{k_b^L}{k_b^R}\right) \\
(2,2) &= 1.0 & (2,4) &= \Delta\eta \\
(3,3) &= \left(\frac{k_b^L}{k_b^R}\right)\left(\frac{k_d^R}{k_d^L}\right) & (4,4) &= \left(\frac{k_d^R}{k_d^L}\right) \\
(5,5) &= \left(\frac{k_b^L}{k_b^R}\right)\left(\frac{k_d^L}{k_d^R}\right) & (6,6) &= \left(\frac{k_b^L}{k_b^R}\right)^2\left(\frac{k_d^L}{k_d^R}\right) \\
(7,4) &= m_o \mu_s \Delta\eta\left(\frac{k_b^L}{k_b^R}\right)\left(\frac{k_d^L}{k_d^R}\right)^2 & (7,5) &= -\Delta\eta\left(\frac{k_b^L}{k_b^R}\right)\left(\frac{k_d^L}{k_d^R}\right)^2 \\
(7,7) &= \left(\frac{k_b^L}{k_b^R}\right)\left(\frac{k_d^L}{k_d^R}\right)^2 & (8,6) &= \Delta\eta\left(\frac{k_b^L}{k_b^R}\right)^2\left(\frac{k_d^L}{k_d^R}\right)^2 \\
(8,8) &= \left(\frac{k_b^L}{k_b^R}\right)^2\left(\frac{k_d^L}{k_d^R}\right)^2
\end{aligned}
$$

in which $\Delta\eta = \eta_o^R(k_d^R/k_d^L) - \eta_o^L$; η_o^L, η_o^R = the values of η_o on the left and the right side elements at point i and k_b^L, k_d^L, k_b^R, k_d^R = the values of k_b and k_d on the left and the right side elements at point i, respectively.

The unspecified elements are equal to zero.

Notation

The following symbols are used in this paper:

a	distance between point on cross section and shear center.
b	flange width.
d	depth of plate girder.
d_w	web height.
E	Young's modulus of elasticity.
F	field transfert matrix.
G	modulus of elasticity in shear.
GK_T	St. Venant torsional stiffness.
$G\overline{K}_T$	equivalent St. Venant torsional stiffness defined by $GK_T + \overline{K}$.

I_w warping moment of inertia.
I_y moment of inertia about weak axis.
K $\int \sigma a^2 dA$.
k_b, k_d ratios of flange width and depth of plate girder at arbitrary point to those at reference point.
k_{bo}, k_{do} ratios of flange width and depth of plate girder at ends to those at reference point.
L span length.
M bending moment.
M_{cr} critical moment.
M_y yield moment of cross section without residual stress.
M_w bimoment produced by warping.
M_z torsional moment.
M_η bending moment about weak axis.
M_o bending moment at midpoint of element.
$(M_y)_o$ yield moment of cross section without residual stress at reference point.
$(M_o)^e_{cr}$ elastic critical moment of simply supported beam under pure bending.
$(M^F_o)^e_{cr}$ elastic critical moment of fixed beam under pure bending.
$(M_o)^e_{cro}$ elastic critical moment of tapered beam under pure bending.
$(m_o)^e_{cr}$ $(M_o)^e_{cr}/M_y$.
$(m^F_o)^e_{cr}$ $(M^F_o)^e_{cr}/M_y$.
$(m_o)^e_{cro}$ $(M_o)^e_{cro}/(M_y)_o$.
m, n dividing number of flange thickness and width.
P point transfer matrix.
R, R' Boundary matrices at left and right ends.
S section modulus.
lateral shear force.
t flange thickness.
u lateral displacement.
w web thickness.
α ratio of flange width to depth of plate girder, $\alpha = b/d$.
β ratio of web height to depth of plate girder, $\beta = d_w/d$.
γ_1, γ_2 sectional constants in inelastic range defined in Eq. 8 c.
Δs movement of shear center.
ε strain at point on cross section.
ε_r residual strain.
ε_y yield strain.
ε_ϕ strain due to bending.
ε_o uniform strain on cross section.
ηd distance from x axis to point on cross section.
$\eta_o d$ distance from x axis to shear center.
θ slope of lateral displacement.
κ reduction factor (subscripts *kt, iw* and *iy* denote K_T, I_w and I_y).
μ coefficient defined by Eqs. 7 (subscripts *kt, s, iw* and *iy* denote K_T, S, I_w *and* I_y).
λ $1/\sqrt{(m_o)^e_{cr}}$

λ_F $1/\sqrt{(m_o^F)_{cr}^e}$.

λ_o $1/\sqrt{(m_o)_{cro}^e}$.

ν Poisson's ratio.

$\bar{\nu}$ E/G.

ξb distance from y axis to point on cross section.

ρ angle of twist per unit length.

σ stress on cross section.

σ_{rc}, σ_{rt} residual compressive and tensile stresses.

σ_y yield-stress level.

ϕ curvature.

angle of twist.

ϕ_y curvature corresponding to first yield in flexure.

Acknowledgments

The writer is grateful to Fumio Nishino of the University of Tokyo and Yuhshi Fukumoto of Nagoya University for their valuable suggestions. He wish to record also his appreciation to Haruko Kitada and Yutaka Hosokawa for their assistance. The numerical calculations were carried out by HITAC 8700/8800 in the University of Tokyo and FACOM 230-35 in Kanazawa University.

References

1. Column Research Council: Guide to Design Criteria for Metal Compression Members. 2nd ed., Ed. B.G. Johnston, John Wiley and Sons, New York, 1966.
2. FUKUMOTO, Y., FUJIWARA, M., and WATANABE, N.: Ineslastic Lateral Buckling Tests on Welded Beams and Girders (in Japanese). Proceedings, Japan Society of Civil Engineers, No. 189, May, 1971, pp. 39-51.
3. GALAMBOS, T.V.: Structural Members and Frames. Prentice-Hall Book Co., Englewood Cliffs, N.J., 1968.
4. GALAMBOS, T.V.: Inelastic Lateral Buckling of Beams. Journal of the Structural Division, ASCE, Vol. 89, No. ST5, Proc. Paper 3683, Oct., 1963, pp. 217–242.
5. HAMAYOSHI, F.: On Torsion of I-Beam with a Web of Variable Height. Memoir, Faculty of Engineering, Hokkaido University, Japan, Vol. 11, No. 2, 1961, pp. 209–228.
6. KITIPORNCHAI, S., and TRAHAIR, N.S.: Elastic Stability of Tapered I-Beams. Journal of the Structural Division, ASCE, Vol. 98, No. ST3, Proc. Paper 8775, Mar., 1972, pp. 713–728.
7. LEE, G.C., and SZABO, B.A.: Torsional Response of Tapered I-Girders, Journal of the Structural Division, ASCE, Vol. 93, No. ST5, Proc. Paper 5505, Oct., 1967; pp. 233–252.
8. LEE, L.H.N.: Non-Uniform Torsion of Tapered I-Beams. Journal of the Franklin Institute, Vol. 262, 1956, pp. 37–44.
9. LEE, L.H.N.: On the Lateral Buckling of a Tapered Narrow Rectangular Beams. Journal of Applied Mechanics, ASME, Vol. 26, Series E, No. 3, Sept., 1959, pp. 457–458.
10. MASSEY, C., and PITMAN, F.S.: Inelastic Lateral Stability Under a Moment Gradient. Journal of the Engineering Mechanics Division, ASCE, Vol. 92, No. EM2, Proc. Paper 4779, Apr. 1966, pp. 101–111.
11. NETHERCOT, D.A.: Factors Affecting the Buckling Stability of Partially Plastic Beams. Proceedings, Institution of Civil Engineers, Part 2, Vol. 53, Proc. Paper 7526, Sept., 1972, pp. 285–304.
12. TRAHAIR, N.S., and KITIPORNCHAI, S.: Elastic Lateral Buckling of Stepped I-Beams. Journal of the Structural Diversion, ASCE, Vol. 97, No. ST10, Proc. Paper 8445, Oct. 1971, pp. 2535–2548.

13. TRAHAIR, N.S., and KITIPORNCHAI, S.: Buckling of Inelastic I-Beams Under Uniform Moment. Journal of the Structural Division, ASCE, Vol. 98, No. ST11, Proc. Paper 9339, Nov. 1972, pp. 2551–2566.
14. UNGER, B.: Elastisches Kippen von beliebig gelagerten und aufgehängten Durchlaufträgern mit einfach-symmetrischem, in Trägerachse veränderlichem Querschnitt unter Verwendung einer Abwandlung des Reduktionsverfahrens als Lösungsmethode. Der Stahlbau, Heft 5, 1970, pp. 135–142, and Heft 6, 1970, pp. 181–184.
15. YOSHIDA, H., and IMOTO, Y.: Inelastic Lateral Buckling of Restrained Beams. Journal of the Engineering Mechanics Division, ASCE, Vol. 99, No. EM2, Proc. Paper 9666, Apr., 1973, pp. 343–366.

Summary

It is shown that the lateral buckling strength of I-shaped plate girders can be expressed by only the ratio of the depth of the cross section to the web height with respect to the cross sectional geometry in both the elastic and inelastic ranges.

Then, the influence of such factors as cross sectional geometry, loading conditions, yield stress levels and residual stress distributions is discussed. Furthermore, the effect of the variations of cross sections with tapering flange widths or web depths is investigated in both the elastic and inelastic ranges.

Résumé

La contrainte critique de déversement de poutres en double té peut s'exprimer, tant dans le domaine élastique que dans le domaine inélastique, à l'aide d'un paramètre de section unique: le rapport de la hauteur totale de la section à la hauteur d'âme. L'auteur envisage de plus l'influence de divers facteurs tels que la forme de la section, les conditions de charge, la valeur de la limite élastique et la répartition des contraintes résiduelles. On étudie enfin, pour les domaines élastique et inélastique, l'effet des variations de sections (largeur des ailes ou hauteur de l'âme variable).

Zusammenfassung

Die kritische Kippspannung eines I-förmigen Trägers lässt sich, sowohl im elastischen als auch im unelastischen Bereich, durch einen einzigen Querschnittsparameter ausdrücken: das Verhältnis der Gesamthöhe des Querschnittes zur Steghöhe. Anschliessend wird der Einfluss der Querschnittsgeometrie, der Belastungsanordnung, der Höhe der Fliessspannung und der Verteilung der Eigenspannungen besprochen, und schliesslich der Einfluss von Querschnittsänderungen (veränderliche Flanschbreite bzw. Steghöhe) im elastischen und unelastischen Bereich.

Erratum

Vol. 35-I of "Publications".
Vol. 35-I des «Mémoires».
Band 35-I der «Abhandlungen».

Article **A.T. Ractliffe:**

Hybrid Yield-Line Finite Element Analysis

Une analyse hybride des lignes de rupture moyennant la méthode des éléments finis

Eine hybride Bruchlinien-Analyse mittels der Methode der finiten Elemente

The legend on Fig. 3, page 174, should be read as follows:

La légende de la fig. 3 en page 174, est la suivante:

Die Legende zu Fig. 3, Seite 174, ist folgende:

a) All edges clamped.
b) Long edges clamped, short edges s.s.
c) Long edges s.s., short edges clamped.
d) All edges s.s.

Leere Seite
Blank page
Page vide